UNIVERSITÀ DEGLI STUDI DI NAPOLI "FERDERICO II"

DIPARTIMENTO DI INGEGNERIA NAVALE

Scuola di Dottorato in INGEGNERIA INDUSTRIALE

Corso di Dottorato in

INGEGNERIA AEROSPAZIALE, NAVALE E DELLA QUALITÀ

Indirizzo INGEGNERIA NAVALE

XXIII ciclo

Human postural stability onboard ship as seakeeping criterion. Stance control model and procedure for validating it: a proposal.

Tutor

prof. Guido BOCCADAMO

prof. Antonio SCAMARDELLA

Coordinatore della Scuola di Dottorato

prof. Antonio MOCCIA

Dottorando

Erica NOCERINO

Ottobre 2010

Dai diamanti non nasce niente
Dal letame nascono i fior
(Via del Campo, Fabrizio de Andrè)

Table of Contents

Chapter 3: Human Postural Stability

Chapter 4: Modelling the Human Postural Control System onboard Ship

Chapter 5: Experimental Procedures for Validating Human Postural Control Model

Introduction

This thesis is focused on human postural stability onboard ships. Within the research conducted, two main objectives have been pursued:

1) the development of a model reproducing human postural control on a moving platform;
2) the realization of experimental procedures for testing and validating the proposed control architecture.

I.1 HUMAN POSTURAL STABILITY: A MULTIDISCIPLINARY TOPIC

Human postural stability is a multidisciplinary topic involving several sciences and disciplines, since it has a profound impact on many aspects of everyday life. How individuals maintain balance, employ correct and efficient postural strategies, are able to prevent falls and occurrence of severe injuries are questions that relate to medicine and neurophysiology (e.g.,[Peterka, 2002], [Mergener, 2004]), biomechanics and robotics (e.g., [Tahboub, 2009]), as well as occupational safety (e.g., [Duncan, 2007]), ergonomics (e.g., [Qu, 2008]) and sport applications (e.g., [Brodie, 2009]).

Many researchers in heterogeneous sectors have worked towards explaining the mechanisms that underlie upright standing and postural stability in different conditions ([Henry et al, 2001], [Mergner, 2005]), during the execution of several tasks on both still and moving platform ([Duncan, 2007], [Punakallio, 2005]). Varied models, aiming to cope with the complicated nature of human postural stability, have been proposed ([Kuo, 1998], [Peterka, 2002], [Tahboub and Merger, 2007], [van der Kooji et al., 1999], [Winter et al., 1998]).

Despite the extensive interest into human balance topic emerges from the numerous published papers and works in different sciences and disciplines, the complete nature of the human postural control is still unknown, and a unified and universally accepted theory or model does not exist.

In field such as human postural control, mathematical models represent an irreplaceable aid for understanding, explaining and analysing the high complexity of the processes involved.

Models may predict human physiological reactions, motion strategies and biomechanics used in maintaining balance. They can also simulate the changes in such strategies and responses among people characterised by different gender, age, balance disorders, or employed in several tasks and in diverse environments. Models can help in analyzing and explaining data obtained from experiments performed on personnel on both fixed and movable platforms, or can be used for designing new experiments. Computational models also allow a systematic manipulation of relevant parameters that can be fine-tuned using experimental data. They may be a useful tool in developing strategies for the improvement of balance and global safety.

Modelling and simulating human body, postural control mechanisms and motions usually involve three sequential steps.

As a first step, the biomechanics of human body is rendered into a geometrical and mechanical framework, whose complexity varies according to the specific questions the model has to address. Existing balance models describe the human body as a multi-link articulated system. The number of segment and the degrees of freedom allowed about the rotational joints depend on the behavioural features that have to be captured. The simplest representation of human body is the single-segment inverted pendulum model, whose motion is limited to a single plane in the antero/posterior direction ([Maurer & Peterka, 2005], [Mergner, 2004], [Peterka, 2002], [Winter, 1995]). Multilink models ([Hsu et al., 2007], [Kuo, 1995], [Stockwell et al., 1981], [Van der Kooij et al., 1999]), models whose motion is allowed in the lateral direction ([Valles et al., 2008], [Wedge & Langlois, 2003], [Winter, 1995]) or in three-dimensions have been also developed ([Langlois, 2010], [Levin & Mizrahi, 1995], [Qu, 2008]).

As second step in model development, the main features of postural equilibrium control as a biological process have to be identified and incorporated into the biomechanical model.

The third step is necessary for testing the validity of the assumptions made and the reliability of the model proposed. The goal of the validation phase is achieved by performing a relevant (statistically) number of experiments, testing many individuals in order to infer significant results. The setting where the experiments are executed ([Langlois et al., 2009], [Peterka, 2002]), the tasks the subjects are instructed to perform and the postural behaviour they have to assume ([Duncan, 2007], [Qu, 2008], [Winter, 1995]) differ according to the specific hypotheses at the base of the study research question.

I.2 HUMAN POSTURAL STABILITY FROM THE NAVAL ARCHITECTS POINT-OF-VIEW

Human postural stability is a critical matter as far as the naval and commercial ship sector is concerned.

The environment and surrounding conditions heavily affect human performance. Noise, vibrations, movements of the operational platform can degrade significantly the ability to carry out the allotted task, and even can represent a risk of injury with different levels of consequence. This is particularly true if the working platform is a ship sailing in a changeable seaway, in which workers not only have to carry out operational activities but also spend their leisure and rest time. Crewmembers of fishing vessels, navy craft, cargo ships, experience conditions of works that are different from those faced by workers in other sectors. There is not a clear separation between working and personal time, since seamen live and operate in conditions that can be cramped and congested. As reported in [ILO, 2007], the fatality rate for fishers is typically several times higher than for other employees, making fishing a very hazardous activity.

Human upright stance is inherently unstable, with most of the body's mass concentrated above the lower extremities, higher up in the trunk; the erect posture is maintained over a relatively small base of support with the pivot point at certain height from the sole. Even in the absence of additional environmental disturbances (movements of the supporting surface, external forces, etc.), a small deviation from upright body orientation is enough to result in an increase of a destabilizing gravitational component, that accelerates the body further away from the upright position. The

maintenance of an upright stance is a "complex task" per se, and ship motion can make it more difficult and cause even routine duties to be hard, demanding and hazardous, or, in harsh conditions, impossible to perform. Weitheim [1998] outlined that motion primarily reduces motivation due to motion sickness, increases fatigue due to increased energy requirements, and creates balance problems.

Currently, the model used to predict the probability that ship motions may cause a person to lose balance or slide on the deck assumes the individual to react as a rigid body having geometrical and inertial proprieties of a human [Graham et al., 1992]. Developments to the Graham model have been proposed in literature. On the one hand, efforts have been made for improving the model prediction, keeping at the same time its mathematical simplicity [Crossland & Rich, 1998]. On the other hand, attempts have been devoted to develop, calibrate and validate more complex and realistic models for human body [Langlois, 2010] and postural control [Boccadamo & Scamardella, 2003].

I.3 OUTLINE OF THE THESIS

In Chapter 1, the key elements of seakeeping theory and approach are outlined for collocating the thesis topic within the naval architecture field and emphasised how the seakeeping performance of ships affects the performance onboard. The human factor issue as it is currently approached during the ship design stage is introduced. Criteria relating human factors to ship operability, that allow quantitative analysis of human performance and its degradation due to motion-induced problem, are discussed.

Chapter 2 reviews existing human models as applied in the naval environment and current approaches to postural stability onboard ships. The classical model developed by Graham is described and the developments successively proposed are discussed.

Chapter 3 covers the physiological and neurological aspects of human postural stability as they emerge from literature. The models for representing human body and the control architecture interesting for the present work are reviewed.

In Chapter 4, a stance control model for modelling postural behaviour of a crewmember onboard ship is proposed. A simple biomechanics model comprising the effects due to ship motions is derived, and the choice of physical parameters is argued. The postural control scheme is incrementally built up for complying with the main features of the biologically-inspired findings described in the previous session. Simulation results, obtained implementing the proposed control model in an own-developed software code, are presented.

Chapter 5 presents the own-developed experimental procedure for testing and validating the proposed control architecture. An "ad hoc" high-flexible multi-technique motion acquisition system has been designed for measuring both ship and human motions during full-scale trials. The whole process for planning, designing, calibrating, and assessing the accuracy of the motion capture system is reported and discussed. The results from the first measurement campaign are presented and compared with the simulated motion obtained from the proposed postural control model.

Finally, Chapter 6 concludes the thesis with a general discussion about the conducted research. The major findings are highlighted and avenues for future investigation and development are shown.

Chapter 1: Seakeeping and Human Factors

1.1 INTRODUCTION

The environment and surrounding conditions heavily affect human performance. Noise, vibrations, movements of the operational platform can degrade significantly the ability to carry out the allotted task, and even can represent a risk of injury with different levels of consequence. This is particularly true if the working platform is a ship sailing in a changeable seaway, in which workers not only have to carry out operational activities but also spend their leisure and rest time.

Crewmembers of fishing vessels, navy craft, cargo ships, experience conditions of works that are different from those faced by workers in other sectors. There is not a clear separation between working and personal time, since seamen live and operate in conditions that can be cramped and congested. As reported in [ILO, 2007], the fatality rate for fishers is typically several times higher than for other employees, making fishing a very hazardous activity.

As pointed out in [Dobbins et al., 2008], human factor, "*a branch of engineering in which the primary emphasis is on the human input*" [Dobie, 2003], has been included as an integral part of the design process in many areas of systems design including the aerospace and automotive sectors. Historically, this process has been slower in the maritime sector, especially because it is made up, in relevant parts, of small enterprises (fishing industries, small craft designers) with restricted budgets that cannot permit to devote time and resources to research and development of topics, such as human factor onboard. On the other hand, the vast amount of literature addressing this and related issues gives evidence of the growing interest, in

particular, in the navy and scientific sectors, as it has been recognised of fundamental importance in order to assure improvements in both safety and efficiency. The human element is becoming a key element in the design process, as well as in the assessment of seakeeping and manoeuvring qualities of existing ships, mainly considering that ship design evolves and, consequently, crew size diminishes.

The International Maritime Organization – IMO, through its Resolution A.947(23) 'Human Element Vision, Principles and Goals for the Organization', recognises "*the need for increased focus on human-related activities in the safe operation of ships, and the need to achieve and maintain high standards of safety, security and environmental protection for the purpose of significantly reducing maritime causalities*" and that "*human element issues have been assigned high priority in the work programme of the Organization*".

The human element is a critical, as well as an intrinsic feature of the whole system-ship lifecycle.

1.2 HUMAN FACTORS ENGINEERING IN SHIP DESIGN

A human factor is a physical or cognitive characteristic of an individual, which influences human-environment equilibriums as well as interaction with technology.

Human Factors – HF, Human Factors Engineering – HFE, and ergonomics can be defined as the scientific branches "*concerned with the understanding of interactions among humans and other elements of a system, and the profession that applies theory, principles, data and methods to design in order to optimize human well-being and overall system performance*" [IEA, website]. These disciplines have been developed only in recent times; their origin is in the military field, during Word War II, to improve aviation safety [Wikipedia, Human factors]. Thenceforth, Human Factors have found a wide range of application domains, including all the fields in which the interaction between human and technology is present.

Today, the requirement to consider Human Elements an integral part of design process is very strong, since it has been recognised that to consider human-systems integration late in the development cycle could result in a degraded system. This is still greatly felt in the military field, as proved by documents, guides and standard developed by military agencies of several countries [Dobbins et al., 2008].

Currently, also the civilian industry is interested in ensuring that the human element would be adequately considered as a key component of any technological system. For example, the aircraft and car industries utilise HF design standards to enhance the performance and safety of their vehicles [Dobbins et al., 2008].

As far as the maritime field is concerned, in the last year efforts have been made to inherit standards that are already available. This issue is discussed in [Dobbins et al., 2008]. The authors, sponsored by the UK MOD Defence Equipment & Support Agency (DE&S), developed a guide for integrating Human Factors features into the classical naval architecture design process. Even if the guide is addressed for small High Speed Craft designers, many aspects underlined could be equally extended to traditional vessel.

The Naval Architect's design process is often referred to as the 'Design Spiral' to describe the iterative procedure that has to be followed during the practical design of craft. Once the specification of the ship has been defined, the process passes through three main stages: the feasibility, main design and end design phases.

In [Dobbins et al., 2008], based on the design stages outlined by the International Organisation for Standardisation (ISO) 'Human-Centred Design Process Standard' (ISO 13407), the Human Factors is introduced during the specification phase. The authors point out that "*the insertion of HF requirements into the specification process is the catalyst to ensuring that HF issues are addressed through the rest of the design and evaluation processes*" and "*in HF terms it may be considered to be the most important section of the design process as without HF insertion at this stage it is unlikely that the project will be successful*".

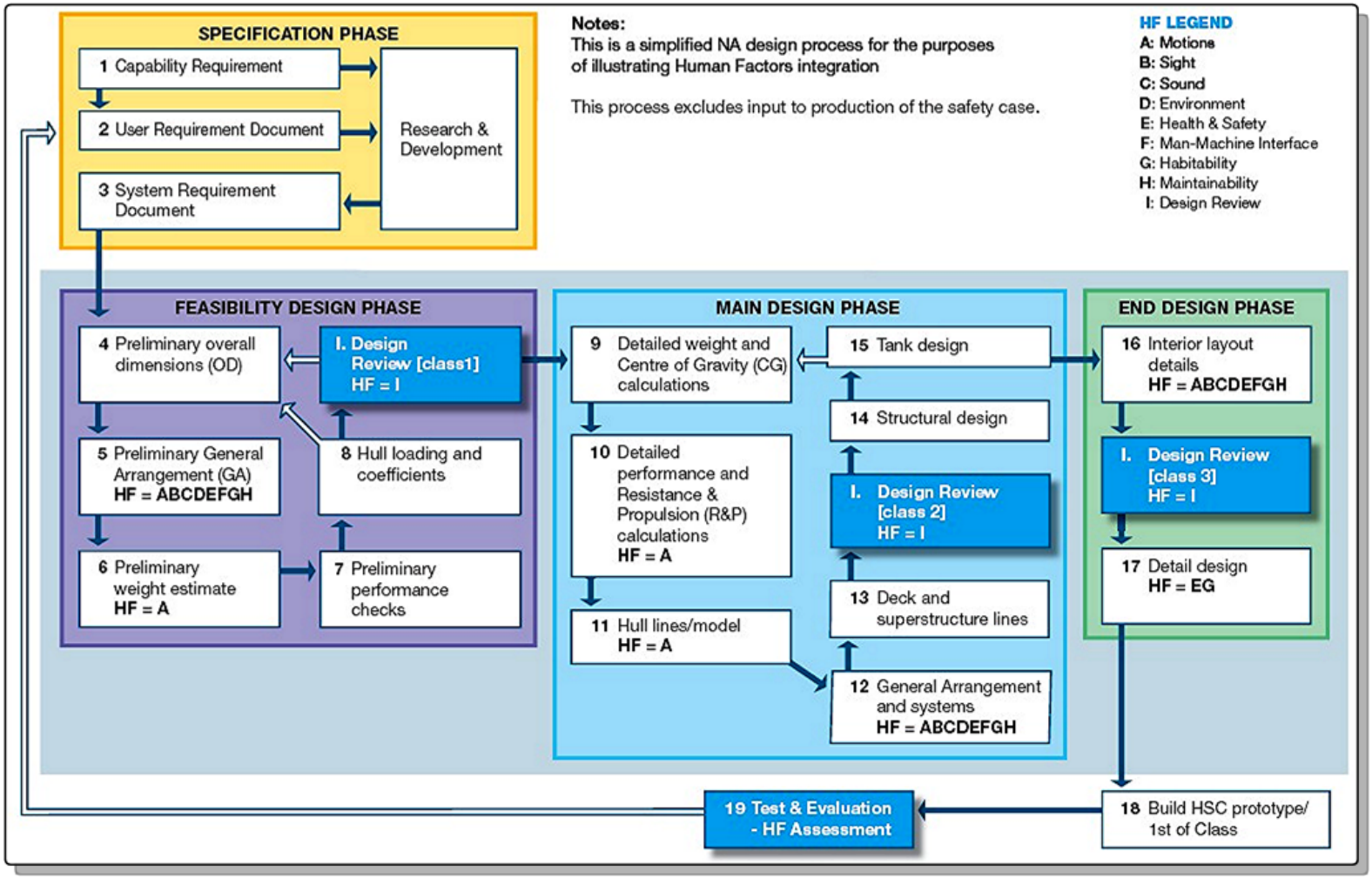

Figure 1.1 - Integrated High Speed Craft design process (overview)

[Dobbins et al., 2008]

Nine Human Factor areas (labelled A through to I in Figure 1.1) have been identified in order to support the integration of HF into the HSC Design Process.

The area named A is related to ship motions, that "*must be considered in the design process due to its potential to degrade performance and increase the risk of acute and chronic injury*".

1.3 THE IMPORTANCE OF GOOD SEAKEEPING

The seakeeping performance influences directly the overall performance of a ship, in terms of structural and machinery functionality, as well as of crew effectiveness. The motions in rough seas limit the capabilities of the vessel to accomplish the mission she has been realized for. The smaller the ship the more severe the performance degradation.

For men operating at sea, the main upsetting factor is the motion of the ship, that not only may affect the execution of onboard activities (direct influence), but can also have collateral effects (sleep disturbance and even deprivation). In heavy seas, severe ship motions limit the human ability from the responsibility tasks (to operate command and control, manage communication systems), up to routinely occupations (to perform ship maintenance or prepare food).

As reported in [Dobie, 2003], the importance of good seakeeping is stated in NATO Standardization Agreement (NATO STANAG 4154: Common Procedures fo Seakeeping in the Ship Design Process), the standard approach to seakeeping that various nations used: "*The general desirability of good seakeeping performance is universally accepted and has been for almost as long as ships have been designed and built. In general terms, good seakeeping qualities permit a warship to operate in adverse weather conditions with minimum degradation of mission effectiveness*".

The NATO standard approach to seakeeping in the ship design is shown in Figure 1.2:

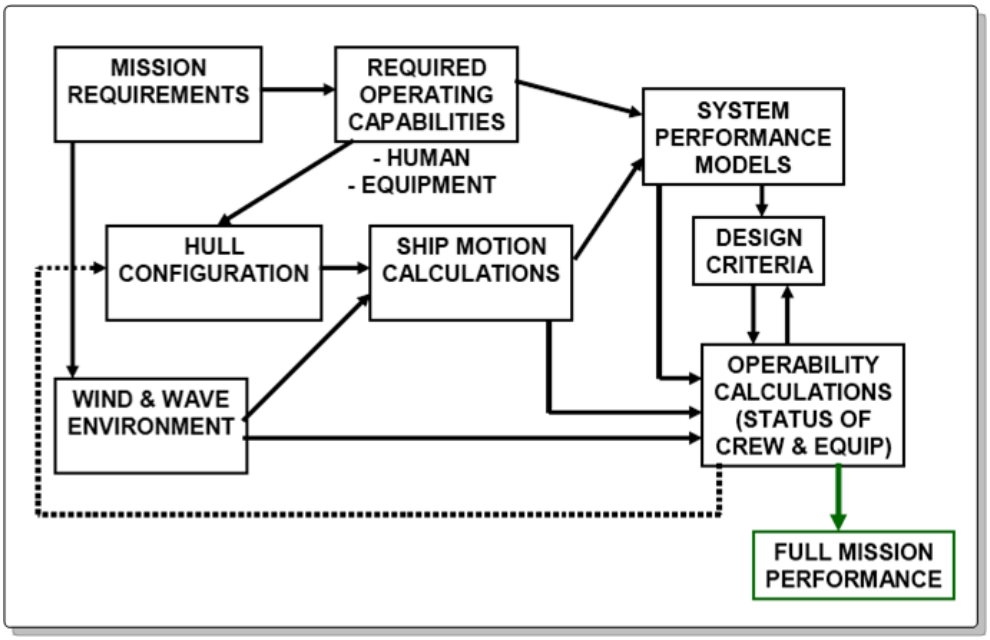

Figure 1.2 - Seakeeping in the Ship Design Process [NATO RTO, 2008]

It can be observed that the human element is incorporated into the seakeeping design process. Indeed, NATO STANAG 4154 also points out the following items related to human issues:

Health and safety of crew

The design manager has an obligation to ensure that the crew has a safe working environment to the extent that is practical for a warship. The problem of injury is particularly relevant, however, given the current trend towards lower manning levels.

Habitability and crew morale

Crew effectiveness is addressed by taking account of motion induced fatigue and motion sickness. However, the longer term peacetime implications such as crew retention should be borne in mind.

Crew tasks

Ship motions can have both direct and indirect effects on crew task performance. Ship motions directly affect physically demanding tasks.

Fine psychomotor tasks such as circuit board repair are also affected directly by the ship motions, but in a different way to physically demanding tasks. Cognitive tasks such as radar monitoring may be indirectly affected by ship motions, in that long exposure to severe

motions may cause nausea and fatigue. Both these may contribute to task performance degradation.

Layout considerations

As the overall ship motion response is minimized for a given sea state the range of locations throughout the ship that satisfy particular motion criteria will be increased. This gives the designer greater flexibility with respect to the location of operationally important compartments and orientation of workstations. Layout considerations are important because they may provide relatively easy (and therefore cheap) solutions to some problems. For example maintaining visibility at the bridge or sheltering certain key locations may help crewmembers perform more effectively.

The same concepts may be well extended also to commercial vessels, since the highlighted issues relate to civil as well as navy ships; only detailed tasks and operational procedures vary.

Before proceeding with a discussion about the human factor and performance onboard, the key elements of seakeeping theory and approach are outlined.

The reader interested in studying such topics in depth can find more detailed theoretical analysis in specialized literature, such as: [Llyod, 1989], [Nabergoj, 2007], [SNAME, 1989].

1.4 SEAKEEPING: MAIN FEATURES

The response of a ship advancing in a seaway is a complicated phenomenon involving the interactions between the vessel dynamics and several distinct hydrodynamic forces. Ship reactions are nonlinear, but, in many cases of practical interest, a linear theory may provide satisfactory predictions. This assumption allows not only to apply the superposition principle, but also to use many powerful analysis techniques derived from other sciences and technologies. E.g., considering the seas encountered by the vessel a random process, spectral techniques can be used to both define the characteristics of the seaway and analyze ship responses.

However, it should be clearly kept in mind the range of applicability the linear hypothesis is applicable for. If the vessel is sailing in high sea states where slamming and water on deck may occur, the linear relation assumed between ship responses and the incident waves will not be further correct.

The linear theory provides results in agreement with the physical evidence for standard ship forms and moderate operating conditions (moderate sea states and vessel speeds), while it does not fit for high speed craft or extreme working conditions (e.g., operation of weapon systems and onboard helicopter deployment in rough seas, crabs fishing in the North Sea).

A ship advancing at a steady mean forward speed with arbitrary heading in regular waves will move in six degrees of freedom: the motion can be considered to be made up of three translational and three rotational components. Consequently, for an arbitrarily shaped vessel, six nonlinear equations of motion must be wrote down and solved simultaneously. For slender vessels in low to moderate sea states, ship motions can be assumed to be small and hence the linear theory can be applied. For the common case of ship with port/starboard symmetry, the six non-linear equations reduce to two sets of three linear equations. That is, the vertical-plane or longitudinal motions (surge, heave and pitch) are uncoupled from the horizontal-plane or transverse motions (sway, roll and yaw).

The linear seakeeping theory is based on three essential assumptions:

- The sea surface elevation is assumed to be a realisation of an ergodico Gaussian stochastic process with zero mean. Thus, the process is entirely described by its power spectral density.
- The wave-excitation loads and ship motion response are assumed to be linear.
- The ship keeps a steady course and moves at a constant average speed (which includes the case of zero speed).

1.4.1 SEAKEEPING REFERENCE SYSTEMS

Three right-handed orthogonal coordinate systems are used to define the ship motions (Figure 1.3).

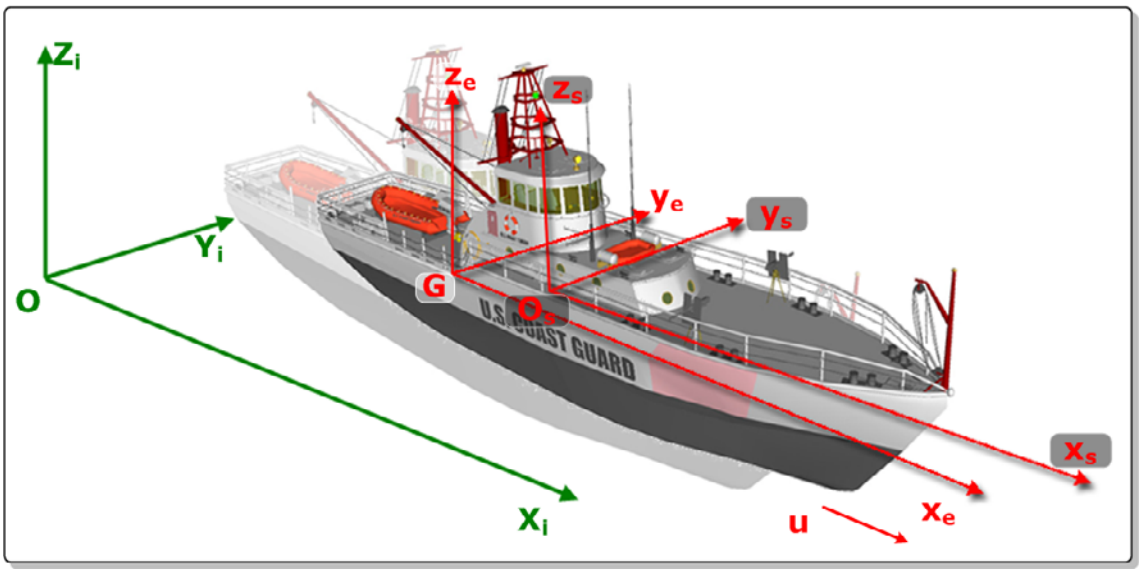

Figure 1.3 – Seakeeping Reference Systems

- *Inertial or Earth-fixed CS* $\{i\} \equiv O(X_i, Y_i, Z_i)$

  The inertial system is fixed in relation to the Earth. The (X_i, Y_i) plane is coincident with the calm-water level. The X_i-axis is in the direction of the wave propagation. The Z_i-axis is positive upwards. If the deep water assumption holds, the incident wave system is defined relative to the $O(X, Y, Z)$ CS as:

$$\zeta = \zeta_a \cos(\omega t - kX_i) \tag{1.1}$$

where:

- ζ_a is the wave amplitude (m)
- $k = 2\pi/\lambda = \omega^2/g$ is the wave number $(\mathrm{rad/m})$
- λ is the wave length (m)
- ω is the circular wave frequency $(\mathrm{rad/s})$
- g is the acceleration of gravity $(\mathrm{m/s^2})$

- *Equilibrium CS* $\{e\} \equiv G(x_e, y_e, z_e)$

This system is moving with a constant velocity *U*, that is the ship forward speed; the system is, then, inertial. The origin can be chosen coinciding with the equilibrium or time-average position of the ship's centre of gravity, *G*. The x_e-axis is positive in the ship forward direction and rotated with an angle μ (wave heading direction) relative to the Earth-fixed X_i-axis. The (x_e, y_e) plane is parallel to the still water surface.

The equilibrium frame is the frame adopted in seakeeping: the motion is described from this RF that represents the equilibrium position and orientation of the vessel. The waves make the ship oscillate with respect to this equilibrium state.

The equilibrium frame can be briefly defined according to the coordinate vector representation [Perez & Fossen, 2007]:

$$\begin{cases} \boldsymbol{u}_{ie}^{i} = \dot{\boldsymbol{r}}_{ie}^{i} = \left[U\cos\bar{\mu}, U\sin\bar{\mu}, 0\right]^T \\ \boldsymbol{\omega}_{ie}^{i} = \left[0,0,0\right]^T \\ \boldsymbol{\Theta}_{ie} = \left[0,0,\bar{\mu}\right]^T \end{cases} \quad \begin{cases} \boldsymbol{u}_{ie}^{e} = \boldsymbol{R}_{i}^{e}\boldsymbol{u}_{ie}^{i} = \left[U,0,0\right]^T \\ U = \left\|\boldsymbol{u}_{ie}^{i}\right\| = \left\|\dfrac{{}^{n}d\vec{r}_{ie}}{dt}\right\| \end{cases} \tag{1.2}$$

where *U* in equation (1.2) is the vessel average forward speed, and the notation $\bar{\mu}$ indicates either equilibrium or slowly varying component [Perez, 2005].

The following relations hold between the equilibrium CS and the Earth-fixed CS:

$$\boldsymbol{r}_{iP}^{i} = \begin{bmatrix} X_{iP} \\ Y_{iP} \\ Z_{iP} \end{bmatrix} = \boldsymbol{r}_{iG}^{i} + \boldsymbol{R}_{e}^{i}\dot{\boldsymbol{r}}_{ie}^{e}\, t + \boldsymbol{R}_{e}^{i}\boldsymbol{r}_{eP}^{e} = \begin{bmatrix} X_{iG} \\ Y_{iG} \\ Z_{iG} \end{bmatrix} + \begin{pmatrix} \cos\mu & -\sin\mu & 0 \\ \sin\mu & \cos\mu & 0 \\ 0 & 0 & 1 \end{pmatrix} \begin{bmatrix} Ut \\ 0 \\ 0 \end{bmatrix} + \\ + \begin{pmatrix} \cos\mu & -\sin\mu & 0 \\ \sin\mu & \cos\mu & 0 \\ 0 & 0 & 1 \end{pmatrix} \begin{bmatrix} x_{eP} \\ y_{eP} \\ z_{eP} \end{bmatrix} \tag{1.3}$$

$$\boldsymbol{r}_{eP}^{e} = \begin{bmatrix} x_{eP} \\ y_{eP} \\ z_{eP} \end{bmatrix} = \boldsymbol{R}_{i}^{e}\left(\boldsymbol{r}_{iP}^{i} - \boldsymbol{r}_{iG}^{i}\right) - \boldsymbol{R}_{i}^{e}\dot{\boldsymbol{r}}_{ie}^{i}\, t = \begin{pmatrix} \cos\mu & \sin\mu & 0 \\ -\sin\mu & \cos\mu & 0 \\ 0 & 0 & 1 \end{pmatrix} \begin{bmatrix} X_{iP} - X_{iG} \\ Y_{iP} - Y_{iG} \\ Z_{iP} - Z_{iG} \end{bmatrix} + \\ - \begin{bmatrix} Ut \\ 0 \\ 0 \end{bmatrix} \tag{1.4}$$

Equation (1.3) transforms from the equilibrium CS to the inertial CS, while equation (1.4) performs the inverse transformation.

- *Ship-fixed CS* $\{s\} \equiv O_s\left(x_s, y_s, z_s\right)$

  This system is connected to the ship, therefore moving with all motions of the ship. The $\left(x_s, y_s\right)$ plane coincides with the ship's calm waterplane, and the direction of the positive axes are:

  - x_s in the longitudinal forward direction,
  - y_s in the lateral port side direction
  - z_s upwards.

  For marine vehicles, the axes of this frame are chosen to coincide with the principal axes of inertia, and this determines the position of the origin of the frame.

  The motions of the ship are determined by the orientation of the ship-fixed system relative to the equilibrium system.

  In order to perform the transformation from the ship-fixed CS to the equilibrium CS the rotation matrix has to be defined. The roll, pitch and yaw is set of Euler angles commonly use in guidance and navigation to describe the attitude of one coordinate system relative to another. The rotation matrix in terms of roll, pitch and yaw is:

$$\boldsymbol{R}_s^e = \boldsymbol{R}_z(\varphi)\boldsymbol{R}_y(\theta)\boldsymbol{R}_x(\psi) = \begin{bmatrix} \mathrm{c}\theta\mathrm{c}\psi & \mathrm{s}\varphi\mathrm{s}\theta\mathrm{c}\psi - \mathrm{c}\varphi\mathrm{s}\psi & \mathrm{c}\varphi\mathrm{s}\theta\mathrm{c}\psi + \mathrm{s}\varphi\mathrm{s}\psi \\ \mathrm{c}\theta\mathrm{s}\psi & \mathrm{s}\varphi\mathrm{s}\theta\mathrm{s}\psi + \mathrm{c}\varphi\mathrm{c}\psi & \mathrm{c}\varphi\mathrm{s}\theta\mathrm{s}\psi - \mathrm{s}\varphi\mathrm{c}\psi \\ -\mathrm{s}\theta & \mathrm{s}\varphi\mathrm{c}\theta & \mathrm{c}\varphi\mathrm{c}\theta \end{bmatrix} \quad (1.5)$$

$\mathrm{s} = \sin(\cdot),\ \mathrm{c} = \cos(\cdot)$

1.4.2 SHIP MOTIONS IN REGULAR WAVES

If the hypothesis of "rigid body" holds, the ship motions can be considered depending only from time. Under this condition, the motions of a ship can be considered a composition of three mutually perpendicular translations of the centre of gravity (*G* or CoG) and three rotations around *G*.

According to the linear theory, the motion components have small amplitude. Therefore, the following generalized perturbation ship-fixed position vector (named seakeeping variables) is defined:

$$\boldsymbol{\eta} \triangleq \begin{bmatrix} r_{es}^e \\ \Theta_{es} \end{bmatrix} = \begin{bmatrix} \left(\delta x_{es}^e, \delta y_{es}^e, \delta z_{es}^e\right)^T \\ \left(\delta\varphi, \delta\theta, \delta\psi\right)^T \end{bmatrix} \equiv \begin{bmatrix} \left(\eta_1, \eta_2, \eta_3\right)^T \\ \left(\eta_4, \eta_5, \eta_6\right)^T \end{bmatrix} \quad (1.6)$$

In equation (1.6) r_{eb}^e includes the three translations of the ship's centre of gravity in the direction of the x_e, y_e and z_e axes:

- η_1: surge in the longitudinal x_e-direction, positive forwards,
- η_2: sway in the lateral y_e-direction, positive to port side,
- η_3: heave in the vertical z_e-direction, positive upwards.

Θ_{es} is the vector of Euler angles:

- η_4: roll about the x_e-axis, positive right turning,
- η_5: pitch about the y_e-axis, positive right turning,
- η_6: yaw about the z_e-axis, positive right turning.

In linear theory, the responses of the vessel, $\eta_i(t)$, to a regular sinusoidal wave (1.1) are harmonic functions proportional to the amplitude of the exciting forces, with the same frequency and with phase shift.

Consequently, the ship motions (described in terms of the three translations of and the three rotations about *G*) have the form:

$$\eta_j(t) = \left|\bar{\eta}_j\right| \cos\left(\omega_e t + \varepsilon_j\right) = \bar{\eta}_j e^{i\omega_e t}, \text{ j=1,...,6} \tag{1.7}$$

where

- $\left|\bar{\eta}_j\right|$ is the magnitude or absolute value of response amplitude
- ε_j is the phase shift of the response.

Together, the two quantities form the complex amplitude $\bar{\eta}_j$:

$$\bar{\eta}_j = \left|\bar{\eta}_j\right| e^{i\varepsilon_j}, \text{ j=1,...,6} \tag{1.8}$$

ω_e is the frequency of encounter, the frequency at which the ship, advancing with a speed *U*, encounters the waves. The period of encounter can be expressed as:

$$T_e = \frac{\lambda}{c - U\cos\mu} \tag{1.9}$$

where

- $c = \frac{\omega}{k} = \frac{\lambda}{T}$ (1.10)

  is the wave speed.

The circular frequency of encounter is given by:

$$\omega_e = \frac{2\pi}{T_e} = \omega - kU\cos\mu = \omega - \frac{\omega^2}{g}\cos\mu \tag{1.11}$$

By introducing the frequency of encounter, the wave elevation becomes:

$$\zeta = \zeta_a \cos\left(\omega_e t - kx_e \cos\mu + ky_e \sin\mu\right) \tag{1.12}$$

The harmonic velocities and accelerations of ship's centre of gravity are found by taking the derivatives of the displacements (1.7):

$$\begin{aligned}
&\dot{\eta}_j(t) = -\omega_e \left|\bar{\eta}_j\right| \sin\left(\omega_e t + \varepsilon_j\right) = \omega_e \left|\bar{\eta}_j\right| \cos\left(\omega_e t + \varepsilon_j + \pi/2\right) = i\omega_e \bar{\eta}_j e^{i\omega_e t} \\
&\ddot{\eta}_j(t) = -\omega_e^2 \left|\bar{\eta}_j\right| \cos\left(\omega_e t + \varepsilon_j\right) = \omega_e^2 \left|\bar{\eta}_j\right| \cos\left(\omega_e t + \varepsilon_j + \pi\right) = -\omega_e^2 \bar{\eta}_j e^{i\omega_e t} \\
&\text{j=1,...,6}
\end{aligned} \tag{1.13}$$

Knowing the motions of and about the centre of gravity, the motions in any point on the ship's structure can be calculated using superposition.

1.4.2a ABSOLUTE AND VERTICAL MOTIONS

Absolute motions are the motions of the ship in the equilibrium CS $\{e\} \equiv G\left(x_e, y_e, z_e\right)$.

Since the ship is assumed to be a rigid body, the rotational motions are the same at all the points on the body, while the three translational motions result from the combined effect of rotation of the body and translation of the centre of gravity.

From basic kinematics, it can be shown that for small motions:

$$\boldsymbol{r}_{eP}^{e} = \boldsymbol{r}_{eG}^{e} + \Theta_{es} \times \boldsymbol{r}_{sP}^{s} \tag{1.14}$$

where

- $\boldsymbol{r}_{eG}^{e}$ (1.15)

  is the vector of translational motions at the origin or CoG;

- $\boldsymbol{r}_{sP}^{s} \triangleq P\left(x_{sP}^{s}, y_{sP}^{s}, z_{sP}^{s}\right)$ (1.16)

  is the position vector of point P on the ship structure in the ship-fixed CS.

Analogously, the same result can be achieved starting from the rotation matrix (1.5) that transforms the ship-fixed coordinates into the equilibrium CS. It is necessary for the linearization to assume the angles of rotation η_4, η_5, and η_6 being small. This implies:

$$\sin(\cdot) \approx \cdot, \ \cos(\cdot) \approx 1 \tag{1.17}$$

making the (1.5):

$$\tilde{\boldsymbol{R}}_s^e = \begin{bmatrix} 1 & -\eta_6 & \eta_5 \\ \eta_6 & 1 & -\eta_4 \\ -\eta_5 & \eta_4 & 1 \end{bmatrix} \tag{1.18}$$

The components of absolute motions at point $P\left(x_{sP}^s, y_{sP}^s, z_{sP}^s\right)$ are given by:

$$\begin{aligned} \eta_{\boldsymbol{1P}} &= \eta_1 - \eta_6 y_{sP}^s + \eta_5 z_{sP}^s \\ \eta_{\boldsymbol{2P}} &= \eta_2 + \eta_6 x_{sP}^s - \eta_4 z_{sP}^s \\ \eta_{\boldsymbol{3P}} &= \eta_3 - \eta_5 x_{sP}^s + \eta_4 y_{sP}^s \end{aligned} \tag{1.19}$$

As (1.19) have been obtain by a linear superposition of harmonic motions, the resultant motion must be harmonic as well. The velocity and acceleration at any point are found by differentiating the individual component amplitudes (1.19) with respect to time:

$$\begin{aligned} &\eta_{mP}(t) = \bar{\eta}_{mP} e^{i\omega_e t} \\ &\dot{\eta}_{mP}(t) = i\omega_e \bar{\eta}_{mP} e^{i\omega_e t} \\ &\ddot{\eta}_{mP}(t) = -\omega_e^2 \bar{\eta}_{mP} e^{i\omega_e t} \\ &\text{m=1,2,3} \end{aligned} \tag{1.20}$$

where $\bar{\eta}_{mP}$ are the motion complex amplitude:

$$\bar{\eta}_{mP} = \left|\bar{\eta}_{mP}\right| e^{i\varepsilon_{mP}}$$
m=1,2,3 (1.21)

The vertical relative motion of the structure with respect to the undisturbed wave surface is the motion that can be perceived looking overboard from a moving ship, downwards toward the waves. For instance, this relative motion is of importance for shipping water on deck. Assuming that the wave is not distorted by the presence of the ship and $z^s_{sP} = 0$, the amplitude of the vertical motion at $P\left(x^s_{sP}, y^s_{sP}, 0\right)$ is defined by:

$$\eta_{\boldsymbol{RP}} = \eta_{\boldsymbol{3P}} - \zeta_P = \eta_3 - \eta_5 x^s_{sP} + \eta_4 y^s_{sP} - \zeta_P \tag{1.22}$$

where the local wave elevation is given by:

$$\zeta = \zeta_P \cos\left(\omega_e t - k x^s_{sP} \cos\mu + k y^s_{sP} \cos\mu\right) \tag{1.23}$$

and $\left(-k x^s_{sP} \cos\mu + k y^s_{sP} \cos\mu\right)$ is the phase shift of the local wave elevation relative to the wave elevation in the centre of gravity.

1.4.3 EQUATIONS OF MOTION

In seakeeping theory the equations of motions are derived in an inertial frame, that is the equilibrium CS, and written according to Newton's second law. Thus, the vector equation of motion is:

$$\boldsymbol{M^e_{RB}}\ddot{\boldsymbol{\eta}} = \boldsymbol{F^e} \tag{1.24}$$

or, equivalently:

$$\sum_{k=1}^{6} M^e_{RB_{jk}} \ddot{\eta}_k(t) = F^e_j(t),\ j = 1,\ldots,6 \tag{1.25}$$

where

- η (1.26)

  are the generalised perturbation coordinates or seakeeping coordinates in the equilibrium frame defined in (1.6);

- $\ddot{\eta}_k$ (1.27)

  are the accelerations in mode *k*.;

- $\boldsymbol{F^e}$ (1.28)

  are the total forces (forces and moments) for the six degrees of freedom expressed in the equilibrium CS;

- F_j^e (1.29)

  represents the total forces or moments acting on the body in direction *j;*

The matrix $\boldsymbol{M_{RB}^e}$ is the generalized rigid-body mass matrix (mass and inertia) with respect to the equilibrium frame:

$$\boldsymbol{M_{RB}^e} \triangleq \begin{bmatrix} \Delta\mathbf{I}_{3\times 3} & \Delta\mathbf{I}\left(\mathbf{r}_{eG}^e\right) \\ \Delta\mathbf{S}\left(\mathbf{r}_{eG}^e\right) & \mathbf{I}^e \end{bmatrix} = \begin{bmatrix} \Delta & 0 & 0 & 0 & \Delta z_{eG}^e & -\Delta y_{eG}^e \\ 0 & \Delta & 0 & -\Delta z_{eG}^e & 0 & \Delta x_{eG}^e \\ 0 & 0 & \Delta & \Delta y_{eG}^e & -\Delta x_{eG}^e & 0 \\ 0 & -\Delta z_{eG}^e & \Delta y_{eG}^e & I_{xx}^e & -I_{xy}^e & -I_{xz}^e \\ \Delta z_{eG}^e & 0 & -\Delta x_{eG}^e & -I_{yx}^e & I_{yy}^e & -I_{yz}^e \\ -\Delta y_{eG}^e & \Delta x_{eG}^e & 0 & -I_{zx}^e & -I_{zy}^e & I_{zz}^e \end{bmatrix} \quad (1.30)$$

where

- Δ (1.31)

  is the mass of the ship;

- $\mathbf{r}_{eG}^e = \left[x_{eG}^e, y_{eG}^e, z_{eG}^e\right]^T$ (1.32)

  is the position vector of the centre of gravity with respect to equilibrium frame;

- $\mathbf{S}(\cdot)$ (1.33)

is the skew-symmetric matrix[1];

- F_j^e (1.34)

  represents the total forces or moments acting on the body in direction *j;*

The inertia tensor with respect to the equilibrium CS $\mathbf{I}^e$ is:

$$\mathbf{I}^e \triangleq \begin{bmatrix} I_{xx}^e & -I_{xy}^e & -I_{xz}^e \\ -I_{yx}^e & I_{yy}^e & -I_{yz}^e \\ -I_{zx}^e & -I_{zy}^e & I_{zz}^e \end{bmatrix}, \ \mathbf{I}^e = \left(\mathbf{I}^e\right)^T > 0 \tag{1.35}$$

Usually, the mass matrix defined in (1.30) is significantly simplified, since, once the equations of motions have been linearised, the distinction between the ship-fixed system and the equilibrium/inertial frame is lost. Therefore, the mass matrix can be defined with respect to the ship-fixed CS, and, under the assumptions that the ship has a port/starboard symmetry with the (x_b, z_b) plane being the plane of symmetry and the origin O_b coinciding with the ship centre of gravity, it results:

$$\boldsymbol{M}_{\boldsymbol{RB}}^{\boldsymbol{b}} = \begin{bmatrix} \Delta & 0 & 0 & 0 & 0 & 0 \\ 0 & \Delta & 0 & 0 & 0 & 0 \\ 0 & 0 & \Delta & 0 & 0 & 0 \\ 0 & 0 & 0 & I_{xx}^b & 0 & -I_{xz}^b \\ 0 & 0 & 0 & 0 & I_{yy}^b & 0 \\ 0 & 0 & 0 & -I_{zx}^b & 0 & I_{zz}^b \end{bmatrix} \tag{1.36}$$

The only product of inertia that appears is I_{xz}^b, the roll-yaw product, which vanishes if the ship has a fore/aft symmetry and is small otherwise.

The total force vector $\boldsymbol{F}^{\boldsymbol{e}}$ (1.37) is assumed to be the linear combination of the components shown in Figure 1.4.

---

[1] A skew-symmetric (or antisymmetric or antimetric) matrix is a square matrix **S** whose transpose is also its negative; that is, it satisfies the equation $\mathbf{S} = -\mathbf{S}^T$, or, equally, $s_{ij} = -s_{ji}$

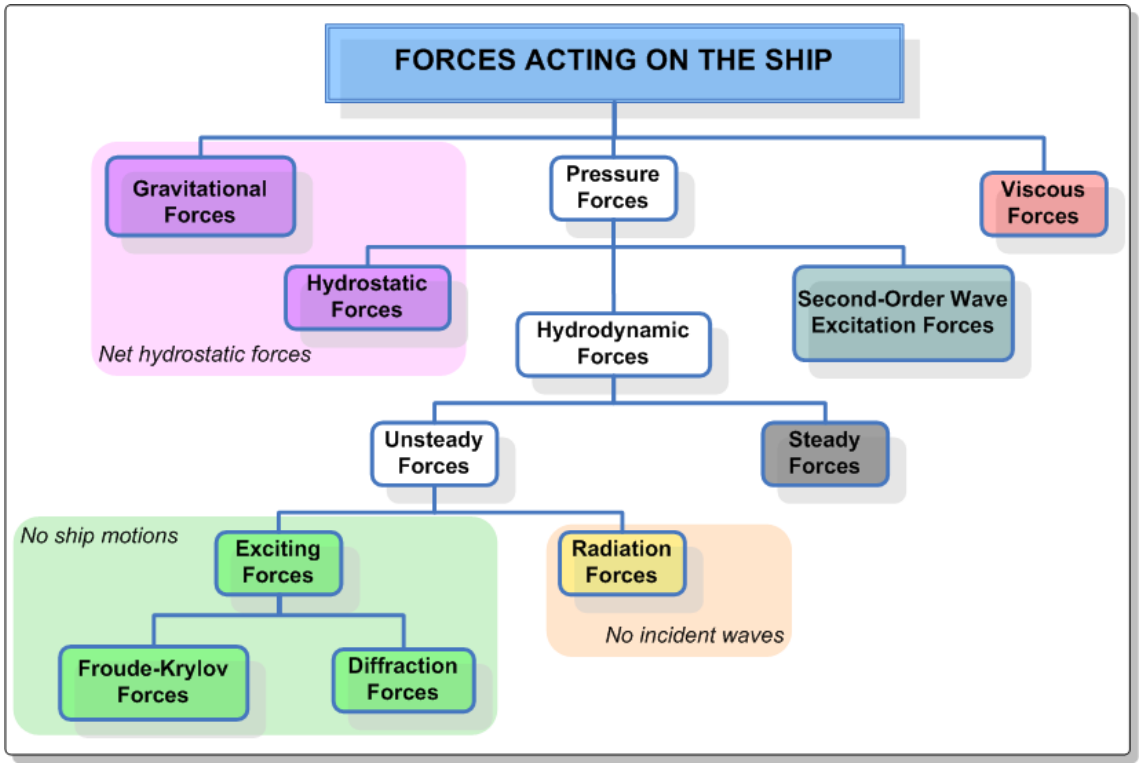

Figure 1.4 - Forces acting on a vessel in a seaway

$$\begin{aligned} \boldsymbol{F}^e &= \boldsymbol{F}_G^e + \boldsymbol{F}_H^e + \boldsymbol{F}_V^e = \boldsymbol{F}_G^e + \left(\boldsymbol{F}_{HS}^e + \boldsymbol{F}_{HD}^e\right) + \boldsymbol{F}_{H_{II}}^e + \boldsymbol{F}_V^e = \\ &= \left(\boldsymbol{F}_G^e + \boldsymbol{F}_{HS}^e\right) + \left(\boldsymbol{F}_{EX}^e + \boldsymbol{F}_R^e\right) + \boldsymbol{F}_{H_{II}}^e + \boldsymbol{F}_V^e = \\ &= \boldsymbol{F}_{HS}^{e\,*} + \boldsymbol{F}_{EX}^e + \boldsymbol{F}_R^e + \boldsymbol{F}_{H_{II}}^e + \boldsymbol{F}_V^e \end{aligned} \tag{1.37}$$

where:

- $\boldsymbol{F}_G^e$ (1.38)

  is the vector of gravitational forces due to the weight of the vessel. Since these forces cancel the mean buoyant forces, they are combined to give the net hydrostatic forces;

- $\boldsymbol{F}_H^e = \boldsymbol{F}_{HS}^e + \boldsymbol{F}_{HD}^e + \boldsymbol{F}_{H_{II}}^e$ (1.39)

  is the vector of the fluid forces acting on the vessel, that may be divided into the hydrostatic, hydrodynamic and second-order wave excitation contributions. Such components are obtained by integrating the fluid pressure over the underwater portion of the hull;

- $\boldsymbol{F}_V^e$ (1.40)

  is the vector of viscous forces. They are nonlinear damping forces due to

nonlinear non-conservative phenomena, such as skin friction, flow separation and eddy making. These forces cannot be studied within a linear framework, as they depend on the relative velocities between the hull and the fluid nonlinearly;

- $\boldsymbol{F}^{e}_{H_{II}}$ (1.41)

  are the second-order wave excitation forces (such as wave-drift loads, etc.) are obtained by integrating the pressure due to second order potentials;

- $\boldsymbol{F}^{e\ *}_{HS} = \boldsymbol{F}^{e}_{G} + \boldsymbol{F}^{e}_{HS}$ (1.42)

  is the net hydrostatic force, that is expressed in terms of restoring/spring coefficients C^{e}_{jk};

- $\tilde{\boldsymbol{F}}^{e}_{HD} = \boldsymbol{F}^{e}_{EX} + \boldsymbol{F}^{e}_{R}$ (1.43)

  is the vector of the unsteady hydrodynamic forces. The hydrodynamic forces $\boldsymbol{F}^{e}_{HD}$ are evaluated starting from the total velocity potential for the fluid flow, that can be subdivided into two main components: the perturbation potential due to steady translation, and the unsteady perturbation potential. The first component is the solution to the wave resistance problem in calm water. In seakeeping approach, only the unsteady part is considered, that is made up of the incident wave and diffracted wave potentials (resulting from the diffraction problem), plus the radiation potential (solution of the radiation problem).

- $\boldsymbol{F}^{e}_{EX} = \boldsymbol{F}^{e}_{EX_I} + \boldsymbol{F}^{e}_{EX_D}$ (1.44)

  are the exciting forces that come from the diffraction problem, in which the body is restrained from oscillating. $\boldsymbol{F}^{e}_{EX_I}$ are the force components due to the incident waves and result from the integration over the body surface of the pressure which would exist in the wave system if the body were not present. They are usually called the Froude-Krylov exciting force. The second component, $\boldsymbol{F}^{e}_{EX_D}$, is caused by the diffraction of the incident waves due to the presence of the vessel;

- $\boldsymbol{F}^{e}_{R}$ (1.45)

  are the radiation forces, that result from the radiation of waves away from a vessel that is forced to oscillate in calm water (there are no incident

waves). These forces are expressed in terms of added mass A_{jk}^{e} and damping coefficients B_{jk}^{e}. The added mass explicates the apparent increased inertia of the vessel that moves in the fluid and spends an amount of kinetic energy to accelerate the surrounding fluid. Therefore, it can be explained as the hydrodynamic pressure induced force. The damping coefficient gives a measure of energy dissipated through the radiated waves.

1.4.4 FREQUENCY DOMAIN FORMULATION

If the incident wave is sinusoidal and the linear approach is valid, the equations of motion can be formulated in the frequency domain framework. This means that the responses of the vessel are considered to be linear with (i.e., directly proportional to) wave amplitude and occur at the frequency at which the ship perceives the incident waves.

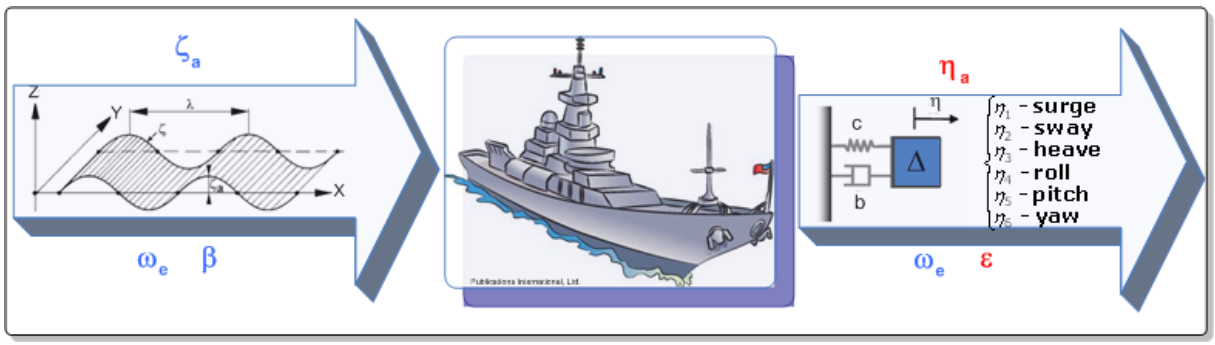

Figure 1.5 – The ship as a linear Input/Output system

Therefore, the time-dependent responses of the vessel will be sinusoidal at the frequency of encounter:

$$\eta_j(t) = \bar{\eta}_j e^{i\omega_e t},\ j = 1,\ldots,6 \tag{1.46}$$

as it has been already shown in section 1.4.2, and equation (1.25) becomes:

$$\sum_{k=1}^{6} -\omega_e^2 M^e_{RB_{jk}} \bar{\eta}_j e^{i\omega_e t} = F^{e\,*}_{HS\,j} + F^e_{EX\,j} + F^e_{R\,j} =$$
$$= -\sum_{k=1}^{6} -C^e_{jk}\bar{\eta}_j e^{i\omega_e t} + F^e_{EX_I\,j} e^{i\omega_e t} + F^e_{EX_D\,j} e^{i\omega_e t} + \sum_{k=1}^{6}\left(\omega_e^2 A^e_{jk} - i\omega_e B^e_{jk}\right)\bar{\eta}_j e^{i\omega_e t} \qquad (1.47)$$
$$j = 1,\ldots,6$$

In vector form, the frequency-domain equations of motion are given by:

$$-\omega_e^2\left[\boldsymbol{M^e_{RB}} + \boldsymbol{A^e}\left(\omega_e\right)\right]\bar{\eta} + i\omega_e \boldsymbol{B^e}\left(\omega_e\right)\bar{\eta} + \boldsymbol{C^e}\bar{\eta} = \boldsymbol{F^e}\left(\omega_e, \mu\right) \qquad (1.48)$$

from which the ship responses can be evaluated:

$$\bar{\eta} = \left(-\omega_e^2\left[\boldsymbol{M^e_{RB}} + \boldsymbol{A^e}\left(\omega_e\right)\right] + i\omega_e \boldsymbol{B^e}\left(\omega_e\right) + \boldsymbol{C^e}\right)^{-1} \boldsymbol{F^e}\left(\omega_e, \mu\right) \qquad (1.49)$$

where

- $\left(\boldsymbol{M^e_{RB}} + \boldsymbol{A^e}\right)$ (1.50)

  is the mass term containing both the mass of the vessel and the hydrodynamic added mass.

- $\boldsymbol{B^e}$ (1.51)

  is the damping term, result of the wave damping of the free surface.

- $\boldsymbol{C^e}$ (1.52)

  is the spring constant terms, that results from the hydrostatic restoring forces and are proportional to the waterplane area

The effects of viscous damping have been neglecting, even if they could be added to the $\boldsymbol{C^e}$ term.

It is worth noting that the equations of motion (1.47) or (1.48) are very similar to the equations of motion for a spring-mass-damper system with six degree of freedom. The principal difference is that the coefficients $\boldsymbol{A^e}$ and $\boldsymbol{B^e}$ are function of frequency. Indeed, by multiplying both sides of expression

(1.48) by $e^{i\omega_e t}$ and taking the real part, this would result in time-domain equations that describe the motion of the ship only if the wave excitation forces are sinusoidal. As for the typical spring-mass-damper, the true time-domain equations (valid for any type of excitation) have constant coefficients.

The hydromechanics coefficients $\boldsymbol{A}^{\boldsymbol{e}}$, $\boldsymbol{B}^{\boldsymbol{e}}$ and $\boldsymbol{C}^{\boldsymbol{e}}$, as well as the wave load components $\boldsymbol{F}^{\boldsymbol{e}}$ can be calculated with existing 2-D or 3-D techniques, that evaluate them and solve equation (1.49) numerically for a discrete set of frequency.

Details on how they perform is beyond the scope of this thesis, and interested readers can refer to specific papers [Salvesen et al., 1970], [Faltinsen, 1990], state-of-art surveys [Beck & Reed, 2001] or hydrodynamic programs ([Fathi, 2010], [Journée & Adegeest, 2003]).

1.4.4a MOTION RESPONSE AMPLITUDE OPERATOR - RAO

Equation (1.49) gives the amplitude and phase of each component of motion (complex amplitude $\overline{\eta}_j$) per unit of wave height (translational motions) or wave slope (rotational motions). These frequency responses, analogous to those defined for the application of generalized linear systems theory, are called transfer functions.

$$\begin{aligned} H_j(\omega,\omega_e,U,\mu) &= \left|\frac{\overline{\eta}_j(\omega,\omega_e,U,\mu)}{\zeta}\right| e^{i\angle\overline{\eta}_j(\omega,\omega_e,U,\mu)},\ \text{j=1,2,3} \\ H_j(\omega,\omega_e,U,\mu) &= \left|\frac{\overline{\eta}_j(\omega,\omega_e,U,\mu)}{k\zeta}\right| e^{i\angle\overline{\eta}_j(\omega,\omega_e,U,\mu)},\ \text{j=4,5,6} \end{aligned} \tag{1.53}$$

where

- $k = \dfrac{\omega}{g}$ (1.54)

  is the wave number
- $\zeta = \zeta_a \cos(\omega_e t + \beta)$ (1.55)

  is the elevation of the free surface at the origin of the equilibrium frame;

- β (1.56)

  is the initial phase of elevation of the free surface at the origin of the equilibrium frame.

The modulus of the transfer functions is defined as Response Amplitude Operator – RAO.

Obtained the motion transfer functions at the centre of gravity of the ship, the frequency responses at any other point of interest on the ship $P\left(x_{bP}^{b}, y_{bP}^{b}, z_{bP}^{b}\right)$ can be derived (analogous to (1.14)) with relation (1.57):

$$\left[H_1^P, H_2^P, H_3^P\right]^T = \left[H_1^G, H_2^G, H_3^G\right]^T + \left[H_4^G, H_5^G, H_6^G\right]^T \times \boldsymbol{r}_{bP}^{b} \tag{1.57}$$

1.4.5 BEHAVIOUR IN IRREGULAR WAVES: SHORT AND LONG TERM STATISTICS

In the analysis conducted so far, the vessel has been considered to proceed in a regular sea, that is the input for the ship-system is a regular sinusoidal wave. Actually, during her life-time the ship will navigate in a complicated seaway of irregular waves, that are random in both time and space.

If the hypotheses of the linear theory are still valid, the superposition principle can be applied to find the ship responses: the resulting motions in irregular waves can be obtained by adding together results from regular waves. In such a way, the superposition principle has been applied for modelling a realistic seaway, as well. Indeed, the irregular sea is seen as a sum of infinite simple, regular harmonic wave components, each with its own random initial phase, amplitude, length, frequency and direction of propagation. So, a convenient way to entirely described these wave components is in terms of a variance spectrum or Power Spectral Density (PSD), also called wave spectrum. Moreover, since the observed wave

elevation, at a certain location and for short periods of time, is assumed to be a realization of a stationary and homogenous zero-mean Gaussian stochastic process, the process is completely characterized by the PSD:

$$\begin{aligned} &\mathrm{E}\left[\zeta(t)\right] = 0 \\ &\mathrm{var}\left[\zeta(t)\right] = \mathrm{E}\left[\zeta(t)^2\right] = \int_0^\infty S_{\zeta\zeta}(\omega)\,d\omega = \sum_{i=1}^{N} \frac{\overline{\zeta}_i^2}{2} \\ &m_\zeta^n = \int_0^\infty \omega^n S_{\zeta\zeta}(\omega)\,d\omega \end{aligned} \tag{1.58}$$

where

- $\mathrm{E}\left[\zeta(t)^2\right]$ (1.59)

  is the variance of surface elevation;

- $S_{\zeta\zeta}(\omega)$ (1.60)

  is the mono-directional wave spectrum;

- m_ζ^n (1.61)

  is the statistical spectral moment of order n.

In some applications, the wave slope spectrum may be necessary:

$$S'_{\zeta\zeta}(\omega) = k^2 S_{\zeta\zeta}(\omega) = \frac{\omega^4}{g^2} S_{\zeta\zeta}(\omega) \tag{1.62}$$

When considering a ship moving with a certain speed, the wave spectrum seen from the vessel is modified due to the Doppler effect according to the encounter frequency:

$$S_{\zeta\zeta}(\omega_e) = \frac{S_{\zeta\zeta}(\omega)}{\left|1 - \frac{2\omega}{g}\cos\mu\right|} \tag{1.63}$$

$S_{\zeta\zeta}(\omega_e)$ is called wave encounter spectrum. The wave energy spectrum can be derived from the analysis of an irregular wave record obtained at a particular place and time. For ship design purposes and vessel response

prediction, current practise is to use standard formulae defining the distribution of wave energy for a geographical area of interest. The idealised wave spectra (Bretschneider, Pierson-Moskowitz, ITTC Two-Parameter, JONSWAP, etc) have been developed according to the location and prevailing weather conditions (see [Lloyd, 1989], [SNAME, 1989]).

The motion RAO defined in section 1.4.4a can be combined with the sea elevation spectrum to obtain the motion spectra:

$$S_{\eta\eta}(\omega_e) = \left|H_j(\omega, \omega_e, U, \mu)\right|^2 S_{\zeta\zeta}(\omega_e), \text{ for j} = 1,\ldots,6$$
or
$$S_{\eta\eta}(\omega_e) = \left|H_j(\omega, \omega_e, U, \mu)\right|^2 S'_{\zeta\zeta}(\omega_e), \text{ for j} = 4,5,6 \qquad (1.64)$$

The principle of this transformation of wave energy to response energy is shown in Figure 1.4.

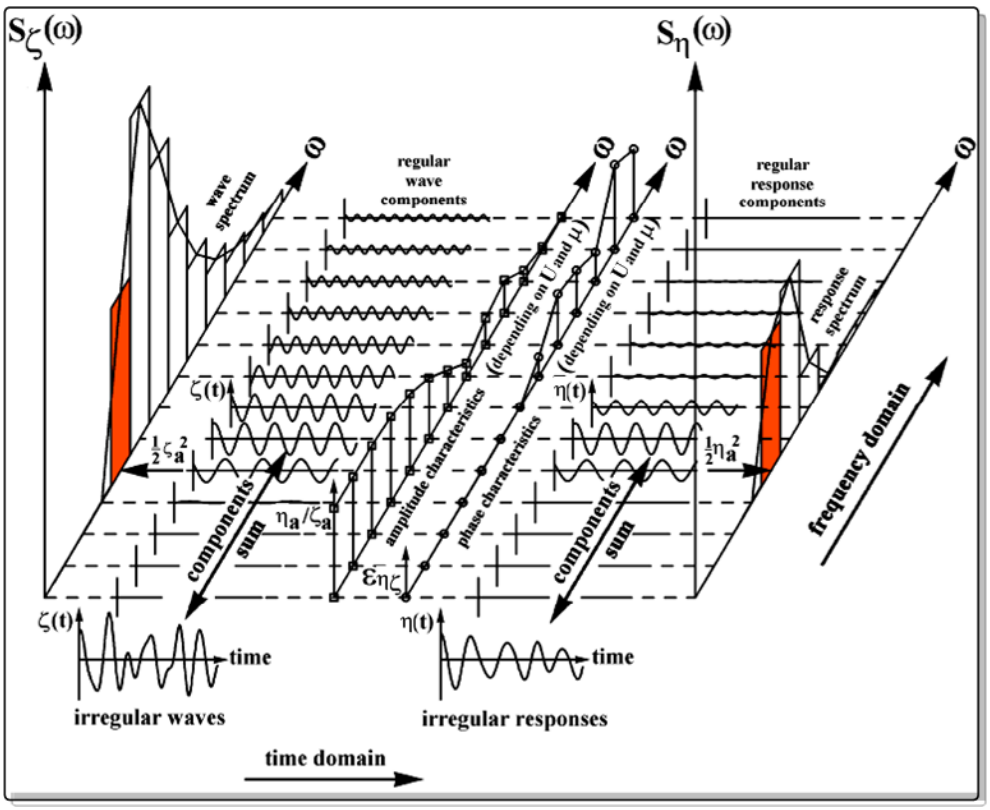

Figure 1.6 - Principle of Transfer of Waves into Responses (after, [Journée & Pinkster, 2002])

The spectral moment of order n of the motion components can be computed either in the encounter or in the wave frequency domain:

$$m_{\eta_j}^n = \int_0^\infty \omega_e{}^n \left|H_j\left(\omega,\omega_e,U,\mu\right)\right|^2 S_{\zeta\zeta}\left(\omega_e\right) d\omega_e = \int_0^\infty \omega_e{}^n \left|H_j\left(\omega,\omega_e,U,\mu\right)\right|^2 S_{\zeta\zeta}\left(\omega\right) d\omega \quad (1.65)$$

where

- $S_{\eta\eta}^*\left(\omega\right) = \left|H_j\left(\omega,\omega_e,U,\mu\right)\right|^2 S_{\zeta\zeta}\left(\omega\right)$ (1.66)

  is called the pseudo spectrum.

The moments of the response spectrum in (1.65), combining the response transfer function with a wave spectrum, make it possible to derive the short term statistics, that is the following statistical quantities of ship responses: standard deviation or Root Mean Square – RSM, significant value, expected maximum, zero-upcrossing period, etc.

The short term statistics are calculated for a fixed sea state, characterised by a certain value of significant wave height and period. During her lifetime, a ship will encounter different sea states, with a specific probability of occurrence. Wave statistics are provided by scatter diagrams (see i.e. Hogben, N., Dacunha, N.M.C. and Oliver, G.F., 1986: Global Wave Statistics. BMT), which are combined together with the ship responses for assessing long term statistics [Fathi, 2010].

1.5 THE HUMAN FACTORS AS SEAKEEPING CRITERIA

1.5.1 DEFINITION OF SEAKEEPING CRITERIUM

Once the responses of a vessel have been calculated for the specific operational sea area, the next step in the seakeeping performance procedure is to establish whether these responses will be satisfactory in practise. This requires establishing limiting value, namely seakeeping criteria, for the response of interest.

For defining a seakeeping criterion, the essential step is to identify the ship responses that are believed to influence the task of interest (e.g., operating fishing gears, handling cargo, etc.) or to degrade the ship or equipment performances (e.g., propeller emergence, slamming, deck wetness, etc.). The combination of the ship response and limit value forms the seakeeping performance criterion. In [Lloyd, 1989] the requirements for the determination of seakeeping criteria are summarised in three "*rules*":

Table 1.1 – Rules for determining seakeeping criteria [Lloyd, 1989]

1)	Criteria must be related to a particular task.
2)	The responses chosen for criteria assessment should be actual concern to the task being considered.
3)	Numerical values of criteria should be determined by monitoring the apparent performance of actual ships at sea

Three methods can be employed for assessing seakeeping criteria and related limiting values:

- full-scale sea trials;
- motion simulators;
- questionnaires.

Full-scale sea trials may have a twofold purpose. Onboard experiments allow measuring in the field the task or phenomena of interest and correlating them with ship motions. In such a way, theoretical models explaining the effect of ship motion can be tuned or validated. Moreover, sea trials make it possible to determine the conditions in which the task becomes

essentially impossible, safety levels for people or equipment are not acceptable, ship performance results no more satisfactory. Unfortunately, full-scale tests have some important drawbacks. It would be very difficult to obtain consistent data since sea state cannot be varied in a controlled manner, and the number of persons involved in the experiments is usually restricted.

Trials in motion simulators have the advantage that the same sequence of motions may be reproduced to obtain controlled experiments on a large number of subjects. However, some simulators cannot reproduce all six degree of freedom (i.e., the Ship Motion Simulator at the Naval BioDynamics Laboratory – NBDL in U.S. is capable of simulating three degree of freedom [Colwell, 2006]) or very large ship motions (in particular as well as translational motions are concerned). Furthermore, practical experiments are limited since it is not possible to simulate all the tasks or phenomena occurring on a real ship.

Questionnaires are a practical method of obtaining data on actual performance at specific tasks at sea. For example, the NATO developed in 1997 a questionnaire to obtain a large database on the effects of ship motions on fatigue, motion sickness and naval task performance [Colwell, 2005]. As highlighted in [Lloyd, 1989], when preparing a questionnaire, it should be borne in mind that ship operators are usually not able to provide direct estimates of ship motions. Instead, seamen have enough experience for estimating wave conditions. For this reason, fruitful results can be obtained by asking for estimates of the worst sea condition in which the task of interest can be completed.

In the common practise, first of all seakeeping criteria are evaluated for a particular mission, and then generalised regarding all possible combinations of sea areas, speeds, courses, etc. that the ships will experience during her lifetime. This procedure allows to calculate the operational effectiveness of the vessel. In numerical terms, operability can be defined as the "*proportion of time the ship can successfully accomplish its mission in a given combination of sea areas and seasons*" [Lloyd, 1989].

Seakeeping criteria typically used for conventional ships are presented in Table 1.2 and Table 1.3.

Table 1.2 – General operability limiting criteria for ships (NORDFORSK 1987) [Faltinsen, 2005] and fishing vessels (Soares et al., 1995) [Boccadamo, 1999]

PHENOMENA	Merchant ships	Naval vessels	Fast small craft	Fishing Vessels
Vertical acceleration at forward perpendicular (RMS value)	0.275g $(L \le 100m)^*$ 0.05g $(L \ge 300m)^*$	0.275g	0.65g	0.35g
Vertical acceleration at bridge (RMS value)	0.15g	0.20g	0.275g	0.20g
Lateral acceleration at bridge (RMS value)	0.12g	0.1g	0.1g	0.15g
Roll (RMS value)	6.0°	4.0°	4.0°	6.0°
Slamming criteria (probability)	0.03 $(L \le 100m)^*$ 0.01 $(L \ge 300m)^*$	0.03	0.03	0.06
Deck wetness criteria (probability)	0.05	0.05	0.05	0.05

* The limiting criterion for lengths between 100 and 330m varies almost linearly between the values $L = 100m$ and $L = 330m$, where L is the length of the ship.

Table 1.3 - Operability-Limiting Criteria for Accelerations and Roll Motions for Various Type of Work and for Passenger Comfort (NORDFORSK 1987) [Faltinsen, 2005]

PHENOMENA	RMS of Vertical Accelerations	RMS of Lateral Accelerations	RMS of Rolls
Light manual work	0.20g	0.10g	6.0°
Heavy manual work	0.15g	0.07g	4.0°
Intellectual work	0.10g	0.05g	3.0°
Transit passengers	0.05g	0.04g	2.5°
Cruise liner	0.02g	0.03g	2.0°

As shown, operational limits for defining an acceptable response differ depending on the missions of the ship. In Table 1.2 operability limiting are presented as functions of ship type. NordForsk defines a 'fast small craft' as a vessel up 35m in length with a speed in excess of 30 knots. It can be noted that the vertical acceleration level for fast small craft is set higher than for merchant ships, naval vessels and even fishing vessel. The reason is that personnel can tolerate higher vertical acceleration when the frequency of oscillation is high [Journée, 2001].

Table 1.3 indicates how ship motions affect humans' ability to perform activities of various nature, and also illustrates the requirement for passenger and cruise liners. Light manual work means work carried out by people adapted to ship motions. This work is not tolerable for longer periods, and causes fatigue quickly. Heavy manual work means work, for instance, on fishing vessels and supply ships. Intellectual work relates to work carried out by people not so well adapted to ship motions, such as scientific personnel on an ocean research vessel. Transit passenger means passengers on a ferry exposed to the acceleration level for about two hours. Cruise liner refers to older passengers on a cruise liner [Faltinsen, 2005].

Table 1.4 – Operability criteria for U.S. Navy and U.S. Coast Guard (after [Stevens, & Parson, 2002])

		NATO STANAG 4154 (U.S. Navy)	U.S. Coast Guard Cutter Certification Plan
SPECIFIC TASK	Motion Sickness Incidence (MSI)	20% of crew in 4 hours	5% in a 30 minute exposure
	Motion Induced Interruption (MII)	1 tip per minute	2.1 tips per minute
GENERAL	Roll Amplitude	4.0° RMS[1]	8.0° SSA[2]
	Pitch Amplitude	1.5° RMS[1]	3.0° SSA[2]
	Vertical Acceleration	0.2g RMS[1]	0.4g SSA[2]
	Lateral Acceleration	0.1g RMS[1]	0.2 g SSA[2]

[1] RMS – Root Mean Square

[2] $SSA = 2 \times \lceil RMS \rceil$ – Significant Single Amplitude

Table 1.4 contains typical personnel performance criteria in use by the U.S. Navy and U.S. Coast Guard. The stated limits are equivalent, but expressed in different units. The Significant Single Amplitude is the average of the one-third of highest amplitudes and is close to what a trained observer would estimate the motions to be.

Definitely, a relatively large variation in published criteria can be pointed out, as reported in [Faltinsen, 2005]. Moreover, since the ship system is made up of several subsystem (hull, plant, human element), different seakeeping criteria can be defined. A coarse classification for operational limits can be set according to [Faltinsen, 2005]:

- structural loading and response,
- machinery and propulsion loading and response,
- safety, comfort, and workability criteria.

1.5.1a A NOTE ABOUT THE USE OF QUESTIONNAIRES FOR DETERMINING LIMITING VALUES FOR SEAKEEPING CRITERIA

The use of questionnaires represents a practical method for obtaining data on specific tasks at sea without interfering with onboard activities.

For being effective, the questionnaire should be made as concise and self-explanatory as possible. Ship operators are usually not able to provide direct estimates of limiting ship motions or other criteria, but are often practised in estimating wave conditions.

If this technique is used, a statistical analysis has to be performed on the collected data. The analysis provides an estimate of the limiting sea state for the task or phenomenon of interest (e.g., deck wetness). If N is the number of questionnaires collected and x_i are the estimates of the limiting sea state in which the task becomes impossible, the mean value $\overline{x}$ and the standard deviation σ_0 of this threshold are respectively:

- $$\overline{x} = \frac{\sum_{i=1}^{N} x_i}{N} \tag{1.67}$$

- $$\sigma_0 = \sqrt{\frac{\sum_{i=1}^{N}(x_i - \bar{x})^2}{N-1}} \qquad (1.68)$$

The lower the standard deviation, the most reliable the estimate of the limiting sea state for the considered seakeeping criterion.

If the investigation is repeated through a "population" of ships (e.g., merchant ships), the threshold for the phenomenon of interest (e.g., the maximum probability of deck wetness events) can be estimated.

Examples of questionnaires and correlated statistical analysis can be found in [Lloyd, 1989].

1.5.2 SEAKEEPING PERSONNEL CRITERIA

Criteria relating Human Factors to ship operability allow quantitative analysis of human performance and its degradation due to motion-induced problem.

Ship motions have adverse effects on both ship passengers and crew and the effect on human performance can be summarised according to the diagram shown in Figure 1.7 (after [Colwell, 2006]).

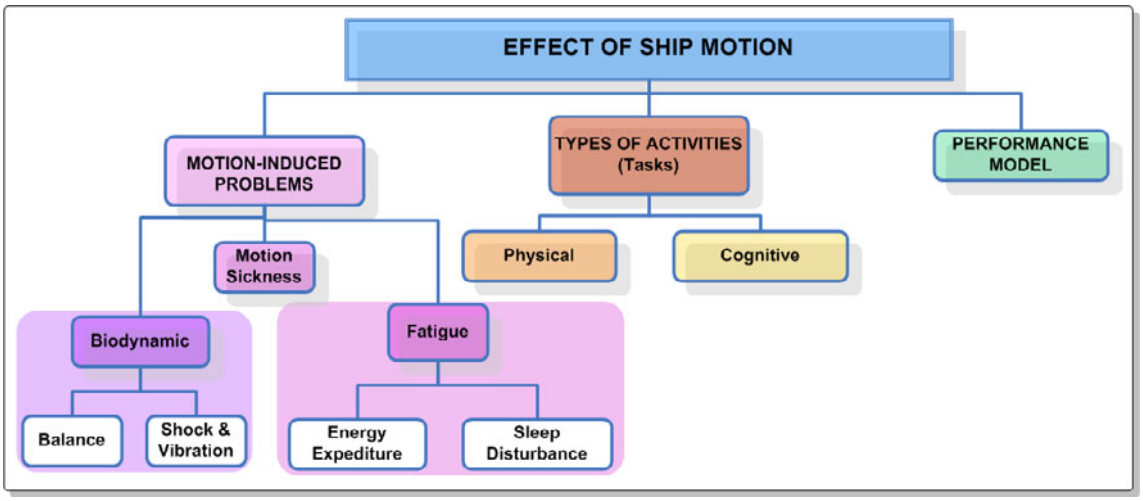

Figure 1.7 – Effect of ship motions on human performance

In [Dobie, 2003] the author observed that working on a moving platform is not only more difficult, but also the individual performs less well because of the difficulties inherent in the situation. Colwell [2005] emphasized that a variety of issues must be considered when evaluating the effects of ship motions on human performance. Ship motions have both an immediate and direct effect on performance (i.e., reduction on the balance of a person standing on deck), and indirect and accumulate effect over time. For example, symptoms of fatigue may arise and, consequently, cognitive performance may lessen.

Important efforts and improvements in understanding and modelling the effects of ship motions on human performance have been achieved by an ad-hoc working group on Human Performance at Sea.

As reported in [Pattison & Sheridan, 2004], in late 1989 the NATO NG/6 Subgroup 5 on Seakeeping, together with behavioural scientists from the University of New Orleans National BioDynamics Laboratory (NBDL), created an American, British and Canadian (ABC-17) Warship Operability group. The aim was to effectively define ship motion effects in the crew, understanding not only "*the mechanics of accelerations that caused a person to stumble*", but also "physiological and mental implications and effects". For this reason, the group established an experimental program in the Ship Motion Simulator at NBDL. In 1991, the Dutch joined to form an ad-hoc, four-nation working group of naval engineers, medical doctors and behavioural scientists. From then on, the ABCD has worked "*to define, cosponsor and/or perform human performance experiments on both land-based ship motion platforms and on sea trials, with the ultimate goal of developing human performance models for use in 'seakeeping' analysis and simulation*" [Colwell, 2005].

The ABCD have summarised the effect of ship motions on human performance in a simplified model, made up of three factors (Figure 1.8).

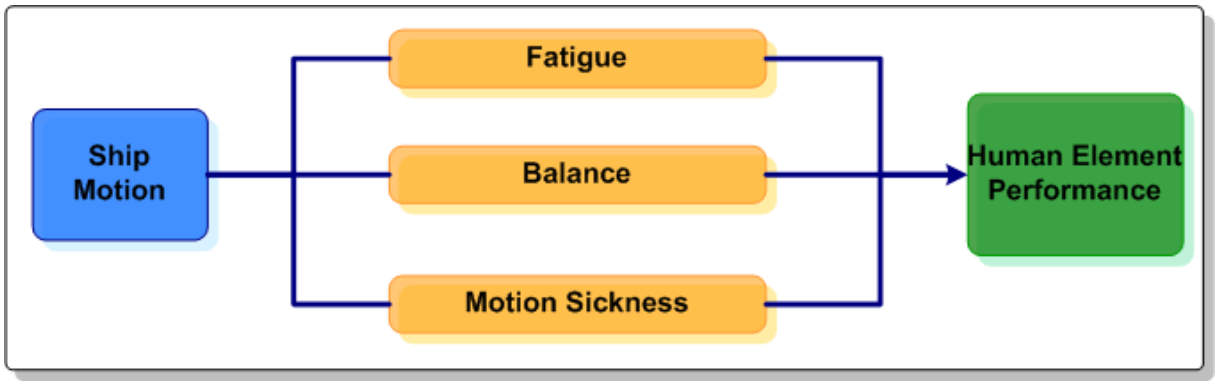

Figure 1.8 - ABCD-WG Model of Human Performance at Sea (after [Dobbins et al., 2008])

The motion experienced on a vessel can cause both fatigue, which degrades physical and cognitive human capability (Motion Induced Fatigue), and postural instability, also referred to as Motion Induced Interruption - MII. Both of these motion induced effects are included in the '*Whole-Body Motion (WBM) problem*' as defined in [Colwell, 1998] and [Dobie, 2003]. These biodynamic problems occur in relatively large-amplitude motions, at frequency below 1 Hz; at higher frequencies, usually 'Whole-Body Vibration (WBV)' problems occur.

Frequency of 1 Hz is also the traditional division between biodynamic and motion sickness problems, unpleasant consequence that characterises cruising vessel as well as many other forms of transport (automobiles, trains, aircraft, etc.).

Wertheim classified the effects of environmental motion on performance based on their consequences on individuals. He identified two categories, distinguishing between "*general effects and specific effects. General effects refer to any task, any performance, carried out in a moving environment. Such effects may be of a motivational nature (motion sickness), of an energetical nature (motion-induced fatigue caused by the continuous muscular effort to maintain balance), or of a biomechanical nature (interference with task performance because of a loss of balance). Specific effects, on the other hand, refer to interference with specific human abilities (e.g. cognition, perception, etc.)*" [Wertheim, 1998].

The present thesis is focused on Motion Induced Interruption, concept that will be explained and deepened in the following chapters.

The next sessions explore briefly the other issues related to the effect of ship motion on human performance and present prediction models, where such models exist.

1.5.2a WHOLE-BODY VIBRATION

Whole-Body Vibration may arise at either low frequency motion induced by sea conditions surrounding the ship and at higher frequency vibrations originated from the engines, propeller shafts and other machineries. Higher frequency vibrations can also originate from severe slamming events in heavy seas. As discussed in [Dobie, 2003], Whole-Body Vibration in the range from 2-12 Hz can have an effect on human performance, but, as reported in [Colwell, 1989], there were significant manual control problems during simulated surface effect ship motions in the range 0.02-0.2 Hz, where the vertical magnitudes were 0.5-1g. The effects of Whole-Body Vibration are many and various, and they may cause performance deficits, fatigue, accident-proneness and even health hazards.

The accepted international standard on biodynamic problems associated with Whole-Body Vibration is the ISO Standard 2631-1 (1997) 'Mechanical vibration and shock - Evaluation of human exposure to Whole-Body Vibration- Part 1: General requirements'. The standard defines limits to exposure to vertical and horizontal vibrations as functions of the frequency and amplitude of accelerations. Current standard methods also include the British Standard 6841 (1987) 'Measurement and evaluation of human exposure to whole – body vibration' [Vibration Injury Network, 2001].

1.5.2.b MOTION INDUCED FATIGUE

Motion Induced Fatigue is an important matter for the maritime community, since operations on moving platform require extra effort to maintain balance and degrade mental capability. MIF may have significant implications in particular for modern minimally manned ships or small vessel with few

crewmembers, since a reduction in performance can imply negative effects on personnel safety, as well as on the ship's operational effectiveness.

Fatigue associated with ship motions is mainly influenced by two factors: energy expenditure and sleep disturbance [Colwell, 2005].

Dobie [2003] relates several studies about the topic. According Powell and Crossland (1998), MIF is a complex matter, including other features such as lack of motivation. Baitis et al. (1995) recognised that the more severe ship motions could well raise the crew's energy expenditure to limits that could be significant. In [Stevens & Parson, 2002], studies conducted by Wertheim et al. in 1997 are reported. Wertheim defined the oxygen consumption to be the best indicator of physical workload and, using the Dutch motion simulator, he found that an individual's maximum capacity for oxygen was significantly reduced in the presence of motions. Empirical data, collected during coastal fishing from Rodahl & Vokac in 1979, also indicated that ship motions were responsible for added energy expenditure, attributed to the need to counterbalance the motions. Årstrand at al. (1973) reported that during coastal fishing heart rate and oxygen consumption were markedly higher in conditions of rough weather than during calm weather. In [Marais et al, 2010] experiments conducted in motion simulator (a 6DOF Stewart platform) are presented with the aim to evaluate the metabolic energy costs associated with maintaining postural stability in a moving environment. Measures of ventilation were collected and the results indicate a systematic increase in metabolic demands associated with the platform motions.

A performance model able to predict expended energy does not yet exist, but it would be desirable to integrate fatigue problem into the existing biodynamic models of balance (described later). As discussed in [Colwell, 2005], such a model could be used as a basis for calculating expended energy.

The relationship between ship motions, sleep disturbance and fatigue has been described in several studies [Colwell, 2005], but there are no models to allow estimating fatigue due to sleep disturbances from ship motion.

Miller and French [2005] developed a Physiological Stress Index – PSI to estimate the impact of exposure to physical stressors, particularly extreme temperature and fatigue related to insufficient sleep.

1.5.2.c MOTION-INDUCED SICKNESS

Motion sickness is one of the most important criteria for the design of passenger vessel and is of growing interest also for navy vessel [Riola et al., 2004], [Khalid, 2010]. Malaise, general discomfort, sweating, nausea, and vomiting characterise motion sickness.

All along, seasickness has affected men involved in the maritime environment. It is interesting to note that the Greek word "$\nu\alpha\tilde{\upsilon}\varsigma$" (*naus*), meaning ship, is the root of *nausea*.

Several factors are involved in the onset of motion sickness symptoms [Dobie, 2003]:

- the characteristics of the stimulus in terms of frequency, intensity, direction, and duration. The most provocative frequency has been shown to be around 0.2Hz;
- the susceptibility of the individual, based upon physiological characteristics, past experiences, psychological and personality factors;
- individual activity at the time of exposure to the stimulus (e.g., passengers are usually worse off than drivers);
- other factors, such as food, ambient air temperature, and certain odours.

The incidence of seasickness is extremely variable: females appear to become sick more often that males; children, below to the age of two, have the highest tolerance to motion sickness; sleep deprivation magnifies the occurrence of seasickness; etc. ([Stevens & Parsons, 2002], [Dobie, 2003]).

It was shown [Colwell, 2005] that the adaptation or habituation reduces the effects of motion sickness over a period of a few days. The time to acquire "*sea-legs*" is generally influenced by individual differences and the type of wave movements encountered [Wertheim, 1998].

Theories on the cause of motion sickness generally agree that a primary contributor is "sensor conflict" and they are known [Stevens & Parson, 2002]: conflict mismatch theory, sensory rearrangement theory by Reason & Brand (1975), neural mismatch theory by Benson (1999). These theories

describe the cause of motion sickness via the same proposition: "*that the vestibular apparatus within the inner ear provides the brain with information about self motion that does not match the sensations of motion generated by visual or kinaesthetic (proprioceptive) systems, or what is expected from previous experience*" [Wertheim, 1998]. Examples of many combination of sensory conflict which are known to produce motion sickness are described in [Colwell, 1989] and [Stevens & Parson, 2002].

- *Empirical/Descriptive Motion Sickness Models*

  There are two empirical models for predicting initial exposure Motion Sickness Incidence – MSI from the amplitude, frequency and duration of exposure to ship motions: the Motion Sickness Incidence – MSI developed by McCauley et al. (1976), and the Vomiting Incidence – VI by Lawther & Griffin (1987, 1988). For a more detailed presentation, Colwell [1989] and Khalid et al. [2010] reviews these models, including a comparison of their relative accuracy for predicting accuracy MSI observed in experiments and at sea.

  In both cases, MSI is expressed in units of percent, representing the percent of population that has vomited after exposure of a specified duration.

  Currently, International Standard Organization (ISO 2631, 1997) and British Standard Organization (BS 6841, 1987) employ the VI model for predicting Motion Sickness Incidence and establishing guidance on the prediction of motion sickness from measurements of vertical oscillation. The 'Motion Sickness Dose Value' (MSDV) is used to predict the percentage of persons likely to vomit after exposure to known magnitudes and durations of vertical oscillation in the frequency range 0.4 to 0.5 Hz [Stevens & Parson, 2002]. The $MSDZ$ $\left(\mathrm{m}\cdot\mathrm{sec}^{-1.5}\right)$ is calculating using equation (1.69), if the frequency-weighted time history of vertical acceleration $a_w(t)$ in known for the complete journey of duration $T(\mathrm{sec})$.

$$MSDZ_z = \sqrt{\int_0^T \left[a_w(t)\right]^2 dt} \tag{1.69}$$

Figure 1.9 graphically illustrates the frequency weighting that was derived from experimental observations and illustrates that the greatest sensitivity to acceleration is in the range 0.125-0.25Hz with a rapid reduction in sensitivity at higher frequencies.

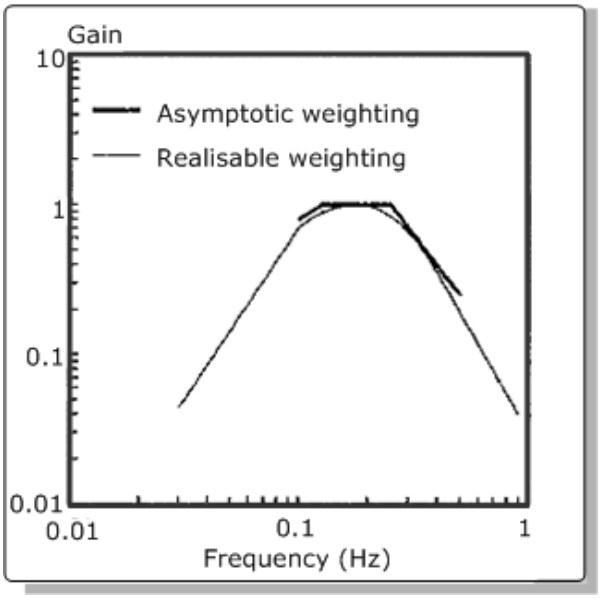

Figure 1.9 – Frequency-weighting as defined in ISO 2631 and BS 6841 (after [Stevens & Parsons, 2002])

Using the MSDV, the percent of people who is likely to vomit is given by:

$$MSI = K_m \cdot MSDZ_z \qquad (1.70)$$

where K_m is a constant that may be approximated to 1/3 for a mixed population of unadapted male and female adults.

- *Analytic/Physiological Motion Sickness Model*

  The first analytic model which allows to calculate the incidence of motion sickness from input of ship motions is due to Bles et al. (1998) [Colwell, 2005]. They postulate the "*Subjective Vertical (SV) conflict theory*" [Khalid et al., 2010]: "*All situations which provoke motion sickness are characterised by a condition in which the 'sensed vertical'*

(sensed gravity) as determined on the basis of integrated information from the eyes, the vestibular system and non-vestibular proprioceptors is at variance with the 'subjective vertical' (expected gravity) as predicted on the basis of previous experience". In SV theory, the sensory conflict that leads to motion sickness occurs when there is a difference between the real and perceived vertical (i.e. gravity vector). The model, developed by the Netherlands TNO Human Factors Institute in conjunction with the ABCD-WG, incorporates a control theory representation of the inner ear otolith and semi-circular canal physiology. Khalid et al. [2010] report further improvements to the original SV theory and suggest an alternative model that explicitly accounts for the horizontal accelerations: "*the new 'Subjective-Vertical-Horizontal (SVH) conflict model', considers two different sensory conflicts to explain variations in the observed sickness incidences aboard passenger ships. The model employs the sensory conflicts between (1) the sensed and expected vertical (SV-conflict) and (2) the sensed and expected horizontal accelerations (SH-conflict) to predict incidences of seasickness*". Several studies have established the role of horizontal accelerations for the occurrence of motion sickness aboard high speed vessels. Khalid et al. [2010] also compared the relative statistical fitness of the descriptive and physiological models applied to full-scale sea trials onboard HSC passenger ferries. The physiological models are found to display improved performance in predicting motion sickness incidence.

As discussed by Colwell [2005], results from the NATO questionnaire suggest an implied interaction between motion sickness and balance; this appears reasonable, as both responses are closely associated with the inner ear. These effects have not been explicitly investigated, and, as reported in [Valk et al., 2010] the relationship between postural stability and seasickness remains of special interest. Although the TNO motion sickness model has been already validated in several ways, a positive correlation between postural instability and sickness severity would add to the validity of using the mechanism to predict motion sickness in general.

Different motion sickness symptoms may affect performance and the sopite syndrome is considered to be one of these. On the web, a definition for sopite syndrome can be found: *"Sopite syndrome is a phrase coined by Graybiel & Knepton (1976) to characterize a poorly understood manifestation of motion sickness. Sopite syndrome is mainly associated with drowsiness and/or fatigue during or after motion. Sopite syndrome may be the result of motion-induced sleepiness that is experienced in situations such as driving, flying and riding aboard a boat. It is also believed to be why babies fall asleep when rocked. Sopite syndrome has been linked to the vestibular system which may modulate the ability of motion to cause (via "rocking") or disturb (via "shaking awake") sleep. Astronauts experiencing sopite syndrome have dubbed it "mental viscosity" or "the space stupids""* [Wikipedia, Sopite Syndrome].

Matsangas et al. [2010] evaluated the decrease of personnel physical activity while underway on two high speed vessels, in order to quantify the effects of sopite syndrome and motion induced fatigue. They found that physical activity was inversely related to ship motion/sea state, and suggest that these reductions in personnel activity levels may be evidence of some combination of sopite syndrome and motion induced fatigue.

1.5.2d MOTOR TASKS

Whole-Body Motion and Whole-Body Vibration have adverse effects on both gross and fine motor skills. The severity of the hull/sea interaction, the weight and complexity of components calling for performing a gross motor task, and the experience of the individual in both carrying out the task and working on a moving platform play roles in motor skill performance [Dobie, 2003]. Stevens & Parson [2002] report different studies indicating a reduced motor control due to ship motions, such as visuo-motor computer tracking tasks, keyboard digit punching, paper and pencil task. In [Pattison & Sheridan, 2004] the results from cognitive experiments from the Battelle Memorial Institute in Columbus, Ohio, are summarised. Such work did not establish how many abilities would be affected by motions during longer exposures where the effects of fatigue would start to play a role. In [Colwell,

2005], report of problems with motion sickness from the NATO questionnaire is discussed. They have significant correlation with physical task performance problems, and with abandoning tasks for subject performing both cognitive and physical tasks.

At the present time, task performance models require a great effort of new research, in particular to relate current postural models with motor tasks, such as, for example, Manual Material Handling [Duncan, 2007].

1.5.2e COGNITIVE PERFORMANCE

In modern ships, the demand of mental work is significantly grown compared with the situation years ago. Numerous studies have, therefore, been conducted to determine whether provocative motion has important effects on cognitive abilities, such as is required working on a computer. Both [Stevens & Parson, 2002] and [Dobie, 2003] report that there is no hard evidence that there are any direct effects of provocative motion on cognitive performance, although there are clearly indirect effects such as degradations of fine motor skills and subject effects of motion sickness. Continued research in this area was recommended in both the surveys, to ascertain the direct effects of the ship movements and the influence of motion sickness on cognitive activity.

In [Colwell, 2005], results from the NATO questionnaire suggest that fatigue correlates significantly with a variety of performance problems for subject performing cognitive tasks.

A multi-national sea trial on the effects of ship motions on human performance was performed on Canadian Forces Auxiliary Vessel Quest, off the coast of Nova Scotia, Canada, in February and March of 2007. The primary goal of these experiments was to obtain subjective and objective measures for human task performance, possibly affected by real ship motion. In [Valk et al., 2010] four types of variables were identified, as shown in Figure 1.10 and Table 1.5.

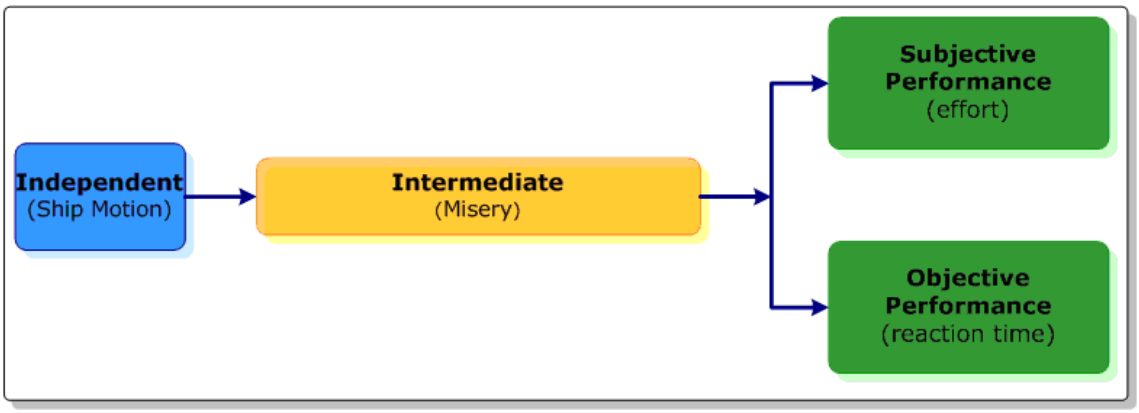

Figure 1.10 - Flow of information from independent via intermediate to performance variables (after [Valk et al., 2010])

Table 1.5 - Variable categories (after [Valk et al., 2010])

Category	Description
1. Independent	Variables that could not have been affected by any of the variables from the other categories (e.g. ship motion)
2. Intermediate	Variables that could have been affected by the independent variables, but which are not performance measures per se (sickness, alertness, sleep, fatigue)
3. Subjective performance	Variables quantifying performance based on subjective ratings, typically obtained from questionnaires (e.g., task effort: cognitive, physical, workload).
4. Objective performance	Variables quantifying performance based on objective ratings, typically obtained from charting task results (dynamic vision, vigilance and tracking, multiple task performance, reaction time).

Results indicate that increased feelings of misery led to impaired visual and cognitive performance. Furthermore, impaired sleep, high levels of fatigue and sleepiness affected cognitive performance. This over-all conclusion confirms what stated in [Bos et al., 2008], i.e., that human performance at

sea is less affected by ship motion per se, but more by its intermediate effects (i.e., by seasickness, fatigue, and impaired sleep).

Colwell [2005] gives some details on cognitive performance models, such as sickness on *situation awareness* and *human behaviour representation*, that are beginning to emerge. He also suggests that new experimental protocols are necessary in order to assess the effects of ship motions, fatigue and motion on situation awareness and decision making.

Chapter 2: Postural Stability as Seakeeping Criterion

2.1 INTRODUCTION

Human postural stability is of great importance in many aspects of everyday life and has application in several scientific and technological fields. These range from medicine, neurophysiology, to sports, biomechanics, robotics, etc. For over fifty years, researches and funds have been devoted to understand postural stability principles and the strategies employed to maintain it, with conceptual and computational model being developed.

Human upright stance is inherently unstable, with most of the body's mass concentrated above the lower extremities, higher up in the trunk; the erect posture is maintained over a relatively small base of support with the pivot point at certain height from the sole. Even in the absence of additional environmental disturbances (movements of the supporting surface, external forces, etc.), a small deviation from upright body orientation is enough to result in an increase of a destabilizing gravitational component, that accelerates the body further away from the upright position. Corrective torque must be generated to counter the destabilizing torque due to gravity; moreover, such a torque generation must be dynamically regulated and changed as the environmental conditions change. The complete nature of the human postural control is unknown yet, since the human body and underlying control system are so complex that a unified and universally accepted theory, explaining how they work, does not exist. Many researchers, in different sectors, have worked towards explaining the mechanism at the basis of upright stance, and a variety of models has been proposed and continues to be developed.

Mathematical models can aid in understanding and explaining complex systems; their purpose is to capture salient features that may differ according to the specific questions they have to address. Their complexity depends on the accuracy required, but, in general, a trade-off between simplicity and accuracy is desirable. While added complexity usually improves the realism of a model, it can make the model more difficult to understand and analyse; in addition, the uncertainty would rise since each single part induces some amount of variance into the whole complex system. Besides, there are practical considerations that make the Occam's Razor [Gibbs & Sugihara, 1997] attractive in modelling the mechanisms and systems involved in human postural stability. The computational cost of adding a huge amount of detail could hinder from using effectively the model, in particular if it were part of a wider simulation/prediction system. Therefore, in order to get a more usable and flexible model it is sometimes appropriate to make some approximations and reduce the model to a suitable form.

Human postural stability is a critical matter as far as the naval and commercial ship sector is concerned. The maintenance of an upright stance is a "*complex task*" per se, and ship motion can make it more difficult and cause even routine duties to be hard, demanding and hazardous, or, in harsh conditions, impossible to perform. Weitheim [1998] outlined that motion primarily reduces motivation due to motion sickness, increases fatigue due to increased energy requirements, and creates balance problems.

Currently, the model used to predict the probability that ship motions may cause a person to lose balance or slide on the deck assumes the individual to react as a rigid body having geometrical and inertial proprieties of a human [Graham et al., 1992]. As stressed in [Duncan, 2007] few studies have specifically examined the biomechanical effects of moving environments and the consequent strategies developed for maintaining postural stability in unstable conditions.

In this chapter, existing human models as applied in the naval environment and current approaches to postural stability onboard ships are reviewed.

2.2 SEAKEEPING CRITERIA FOR PERSONNEL ON DECK: THE MOTION INDUCED INTERRUPTION

In any motion environment, losing balance is a likely event and potentially its occurrence increases with worsening sea conditions. Motion Induced Interruptions (MIIs) have been employed as a seakeeping criteria for personnel operating on ship deck.

A Motion Induced Interruption is defined as an incident where ship motions cause a person to slide or lose balance unless the ongoing task is temporarily abandoned in order to keep the upright stance. MIIs include the ship motion induced interruptions of the crew in all non-seated tasks such as standing, walking, lifting and moving objects [Crossland & Rich, 1998]. This concept was introduced by Applebee, Baitis and McNamara in 1980's. In their works the researchers showed that performance of crew on the flight deck of frigates could be characterised by MII. They proposed a time-domain method for calculating the number of loss-of-balance events and defined the notion of Lateral Force Estimator (LFE) as "*combination of the earth-referenced lateral acceleration, and the ship-referenced lateral acceleration due to ship roll*" [Graham, 1990]. It was shown that the value of LFE, the apparent lateral acceleration parallel to the ship deck, can be related to the incidence of MIIs. Since implicit in the LFE concept is the assumption that the ship-referenced vertical acceleration is negligible, the LFE is only a valid estimator of MIIs under conditions in which the vertical acceleration is small [Graham, 1990]. Graham [1990], [1992] developed a generalization of the LFE including non-zero vertical acceleration. He also proposed a method for calculating the number of MIIs in the frequency domain, a form more suitable for the prediction methods of ship motions.

2.2.1 THE CLASSICAL APPROACH TO MII THEORY

To define the LFE, let us consider two different coordinate frames (Figure 2.1):

- the $\{e\} \equiv G(x_e, y_e, z_e)$ equilibrium coordinate system, as defined in section 1.4.1;

- the $\{p_s\} \equiv P(x_s, y_s, z_s)$ coordinate system, a ship-fixed CS with axes parallel to the ship axes and origin located at the centre of gravity of an object of mass m fixed to ship.

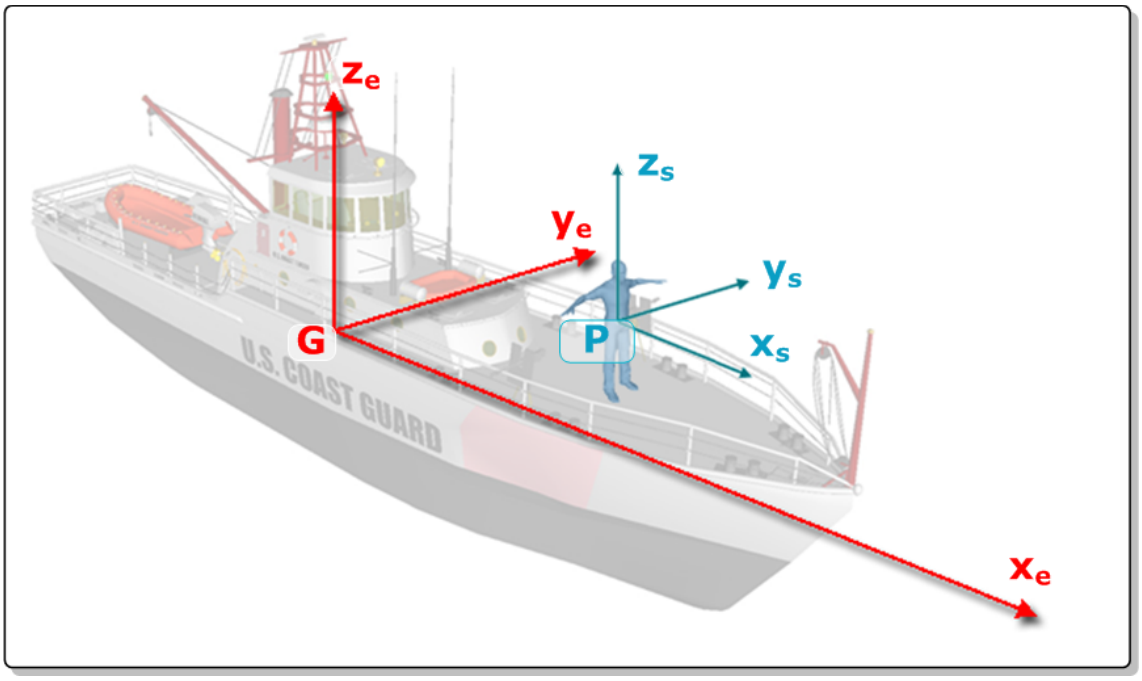

Figure 2.1 – Reference Systems for defining the LFE

The object could be a container, an unsecured helicopter on deck, a crew member, etc.

As derived in Chapter 1, the displacement at the point $P(x^s_{sP}, y^s_{sP}, z^s_{sP})$ on the ship is given by:

$$\boldsymbol{r}^e_{eP} = \boldsymbol{r}^e_{eG} + \Theta_{es} \times \boldsymbol{r}^s_{sP} \tag{2.1}$$

The velocities and accelerations at P are obtained by differentiating equation (2.1) with respect to time:

$$\dot{\boldsymbol{r}}^e_{eP} = \dot{\boldsymbol{r}}^e_{eG} + \dot{\Theta}_{es} \times \boldsymbol{r}^s_{sP} \tag{2.2}$$

$$\ddot{\boldsymbol{r}}^e_{eP} = \ddot{\boldsymbol{r}}^e_{eG} + \ddot{\Theta}_{es} \times \boldsymbol{r}^s_{sP} \tag{2.3}$$

The object of mass m at the point P experiences an inertial force in the equilibrium frame given by:

$$\boldsymbol{F}_{eP}^{e} = -m\left(\ddot{\boldsymbol{r}}_{eP}^{e} + \boldsymbol{g}_{e}^{e}\right) \tag{2.4}$$

where

$$\boldsymbol{g}_{e}^{e} \triangleq \left[0,0,g\right]^{T} \tag{2.5}$$

is the acceleration of gravity vector expressed in the equilibrium frame.

For the development of seakeeping criteria, the forces perpendicular and parallel to the ship deck are more relevant, i.e. the forces in the $\left\{p_s\right\} \equiv P\left(x_s, y_s, z_s\right)$ reference system interest. The coordinate transformation from the equilibrium to the ship-fixed reference system is performed through the rotation matrix $\boldsymbol{R}_{e}^{s}\left(\Theta_{es}\right)$:

$$\boldsymbol{F}_{sP}^{s} = -m\boldsymbol{R}_{e}^{s}\left(\Theta_{es}\right)\left(\ddot{\boldsymbol{r}}_{eP}^{e} + \boldsymbol{g}_{e}^{e}\right) \tag{2.6}$$

where

$$\boldsymbol{R}_{e}^{s}\left(\Theta_{es}\right) = \left[\boldsymbol{R}_{s}^{e}\left(\Theta_{es}\right)\right]^{T} \approx \begin{bmatrix} 1 & \eta_6 & -\eta_5 \\ -\eta_6 & 1 & \eta_4 \\ \eta_5 & -\eta_4 & 1 \end{bmatrix} \tag{2.7}$$

Keeping only the linear terms, we get:

$$\boldsymbol{F}_{sP}^{s} = m\begin{bmatrix} F_{long} \\ F_{lat} \\ F_{v} \end{bmatrix} = m\begin{bmatrix} -\ddot{\eta}_{\boldsymbol{1P}} + g\eta_5 \\ -\ddot{\eta}_{\boldsymbol{2P}} - g\eta_4 \\ -\ddot{\eta}_{\boldsymbol{3P}} - g \end{bmatrix} = m\begin{bmatrix} -\ddot{\eta}_1 + \ddot{\eta}_6 y_{sP}^{s} - \ddot{\eta}_5 z_{sP}^{s} + g\eta_5 \\ -\ddot{\eta}_2 - \ddot{\eta}_6 x_{sP}^{s} + \ddot{\eta}_4 z_{sP}^{s} - g\eta_4 \\ -\ddot{\eta}_3 + \ddot{\eta}_5 x_{sP}^{s} - \ddot{\eta}_4 y_{sP}^{s} - g \end{bmatrix} \tag{2.8}$$

The quantities F_{long} and F_{lat} are the linearized longitudinal and lateral forces per unit mass (accelerations) and are called by Baitis et al. the longitudinal and lateral force estimator. F_v is the linearized vertical force per unit mass.

According to Baitis et al. [Stevens & Parson, 2002], MIIs include three distinct phenomena:

1) *sliding* due to the forces induced by the ship against the frictional forces between movable objects (e.g., the individual's shoes) and the deck;
2) stumbling due to a momentary loss of postural stability (*tipping*);
3) the occasional and potentially the most serious conditions where *lift-off* occurs due to motion forces exceeding the restraining force of gravity.

The most frequent types of MII are usually due to sliding or to loss of balance. These events have a major interest for the sake of safety onboard, since the third type of MII, crewmembers rising on the deck, usually occurs when ship motions become more severe.

Graham ([1990], [1992]) derived simple mathematical models for predicting sliding and losing of balance events (tipping).

2.2.1a SLIDING

For deriving the sliding condition, let us define the *static coefficient of friction* μ_s between the deck and the object under consideration, i.e. the crewmember shoes. Assuming that the forces in the longitudinal direction are small, slides can only occur in the port or starboard directions.

In Table 2.1 the expression for predicting occurrence of sliding in the case of zero longitudinal forces are reported.

Following [Graham et al., 1992], the quantities in equation (2.10) and (2.12) are called *Sliding Estimator Functions*.

The value of μ_s depends on the deck conditions. For dry decks, an empirical value of 0.7 for μ_s is suggested by [Baitis et al., 1984].

Table 2.1 – Port and Starboard Sliding Estimator Functions

SLIDING ESTIMATOR FUNCTIONS $\left(F_{long} = 0\right)$		
Sliding to Port	$F_{lat} > -\mu_s F_v$ $-\ddot{\eta}_{2P} - g\eta_4 - \mu_s \ddot{\eta}_{3P} > \mu_s g$	(2.9)
	$S_p = -\ddot{\eta}_{2P} - g\eta_4 - \mu_s \ddot{\eta}_{3P}$	(2.10)
Sliding to Starboard	$F_{lat} < -\mu_s F_v$ $\ddot{\eta}_{2P} + g\eta_4 - \mu_s \ddot{\eta}_{3P} > \mu_s g$	(2.11)
	$S_s = \ddot{\eta}_{2P} + g\eta_4 - \mu_s \ddot{\eta}_{3P}$	(2.12)

If the ship presents a *steady heel angle* ϕ_m (positive starboard side down), the right hand sides of equations (2.9) and (2.11) should be respectively replaced by:

$$S_p > \mu_s g + \phi_m g \tag{2.13}$$

$$S_p > \mu_s g - \phi_m g \tag{2.14}$$

As it can be observed from expressions (2.13) and (2.14), sliding are more likely to occur in the downward direction.

In the case of non-zero longitudinal forces, a slide will occur in some direction whenever:

$$\sqrt{F_{long}{}^2 + F_{lat}{}^2} > \mu_s F_v \tag{2.15}$$

For case in which the longitudinal acceleration is small compared with the lateral acceleration, it is reasonable to assume that all of the slides will occur near the port and starboard directions. Graham et al. [1991] showed that in this case, the presence of longitudinal acceleration increases the sliding incidence evaluated with (2.10) and (2.12) by about 14%.

For longitudinal acceleration larger than about half the lateral acceleration, the *forward and aft Sliding Estimator Functions* can be defined by [Graham et al., 1991]:

Table 2.2 - Forward and Aft Sliding Estimator Functions

SLIDING ESTIMATOR FUNCTIONS $\left(F_{long} > \left(0.5 \cdot F_{lat}\right)\right)$		
Forward Sliding	$F_{long} > -\mu_s^* F_v$ $-\ddot{\eta}_{1P} + g\eta_5 - \mu_s^* \ddot{\eta}_{3P} > \mu_s^* g$	(2.16)
	$S_f = -\ddot{\eta}_{1P} + g\eta_5 - \mu_s^* \ddot{\eta}_{3P}$	(2.17)
Aft Sliding	$F_{long} < -\mu_s^* F_v$ $\ddot{\eta}_{1P} - g\eta_5 - \mu_s^* \ddot{\eta}_{3P} > \mu_s^* g$	(2.18)
	$S_a = \ddot{\eta}_{1P} - g\eta_5 - \mu_s^* \ddot{\eta}_{3P}$	(2.19)

where a reasonable value for μ_s^* should be:

$$\mu_s^* = 0.886\mu_s \tag{2.20}$$

The authors pointed out that while the method developed for small longitudinal acceleration is accurate, the method developed for comparable longitudinal and lateral accelerations is more approximate [Graham et al., 1991].

2.2.1b TIPPING

To derive the tipping condition another coordinate system will be used (Figure 2.2):

- the $\{p\} = P\left(x_p, y_p, z_p\right)$ coordinate system is a "personnel coordinate system" fixed to the crew member with the origin at the subject's centre of gravity and axes parallel to the principal axes of the person.
  If the person is facing forwards upright with zero lean angle, this coordinate system coincides with the $P\left(x_s, y_s, z_s\right)$ CS.

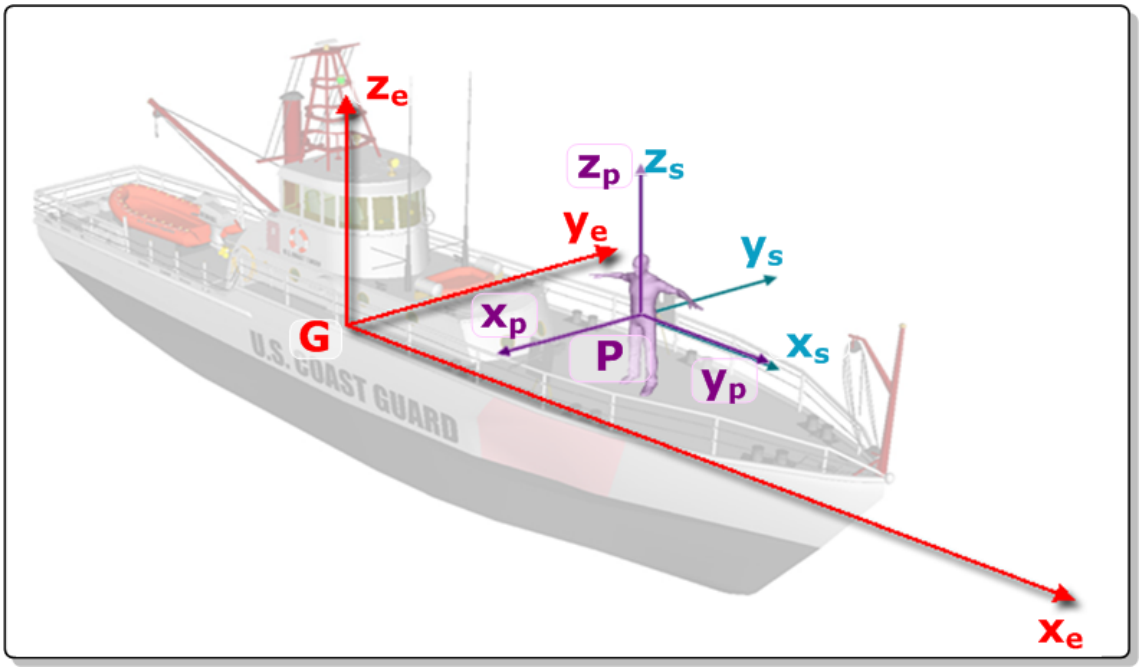

Figure 2.2 – Reference systems for deriving the tipping condition

In the classical model developed by Graham, the person is considered to be a rigid body with the centre of gravity at a height *h* above the deck, the half-stance width equal to *b*, and the half-foot length being *d*. The personnel principle moments of inertia can be approximated by:

$$\left(I_{xx}^{p}, I_{yy}^{p}, I_{zz}^{p}\right) \approx m\left(\frac{h^2}{3}, \frac{h^2}{3}, 0\right) \tag{2.21}$$

A tipping will occur when the moment of the forces parallel to the deck (composed of the lateral and horizontal accelerations) about the person's feet is greater than the moment of the normal forces (composed of the vertical accelerations including gravity).

If the person stands facing towards the stern or the bow and the longitudinal acceleration is assumed to be small, all tips occur in the port or starboard directions.

The forces $\boldsymbol{F}_{sP}^{s}$ acting on the centre of gravity of the person result in destabilizing moment about the feet; e.g. for the left foot LF this moment $\left(\boldsymbol{M}_{p/LF}^{p}\right)^{F}$ is given by:

$$\left(\boldsymbol{M}_{p/LF}^{p}\right)^{F} = -\boldsymbol{r}_{pLF}^{p} \times \boldsymbol{F}_{pP}^{p} = \begin{bmatrix} -mbF_{v} - mhF_{lat} \\ mhF_{long} + mdF_{v} \\ -mdF_{lat} + mbF_{long} \end{bmatrix} \tag{2.22}$$

where

- $\boldsymbol{r}_{pLF}^{p} \triangleq LF\left(x_{pLF}^{p}, y_{pLF}^{p}, z_{pLF}^{p}\right) = (d, b, -h)$ (2.23)

  is the position vector of the person's left foot in the person-fixed CS;

Under the assumptions made, the forces $\boldsymbol{F}_{pP}^{p}$ in the person-fixed CS coincide with forces $\boldsymbol{F}_{sP}^{s}$ expressed in the $P\left(x_{s}, y_{s}, z_{s}\right)$ frame.

In addition, the rotation of the ship induces a moment that in the inertial frame is expressed by:

$$\left(\boldsymbol{M}_{e/LF}^{e}\right)^{I} = -\boldsymbol{I}_{p}^{e}\ddot{\Theta}_{es} \approx -\frac{1}{3}mh^{2}\left(\ddot{\eta}_{4}, \ddot{\eta}_{5}, 0\right) \tag{2.24}$$

where $\boldsymbol{I}_{p}^{e}$ is the person moment of inertia tensor at the centre of gravity

Making the transformation to the personnel reference system and keeping only the linear terms, it results that:

$$\left(\boldsymbol{M}_{p/LF}^{p}\right)^{I} = \boldsymbol{R}_{e}^{s}\left(\Theta_{es}\right)\left(\boldsymbol{M}_{e/LF}^{e}\right)^{I} = -\frac{1}{3}mh^{2}\left(\ddot{\eta}_{4}, \ddot{\eta}_{5}, 0\right) \tag{2.25}$$

The condition for tipping is given by the first component of the total moment about the left foot:

$$\left(\boldsymbol{M}_{p/LF}^{p}\right)_{1} = \left(\boldsymbol{M}_{p/LF}^{p}\right)_{1}^{I} + \left(\boldsymbol{M}_{p/LF}^{p}\right)_{1}^{F} = -\frac{1}{3}mh^{2}\ddot{\eta}_{4} - mbF_{lat} - mhF_{v} \tag{2.26}$$

Table 2.3 reports the expression for tipping events in the transversal directions.

Following [Graham et al., 1992], the quantities in equation (2.28) and (2.30) are called *Tipping Estimator Functions*. The quotient b/h is called the *Lateral Tipping Coefficient*, for which Graham et al. [1992] assumed a representative equal to 0.25.

Table 2.3 – Port and Starboard Tipping Estimator Functions

TIPPING ESTIMATOR FUNCTIONS $\left(F_{long} = 0\right)$		
Tipping to Port	$\left(\boldsymbol{M}^{p}_{p/LF}\right)_1 = -\frac{1}{3}mh^2\ddot{\eta}_4 - mbF_v - mhF_{lat} < 0$ $\frac{1}{3}h\ddot{\eta}_4 - \ddot{\eta}_{\boldsymbol{2P}} - g\eta_4 - \frac{b}{h}\ddot{\eta}_{\boldsymbol{3P}} > \frac{b}{h}g$	(2.27)
	$T_p = \frac{1}{3}h\ddot{\eta}_4 - \ddot{\eta}_{\boldsymbol{2P}} - g\eta_4 - \frac{b}{h}\ddot{\eta}_{\boldsymbol{3P}}$	(2.28)
Tipping to Starboard	$\left(\boldsymbol{M}^{p}_{p/LF}\right)_1 = -\frac{1}{3}mh^2\ddot{\eta}_4 - mbF_v - mhF_{lat} > 0$ $-\frac{1}{3}h\ddot{\eta}_4 + \ddot{\eta}_{\boldsymbol{2P}} + g\eta_4 - \frac{b}{h}\ddot{\eta}_{\boldsymbol{3P}} > \frac{b}{h}g$	(2.29)
	$T_s = -\frac{1}{3}h\ddot{\eta}_4 + \ddot{\eta}_{\boldsymbol{2P}} + g\eta_4 - \frac{b}{h}\ddot{\eta}_{\boldsymbol{3P}}$	(2.30)

In the case of non-negligible longitudinal acceleration, suppose that the resultant force in the plane of the deck is in the direction δ, the resultant moment in the direction $\delta + 90°$; the tipping, if it occurred, would be in the direction δ. The occurrence of a tipping event is restricted in the rectangle defined by the location of the crewmembers' feet. For deriving the expression of the resultant moment, the forces acting on the person must be written in the person-fixed CS rotated by the angle δ with respect to the $P\left(x_s, y_s, z_s\right)$ CS:

$$\begin{aligned} \boldsymbol{F}_{pP}^{p} &= \boldsymbol{R}_{s}^{p}\left(\Theta_{sp}\right)\boldsymbol{F}_{sP}^{s} \\ \left(\boldsymbol{M}_{p/F_\delta}^{p}\right)^{I} &= \boldsymbol{R}_{s}^{p}\left(\Theta_{sp}\right)\left(\boldsymbol{M}_{p/LF}^{p}\right)^{I} \end{aligned} \tag{2.31}$$

where:

- $\boldsymbol{R}_{s}^{p}\left(\Theta_{sp}\right) = \begin{bmatrix} \cos\delta & \sin\delta & 0 \\ -\sin\delta & \cos\delta & 0 \\ 0 & 0 & 1 \end{bmatrix}$ (2.32)

  is the rotation matrix that performs the transformation to the new coordinate system.

The moment acting about the point F_δ can be expressed by:

$$\begin{aligned} &\left(\boldsymbol{M}_{p/F_\delta}^{p}\right)_2 = \left(\boldsymbol{M}_{p/F_\delta}^{p}\right)_2^{I} + \left(\boldsymbol{M}_{p/F_\delta}^{p}\right)_2^{F} = \left(\boldsymbol{r}_{pF_\delta}^{p} \times \boldsymbol{F}_{pP}^{p}\right)_2^{I} + \left(\boldsymbol{M}_{p/F_\delta}^{p}\right)_2^{F} = \\ &= \left(F_{long} - \frac{1}{3}h\ddot{\eta}_5\right)\cos\delta + \left(F_{lat} + \frac{1}{3}h\ddot{\eta}_4\right) + \frac{b(\delta)}{h}F_v \end{aligned} \tag{2.33}$$

where:

- $\boldsymbol{r}_{pF_\delta}^{p} \triangleq F\left(x_{pF_\delta}^{p}, y_{pF_\delta}^{p}, z_{pF_\delta}^{p}\right) = \left(b(\delta), 0, -h\right)$ (2.34)

  is the position vector of the person's foot (about which the tipping would occur) in the person-fixed CS rotated by the angle δ;
- $b(\delta)$ is the half-stance width in the direction δ

The *Forward* and *Aft Tipping Estimator Functions* can be derived considering that $\delta = 0$ in these directions and $d = b(0)$ is the half-foot length (Table 2.4).

The quantity d/h is called the *Longitudinal Tipping Coefficient* and was estimated by [Graham et al., 1992] to be 0.17. Since a person can resist a larger force from the back than from the front, different values for the forward and aft tipping coefficients can be chose.

Comparing the values for both the lateral and longitudinal tipping coefficients with the value defined for μ_s, it can be noted that for dry-deck conditions tipping becomes a problem before sliding.

Baitis et al. [Dobie, 2003] confirmed such hypothesis through simulator experiments. They found that the coefficient of friction for interior and exterior surfaces of a ship is usually larger than either the lateral or longitudinal tipping coefficient. So, tipping MII will usually occur before sliding events.

Table 2.4 – Forward and Aft Tipping Estimator Functions

TIPPING ESTIMATOR FUNCTIONS $\left(F_{long} \neq 0\right)$		
Forward Tipping	$F_{long} - \frac{1}{3}h\ddot{\eta}_5 - \frac{d}{h}\ddot{\eta}_{\mathbf{3P}} > \frac{d}{h}g$	(2.35)
	$T_f = F_{long} - \frac{1}{3}h\ddot{\eta}_5 - \frac{d}{h}\ddot{\eta}_{\mathbf{3P}}$	(2.36)
Aft Tipping	$-F_{long} + \frac{1}{3}h\ddot{\eta}_5 - \frac{d}{h}\ddot{\eta}_{\mathbf{3P}} > \frac{d}{h}g$	(2.37)
	$T_a = -F_{long} + \frac{1}{3}h\ddot{\eta}_5 - \frac{d}{h}\ddot{\eta}_{\mathbf{3P}}$	(2.38)

Finally, for the case of a person facing in an arbitrary direction κ the tipping estimator functions become:

Table 2.5 - General Tipping Estimator Functions

TIPPING ESTIMATOR FUNCTIONS $\left(\text{whatever } \kappa\right)$		
$T_\kappa, T_{\kappa+180^\circ}$	$\left(F_{long} - \frac{1}{3}h\ddot{\eta}_5\right)\cos\kappa + \left(F_{lat} + \frac{1}{3}h\ddot{\eta}_4\right)\sin\kappa - \frac{d}{h}\ddot{\eta}_{\mathbf{3P}} > \frac{d}{h}g$	(2.39)
$T_{\kappa+90^\circ}, T_{\kappa+270^\circ}$	$\left(F_{long} - \frac{1}{3}h\ddot{\eta}_5\right)\cos\left(\kappa+90^\circ\right) + \left(F_{lat} + \frac{1}{3}h\ddot{\eta}_4\right)\sin\left(\kappa+90^\circ\right) - \frac{l}{h}\ddot{\eta}_{\mathbf{3P}} > \frac{l}{h}g$	(2.40)

2.2.2 MIIs ESTIMATION IN THE FREQUENCY DOMAIN

Under the assumption that the sliding and tipping estimator functions followed the Rayleigh distribution, a frequency domain method was derived for predicting the number of MII events per unit time ([Graham, 1990], [Graham et al., 1991], [Graham et al., 1992]).

Let $S_{T_p}(\omega_e)$ be the *Power Spectral Density of the Tipping Port Estimator Function* in equation (2.28) as function of the encounter frequency ω_e; the *spectral moments* of $S_{T_p}(\omega_e)$ are:

$$m_{n_{T_p}} = \int_0^\infty \omega_e{}^n S_{T_p}(\omega_e)\, d\omega_e = \int_0^\infty \omega_e{}^n \left|H_{T_p}(\omega_e, \mu)\right|^2 S_{\zeta\zeta}(\omega_e)\, d\omega_e \tag{2.41}$$

where:

- $H_{T_p}(\omega_e, \mu)$ is the transfer function of the Tipping Port Estimator Function
- $S_{\zeta\zeta}(\omega_e)$ is the wave spectral density.

The number of upcrossings (or downcrossings) per unit time of a threshold at level *t* is then given by:

$$N_{T_p} = \frac{1}{2\pi}\sqrt{\frac{m_2}{m_0}}\exp\left(-\frac{t_{T_p}}{2m_0}\right) \tag{2.42}$$

where:

- N_{T_p} is the number of tipping events per unit time in the port direction
- t_{T_p} is the threshold that, in the specific case, is equal to $(b/h)g$

The total number of MIIs per unit time can be obtained evaluating equation (2.42) for all the estimator functions defined previously and considering the threshold levels summarised in (

Table 2.6).

Table 2.6 – Threshold levels for Sliding and Tipping estimations

THRESHOLD LEVELS FOR MIIs DETECTION			
Sliding to Port/Starboard	Sliding to Forward/Aft	Tipping to Port/Starboard	Tipping to Forward/Aft
$t_{S_{p/s}} = \mu_s g$	$t_{S_{f/a}} = 0.886\mu_s g$	$t_{T_{p/s}} = (b/h)g$	$t_{T_{f/a}} = (d/h)g$

2.2.3 MII AS OPERABILITY CRITERION

Before the development of the MII theory, limiting criteria for personnel operations on deck were expressed in terms of Root Mean Square (RMS) roll or pitch limits or by limitation on vertical and lateral accelerations [Graham, 1990]. Typically, a RMS roll angle of four degrees was employed. It should be noted that it is not the inclination of the deck per se that constitutes a problem, but rather the combination of deck inclination with lateral and vertical accelerations. Moreover, if one of the limits is exceeded, the entire system has to be considered inoperable.

The MII model incorporates roll, pitch and accelerations, and a limit on the numbers of MIIs that can be tolerated is a good indicator for personnel performance onboard.

Graham [1990] defined risk levels based on the number of MIIs per minute (Table 2.7).

Table 2.7 – MII Risk Level

RISK LEVEL	MIIs PER MINUTE
1. Possible	0.1
2. Probable	0.5
3. Serious	1.5
4. Severe	3.0
5. Extreme	5.0

These risk levels were derived for the initial hook-up of the helicopter message line to the arresting system on the desk. This task is considered to be hazardous for crew safety due to the balance problems induced by the moving and slippery deck, the wind, etc.

The criterion adopted by NATO STANAG 4154 is one MII per minute, being regarded as a reasonable level of risk for many onboard tasks.

2.3 DEVELOPMENTS IN MII MODELLING

The MII model proposed by Graham significantly simplifies the complexity of human body and postural stability mechanisms, modelling the person as a passive rigid body unable to counteract the external stimuli. Despite this extreme simplification and due its flexibility, such a model has become widely used as part of ship design tools. The predicted incidence of loss of balance events is useful to assess the effect of motion on people onboard and, for instance, to compare different designs from the personnel performance point of view. However, several studies ([Boccadamo, 1999], [Crossland & Rich, 1998], [Wedge & Langlois, 2003]) have shown that the MII model by Graham tends to overestimate the number of MII occurrences.

Modelling human postural stability onboard and developing a more realistic MII model is a challenging task as it involves complex mechanisms related to human cognition and personnel experience.

As reported in [Dobie, 2003], Baitis et al. noted that subjects apply different techniques for maintaining the equilibrium stance. Moreover, a significant variability in propensity to experience MIIs among people has been proved by Langlois et al. [2009]. Experimental studies by [McCauley & Pierce, 2008] have suggested that a long term adaptation (on the order of months or years) to mild ship motion can explain the differences in MIIs occurrence between civilians, and skilled and adapted crewmembers. However, beyond

certain levels of motion severity, even individuals that have already gained "sea legs" will experience a higher incidence of MII events.

The occurrence of MII depends on the ship location and on the type of tasks to be performed. Indeed, the values of acceleration onboard differ depending on the distance from the centre of gravity. Moreover, the acceptable number of MIIs would vary according to the allotted task. For instance, a crewmember employed in a watchkeeping can tolerate a higher number of MIIs events than a person engaged in manual lifting.

Starting from the model developed by Graham, the researches on the effects of ship motion on human balance have followed two main directions. Efforts have been made, on the one hand, to improve the estimates of MII incidence, keeping the simplicity of the Graham model and developing empirical tipping coefficients that consider different deck motions, accelerations, and shipboard tasks.

On the other hand, attempts have been devoted to develop, calibrate and validate more complex and realistic models for human body and postural control.

2.3.1 EMPIRICAL METHODS FOR DERIVING MII CRITERIA

Several simulator and onboard tests have been conducted to experimentally determine tipping coefficients for improving the prediction of MIIs occurrence.

Crossland & Rich [1998] performed experiments with the Large Motion Simulator (LMS) at DERA Bedford, UK. These tests were conducted to investigate the effects of ship motion on the postural stability of Royal Navy personnel and to provide data for validating the proposed model.

Sailors were asked to execute simple shipboard tasks (standing facing aft and athwartships, weapon loading, etc.) and empirical tipping coefficients were derived for each task.

The lower the tipping coefficient the harder the task is to perform. The empirical tipping coefficients were found to be greater than equivalent theoretical values, suggesting that the person can withstand the motion

better than the model would predict. This means that the empirical tipping coefficients improve the predictions of MII incidence. It was also noted that the tipping coefficients significantly differ depending on the direction considered, i.e. varies from the side to side versus the front to back direction.

For general seakeeping assessment purposes, since people tend to adopt the most resistant stance by standing sideways to the predominant motions, the authors advised to consider only the transverse tipping. In more complex shipboard task scenarios or if the person is constrained to adopt a specific stance, a weighted tipping coefficient was recommended.

In [Crossland et al.,2007] results from experiments on postural stability during task performance (standing facing aft and athwartships, weapon loading, fire fighting, etc.) onboard a fully instrumented vessel were presented.

Longitudinal and lateral tipping coefficients were calculated as continuous time histories directly from the ship motion data. The obtained average tipping coefficients compared well with those previously obtained by [Crossland & Rich, 1998] as it was expected, being the motion frequencies similar for the full-scale trials and the simulator studies. The differences found were attributed to the subject differences.

In addition, the length of time it takes to recuperate from an MII was valued. The number of MII events per minute $\left(MII_{RATE}\right)$ together with the interval of time for recovering from them $\left(D_{MII}\right)$ enable the derivation of task effectiveness $\left(E_{TASK}\right)$ by relationship (2.43):

$$E_{TASK} = 1 - \frac{MII_{RATE} D_{MII}}{60} \tag{2.43}$$

If the condition

$$\left(MII_{RATE} D_{MII} / 60\right) \geq 1 \Rightarrow E_{TASK} = 0 \tag{2.44}$$

is verified, the task will not be completed.

Analogously, given an acceptable level of task effectiveness, an MII criterion can be derived from:

$$MII_{CRIT} = \left(\frac{1 - E_{TASK}}{D_{MII}} \right) 60 \tag{2.45}$$

2.3.2 CONTROL MODEL FOR POSTURAL STABILITY ONBOARD

During the early years of 2000, Boccadamo et al. ([1999], [2003]) conducted, in cooperation with Occupational Medicine Scientists, a survey aiming to assess the effect of ship motions on working conditions and postural behaviour onboard fishing boats. Accidents occurred to Italian (Campania region) fishermen were analysed. For dangerous tasks performed by crewmember on deck, levels of risk were defined. The study pointed out that sliding was the most frequent event that made unsafe the activities onboard. It was also highlighted that, onboard small vessels, ship motions heavily affect human performance and produce serious accidents.

The authors noted that the Graham model was not suitable for predicting the MIIs incidence when the frequency of ship motions is high, such as onboard small fishing vessels. They proposed a "*dynamic model*" able to control the upright stance.

The human body was modelled as a simple inverted pendulum, with damping and restoring characteristics of an average man; the control mechanism for assuring the vertical equilibrium was implemented as a classical Proportional-Integral-Derivative (PID) controller (Figure 2.3).

The "*human-like*" system reacts to the total moment due to ship motions with an angle γ, that is the angle by which the pendulum tilts to withstand the external disturbances.

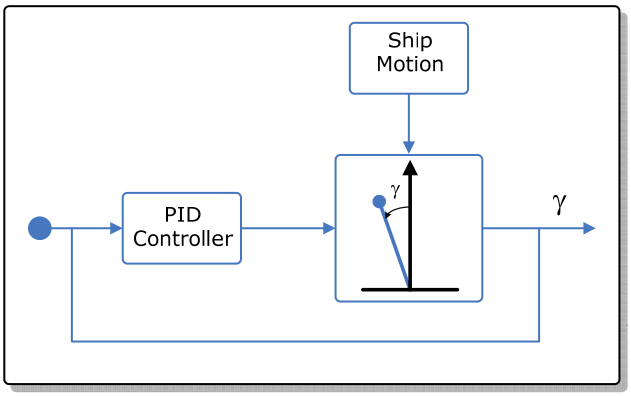

Figure 2.3 – Control model for postural stability onboard by Boccadamo

The controller gains were selected so that the developed controlling torque at the ankle joint was in phase opposition with the destabilising moment. This would correspond to a person that shifts his weight to counteract an external stimulus and stay upright.

For a crewmember facing forward, the tipping conditions were modified to take into account the proposed model formulation as following.

$$T_p^B = T_p - \gamma g \tag{2.46}$$

$$T_s^B = T_s + \gamma g \tag{2.47}$$

where:

- T_p^B and T_s^B are the Port and Starboard Tipping Coefficients according to Boccadamo, respectively;
- γ is the leaning angle of the inverted pendulum.

For validating the proposed model and defining a proper seakeeping criterion for fishing activities onboard (in terms of frequency of MIIs events), a questionnaire survey was conducted among Italian fishermen [Boccadamo & Scamardella, 2003] (see section 1.5.1a).

According to the subjects interviewed, one MII event per minute was a safe limit for operations on deck. The significant wave heights at which fishing tasks became hazardous were then determined with respect to the ships' length. For each vessel, the MII occurrence was calculated according to the classical model by Graham and the dynamic model by Boccadamo. Both of

the methods estimated a high number of MIIs and, then, a threshold value not fitting in the MII limit assessed by fishermen.

The standard deviation of the MII threshold (maximum number of MII events) calculated by using the model by Boccadamo was smaller than the standard deviation obtained from the Graham model. Moreover, the method by Boccadamo provided an MII limiting value lower (by the 50%) than the MII limit from the method by Graham.

Careful assessment of the controller gains was necessary to improve the accuracy of the proposed dynamic model in predicting MII incidence.

2.3.3 ARTICULATED POSTURAL STABILITY MODEL

Articulated dynamic modelling of humans has been introduced in the naval sector by Langlois and his group ([Langlois, 2010], [Langlois et al., 2009], [Wedge & Langlois, 2003]), whose researches were conducted in conjunction with the ACBD working group.

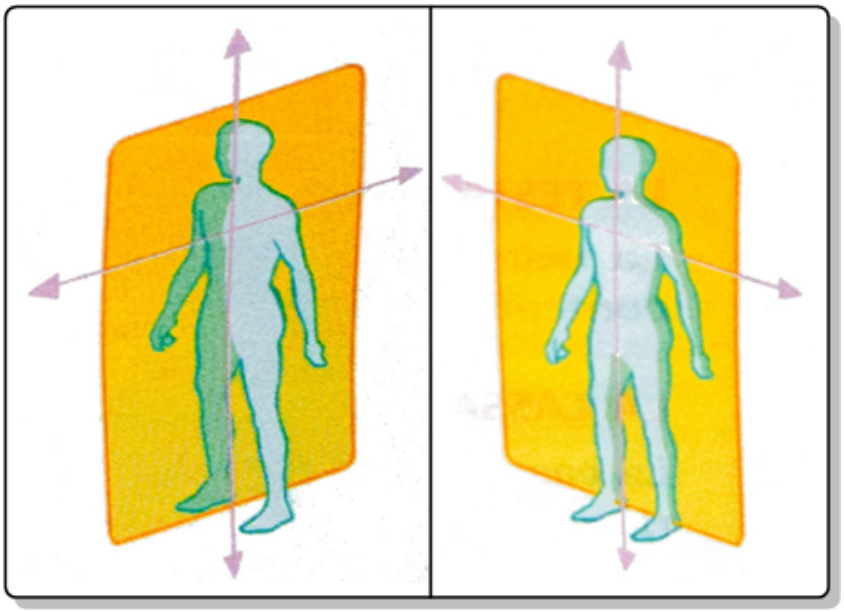

Figure 2.4 – Human body planes.
Left: Sagittal Plane. Right: Coronal Plane

In [Wedge & Langlois, 2003], two planar models were proposed for predicting MII frequency as a function of ship operating conditions. The idea comes from models used for human quiet standing, which generally divide human body into two perpendicular planes: the sagittal (Figure 2.4 left) and the coronal planes (Figure 2.4 right).

The median sagittal plane cuts the body into left and right halves passing through the centreline (a bilateral symmetry is assumed); within this plane, the model moves in the front/anterior and back/posterior (A/P) direction.

The mid-coronal or frontal plane bisects the body into front-back or anterior-posterior sections. In this plane, the body moves in the left-right or medio-lateral (M/L) direction.

In the sagittal plane, the model proposed by Wedge & Langlois [2003] is an inverted pendulum, with revolute joints at the ankles that allow motion in the A/P direction (Figure 2.5 left).

In the frontal plane, the human body was represented by a four-bar linkage, where the four links are the torso (included the trunk, arms, and head), the right and left legs, and the ground. Both ankles and hips are rotational joints permitting movements in the M/L direction (Figure 2.5 right).

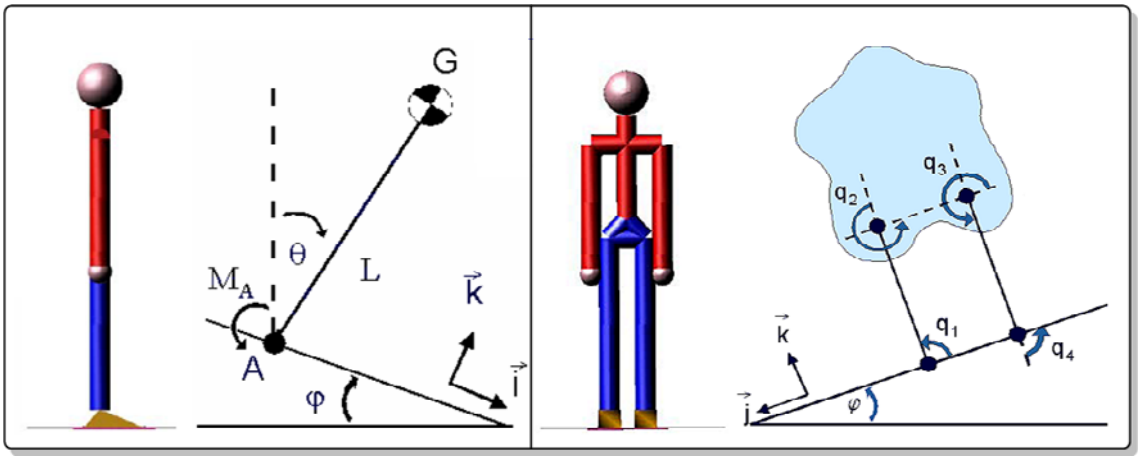

Figure 2.5 – Articulated model by Wedge and Langlois [2003].
Left: Inverted pendulum. Right: Four-bar linkage

The articulated models were based on realistic average human geometry, physical and inertial properties.

Derived the governing dynamic equations for the two models, a control methodology was designed to maintain the vertical orientation by actively controlling ankle torque. Both the models were put in the Single-Input-Single-Output (SISO) form, that is a system with one input, the controlling variable (e.g., the ankle torque), and one output, the controlled variable (e.g., one ankle angle). A simple linear controller was developed using the pole placement approach to design the controller gains.

The models were tuned and validated using experimental data from the US Naval Biodynamics Laboratory (NBDL). Acceptable results in terms of MII incidence prediction were obtained for the conditions for which the models were tuned; in different conditions, generally an over-prediction was observed.

The postural stability model in the sagittal plane (i.e., the dynamic inverted pendulum) was tuned based on sea trials, sponsored by Defence Research and Development Canada, onboard a research vessel [Langlois et al., 2009]. The controller gains were selected so that the MII occasions predicted by the model could closely match with the number and agree in time with the observed events during the trials. Inputs to the dynamic models included the time histories of deck motion, while the generated interface forces and moments, between the revolute joint (i.e., the ankle) and the deck, were used to derive postural stability indices.

Recognised that MIIs occur from either sliding or tipping, a composite index was defined as:

$$C_c = \frac{C_S + C_T}{2} = \left| \frac{\frac{F_y}{\mu} + \frac{M_x}{d}}{2F_z} \right| = \left| \frac{dF_y + \mu M_x}{2\mu d F_z} \right| > 1 \qquad (2.48)$$

where:

- $C_S = \left| \frac{F_y}{\mu_s F_z} \right|$ (2.49)

  is the sliding index;

- $C_T = \left| \frac{M_x}{dF_z} \right|$ (2.50)

  is the tipping index;

- F_y is the interface force component in the direction parallel to the deck;
- F_z is the interface force component in the direction normal to the deck;
- M_x is the restoring moment actuated by the subject's ankle joints;
- μ_s is the friction coefficient;
- d is the distance between the subject's ankle joint and toes.

An MII is expected whenever the inequality (2.48) is satisfied.

The single-segment single-degree-of-freedom planar inverted pendulum was extended into a more complex spatial inverted pendulum [Langlois, 2010]. This new proposal combines the previous distinct models (Figure 2.5) that divided postural stability into two separate planes. The spatial inverted pendulum consists in a single segment, whose motion is not limited in the antero/posterior direction: movements in three dimensions are allowed. The model could be improved by including additional articulated segments for simulating complex tasks (e.g., manual materials handling activities).

The ideas at basis of the model were several. The spatial pendulum would have to be suitable for predicting MII events at arbitrary shipboard locations, easily expandable, and able to "turn into" the simple rigid body model (e.g., locking articulation joints).

The spatial model was verified and validated against planar results obtained in [Langlois et al., 2009], and the procedure for adding segments and multi-degree-of-freedom was sketched out. It should be emphasized that expanding the model complexity would increase the challenges associated with defining appropriate control strategy and model parameters. Moreover, without validation against additional dataset, the proposed articulated postural stability models are limited for the conditions in which the models were tuned.

2.4 DISCRIMANT INDEX FOR ASSESSING THE POSTURAL STABILITY BOUNDARY ONBOARD

At the same time as the studies conducted by Baitis et al., Japanese researchers [Kimura et al., 1988] proposed to assess stability and safety boundaries for fishermen operating in oscillatory environment employing a statistical empirical index.

They conducted a survey on man-overboard and injury accidents occurred on Japanese fishermen, and estimated that the most important factor causing onboard accidents was ship oscillatory motions. Analysing the time-histories of the acceleration of human centre of gravity and of the ship motions, the authors found linear relationship between the two variables.

Experiments onboard were performed. The accelerations of the ship deck and experienced by crewmembers were measured by accelerometers; a force-plate was used to collect data of the person centre of gravity movements. A discriminate analysis was performed and the following linear function was proposed:

$$T = m_{1_{x_s}} + 0.166 m_{1_{y_s}} + 0.113 m_{1_{z_s}} < 0.220 \tag{2.51}$$

where:

- T is the discriminant score found to be equal to 0.22;
- $m_{1_{x_s}}, m_{1_{y_s}}, m_{1_{z_s}}$ are the first spectrum moment of the ship accelerations in the ship-fixed coordinate system.

A value of T greater than 0.22 would mean that the subject was not stable on the ship deck.

The method proposed by Kimura is attractive due to its simple expression; the formulated criterion could be useful to assess the effect of ship motion on postural stability in a straightforward way. Nevertheless, the use of force plates to derive the movements of a person's centre of gravity arouses some doubts. Force platforms measure human ground reaction force and the location of the centre of pressure; optical systems are used to quantify the subject's centre of gravity displacements [Winter, 2005].

Chapter 3: Human Postural Stability

3.1 INTRODUCTION

Human postural control is an interdisciplinary problem, involved different sciences and disciplines (orthopaedic and rehabilitation surgeries, kinesiology and biomechanics, prosthetics and orthotics, etc.). The extensive interest into human balance topic emerges from numerous papers and publications in which the ultimate goal is to identify the mechanisms beyond the maintenance of upright stance. Several models, aiming to cope with the high complexity of the processes involved (multi-segments dynamics, multisensory integration, cognition, etc.), have been proposed.

In field such as human postural control, models can help in analyzing and explaining data obtained from experiments performed on personnel on both fixed and motion platforms, or can be used for designing new experiments [Mahboobin, 2007]. Computational models also allow a systematic manipulation of relevant parameters that can be fine-tuned using experimental data.

Modelling and simulating human body, postural control mechanisms and motions involves aspects such as enhancement of ergonomics and occupational efficiency, effectiveness and safety [Qu, 2008]. Extensive work has been conducted for occupational activities, in particular as far as task and product design is concerned. Control models and motion simulations may be very helpful to understand and prevent occupational incidents, such as falls and low-back pain (LBP) that are very common and costly occupational injuries in motion [Duncan, 2007] as well as in still environment [Qu, 2008].

Qu [2008] gives the major reasons underlying the values of human balance control models and simulation. Models may predict human physiological reactions, motion strategies and biomechanics used in maintaining balance. They can also simulate the changes in such strategies and responses among people characterised by different gender, age, balance disorders, or employed in several tasks and in diverse environments. This may be a useful tool in developing strategies for the improvement of balance and global safety, as well can help to better understand human postural balance avoiding the need for executing actual tests.

Biological research uses dynamic models to formalize and simulate proposed human postural control system and these models may well serve as "blueprints" for designing equilibrium control system for biped robots [Mergner et al., 2006]. Mergner and his group [PostuRob, Website] has implemented biological models into a biped robot, applying a new biorobotics method, the so-called "*Hardware-In-the-Loop (HIL) simulation*". In this approach, only the control mechanism under consideration is implemented as a software model, while all other components (body parts) remain hardware. Both medicine research and bionics could take advance, replacing the human body by a humanoid robot whose "*brain*" (embedded PC) contains a software model for human stance control. On one hand, the researchers show that equilibrium control principles of human upright stance, derived from biological studies, can successfully be implemented in the equilibrium control of biped humanoid robots. On the other, the proposed approach allows to explore into human sensorimotor control functions and to understand the malfunctions causing sensorimotor deficits. This would also help to design and construct neural prostheses and orthoses, that can be directly included as parts of the robot and *HIL* system.

This chapter is organised into four main sections.

In the first part, physiological concepts relevant for human postural stability are introduced (section 3.2).

Then, the models for representing human body are described (section 3.3).

The third section explains the main neurological aspects of human postural control (section 3.4). Control models, proposed in literature and interesting for the present work, are reviewed (section 3.5). Finally (section 3.6),

experimental methods now used for identifying and validating human balance model are briefly discussed.

3.2 HUMAN POSTURAL STABILITY: PHYSIOLOGICAL FEATURES

The terms "equilibrium", "postural stability" and "postural control" are used as synonyms for balance control [Punakallio, 2005].

Balance is an integral component of almost all daily activities, which require continuous changes in stability and orientation mechanisms. The unceasing modifications in postural strategies are highly related to the force, velocity and magnitude characterising the task that has to be executed.

According to Shumway-Cook and Woollacott (Figure 3.1), balance control is the result of the interaction among the individual (body segments), the task-related factors and environmental conditions [Punakallio, 2005].

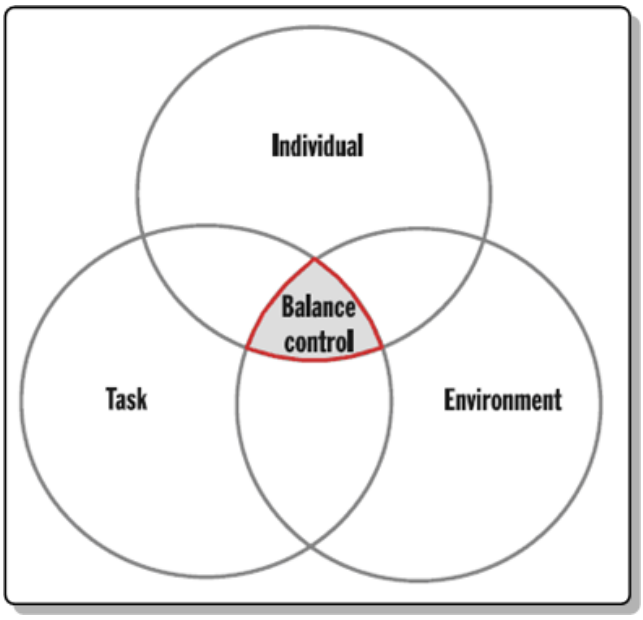

Figure 3.1 - Conceptual model for balance control defined by Shumway-Cook and Woollacott (after [Punakallio, 2005])

The word p*osture* describes the orientation of a body relative to the gravitational vector; it is an angular measure from the vertical [Winter, 1995].

The spatial orientation of human body is described according to a coordinate system that identifies the following three plane (Figure 3.2):

- the *transverse* (also known as *axial* or *horizontal*) *plane*, parallel to the ground, which separates the superior (the head) from the inferior part (the feet) of the body;
- the *mid-coronal* (also referred to as *medial/lateral* or *frontal*) *plane*, perpendicular to the ground, which divides the body into antero/posterior, front/back or ventral/dorsal parts;.
- the *sagittal plane*, perpendicular to the ground, which bisects the body into left and right halves. The *median sagittal plane* is the specific sagittal plane that passes through the middle of the body; it is the plane of symmetry for a person.

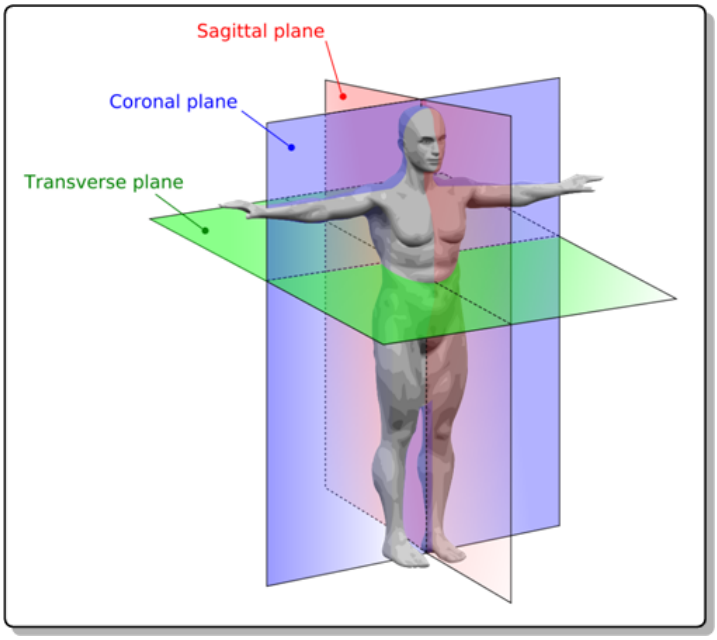

Figure 3.2 - Anatomical planes in a human [Wikipedia, Anatomical terms of location]

The dynamics of body posture allows to avoid falling and to preserve balance, which is related to the inertial forces acting on the body.

A person is said to be stable or in a stable posture as long as the line of action of the person's weight vector passes through (within) his or her base

of support. In other words, postural stability is the ability to maintain the *Centre of Mass* – CoM (or *Centre of Gravity* – CoG)[1] position and its displacements within the *Base of Support* – BoS, identified by the position of the feet in both antero/posterior and lateral directions.

Experiments have demonstrated that, during upright stance, the CoM is not fixed, but it moves away from its equilibrium position. This condition is inherently unstable and results from the action of the gravitational component, that makes the CoM to accelerate away from the erect position. In order to maintain the equilibrium, the CoM has to be kept inside the BoS and a restoring moment has to be developed to counteract the destabilising force of gravity. The *Centre of Pressure* – CoP correspondes to neuromuscular reaction produced for controlling the CoM locus [Valles et al., 2006]. The CoP is the active controlling variable, while the CoM is the passive controlled variable.

The Base of Support, or *supporting area*, represents the possible range of the CoP, which is defined as the origin of the ground reaction vector [Hof et al., 2005]. This point is the weighted average of all the pressures over the feet's surface in contact with the ground, and it is independent of the CoM [Winter, 1995].

Figure 3.3 shows a seven-second record of simultaneous CoM and CoP fluctuation for a subject in quiet standing. CoP oscillates from side to side of the CoM with a higher frequency and greater amplitude.

If one foot is on the ground, the net CoP is located within this foot. If both feet are in contact with the ground, there are two different CoPs under each foot. The net CoP lies in a position between the two feet, depending of the weight that rests on each foot.

[1] The term *Centre of Mass* has a more general meaning, while the *Centre of Gravity* refers to the centre of mass in one axis only, defined by the direction of gravity [Winter, 2005].

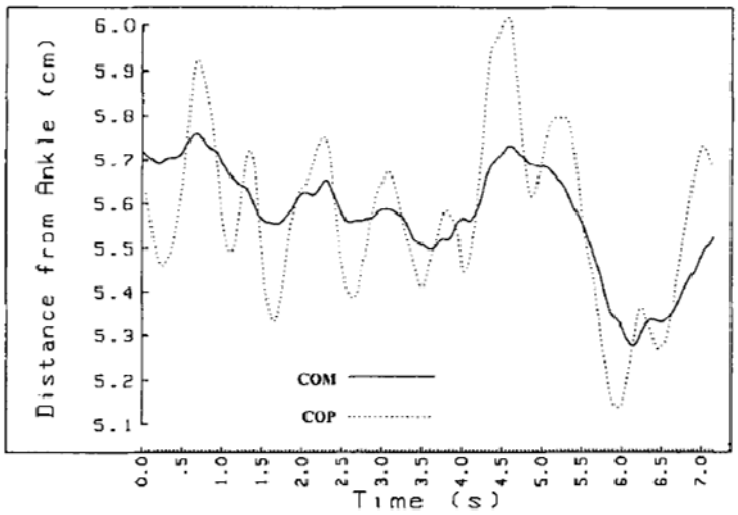

Figure 3.3 – CoP and CoM displacements [Winter, 1995]

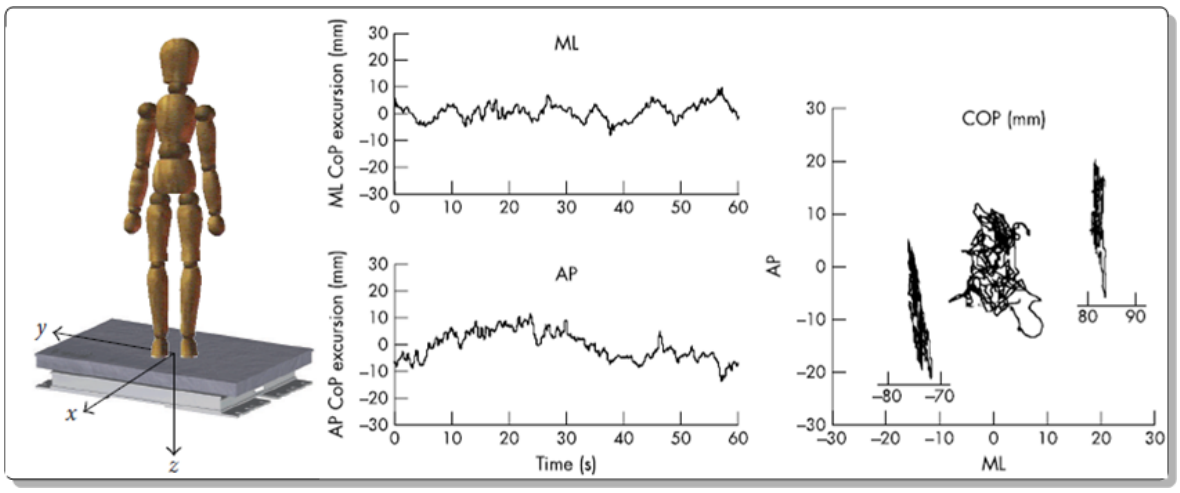

Figure 3.4 – Left: Centre of foot pressure (CoP) trajectory of a representative subject on force plate (after [Amoud et al., 2008]). Centre: Monodimensional time series in Medio/Lateral and Antero/Posterior directions, obtained from total body CoP. Right: Bidimensional displacement of CoP sway in the horizontal plane of each single foot and of the total body (centre) (after [Rocchi et al., 2002])

Figure 3.4 shows displacements of CoP recorded separately from left and right feet during quiet standing in the side-by-side position. COPnet is calculated as a weighted average of COPl and COPr. It appears that the

average of COPl and COPr would result in an A/P movement of the COPnet but negligible M/L displacement.

The Limits of Stability (LoF) define how far a person is able to lean in any direction without changing its base of support. Spirduso et al. [2005] report that adults able to align their CoM directly above their BoS during quiet standing may sway 12° in a forward and backward direction and 16° laterally before requiring to take a step.

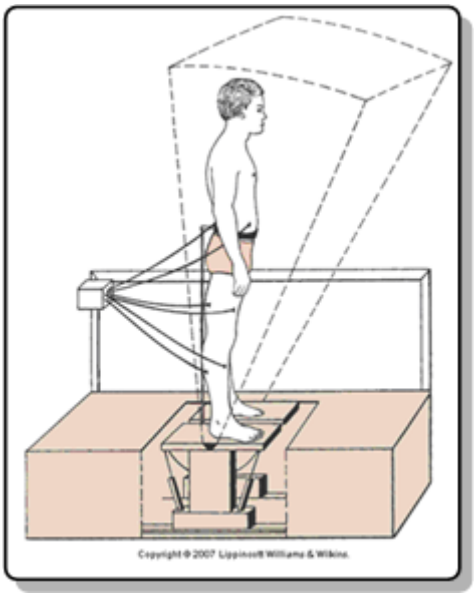

Figure 3.5 – Cone of Stability (after [McKeough, 2010])

As drawn in Figure 3.5, the cone of stability is not symmetric with respect to the antero/posterior direction, but the LoS are greater for a leaning angle in the forward sense.

Biomechanics researches have revealed that at least three distinct postural control strategies are commonly employed, either consciously or subconsciously, for maintaining postural stability. These strategies are referred to as the ankle, hip, and step strategies (Figure 3.6).

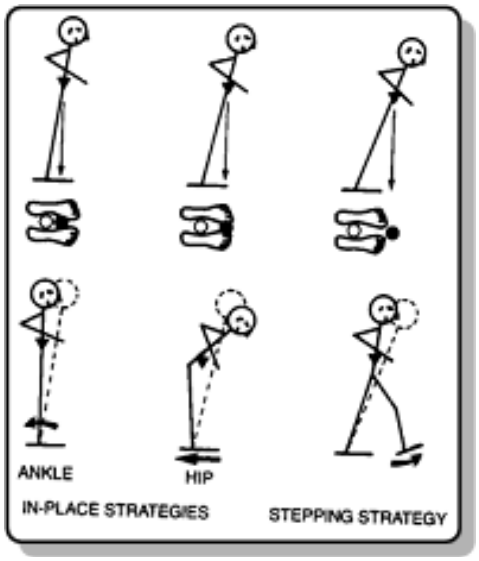

Figure 3.6 – Human postural stability strategies depend on the CoM position relative to the BoS or LoS (after [McKeough, 2010])

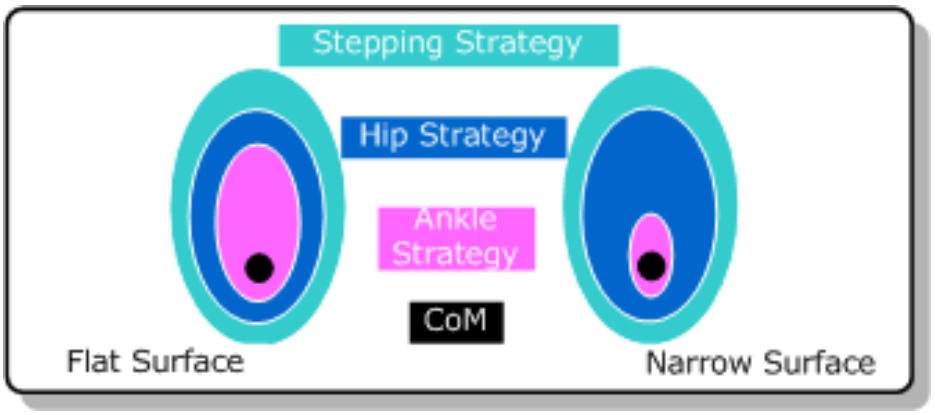

Figure 3.7 – Human postural stability strategies in relation to support surface (after [McKeough, 2010])

Many factors affect the choice of postural sway strategy:

- kind and motion of supporting surface (Figure 3.7),
- stability of external environment,
- age (elderly people are more subject to falling then young individuals),
- type of the executing task, that can produce fatigue or stress,
- individual characteristics, such as obesity,
- injuries and deficits of postural system (diseases of the neuromuscular system or sense organs).

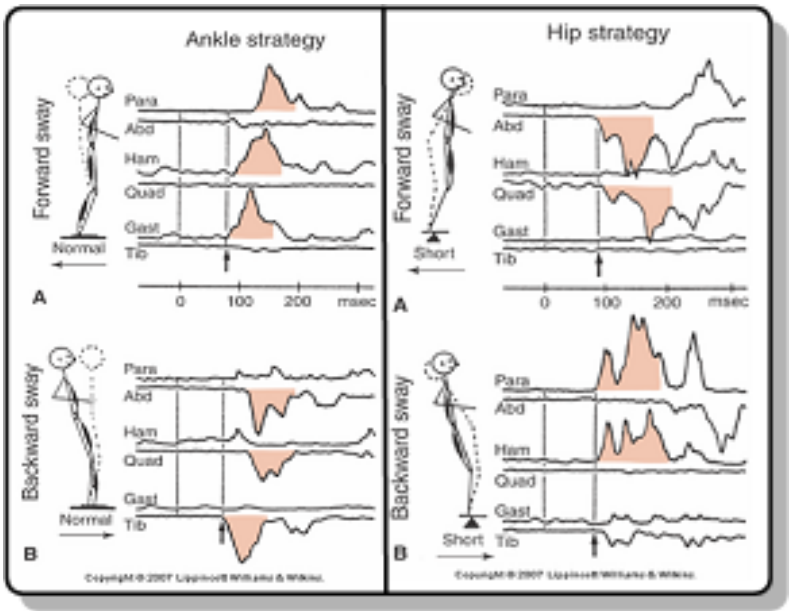

Figure 3.8 – Active muscles during ankle (left) and hip (right) strategies (after [McKeough, 2010])

In the case of ankle strategy (Figure 3.8 left), the body moves as a single link with "frozen" muscles about the ankle joint. The upper and lower parts of the body move in the same direction, namely are in phase. The force that can be generated by the muscles involved in such a strategy is relatively small, so the ankle strategy is mainly used to control upright stance in quiet standing on a flat and broad surface (a sufficient force to restore balance can be generated pushing against the surface), and with small and low external perturbations.

In more perturbed situations (i.e., the movement of the base of support is large, fast, nearing the limit of stability) or when the ankle muscles cannot act efficiently (e.g., the surface is too narrow or unstable to allow an opposing pressure), the hip strategy is activated (Figure 3.9 right).

Because of the small width of the foot, the maximum moment that could be generated by the ankle muscles would be about 10Nm. A destabilising torque above this limit would cause the foot to roll over on its lateral borders. On the contrary, each of the hip groups could generate in excess of 100 Nm in emergencies [Winter, 1995].

The postural sway control is achieved by the muscles of the hip, pelvis and trunk, moving the upper and lower parts of the body in opposite directions (out of phase).

When either the CoM displacement has exceed the original BoS or the individual's maximum LoS, or when the external perturbations have been so high that the hip strategy was not sufficient to avoid a fall, a person responds actuating the step strategy. One or more steps are taken for attempting to establish a new base of support and preserve stability. However, as reported in [Spirduso et al., 2005], for individual not constrained to maintain feet in place but free to respond naturally, stepping appears to be the preferred strategy, even when the external disturbances are small, and occurs before the LoS have actually been exceeded.

As reported in [Krell et al., 1998] and [Spirduso et al., 2005], several experiments have demonstrated that, in a standing position under different platform conditions, various combinations of the discussed balance strategies may be used in conjunction to maintain the upright stance.

During quiet standing, the most common stance is with the feet in a side-by-side position [Winter, 1995]. In perturbed conditions, people free to adopt the most resistant stance tend to stay sideways to the predominant motions [Crossland & Rich, 1998]. Moreover, the wider the stance, the smaller active and the larger passive mechanisms required for controlling the posture [Henry et al., 2001].

Human balance control can be studied considered two different scenarios:

- *unperturbed* or *Quiet Standing* (QS), that is the classical biomechanics problem [Winter, 1995];
- *Perturbed* or *dynamic Standing* (PS), where the mechanisms employed for facing external disturbances (e.g., motion platform) are examined;

Usually, researches employing the PS method aim to isolate recovering strategies, identify the role of individual systems involved in stability mechanisms, and recognise deficits and disorders of the postural system [Winter, 1995]. Dynamic tests are also oriented to measure a person's ability

to maintain balance while walking or performing tasks and actions of daily activities and work [Punakallio, 2005].

Perturbations to the systems can be either internal or external.

Internal disturbances, or self-perturbed stance, result from voluntary movement of the body (such as raising the arms or bending the trunk), closing eyes, changing in base of support (e.g. wide-base stance, tandem stance[2], or one-leg stance). Since in this case the individual response is proactive[3], the anticipatory behaviour of the equilibrium control system can be studied [Winter, 1995].

External perturbations are applied without the knowledge of the subject and have the goal of testing the reactive response of the control systems. A wide variety of perturbation methods are in use:

- movable (tilting and translating) platforms ([Maurer et al, 2006], [Mergner et al., 2005], [Peterka, 2002], [Schweigart & Mergner, 2007]),
- push and pull force stimuli ([Maurer et al, 2006], [Cnyrim et al., 2009]),
- changes in surrounding environment ([Mergner et al., 2005], [Peterka, 2002]).

Applying this method allows to identify different mechanisms, strategies and the role of each part of the system required for controlling the stance.

Even if the musculoskeletal structure involved in regulating posture in quiet and dynamic conditions is the same, mechanisms and strategies for balance control may differ. For example, during quiet standing balance is usually controlled by the ankle strategy, whereas ankle muscle activity alone is not sufficient to maintain balance in presence of large and fast platform movements.

Furthermore, in quiet or static standing condition the CoP is maintained as fixed as possible, while the body sways back and forth pivoting about the ankle. As far as dynamic standing is concerned, the CoP moves actively while

[2] A tandem stance is characterised by standing with one foot ahead the other.

[3] Acting in advance to deal with an expected difficulty [thefreedictionary.com, Proactive].

standing, walking or different tasks of daily activities are performed [Punakallio, 2005].

3.3 BIOMECHANICAL MODELS

Biomechanical models of balance are useful for understanding the mechanisms of postural control.

3.3.1 MODELLING HUMAN BODY IN THE SAGITTAL PLANE: THE INVERTED PENDULUM BODY MODEL

Many existing balance models have focused on investigating postural equilibrium in the sagittal plane, where the postural sway is described in the antero/posterior direction ([Maurer & Peterka, 2005], [Mergner, 2004], [Peterka & Loughlin, 2004], [Schweigart & Mergner, 2008], [van der Kooij et al., 2005], [Winter, 1995], [Winter et al., 1996]).

In this framework, the simplest representation of human body is the single-segment *inverted pendulum* model, whose motion is limited to a single plane. It is assumed that the human-body/inverted-pendulum responds adopting an "ankle joint strategy" for balance recovery, namely only the ankle control torque is developed for controlling the upright stance.

The inverted pendulum is a suitable model for embodying the intrinsic instability of human posture, with most of the body's mass concentrated above the pivot point.

The relationship between the CoM and CoP can help in explaining and understanding the validity of the inverted pendulum as model for human balance.

In Figure 3.9 a subject swaying in the antero/posterior direction while standing quietly is shown. Five different instants of time are drawn, in which the changing relative position between the CoP (the controlling variable) and the CoM (the controlled variable) are illustrated.

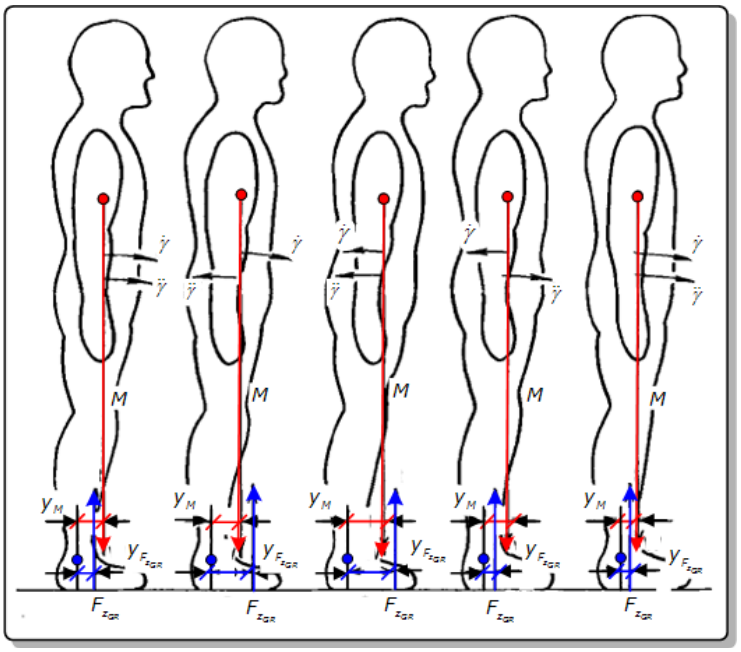

Figure 3.9 - A subject swaying back and forth while standing quietly on a force platform (after [Winter, 1995])

The following quantities are recognisable in the figure:

- $\dot{\gamma}$ is the CoM angular velocity
- $\ddot{\gamma}$ is the CoM angular acceleration
- $M = mg$ is the body weight
- y_M is the distance of the body weight from the ankle joint
- $F_{z_{GR}}$ is the vertical ground reaction force.
- $y_{F_{z_{GR}}}$ is the distance of the vertical reaction force from the ankle joint

When the CoM is ahead of the CoP, a clockwise moment is present at the ankle joint resulting in a forward rotation of the trunk. To correct the forward angular velocity, the CoP must be moved anterior to the CoG and a counter-clockwise moment and angular acceleration rise until the angular velocity is turned back.

The CoP has to be continuously moving anteriorly and posteriorly with respect to the CoM to restore a stability position. The muscles that control the ankle moment and cause the CoP to move for regulating the CoM are the plantarflexors and dorsiflexors of the foot.

The stabilizing control torque is provided by the neural control system ([Perterka, 2002], [Mergner 2004]) that activates the related ankle-joint muscles, generating the body's angular acceleration.

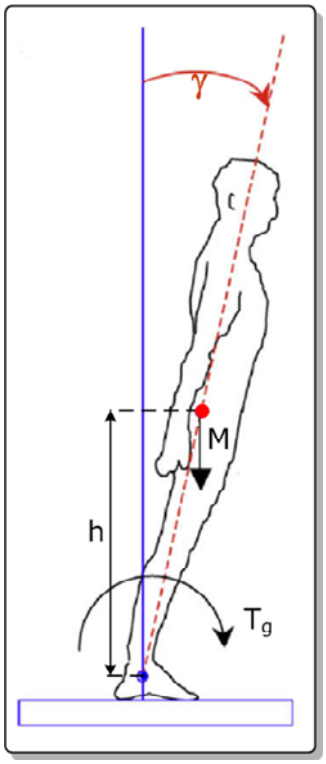

Figure 3.10 - A single inverted-pendulum model representing a human standing on a platform where body motion takes place in the sagittal plane by rotations about the ankle joint (after [Tahboub, 2009])

To derive the equation describing the body's dynamics, consider Figure 3.10 shown a human sketch leaning forward, where:

- γ is the sway angle from the ankle joint
- h is the distance of the CoM from the ankle joint

The destabilizing gravitational torque

$$T_g = mgh\sin(\gamma) \tag{3.1}$$

whose magnitude depends on the body-in-space angle, acts on the body due to a shift of the COM from the vertical equal to:

$$y_{COM} = h\sin(\gamma) \tag{3.2}$$

To bring back the COM to the desired lean angle (i.e. to the vertical position) and stabilize posture, the counteractive muscle torque

$$T_C = T_g \tag{3.3}$$

has to be generated.

The equation of motion can be derived both applying Newton's law and using the method of Euler-Lagrange:

$$J_A\ddot{\gamma}(t) - mgh\sin(\gamma(t)) = T_C(t) \tag{3.4}$$

where

$$J_A = J_{COM} + mh^2 \tag{3.5}$$

is the mass moment of inertia of the human body at the ankle joint.

The single-segment inverted pendulum is a good body model especially when the sway amplitude is small and the ankle strategy dominates ([Borg, 2005], [Schweigart & Mergner, 2008]).

However, some researchers have argued that such approach is oversimplified (see [Qu, 2008]). While a single link is suitable for modelling the ankle strategy, at least two segments are necessary for representing the hip strategy.

In [1981] Stockwell et al. described the human body in the sagittal plane as a system composed of five rigid segments (triangular foot, shank, thigh, torso including arms, head), with four degrees of freedom about the ankle, knee, hip and neck joint. The authors asserted that such a multilink model was necessary for obtaining an adequate description of postural sway from measurements and tests.

Kuo [1995] adopted a multi-segment inverted pendulum body model to fake into account the contribution of hip torque in balance control into the anterior and posterior direction.

Van der Kooij et al. [1999] proposed a three-link segment model of a standing human on a movable support base.

In their study, Hsu et al. [2007] showed that six major joints along the longitudinal axis of the body are equally activated during quiet standing and their motions are coordinated to stabilize the spatial positions of the COM and head.

Tahboub [2010a, 2010b] presented a human-based framework for postural control of a multi-segment humanoid robot in environment characterised by a variety of external disturbances.

It may be argued that adding multiple links and joints can refine and improve the fidelity of the model but also increases the complexity of the model itself.

3.3.2 MODELLING HUMAN BODY IN THE MID-LATERAL PLANE

The vast majority of the investigations in postural stability have been confined to the sagittal plane, since antero/posterior sway amplitude is usually larger then medial/lateral sway. In fact, the magnitude of antero/posterior sway in healthy young adults is often double that of medial/lateral sway [Valles et al., 2008]. Natural body sway in the frontal plane also decreases with stance width [Wing et al., 1995].

Moreover, the ability to withstand lateral disturbances is greater, as the lateral movement is dominated by the hip strategy, controlled by the hip muscles [Winter et al., 1996].

The medial/lateral sway is important in some condition, such as when external loading increases during upright stance. In this situation, a significant intensification of leaning excursion in the lateral direction may result [Qu, 2008].

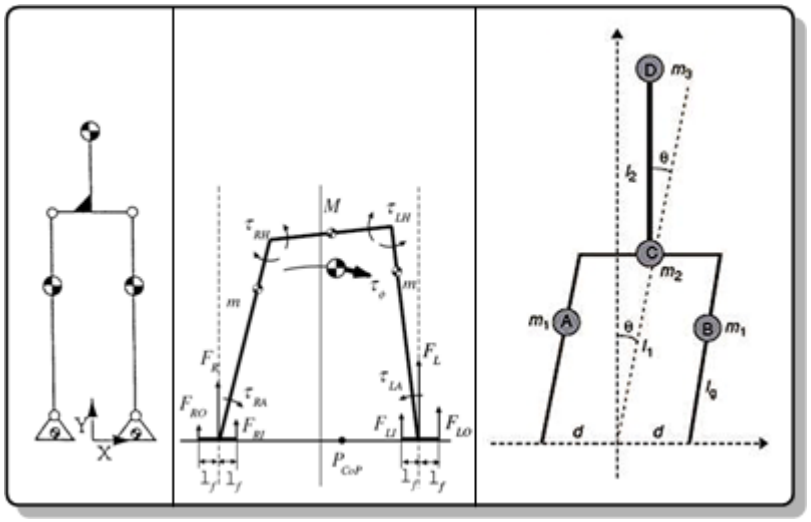

Figure 3.11 – Biomechanical models for standing in the frontal plane proposed by Winter [1995] (left), Ito et al. [2003] (centre), Hidenori & Jiang [2006] (right)

In the frontal plane the simpler biomechanical model for describing human body is a parallelogram pivoting about both ankle and hip joints (Figure 3.11 left). This model has the CoM in a position similar to those in the single-segment inverted pendulum. Four torques are developed at the four joints that can control the upright position. However, the dominant control in the medial/lateral direction is due to the load/unloading mechanism at the hip joint and not to the ankle muscle as in the sagittal plane [Winter, 1995].

In double feet support phase, that is with both the feet in contact with the ground, the model reduces to a four-bar closed mechanism, where the links are the upper part of the body (torso, arms and head), two legs and the feet making a single element together with the ground (Figure 3.11 centre). The knees are considered locked. Although the first three links actually move, the system possesses only one degree of freedom ([Ito et al., 2003], [Tang, 2006]). Theoretically the same magnitude of torque acting at any one of the four joints would have the same results. Even if due to the biomechanics and anatomy of the ankle and hip joints this theoretical situation never occurs [Winter, 1995], it could represent a useful finding from a modelling and controlling perspective [Ito et al., 2003].

Winter et al. [1998] proposed that also in the medial/lateral plane an inverted pendulum model relationship can be established between the CoM (the controlled variable) and the CoP (the controlling variables). Van der Kooij et al. [2005] disapproved the methodologies used by Winter and his group for identifying the rigid body dynamics and the physiological mechanism that controls the body balance. However, they agreed that in quiet standing the CoP and CoM move in phase.

Valles et al. [2006, 2008] extended the classical inverted pendulum to the lateral plane, combining the antero/posterior and medial/lateral sway.

Hidenori & Jiang [2006] derived a multilink model of human body (Figure 3.11 right) based on experimental results showing that the lumbosacral joint moves opposite to the direction of ankle joint in order to keep the trunk perpendicular to the horizontal.

3.3.3 THREE-DIMENSIONAL MODELS

Many existing human body models, either single or multi-link, are developed separately in the sagittal and frontal planes.

Two-dimensional balance models can not be able to reflect the complex nature of human upright stance and simulate the different balance strategies.

Levin & Mizrahi [1995] presented a three-dimensional, four-joint, five-segment model of the human body to estimate the CoM trajectory and describe postural standing sway dynamics.

In [Qu, 2008] a two-links three-dimensional inverted pendulum was used to describe human body dynamics. The two rigid linked segments represented the legs and upper body; two joints at the ankle and hip were considered. By modelling the human body in this form both the ankle and hip strategies could be accounted for. The lower segment (legs) was allowed to rotate only in the sagittal plane, being controlled by ankle torque. Whereas the upper body part was assumed to rotate only in the frontal plane, activated by hip torque. Transversal rotation between the two links was not permitted.

3.4 HUMAN POSTURAL STABILITY: NEUROLOGICAL FEATURES

Postural stability is a complex process that requires the interaction among three different components (Figure 3.12):

- combination of input from the *sensory systems*: somatosensory, vestibular and vision systems;
- *motor reactions* via the activation of muscles of the feet, legs and trunk;;
- central integration of the sensory input and motor processes by the *Central Nervous System* (CNS).

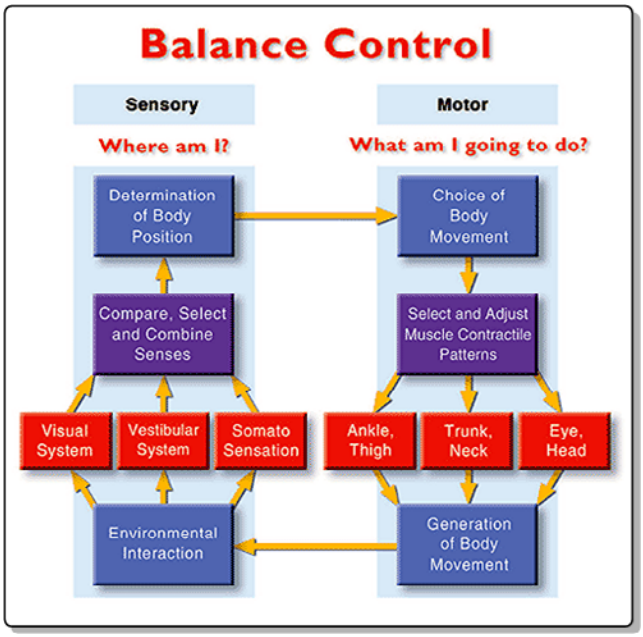

Figure 3.12 – Balance control: conceptual map
[NeuroCom International, Inc. 2009]

The ability to control and maintain balance relies on sensory inputs from somatosensory, visual and vestibular systems.

The somatosensory system[4], the proprioceptors[5] and the mechanical sensitivity of cutaneous and subcutaneous tissue provide awareness of

[4] The somatosensory system receives and interprets sensory information from organs in the joints, ligaments, muscles, and skin. This system processes information about the length, degree of stretch, tension, and contraction of muscles, pain, temperature, pressure and joint position [thefreedictionary.com, Somatosensation].

position and movement of body segments with reference to each other and the support surface [Punakallio, 2005].

The plantar pressure sensors (somatosensory graviceptors) measure CoP shifts and ground reaction forces [Mergner, 2007]. Body angular position and velocity with respect to the foot stem mainly from joints along the body axis. If the inverted pendulum simplification is adopted, the proprioceptive signal only derives from the single ankle joint ([Mergner, 2007], [Mergner et al., 2003]).

The visual and vestibular systems provide information about the body's position in relation to the environment: gaze and eyes give a reference for horizontal, while the vestibular system helps in determining a reference for vertical [McKeough, 2010].

The role of visual orientation cues for balance control is still not well identified [Mergner et al., 2005]. Vision can also be compensated by other sensory inputs [Punakallio, 2005]. For example, when the focusing distance is great, the visual input becomes unreliable and inputs from the other sensors turn out to be important.

The vestibular system provides the dominant input about movement and the sense of balance [Wikipedia, Vestibular system], supplying information concerning the position of the head in relation to gravity. The vestibular system comprises two components that act as a biological six degrees of freedom inertial measuring device [Mergner & Glasauer, 1999]: the semicircular canals, which sense rotational movements, and the otoliths, which are sensitive to linear accelerations.

Vertical and horizontal semicircular canals sense rotational movement of the head in the sagittal and frontal, as well as horizontal, planes, respectively. Saccular otoliths sense vertical linear accelerations of the head (e.g., gravity), whereas utricular otoliths sense horizontal linear accelerations like head movements generated during forward walking [Punakallio, 2005].

---

[5] Proprioceptors are sensory receptors (located within the muscles, tendons, joints, and the inner ear) that detect the motion or position of the body or a limb and provide information about posture and balance [thefreedictionary.com, Proprioceptor].

The Central Nervous System (CNS) is the part of the nervous system that integrates the information that it receives from, and coordinates the activity of, all parts of the bodies. It consists of the brain and the spinal cord [Wikipedia, Central Nervous System].

The CNS is designated to organise sensory information, and select the motor responses for stabilising posture and preventing falls depending on environmental conditions.

Information from the three sensory systems is processed by the CNS, which selects the most appropriate and accurate in relation to the specific task and actual surrounding circumstances. This adaptive interaction makes it possible to ignore sensory input creating conflict and producing disorientation and instability. For example, a healthy young individual standing on rigid flat platform, while observing fixed vertical walls, receives correct and reliable proprioceptive and visual orientation references. Irregular and movable floors, moving objects in the visual field, active head movements generate balance information and sensory cues from proprioceptive, visual and vestibular systems respectively, that can negatively affect equilibrium.

The ability to adopt proper sensory strategy and, consequently, ready biomechanical and musculoskeletal responses depends on individual aspects such as age, habituation, sensory and motor impairments and pathologies ([Mergner et al., 2009], [Punakallio, 2005]).

The mechanisms and processes that drive the complex system described above and make the balance control effective are not completely identified.

Traditionally, the control of posture was considered to be based upon simple postural responses known as the postural reflexes ([Mergner, 2004], [Punakallio, 2005]). The reflexes[6] are stereotype (standardized and simplified) reactions to sensory stimuli.

Mergner [2004] asserted that postural reflexes are evoked as long as the CNS is in an immature state, or if it is damaged, while in normal and adult

[6]A reflex action is an involuntary and nearly instantaneous movement [Wikipedia, Reflex]

individuals the postural responses are no longer stereotype and therefore cannot be termed reflexes.

Soon after birth, postural reflexes are replaced by automatic reaction that allow for volition and cognition [Mergner, 2004].

Voluntary postural movements can be initiated in response to an external stimulus. According to Massion (1994), voluntary postural adjustments are organised on the basis of internal representations of body geometry (provided by the postural body scheme), body dynamics (support and surrounding conditions) and body orientation (from sensory input) [Punakallio, 2005].

Shumway-Cook and Woollacott (1995) asserted that the CNS must have an accurate picture of where the body is in space and whether it is stationary or in motion, to know when and how to apply restoring forces to keep the COG within the BOS [Punakallio, 2005].

As reported in [Mergner, 2007], von Holst and Mittelstaedt (1950) proposed a model (*reafference principle*) based on the decomposition of sensory signals into self-produced sensory input (*reafferent input*) and input stemming from external disturbances (*exafferent input*). The CNS uses an "internal model" (*afferent copy*) of the body and its dynamics to simulate its behaviour in parallel to the actual outside behaviour. Motor responses are then produced in order to minimize the difference between the simulated internal behaviour and the actual (monitored by sensory systems).

3.5 POSTURAL CONTROL MODELS

Currently, the complete nature of the human postural control system is not completely understood. Little is known about how information from the senses is processed and combined to generate appropriate corrective torque when conflicting or inaccurate orientation information derives from different sensory systems.

Numerous studies have tried to contribute in modelling balance mechanisms. These start from the idea that human body acts as a controlled dynamical system, that is upright posture is maintained via control-like strategies (namely, feedback control) based on information provided by the three main sensory systems (see section 3.4) [Mahboobin, 2007].

As the body deviates from the upright stance, gravity induces a destabilising torque that accelerates the CoM far from its equilibrium position. In order to maintain balance the body has to produce a counteracting torque, based on the information provided by the sensory systems. This information is integrated and processed by the CNS that activates the motor strategies (see section 3.2) required for generating the reaction moment.

Then, the CNS acts as a controller that generates a corrective torque for stabilizing the inherently unstable erect body posture.

Experiments in human balance suggest that feedback control plays a dominant (although possibly not exclusive) role in maintaining upright posture in humans [Mahboobin, 2007].

As suggested by Davidson [2007] and Mahboobin [2007], published literature on human postural control can be broadly classified in: models that implement *Proportional-Integral-Derivative* (PID) or Proportional-Derivative (PD) *control*, and models that employ *optimal control* techniques.

The following section contains a description of some models that has incorporated PID controller to analyse human postural stability and are of interest in this work. A comprehensive review of investigations that uses optimal control approach can be found in [Davidson, 2007], [Qu, 2008] and in related bibliography.

3.5.1 POSTURAL CONTROL MODELS USING PID CONTROLLER

The *Proportional-Integral-Derivative* – PID (Figure 3.13) controller is the most common feedback controlling method for dynamic system, widely used in industrial as well as other engineering contexts.

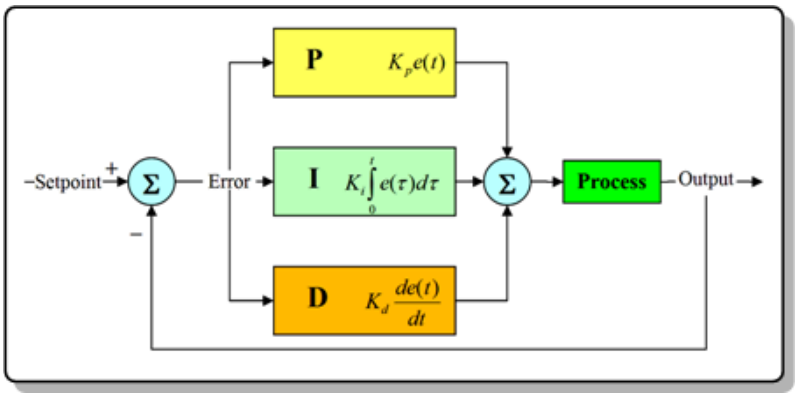

Figure 3.13 – A block diagram of a PID controller [Wikipedia, PID controller]

Many authors ([Mahboobin et al., 2008], [Maurer & Perterka, 2005], [Mergner, 2004], [Peterka, 2002], [Tahboub, 2009], [van der Kooij & al., 2005]) modelled the human body (the box named "*Process*" in Figure 3.13) as a linearized single-link inverted pendulum and the CNS as a PID controller generating the corrective torque about the ankle joint.

The ankle joint and its muscles are considered an ideal angular actuator that receives its input from the "neural controller" and transforms the neural command signal (or error signal in a simple feedback system) into the stabilising torque [Mergner, 2004].

From a theoretical perspective, the stabilisation of an inverted pendulum requires that the controlling torque contains at least two components: a *stiffness factor* (resulted from position feedback, box "*P*" in Figure 3.13) and a *damping factor* (resulted from velocity feedback, box "*D*" in Figure 3.13)) ([Peterka, 2002], [Mergner, 2004]). The stiffness component is proportional to the actuating error signal and has the task of compensating for the negative stiffness due to gravity. The damping factor is proportional to the rate of change of the error signal and is required to avoid oscillations [van der Kooij et al., 2005].

A third component (*swiftness factor*), proportional to the time integral of the error signal (box "*I*" in Figure 3.13), can be added optionally. This contribution takes into account both the magnitude and the duration of the error and gives the accumulated offset that should have been corrected. The swiftness factor adds low frequency error correcting properties, but is not necessary for stability [Peterka, 2002].

The torque produced by the PID controller is indicated as active feedback [Peterka, 2002], and is also named reflexive or sensory feedback [van der Kooij et al., 2005]. The term "active" indicates that the generated corrective torque rises in response to an external perturbation [Mahboobin, 2007].

In the model, a time delay is included in order to represent the effective time delay of the system, due to sensory transduction, neural transmission, nervous system processing, muscle activation, and force development ([Mahboobin, 2008], [Maurer et al., 2006], [Peterka, 2002], [Tahboub, 2009]).

To model the passive torque generated from muscle/tendon stretch caused by body sway relative to the support surface, another feedback loop without time delay is include into the postural control scheme ([Peterka, 2002], [Peterka, 2003], [van der Kooij et al., 2005]).

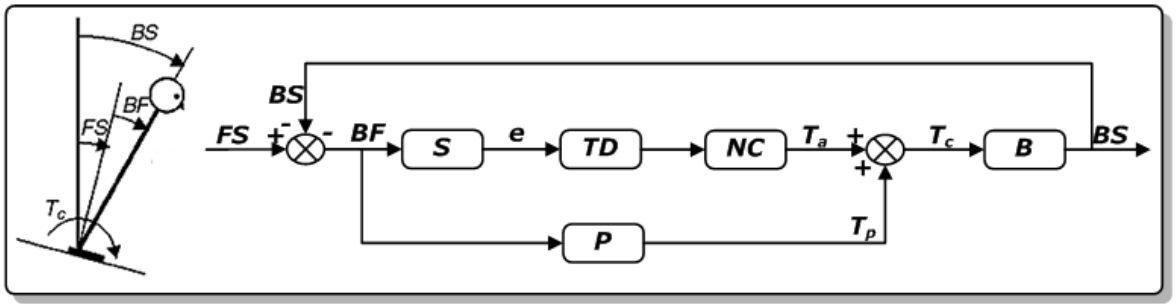

Figure 3.14 - A simplified postural control model including time delay and passive feedback loop (after, [Peterka, 2003])

In Figure 3.14 a simplified version of the postural model proposed by Peterka is shown, where:

- BS (Body-in-Space) is body orientation relative to earth-vertical;
- BF is body orientation relative to the feet;
- FS is Foot-in-Space orientation;
- S is the sensory system that senses the BF angle;
- TD is the system time delay;
- NC is the neural PID controller;
- B is the human body modelled as an inverted pendulum;

- P is the muscle and tendon dynamics, modelled as a PD controller;
- T_C is the total corrective torque applied to counter the destabilising torque due to gravity;
- T_a is the corrective active torque derived from sensory information;
- T_p is the corrective passive torque due to muscle dynamics;
- e is the internal error signal, produced by the sensed BF angle, that is used by neuromuscular systems to generate T_C.

The model includes passive muscle dynamics and a feedback loop conveying force-related sensory information. Muscles generate passive corrective torque that sums with active torque derived from sensory information to give the overall corrective torque to the body.

The "passive" control, made up of a stiffness and damping contributions, appeared to be negligible during perturbations (a factor of ten smaller than the active torque generation). Thus, adding the passive feedback loop did not increase significantly the accuracy of the whole model ([Alexandrov et al., 2005], [Mahboobin, 2007], [Peterka, 2002]).

Tahboub [2009] included in his postural control model feed-forward or anticipatory control terms.

In motor control theory, the feedback loop and the controlled plant constitute a "closed-loop" system, while the feed-forward control provides external input signals to the dynamic system in the "open-loop" manner (Figure 3.15).

The anticipatory body inclination in a standing passenger before the start of a train is an example of involuntary feed-forward correction. Such anticipatory adjustment is possible only when the forthcoming perturbations are predictable [Alexandrov et al., 2005].

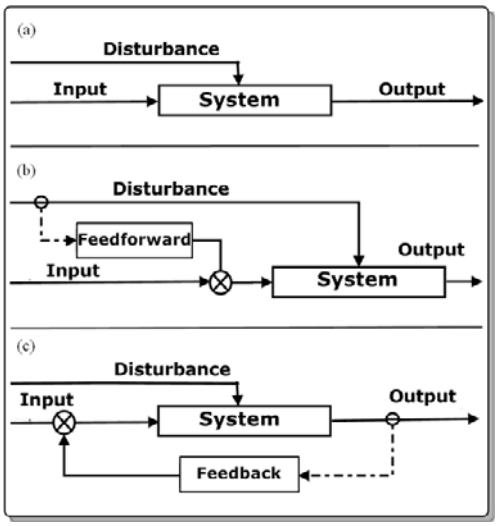

Figure 3.15 - The Three types of Control System: (a) Open Loop, (b) Feed-forward, (c) Feedback (after [Wikipedia, Feed-forward])

Alexandrov et al. emphasized that the feed-forward path did not control directly muscle forces, but acted modifying the parameters of the feedback loop. This concept was confirmed on the basis of the study of Gurfinkel et al. (1995). They found that the characteristic time for adjustment of the feedback loop parameters during orthograde posture is about 10 seconds. Therefore, it was hypothesised that, during the short, early phase of the response, feed-forward control was small and posture maintenance was mainly achieved by the feedback mechanisms [Alexadrov et al., 2005].

Wagner & Smith [2008] suggested that the neural processes based on feedback control must contain a forward path. This control mechanism, combined with an internal model, can explain how humans learn motor abilities for executing a given task.

From studies conducted by Hay & Rendon [1999], it resulted that feed-forward control emerges and becomes more efficient later in time (as individuals grow up) than feedback mechanisms.

According to Tahboub [2009], feed-forward control is associated with learning and can be employed for reproducing observed behaviour during specific tasks.

In order to take into account the information stemming from the sensory cues, Perterka ([Perterka, 2002], [Perterka, 2003], [Peterka & Loughlin, 2004]) proposed a feedback control model where the generated corrective

torque depended on orientation and movement input provided by the sensory systems (Figure 3.16).

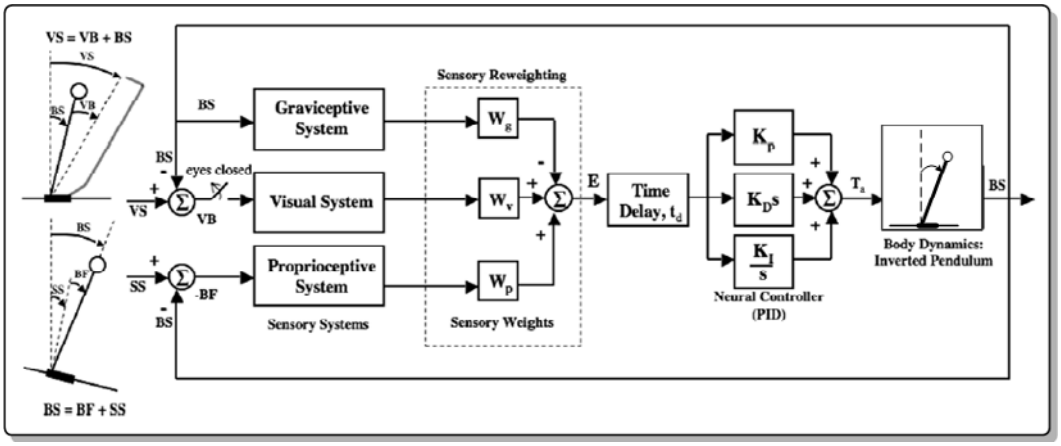

Figure 3.16 – Feedback model of postural control proposed by Peterka (after [Mahboobin et al., 2008])

In the feedback model shown in Figure 3.16, the body is modelled as an inverted pendulum. The sensory pathways include variable sensory weights that can change as environmental factors change. BS, VS and SS are angles, with respect to earth-vertical, of the body, visual scene and support surface, respectively. VB and BF are the relative angles of the visual scene and the support surface with respect to the body. Corrective torque about the ankle T_a is generated by a PID controller, acting on the combined delayed sensory error signal E.

The contribution of each sensory system (vestibular or graviceptive, visual and proprioceptive) is determined by variable sensory weights, that differ under different environmental conditions. According to sensory re-weighting hypothesis proposed by Peterka, the overall sensory weight $\boldsymbol{W}$ in (3.6) is the sum of the sensory weights of those sensory inputs that provide accurate information about body orientation:

$$\boldsymbol{W} = W_g + W_v + W_p \tag{3.6}$$

where

- W_g is weight for the graviceptive sensory system;

- W_v is weight for the visual sensory system;
- W_p is weight for the proprioceptive sensory system;

For example, the effective overall sensory weight is $\boldsymbol{W} = W_g + W_v + W_p$ during quiet standing on a fixed platform with eyes-open. But, for eyes-closed stance, the visual system does not contribute information about body sway, so the effective overall sensory weight in this case is $\boldsymbol{W} = W_g + W_p$ [Mahboobin, 2007].

Following the postural control model proposed by Peterka ([Peterka, 2002], [Peterka, 2003], [Peterka & Loughlin, 2004]), Mabhboobin et al. [2008] combined sensory re-weighting concept with optimal filtering theory. A Kalman filter was adopted for estimating sensor noise and disturbance size; consequently, the filtering process automatically generated sensory weights.

The control system was implemented into a humanoid robot model resulting in stable stance for the robot on a sway-referenced platform. Traditionally, in robotics the emphasis has been on controlling the location of the CoP based on proprioception, with little use of vestibular signals (via accelerometers) and no use of vision. As in humans, multiple sensory sources and combinations may contribute to stabilise humanoid robots in perturbed environments.

Valles et al. ([2006], [2008]) extended the feedback control balance model developed by Maurer and Peterka [2005] in the sagittal plane for investigating postural sway also in the medial/lateral direction. They proposed a bi-planar model (Figure 3.17) that assumed an inverted pendulum in both antero/posterior and lateral plane. The postural model was stabilised by a PID controller whose parameters were changed for taking into account the sway direction. For healthy young adults, they found that the in medial/lateral plane the damping factor was higher (24% circa), whereas the disturbance torque was lower (46% circa) than in the sagittal plane. This was reasonable being the human body more stable in the lateral than in the antero/posterior direction.

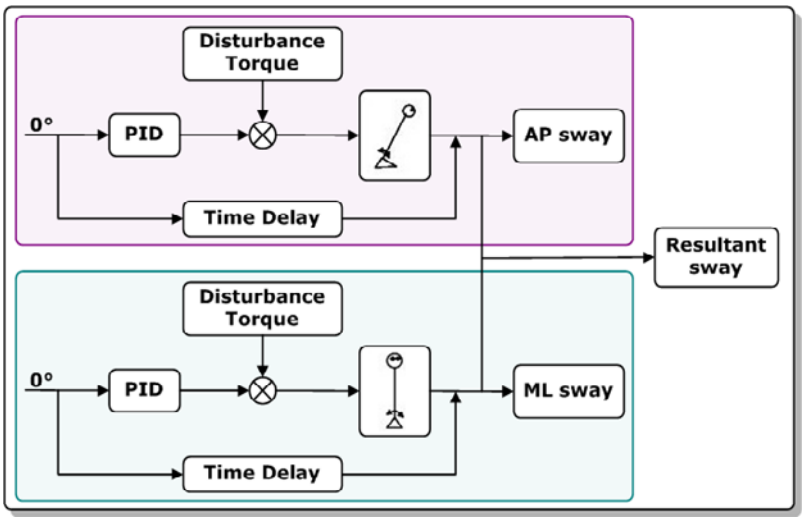

Figure 3.17 – Bi-planar model (afert [Valles et al., 2006])

Mergner and his group ([Maurer et al., 2005], [Mergner, 2004], [Mergner, 2007], [Mergner et al., 2003], [Mergner et al., 2005]) conducted experiments in which the postural responses of both normal subjects and patients with sensory impairments were measured during perturbed stance conditions. The data collected were compared to simulated results obtained from a feedback control model.

In the proposed model, a sensory interaction was obtained by weighing the sensory signals on the basis of thresholds having a physiological meaning. These thresholds represent an ideal "switch" for selecting the most reliable and suitable sensory input according to environmental conditions.

The body lean movement, raised as postural stimulus compensation, did not derive form the sensory cues proper, but from internal estimates of external disturbances. Therefore, the main control principle is that the external disturbances are compensated for by creating internal estimates of each disturbance, and feeding these estimates into the feedback control loop.

The multisensory postural control model proposed by Mergner and his colleagues ([Maurer et al., 2005], [Mergner, 2004], [Mergner, 2007], [Mergner et al., 2003], [Mergner et al., 2005]) is based on neurological studies and is conceived in a biological framework, being developed for understanding human postural mechanisms. To avoid the difficulty in comparing simulation results with real human postural behaviour in a wide range of situations, the proposed model was "transformed" in a traditional

engineering control architecture that was embodied in a biped humanoid robot ([Mergner, 2007], [Schweigart & Mergner, 2008], [Tahbuoub et al., 2006]). The "PostuRob" [PostuRob. Website] was equipped with three sensory systems: the vestibular system was mimicked by combining a 3D accelerometer with a 3D gyrometer; the ankle-foot ankle was measured with a goniometer; the somatosensory foot sole pressure receptors were embodied by a set of force sensors. The "muscles" consisted of pneumatic actuators with springs as "tendon" that generated the controlling torque. The robot represented the core of a Hardware-In-the-Loop (HIL) simulation environment for testing and validating the postural control engineering approach inspired by biological findings.

In [Tahboub, 2009], [Tahboub, 2010a] and [Tahboub, 2010b], [Tahboub & Mergner, 2007] the latter control model (Figure 3.18) is extensively discussed. Briefly, it was made up of three main sub-systems.

Instead of using a classical PID controller, an alternative scheme was chosen, namely "*a robust tracking and disturbance rejection scheme*" [Tahboub, 2009]. It was composed of PD-feedback and I-cascade parts, the former component acting on the system output, whereas the latter acting on the tracking error. A PD feed-forward term could be introduced for speeding the response and enhancing tracking ability to generate desired voluntary motion [Tahboub, 2009].

The controlling architecture was also composed of an extended observer, which estimated the external disturbances such as platform tilt ([Tahboub, 2009], [Tahboub, 2010a], [Tahboub, 2010b]), pull forces [Tahboub, 2009], platform translational acceleration ([Tahboub, 2010a], [Tahboub, 2010b]). As an alternative solution, a Kalman filter was implemented too. It was proved that the first estimation option (which incorporated an internal model of the dynamic system) provided better results [Tahboub, 2010a].

The compensation mechanism produced the actuating torque that had a twofold aim: to stabilise the unstable system (humanoid body) and cancel the external disturbances.

It has to be mentioned that the control scheme was applied not only to an inverted pendulum model, but it was also extended to a multilink model ([Tahboub, 2010a], [Tahboub, 2010b]).

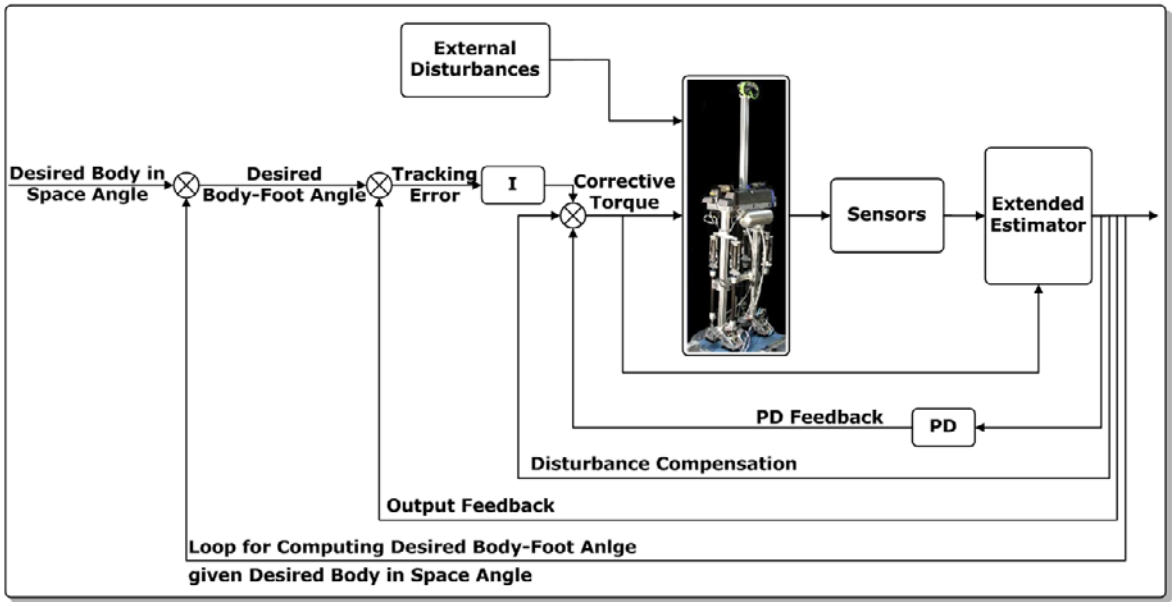

Figure 3.18 - Control architecture and simulation model showing the plant, extended observer, estimated-disturbances compensation, state-feedback inner loop, and internal model integral controller (after [Tahboub & Mergner, 2007])

Some considerations can be outlined about the balance control models discussed above.

In analyses of balance stability in humans, the body is usually represented as a one-dimensional inverted pendulum rotating about the ankle joints and the problem is approached mainly in the sagittal plane. The human body as a biomechanical system can be more accurately modelled by a multi-joint chain. In such a model, due to the interaction among links in the chain, the change of torque in any joint influences on the movement in all the joints [Alxandrov et al., 2005]. Although it was recognised that such an approach may be valid if the movements in all the joints, except the ankle, are artificially blocked [Peterka 2002], Schweigart & Mergner [2008] showed that the "inverted pendulum" simplification is a legitimate simplification. This is particularly true when it is employed for testing and validating novel ideas or findings.

Moreover, although the presented models reveal important features of human postural control mechanisms, they significantly simplify the high complexity and non-linearities of the real system. For example, the model proposed by Peterka [2002, 2003] is able to simulate the steady-state response of system, as well as transient conditions [Peterka & Loughlin,

2004], but it does not describe how sensory weights change under different environmental conditions ([Peterka, 2003], [Mahboobin, 2007]). The model discussed in [Schweigart & Mergner, 2008] is not able to predict well transient responses, showing an immediate compensation of the platform tilt that was not observed in the experiments. It also does not describe the observed for-aft asymmetry behaviour.

More sophisticated models, employing optimal estimation concepts and multilink geometries, are needed to take into account such aspects (see, for example, [Alexandrov et al., 2005], [Davidson, 2007], [Kuo, 1995], [Qu, 2008], [van der Kooij et al., 1999]).

3.6 APPROACHES FOR IDENTIFYING HUMAN BALANCE CONTROL SYSTEM

To identify the rigid body dynamics and the physiological mechanisms that control the body, the human body has to be perturbed with known external disturbances. To deepen human balance control, CoM, CoP, electromyogram[7] (EMG), joint moments, joint angles and angular velocities, or related measures are commonly recorded. Studies on postural control can be classified according to the experimental approach they employed. According to van der Kooij et al. [2005], two major approaches can be distinguished:

- system identification methods;
- descriptive measure methods.

System identification is the process that allow building dynamic models from experimental data. In this method, two signals (e.g., CoP and CoM time

[7] Electromyography (EMG) is a technique for evaluating and recording the electrical activity produced by muscle cells, when they are electrically or neurologically activated. The signals, tracing in a record called electromyogram, allow to analyze the biomechanics of human movement [Wikipedia, Electromyography].

series) are used to identified the dynamics between both the signals, i.e. the mechanisms involved in balance control. For example, the frequency response functions of CoP, CoM, etc. obtained stimulating the system with external or internal perturbations are employed for identifying parameters of balance control models ([Peterka, 2002], [Tahboub, 2009], [van der Kooij, 2001]).

System identification methods have been frequently used in balance control studies. Among them, van der Kooij et al. [2005] criticise direct approach (e.g., linear regression [Winter et al., 1998] or cross-correlation function of CoP and CoM [Winter et al., 2001]) when applied in systems with feedback (like human balance system). Actually, direct approaches are well suited to study open-loop systems.

The descriptive method makes use of statistical or stochastic measures such as, for example, the power spectral densities of the CoP and CoM [Winter et al., 1998].

According to van der Kooij et al. [2005] direct approach and descriptive methods can ignore or mask important dynamics of the human balance control system. Therefore, they recommend to employ identification methods allowing to study the dynamics that control the body and the dynamics that perturb the body separately. In such a way, these methods allow to retrieve reliable estimates of the feedback mechanisms that control balance.

Chapter 4: Modelling the Human Postural Control System onboard Ship

4.1 INTRODUCTION

In this chapter, a stance control model for modelling postural behaviour of a crewmember onboard ship is proposed. The model complies with the main features of the biologically-inspired frameworks described in Chapter 3.

The most interesting findings of published postural control studies have been synthesized and applied to the issue of postural stability onboard a sailing ship.

In developing such a model, the Occam's Razor [Gibbs & Sugihara, 1997] has been followed. That is, a simple model able to capture the salient aspects of human postural control system in a moving environment has been derived. In this way, the complex mechanisms that underlie the maintaining of balance could be easily understood and implemented in a wider procedure.

The goal of the proposed model is, on one hand, to extract the principles of human stance control for reproducing an individual that tries to restore postural equilibrium on a moving ship. Modelling a person as a dynamic and active system would result in a more realistic scenario than the reference model commonly employed for predicting loss of balance events onboard ship. The latter model, proposed by Graham and described in section 2.2, regards a crewmember as a dummy, namely a passive rigid body unable to counteract the external disturbances due to ship motions.

On the other hand, the present model has been planned with a simple and flexible approach, that makes it possible to develop a more general procedure to be used as part of conventional ship design tools or for assessing safety working conditions aboard.

As a first step in model development, the biomechanics of human body were simplified. The body has been represented as a single-link inverted pendulum with body rotation occurring about the ankle joint axis. The equations of motion describing the inverted pendulum dynamics are quite simple and can be linearised about the vertical position (i.e. the equilibrium point). That allows superimposing the ship dynamics (in the form of linear motions) in a straightforward manner.

As a second step, the main features of postural equilibrium as a biological process have been translated into a control engineering approach to model the human upright control system. Among the heterogeneous aspects emphasised by postural stability studies (as also shown in [Tahboub, [2009]), a set of principles, meaningful for modelling an individual on a movable platform, has been identified and included into the proposed control model:

- Both proactive and reactive control efforts exist (e.g. [Peterka, 2002]).
- Postural control system shows anticipatory, adaptive and learning properties (e.g. [Alexadrov et al., 2005], [Wagner & Smith, 2008]).
- Postural stability is achieved by feedback mechanisms and rejection of external disturbances (e.g. [Mergner et al., 2003], [Peterka, 2002]).
- Feedback control implies proportional, derivative, and integral contributions (e.g. [Peterka, 2002], [Tahboub, 2009]).
- External disturbances and voluntary motion can be handled simultaneously (e.g. [Mergner, 2004], [Tahboub & Mergner, 2007]).
- Postural control is based on an internal model reproducing body dynamics (e.g. [Mergner, 2007]).
- Postural stability is based on multisensory information, integrated and processed by the Central Nervous System, rather than on simple reflexes (e.g. [Mergner, 2004], [Peterka, 2002]).

- Both global sensor inputs (from vision and vestibular system) and local sensor contributions (from proprioception system) are employed and automatically combined depending on environmental conditions (e.g. [Mergner et al., 2003], [Peterka, 2002]).
- External disturbances are estimated separately from each other and their destabilising effect is contrasted by a reactive control action based on these estimates (e.g. [Mergner, 2004], [Tahboub, 2009]).

In particular, the proposed model is based on work by Tahboub and his group ([Thaboub, 2009], [Tahboub & Mergner, 2007]) that designed and implemented a control framework for stabilising a humanoid robot with the ultimate goal to yield a deeper understanding of neurological aspects underlying human postural control.

In the model discussed in the next sections, other biological features (such as system delays and nonlinearities, dynamics, noise and drifts of sensory systems) are omitted since these aspects have been considered negligible (at the moment) for the purposes of the conducted study.

The present chapter is organised as follow.

First of all, a simple biomechanics model comprising the effects due to ship motions is derived, and the choice of physical parameters is argued.

Then, the postural control scheme is incrementally built up, by incorporating a single element one-step at a time up to compose the complete model.

4.2 MODELLING A CREWMEMBER ONBOARD SHIP

In this work, a single-segment inverted-pendulum model is used to describe the postural stability behaviour of a crewmember onboard a ship. It is assumed that the person is on the deck, facing out in the lateral positive direction.

First of all, only the sway motion in the anterior-posterior (A/P) direction is considered (i.e. the pendulum motion is limited to a single plane), assuming an "ankle joint strategy" for balance recovery.

Human upright stance is inherently unstable, with most of the body's mass concentrated above the lower extremities, higher up in the trunk; the erect posture is maintained over a relatively small base of support with the pivot point at certain height from the sole. Even in the absence of additional environmental disturbances (movements of the supporting surface, external forces, etc.), a small deviation from upright body orientation is enough to result in an increase of a destabilizing gravitational component.

Figure 4.1 Left explains the idea stated above.

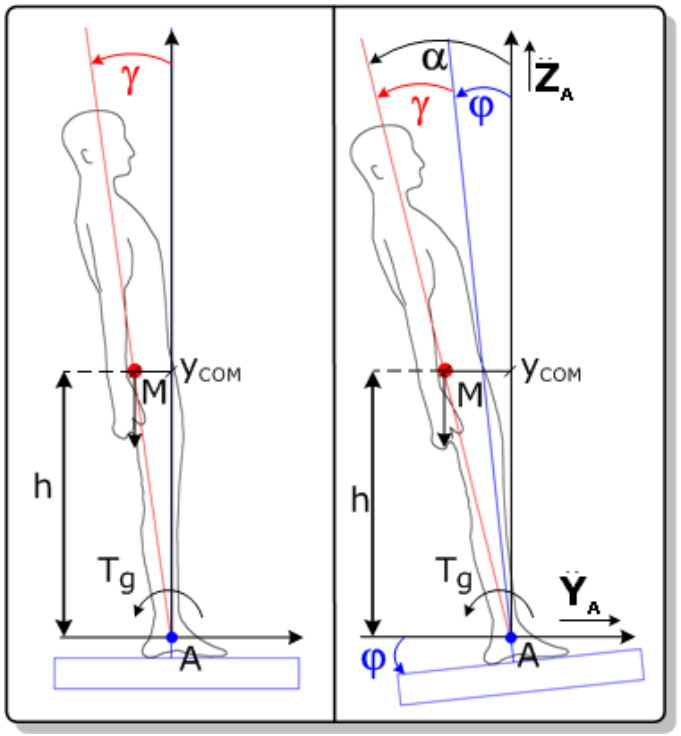

Figure 4.1 – A single inverted-pendulum model representing a crewmember standing on ship deck. Left: The deck is horizontal and stationary. Right: The deck is moving. (after [Tahboub, 2009])

where:

- γ (4.1)

  is the leaning angle from the ankle joint;

- h (4.2)

  is the distance of the Centre of Mass (CoM) from the ankle joint;

- $M = mg$ (4.3)

  is the body weight;

- $T_g = mgh\sin(\gamma)$ (4.4)

  is the destabilising gravitational torque.

- $y_{COM} = h\sin(\gamma)$ (4.5)

  is the shift of the COM from the vertical.

The individual is shown leaning backward at the angle γ from the ankle joint (relative to the deck). The destabilising torque T_g in (4.4) is due to the gravity that acts on the CoM shifted away from the upright equilibrium position (4.5). The magnitude of the gravitational torque depends on the body-in-space angle.

To bring back the COM to the desired lean angle (i.e. to the vertical position) and stabilize posture, a counteractive muscle torque

$$T_C = T_g \tag{4.6}$$

has to be generated.

As discussed in section 3.3.1, the stabilizing control torque is provided by the neural control system that activates the related ankle-joint muscles, generating the body's angular acceleration.

The equation describing the body's dynamics can be derived both applying Newton's law and using the method of Euler-Lagrange:

$$J_A\ddot{\gamma}(t) - mgh\sin(\gamma(t)) = T_C(t) \tag{4.7}$$

where

- $J_A = J_{COM} + mh^2$ (4.8)

  is the mass moment of inertia of the human body at the ankle joint (*Parallel-Axis Theorem*);

- J_{COM} (4.9)

  is the mass moment of inertia respect to the CoM;

Taking the ship reference system as a basis, also here torques and angles are assumed to be positive in the anticlockwise direction.

Assuming a small lean angle γ, the nonlinear second-order differential equation (4.7) can be linearised about the vertical position (i.e. the equilibrium point):

$$J_A\ddot{\gamma}(t) - mgh\gamma(t) = T_C(t) \tag{4.10}$$

Now, let us introduce the effect of a moving supporting surface (in this case we are talking about the motion of the ship, Figure 4.1 Right) in the equation of the inverted pendulum dynamics.

Here, the human body motion is restricted to the sagittal or A/P plane, and the linear hypothesis also holds for the ship motion, so ship's longitudinal acceleration is negligible. In this hypothesis, only three DOF motion platforms can affect the stability of a man standing on the deck and they have to be included in the pendulum dynamics:

$$\begin{aligned} &J_A\left(\ddot{\gamma}(t) + \ddot{\varphi}(t)\right) - mgh\sin\left(\gamma(t) + \varphi(t)\right) - mh\ddot{Y}_A(t)\cos\left(\gamma(t) + \varphi(t)\right) + \\ &-mh\ddot{Z}_A\sin\left(\gamma(t) + \varphi(t)\right) = T_C(t) \end{aligned} \tag{4.11}$$

where:

- φ (4.12)

  is the deck roll angle;

- $\alpha = \gamma + \varphi$ (4.13)

  is the inclination angle of body COM relative to the vertical;

- $\ddot{\varphi}$ (4.14)

  is the deck roll angle acceleration;

- $\ddot{Y}_A$ (4.15)

  is the deck lateral acceleration;

- $\ddot{Z}_A$ (4.16)

  is the deck vertical acceleration.

Both the linear accelerations are determined in the point A, the individual ankle joint, considered to be fixed with the ship's deck.

In the case of equation (4.11), for stabilising posture the counteractive muscle torque has to face not only the gravitational destabilising effect, but also the effect due to ship motions:

$$T_C = mgh\sin\left(\gamma(t)+\varphi(t)\right) + mh\ddot{Y}_A(t)\cos\left(\gamma(t)+\varphi(t)\right) + \\ +mh\ddot{Z}_A\sin\left(\gamma(t)+\varphi(t)\right) - J_A\ddot{\varphi}(t) \tag{4.17}$$

Linearising equation (4.11) and neglecting the terms higher than the second order, we get:

$$J_A\left(\ddot{\gamma}(t)+\ddot{\varphi}(t)\right) - mgh\left(\gamma(t)+\varphi(t)\right) - mh\ddot{Y}_A(t) = T_C(t) \tag{4.18}$$

In [Tahboub, 2009] and [van der Kooij et al., 2005] similar expressions were derived for an inverted pendulum on a surface tilting about an axis passing through the ankle joint, and subjected to a horizontal disturbing force acting at a known height from the ankle joint.

4.3 CHOICE OF ANTHROPOMETRIC PARAMETERS

For analysing the dynamics of the proposed model, the anthropometric parameters (body segments, mass and inertial characteristics) included in the equations of motion have been selected carefully. Taking care to employ suitable physical values for humans is important as this choice can influence the results of computations and simulations (e.g. [Lenzi et al., 2003], [Rao et al., 2005]). Rao et al. [2005] recommend to use values for body segment parameters obtained from multiple regression estimation functions over a significant sample of individuals.

In the present study, the human body parameters have been decided based on the following elements. First of all, the model has been designed in order to simulate the behaviour of a representative mean-experienced (*archetypal*) subject onboard ship. Moreover, neither anthropometric data characterising the worldwide population of seamen are available, nor a survey for deriving anthropometric measurements was conducted (for the moment) within the present investigation.

On the contrary, an extensively bibliography research has been performed, that has led to assume the following values for characterising body's parameters of a mid-size man:

- $m = 77.3$ kg (4.19)

  is the body mass from Anthropometry Databases [Moss et al., 2000];
- $h_{Body} = 1.754$ m (4.20)

  is the body height from Anthropometry Databases [Moss et al., 2000];
- $h_{COM} = 0.56 \cdot h_{Body} = 0.982$ m (4.21)

  is the distance of the CoM from the base of support computed as fraction of body height h_{Body} [Gambino et al., 2006)]
- $h_A = 0.04 \cdot h_{Body} = 0.070$ m (4.22)

  is the distance of the ankle joint from the base of support computed as fraction of body height h_{Body} [Winter, 2005].
- $h = h_{COM} - h_A = (0.56 - 0.04) \cdot h_{Body} = 0.912$ m (4.23)

is the distance of the CoM from the ankle joint.

- $J_{COM} = 3.44 \cdot h_{Body}{}^2 + 0.144 \cdot m - 8.04 = 13.67 \text{ kg} \cdot \text{m}^2$ (4.24)

  is the moment of inertia in the anterior/posterior or sagittal plane of supine position respect to the centre of mass [Matsuo et al., 1995].

- $J_A = J_{COM} + mh^2 = 77.98 \text{ kg} \cdot \text{m}^2$ (4.25)

  is the mass moment of inertia of the human body at the ankle joint (*Parallel-Axis Theorem*);

The body segment lengths are expressed as a percentage of body height h_{Body} as defined by Drillis and Contini (1966). As reported in [Winter, 2005], these segment proportions serve as a good approximation in the absence of better data (i.e. direct measurements from the individual).

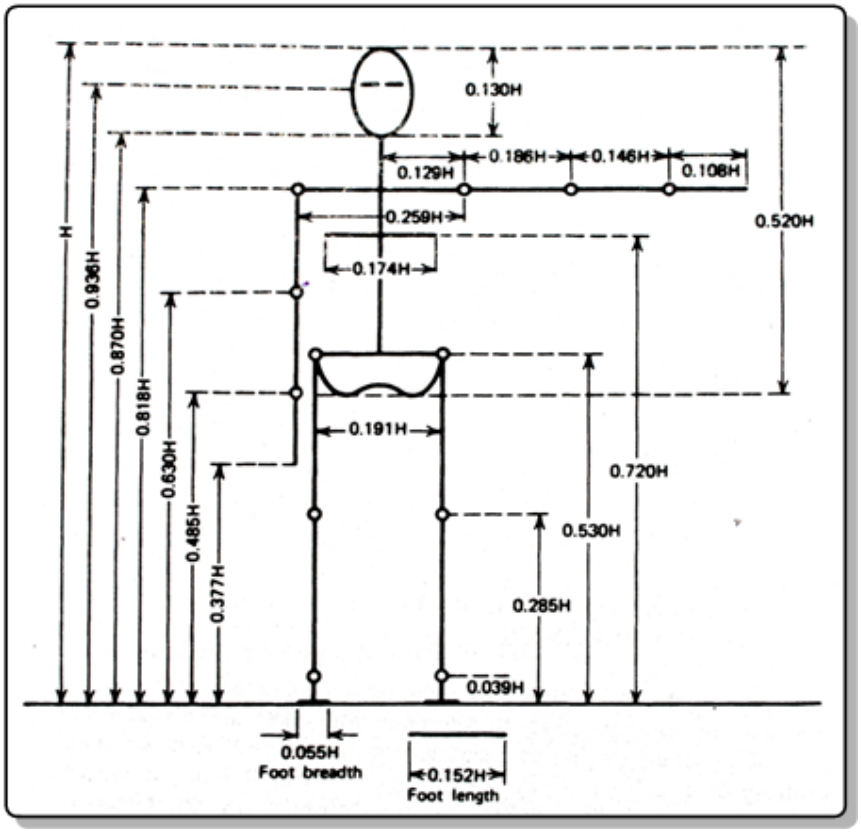

Figure 4.2 – Body segment lengths expressed as a fraction of body height H (after, [Winter, 2005])

4.4 MODELLING THE POSTURAL CONTROL SYSTEM: WITHOUT SHIP MOTIONS

Starting from the linearised equation of motion (4.10), the transfer function of the human-like inverted pendulum can be derived:

$$\mathrm{P}(s) = \frac{\Gamma(s)}{\mathrm{U}(s)} = \frac{1}{J_A s^2 - mgh} \tag{4.26}$$

By inspecting (4.26), it is evident that the system is inherently unstable as one pole of the system transfer function is in the right half s-plane (RHP).

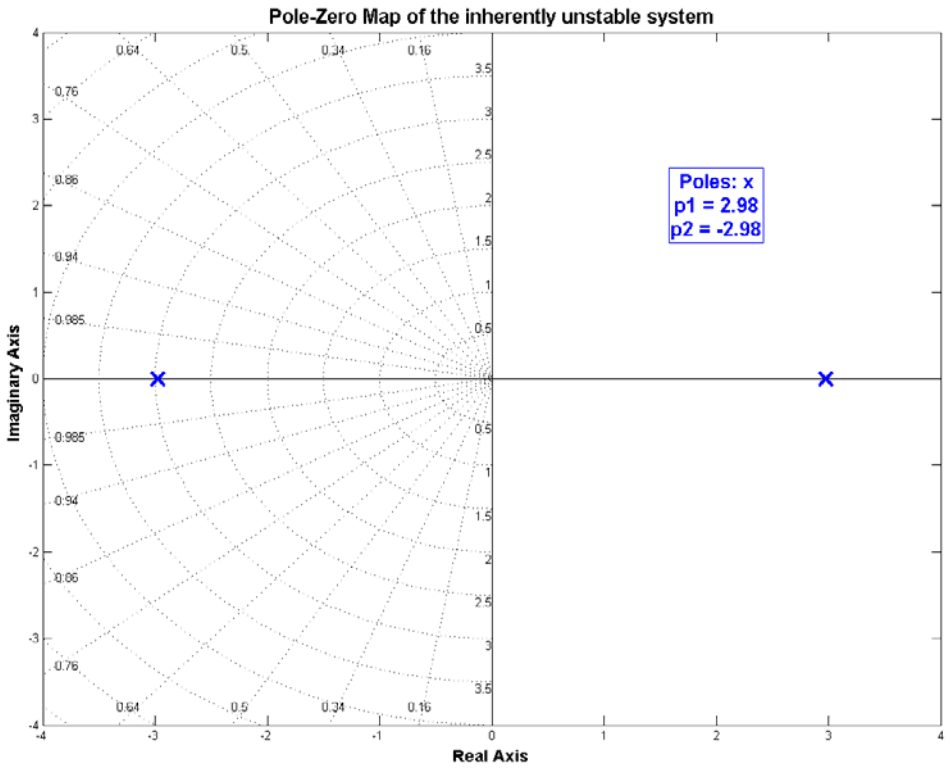

Figure 4.3 - Pole-Zero Map of the unstable inverted pendulum system

The poles of the system are equal to:

$$p_1 = +\sqrt{\frac{mgh}{J_A}} = 2.98$$
$$p_2 = -\sqrt{\frac{mgh}{J_A}} = -2.98 \tag{4.27}$$

and are shown in Figure 4.3, together with loci of constant damping factors and natural frequencies (dotted lines).

In order to stabilize the system dynamics a control strategy is required, so that the positive pole can be cancelled and possibly replaced to achieve the desired human-like behaviour.

Before examining the designed control scheme in detail, it may be helpful to write the inverted pendulum model in the state-space form.

Once the angular position and velocity of the COM have been chosen as state variables, it is straightforward to draw the system matrices:

$$\dot{\mathbf{x}} = \mathbf{A}\mathbf{x} + \mathbf{B}u$$
$$y = \mathbf{C}\mathbf{x} + Du \tag{4.28}$$

$$\begin{bmatrix} \dot{x}_1 \\ \dot{x}_2 \end{bmatrix} = \begin{bmatrix} \dot{\gamma} \\ \ddot{\gamma} \end{bmatrix} = \begin{pmatrix} 0 & 1 \\ \frac{mgh}{I_A} & 0 \end{pmatrix} \begin{bmatrix} x_1 \\ x_2 \end{bmatrix} + \begin{pmatrix} 0 \\ \frac{1}{I_A} \end{pmatrix} u$$
$$y = \begin{bmatrix} 1 & 0 \end{bmatrix} \begin{bmatrix} x_1 \\ x_2 \end{bmatrix} \tag{4.29}$$

where:

- $y = x_1 = \gamma$ (4.30)

  is the pendulum position compared with the vertical;
- $x_2 = \dot{\gamma}$ (4.31)

  is the pendulum angular velocity.
- $\mathbf{x} = \begin{bmatrix} x_1 \\ x_2 \end{bmatrix}$ (4.32)

  is the state of the system;

- $\mathbf{A} = \begin{pmatrix} 0 & 1 \\ \frac{mgh}{I_A} & 0 \end{pmatrix}$ (4.33)

  is the system matrix

- $\mathbf{B} = \begin{pmatrix} 0 \\ \frac{1}{I_A} \end{pmatrix}$ (4.34)

  is the input matrix,

- $u = T_C$ (4.35)

  is the input for the system, that is the controller torque.

- $\mathbf{C} = \begin{bmatrix} 1 \\ 0 \end{bmatrix}^T$ (4.36)

  is the output matrix,

- $D = 0$ (4.37)

  is the direct transmission term.

4.4.1 THE STATE-FEEDBACK PD CONTROL FOR STABILISING THE UNSTABLE SYSTEM

The first step in obtaining the desired control over the system dynamics is to increase its stiffness by feeding back the angular position and to add artificial damping by feeding back the angular velocity. That results in a classical Proportional-Derivative (PD) control scheme.

For achieving the preferred system response, the Proportional gain must satisfy the following condition:

$$K_P > mgh \tag{4.38}$$

Rather, the velocity or Derivative gain has to be selected depending on the desired damping ratio that dominates the overshoot and speed of response.

The inverted pendulum system (4.29) is controllable for any parameter. This means that any chosen dynamics of the system states can be

theoretically enforced by designing a suitable controller (namely selecting proper controller gains). This is equivalent to fix the poles of the system in a desired position and force it to mimic a desirable response.

In this work, the poles of the system have been selected in order to reproduce human behaviour observed during postural experiments. The values reported in [Peterka, 2002] and [Mahboobin et al., 2008] for the natural frequency (4.39)

$$\omega_n = 2.02 \text{ rad/s} \tag{4.39}$$

and the damping ratio (4.40)

$$\zeta = 1.06 \tag{4.40}$$

have been employed.
These values determine important features that characterise the response of the system in the time-domain. In particular, since

$$\zeta > 1 \tag{4.41}$$

the system is overdamped. Then, it is characterized by no overshoot, and long rise and settling times:

- rise time:
  $$t_r \cong 1.8/\omega_n = 0.89 \text{ s} \tag{4.42}$$
- settling times:
  $$t_s = 4.6/(\zeta \cdot \omega_n) = 2.15 \text{ s} \tag{4.43}$$

With the chosen natural frequency (4.39) and damping ratio (4.40), the resulting poles are:

$$p_{1,2} = -\sigma \pm j\omega_d = \begin{cases} p_1 = -1.43 \\ p_2 = -2.85 \end{cases} \tag{4.44}$$

where:

- $\sigma = \zeta \cdot \omega_n = 2.14$ (4.45)

  is the real part of the complex poles;

- $\omega_d = \omega_n \cdot \sqrt{1-\zeta^2} = 0 + j0.71$ (4.46)

  is the damped natural frequency of the system.

4.4.2 THE INTEGRAL CONTROL FOR ROBUST TRACKING

In addition to reproduce the "natural" behaviour of a person in quite standing condition, the proposed model has to mimic an individual standing on a moving platform that continuously tries to move back to the equilibrium position, namely the vertical.

To minimise steady-state errors and obtain robust tracking of a reference input, a compensation containing an integral term has to be introduced.

For the case study, the reference input coincides with assuring a zero lean angle with respect to the vertical direction:

$$r_\gamma = 0^\circ \tag{4.47}$$

The integral of the error

$$e = r_\gamma - \gamma \tag{4.48}$$

between the reference and the actual pendulum angle can be feed-back together with the state of the system (4.32). This is achieved by augmenting the system state with the new integral state

$$\begin{aligned} x_I &= \int^t \mathrm{e}\ dt = \int^t \left(r_\gamma - \gamma\right)\ dt \\ \dot{x}_I &= e = r_\gamma - \gamma \end{aligned} \tag{4.49}$$

The augmented system in the state-space form becomes:

$$\begin{aligned} \begin{bmatrix} \dot{\mathbf{x}} \\ \dot{x}_I \end{bmatrix} &= \begin{bmatrix} 0 & \mathbf{A} \\ 0 & \mathbf{H} \end{bmatrix} \begin{bmatrix} \mathbf{x} \\ x_I \end{bmatrix} + \begin{bmatrix} \mathbf{B} \\ 0 \end{bmatrix} u + \begin{bmatrix} \mathbf{0} \\ 1 \end{bmatrix} r \\ \begin{bmatrix} \dot{x}_1 \\ \dot{x}_2 \\ \dot{x}_I \end{bmatrix} &= \begin{bmatrix} 0 & 1 & 0 \\ \dfrac{mgh}{I_A} & 0 & 0 \\ -1 & 0 & 0 \end{bmatrix} \begin{bmatrix} x_1 \\ x_2 \\ x_I \end{bmatrix} + \begin{bmatrix} 0 \\ \dfrac{1}{I_A} \\ 0 \end{bmatrix} u + \begin{bmatrix} 0 \\ 0 \\ 1 \end{bmatrix} r \end{aligned} \tag{4.50}$$

The total feedback low, including both the PD and the Integral parts, is:

$$u = -\mathbf{K} \begin{bmatrix} \dot{\mathbf{x}} \\ \dot{x}_I \end{bmatrix} = -\begin{bmatrix} \mathbf{K}_{PD} & K_I \end{bmatrix} \begin{bmatrix} \dot{\mathbf{x}} \\ \dot{x}_I \end{bmatrix} = -\begin{bmatrix} K_P & K_D & K_I \end{bmatrix} \begin{bmatrix} x_1 \\ x_2 \\ x_I \end{bmatrix} \tag{4.51}$$

or, correspondingly,

$$T_C(t) = -\left(K_P \gamma(t) + K_D \dot{\gamma}(t) + K_I \int^t \left(r_\gamma(t) - \gamma(t)\right)\ dt\right) \tag{4.52}$$

From a theoretical perspective, two alternative schemes exist for implementing a PID controller.

Many authors (e.g. [Mergner, 2004], [Peterka, 2002]) proposed the classical design with the PID or PD controller inserted in series (cascade) with the plant or system (human inverted pendulum). In this way, the tracking error is feed-back to the whole controller. According to Tahboub [2009], this choice undermines the overall damping of the system, due to its intrinsic instability.

On the other hand, to let only the Integral part act on the tracking error (4.48) allow implementing the classical "robust tracking control scheme" [Franklin et al., 1994]. At the same time, the state-feedback part involving the PD controller allows stabilising the originally unstable system (also see

[Tahboub, 2009]). This scheme produces limited and smoother control action than the classical cascade form [Bolzern et al., 1998]. This is an important requirement for system with time delays, like the human postural control system, in order to avoid the occurrence of instability.

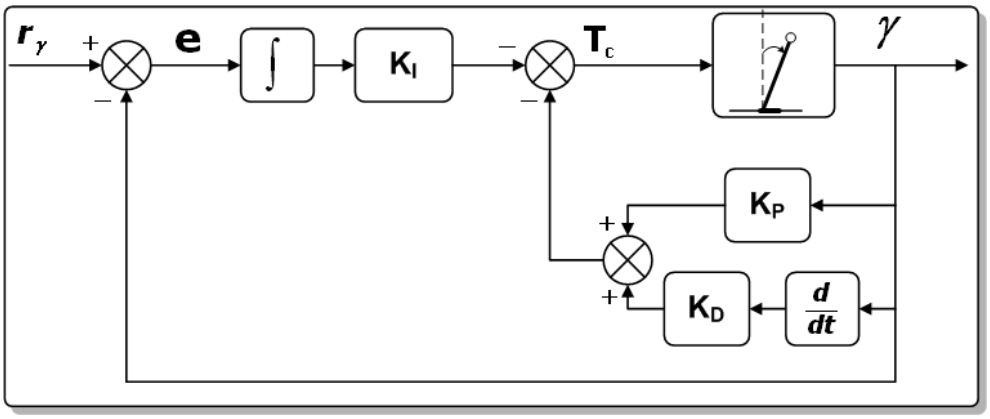

Figure 4.4 – Modelling the human postural control system: State-feedback PD and Integral Tracking control

The transfer function of the complete system, made up of the plant (human inverted pendulum) and the PID controller (PD terms in parallel and Integral part in cascade with the plant, Figure 4.4), from the output γ to the reference angle r_γ results:

$$\frac{\Gamma(s)}{R(s)} = \frac{-K_I}{J_A s^3 + K_D s^2 + (K_P - mgh)s - K_I} \tag{4.53}$$

Since the augmented system (4.50) is still controllable, the values of the controller gains can be selected for assuring any chosen system dynamics.

The gains have been then set to fix two of the three poles of the closed loop system at $p_1 = -1.43$ and $p_2 = -2.85$ for fitting the requirements discussed in the previous section.

The third pole has been chosen conservatively for keeping low the values of the controller gains. Otherwise stability would occur [Tahboub, 2009]. Moreover, an additional pole in the left half-plane would increase the rise time significantly if the extra pole is within a factor of 4 of the real part of the complex poles [Franklin et al., 1994]. In the present case, the poles are real,

and the third pole has been then assigned starting from the poles (4.27) of the instable system (4.26):

$$p_3 = -2.98/4.5 = -0.66 \tag{4.54}$$

The resulted gains, determined with pole-placement method, are:

- $K_P = 1230.56$ Nm/rad (4.55)
- $K_D = 385.54$ Nms/rad (4.56)
- $K_I = -210.55$ Nm/rads (4.57)

The poles for the controlled system in the s-plane are shown in Figure 4.5. The locus of constant damping factor $\zeta = 1.06$ and natural frequency $\omega_n = 2.02$ rad/s, as chosen for the human inverted pendulum system, is also drawn.

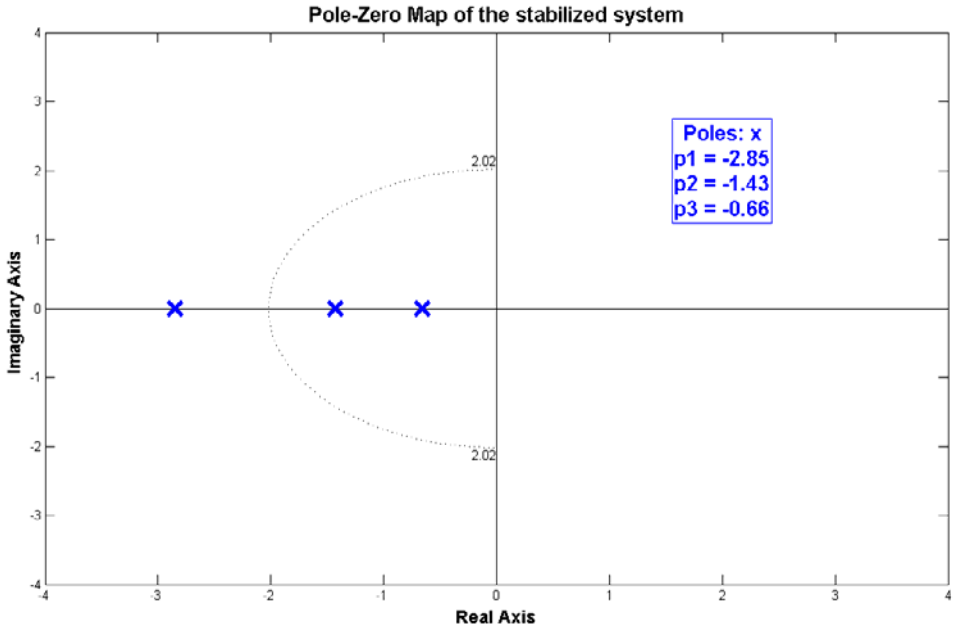

Figure 4.5 - Pole-Zero Map of the stabilised inverted pendulum system

Figure 4.6 shows the frequency response plot (magnitude and phase) of system (4.53).

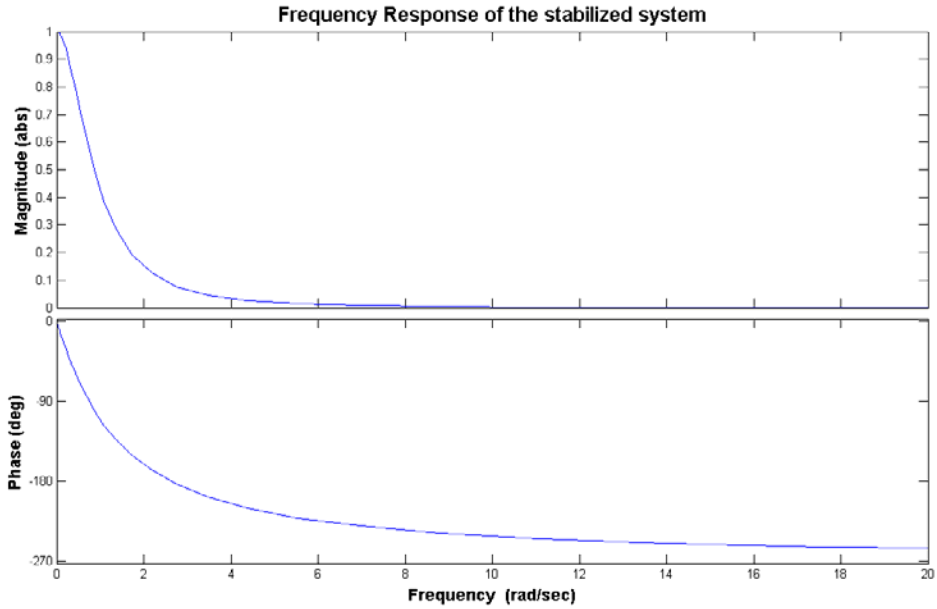

Figure 4.6 - Frequency response of the stabilised inverted pendulum system

4.4.3 THE FEED-FORWARD CONTROLLER FOR ANTICIPATORY RESPONSE

As reported in [Tahboub, 2009], the decision of keeping low the gains of the PID controller can lead to a system characterised by slow response and weak tracking abilities.

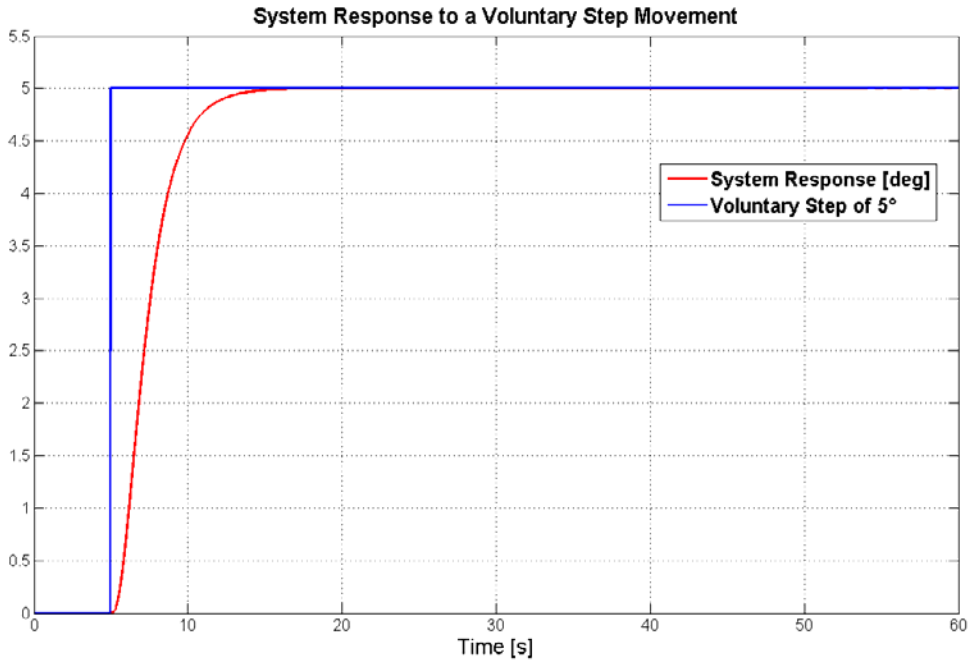

Figure 4.7 - Response to a desired voluntary step of 5°

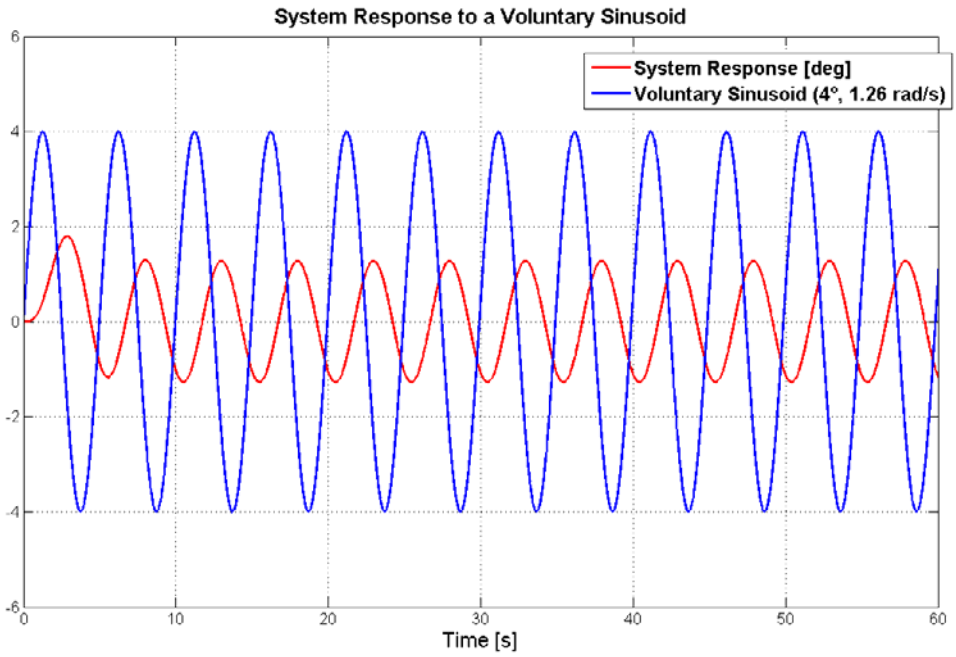

Figure 4.8 - Response to a desired voluntary sinusoid of 4° and 1.26 rad/s

For example, in Figure 4.7 and Figure 4.8 the response of the system to voluntary motions is shown.

The choice of the reference inputs used for the simulation is not fortuitous, rather it is based on the work by Tahboub [2009].

In the case of a voluntary step of 5° (Figure 4.7), the system responds with a zero overshoot and approximately 10-s rise time.

When the desired voluntary motion is a sinusoid (Figure 4.8), the system is not able to track the reference signal, showing lower amplitude and phase lag.

To improve the system tracking characteristics feed-forward terms can be added.

As already discussed in section 3.5.1, feed-forward control can explain the anticipatory response to expected or predictable external disturbances, such as, for example, the anticipatory body inclination of standing passengers before the train or the bus starts. Feed-forward terms also account for learning ability in executing allotted working tasks.

The control law has been modified for including feed-forward control, resulting in:

$$T_C(t) = -\left(K_P\gamma(t) + K_D\dot{\gamma}(t) + K_I\int^t\left(r_\gamma(t) - \gamma(t)\right)\,dt\right) + \\ +K_{P_{ff}}r_\gamma(t) + K_{D_{ff}}\dot{r}_\gamma(t) \tag{4.58}$$

In this case, the transfer function of the system, made up of the plant (human inverted pendulum) and both the PID and feed-forward controllers, from the output γ to the reference angle r_γ is:

$$\frac{\Gamma(s)}{R(s)} = \frac{K_{D_{ff}}s^2 + K_{P_{ff}}s - K_I}{J_A s^3 + K_D s^2 + (K_P - mgh)s - K_I} \tag{4.59}$$

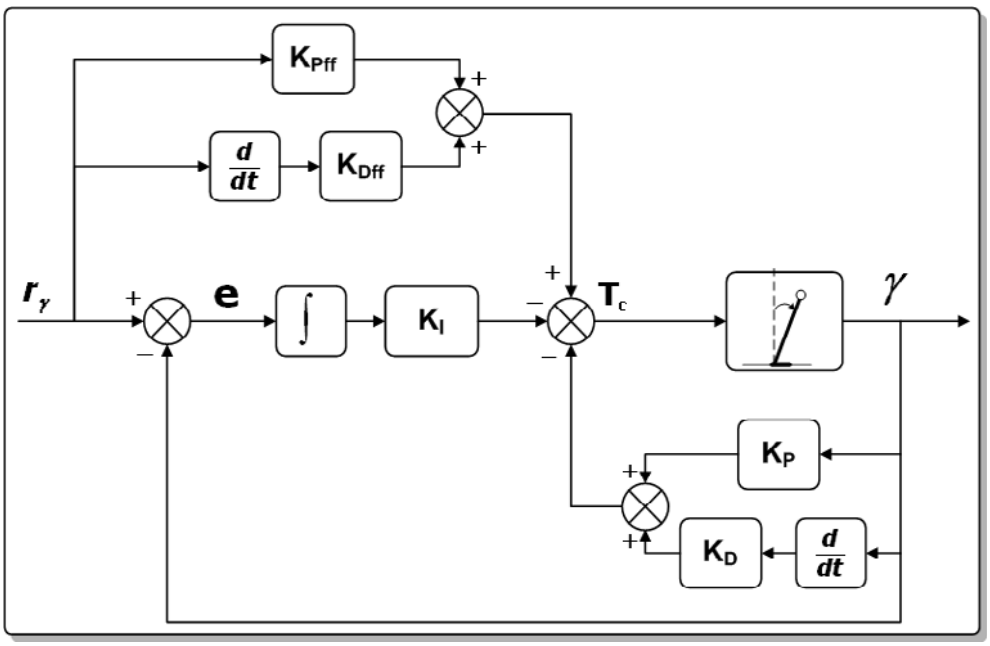

Figure 4.9 - Modelling the human postural control system: State-feedback PD control, Integral Tracking and Feed-Forward control

By inspecting (4.59), it is evident that including feed-forward terms add two zeros to the original system, whose position in the s-plane depends on the values assigned to the feed-forward gains.

Additional zeros effect the system response [Franklin et al., 1994].

For assessing the consequence of this additional control effort on system dynamics, different values of stiffness and damping feed-forward contributions have been tested.

As first choice, $K_{D_{ff}}$ and $K_{P_{ff}}$ have been fixed in order to reproduce "passive" control effort due to muscle torque (see section 3.5.1), that is equal to the ten percent of K_D and K_P:

- $K_{P_{ff}} = 10\%K_P = 123.06$ Nm/rad (4.60)
- $K_{D_{ff}} = 10\%K_D = 38.55$ Nms/rad (4.61)

It has to be pointed out that researchers (e.g. [Peterka, 2002]) have proposed to model passive control by adding a second feedback loop to the original postural control system with PID controller (section 3.5.1). They also found that this additional feedback control action did not increase significantly the accuracy of the whole model.

In the author's opinion, the passive torque generated by muscles can be viewed as an automatic reaction and, therefore, can be included as well in the anticipatory feed-forward control effort.

Figure 4.10 and Figure 4.11 show the frequency response and the position of the zeros due to the additional feed-forward path, respectively.

As shown in Figure 4.12 and Figure 4.13, the selected values for $K_{D_{ff}}$ and $K_{P_{ff}}$ does not change significantly the dynamics of the system, as far as the overshoot, response amplitude and rise time are concerned. On the other hand, the phase lag is slightly reduced.

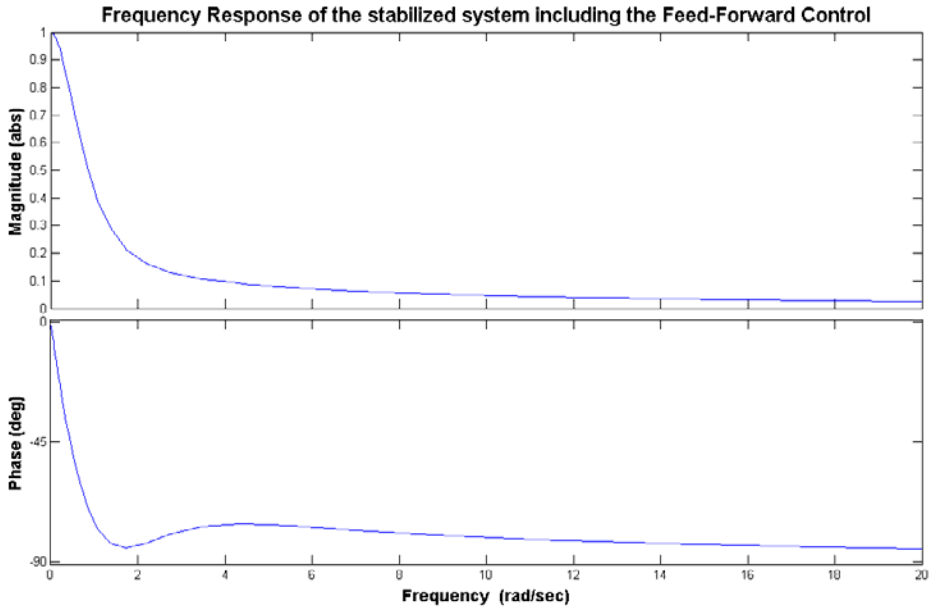

Figure 4.10 - Frequency response of the stabilised inverted pendulum system with Feed-Forward controller $\left(K_{P_{ff}} = 10\%K_P, K_{D_{ff}} = 10\%K_D\right)$

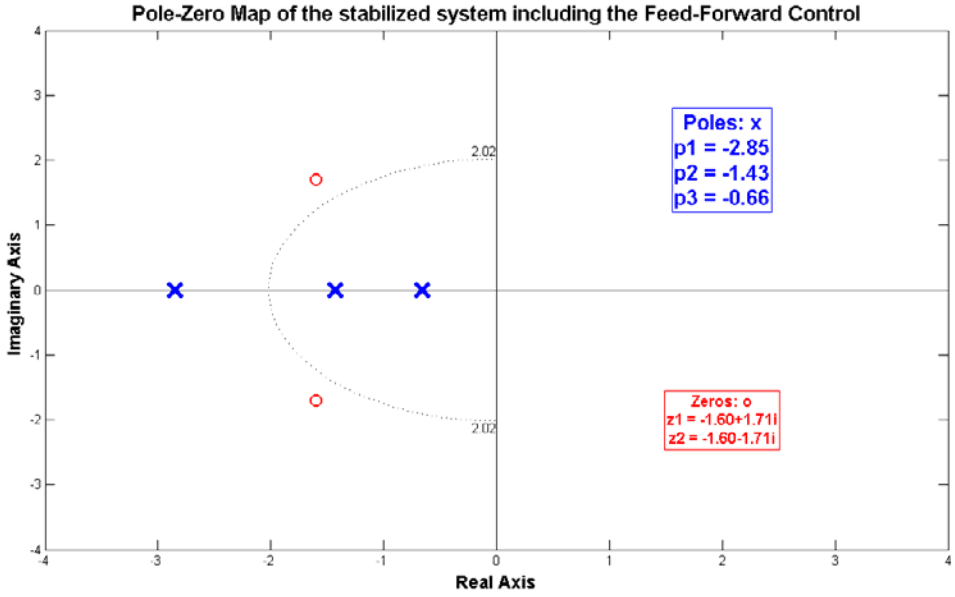

Figure 4.11 - Pole-Zero Map of the stabilised inverted pendulum system with Feed-Forward controller $\left(K_{P_{ff}} = 10\%K_P, K_{D_{ff}} = 10\%K_D\right)$

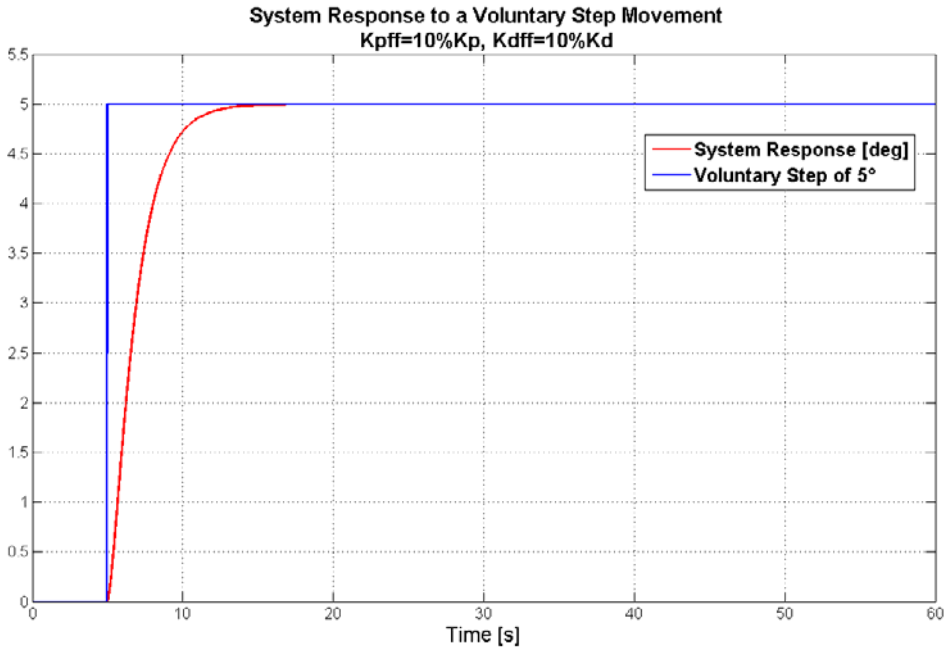

Figure 4.12 - Response to a desired voluntary step of 5° with Feed-Forward controller $\left(K_{P_{ff}} = 10\%K_P, K_{D_{ff}} = 10\%K_D\right)$

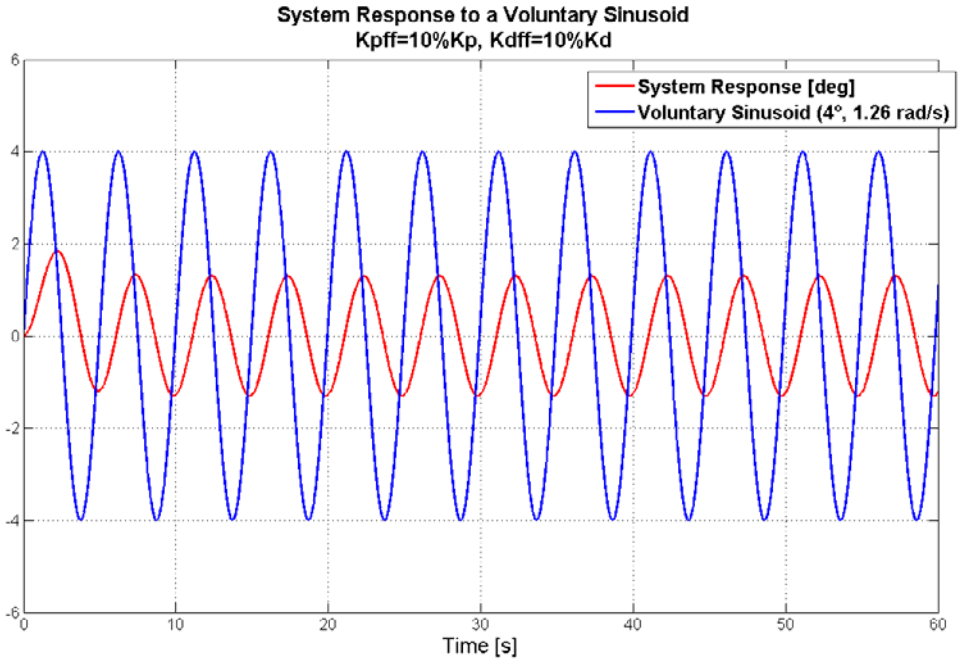

Figure 4.13 - Response to a desired voluntary sinusoid of 4° and 1.26 rad/s with Feed-Forward controller $\left(K_{P_{ff}} = 10\%K_P, K_{D_{ff}} = 10\%K_D\right)$

For improving the system tracking response, $K_{D_{ff}}$ and $K_{P_{ff}}$ have been then varied on the basis of the values proposed by Tahboub [2009]. In that work,

the feed-forward gains have been fixed to produce a desirable tracking response to a voluntary step movement of 5° and a sinusoidal voluntary motion of 4° at 1.26 rad/s.

The resulted values for $K_{D_{ff}}$ and $K_{P_{ff}}$ are respectively:

- $K_{P_{ff}} = 18\%K_P = 221.50$ Nm/rad (4.62)
- $K_{D_{ff}} = 93\%K_D = 358.55$ Nms/rad (4.63)

The frequency response and the position of the additional zeros corresponding to the chosen parameters are shown in Figure 4.14 and Figure 4.15.

In this case, the rise time is approximately 9.3 seconds (Figure 4.16) and the phase lag is cancelled (Figure 4.17).

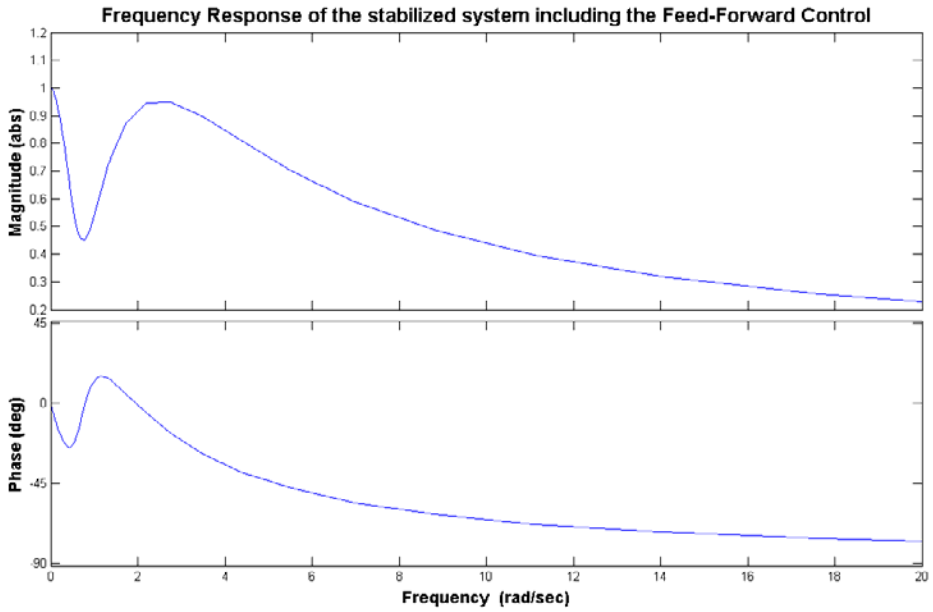

Figure 4.14 - Frequency response of the stabilised inverted pendulum system with Feed-Forward controller $\left(K_{P_{ff}} = 18\%K_P, K_{D_{ff}} = 93\%K_D\right)$

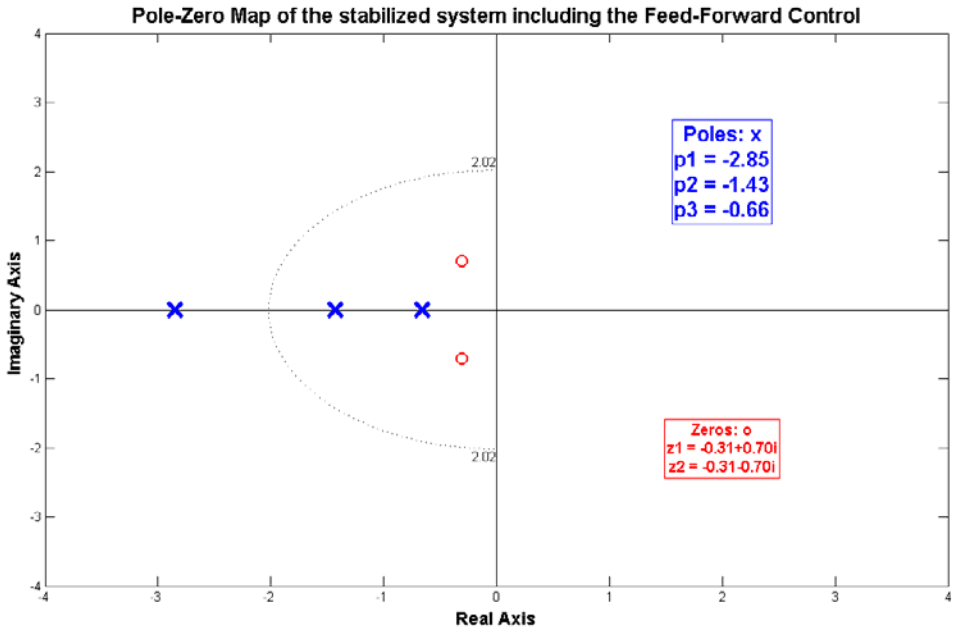

Figure 4.15 - Pole-Zero Map of the stabilised inverted pendulum system with Feed-Forward controller $\left(K_{P_{ff}} = 18\%K_P, K_{D_{ff}} = 93\%K_D\right)$

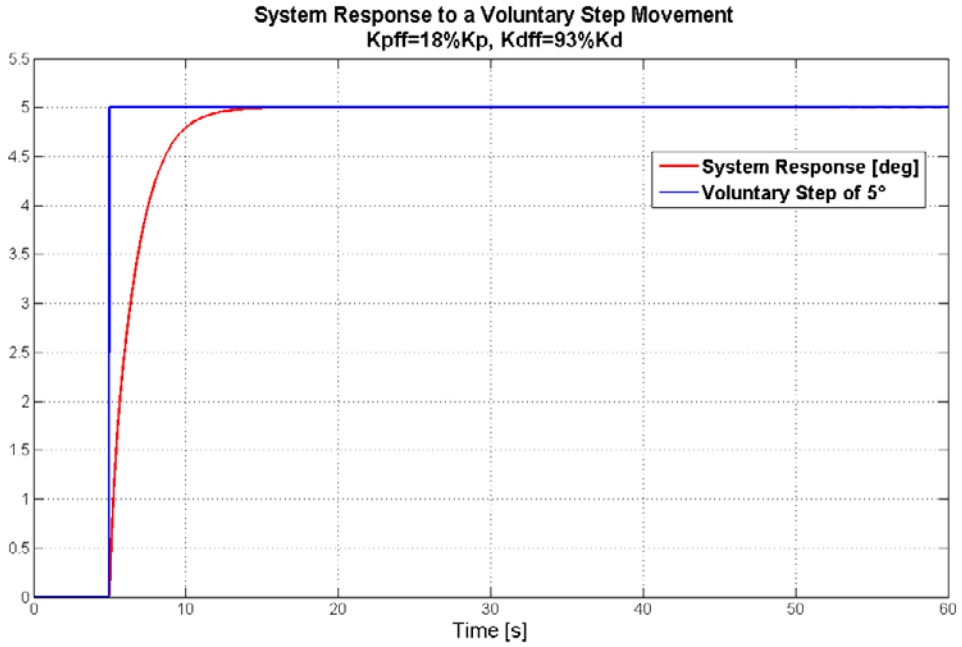

Figure 4.16 - Response to a desired voluntary step of 5° with Feed-Forward controller $\left(K_{P_{ff}} = 18\%K_P, K_{D_{ff}} = 93\%K_D\right)$

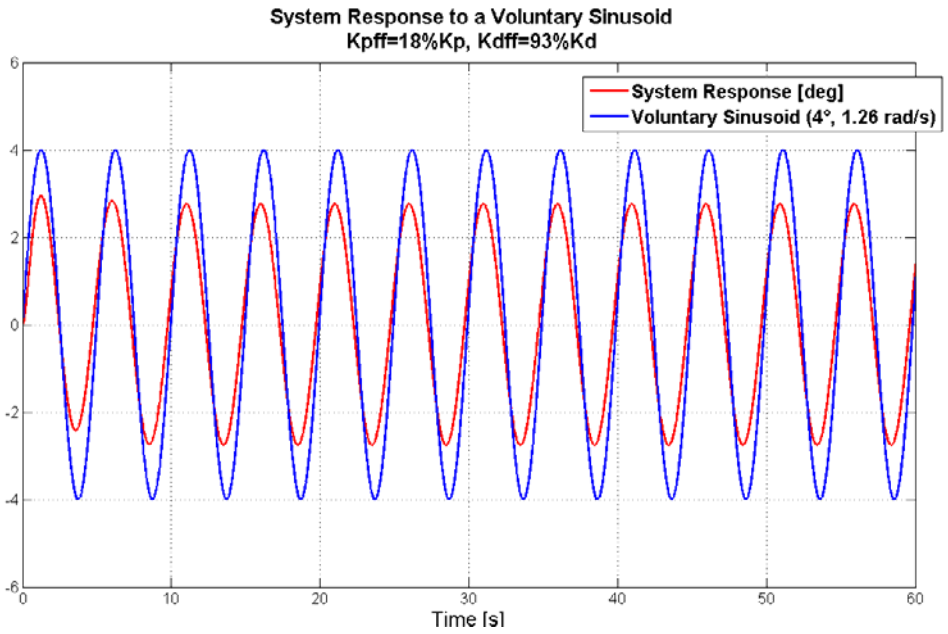

Figure 4.17 - Response to a desired voluntary sinusoid of 4° and 1.26 rad/s with Feed-Forward controller $\left(K_{P_{ff}} = 18\%K_P, K_{D_{ff}} = 93\%K_D\right)$

The best tracking performance to a voluntary step motion is achieved by assuming the feed-forward parameters to be equal to:

- $K_{P_{ff}} = 30\%K_P = 369.17$ Nm/rad (4.64)
- $K_{D_{ff}} = 95\%K_D = 366.26$ Nms/rad (4.65)

The zeros introduced by the feed-forward path move closer the real pole of the inverted pendulum system with PID controller (Figure 4.19). As shown in Figure 4.20 and Figure 4.21, this configuration increases system overshoot, reduces significantly the rise time (about 6.4 seconds) and produces a satisfying response to the sinusoidal motion.

Increasing the value of the stiffness feed-forward contribution results in considerable undesirable overshoot (Figure 4.24, Figure 4.25):

- $K_{P_{ff}} = 50\%K_P = 615.28$ Nm/rad (4.66)

- $K_{D_{ff}} = 95\%K_D = 366.26$ Nms/rad (4.67)

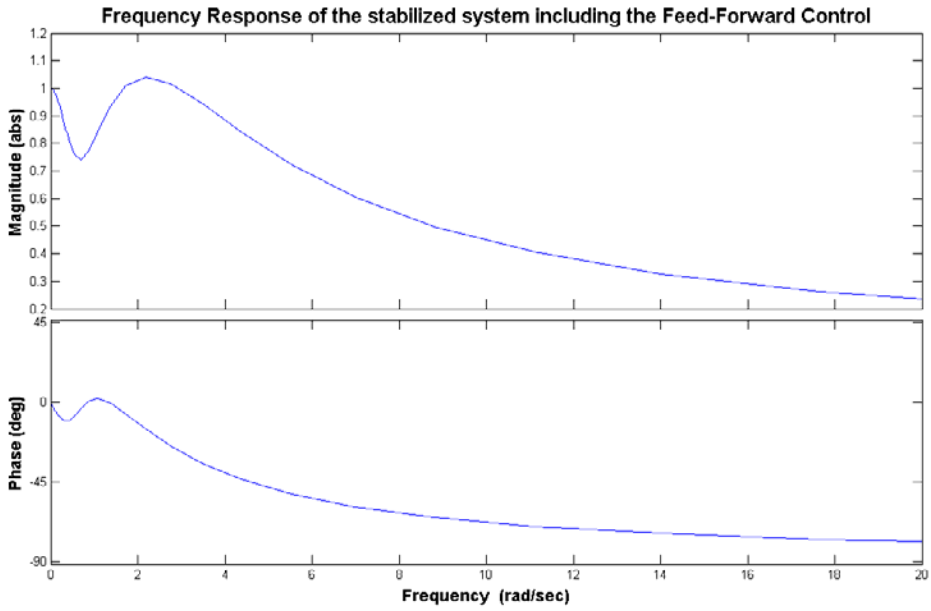

Figure 4.18 - Frequency response of the stabilised inverted pendulum system with Feed-Forward controller $\left(K_{P_{ff}} = 30\%K_P, K_{D_{ff}} = 95\%K_D\right)$

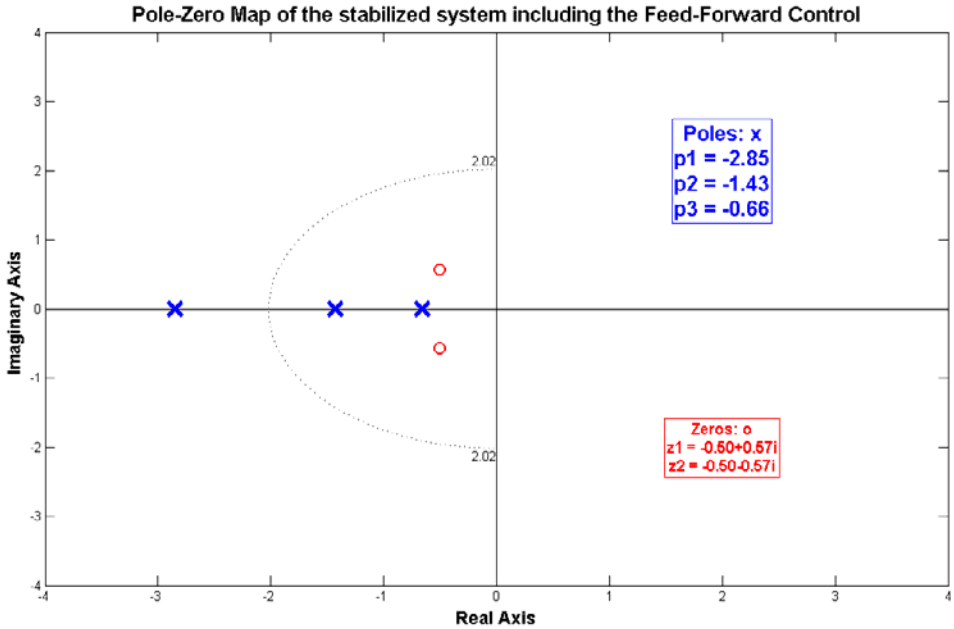

Figure 4.19 - Pole-Zero Map of the stabilised inverted pendulum system with Feed-Forward controller $\left(K_{P_{ff}} = 30\%K_P, K_{D_{ff}} = 95\%K_D\right)$

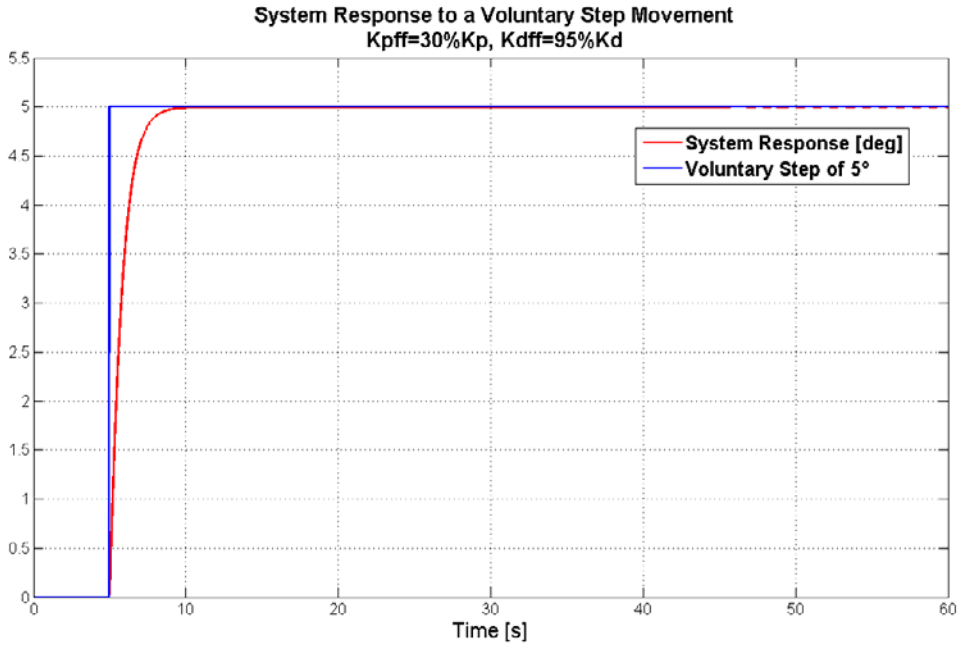

Figure 4.20 - Response to a desired voluntary step of 5° with Feed-Forward controller $\left(K_{P_{ff}} = 30\%K_P, K_{D_{ff}} = 95\%K_D\right)$

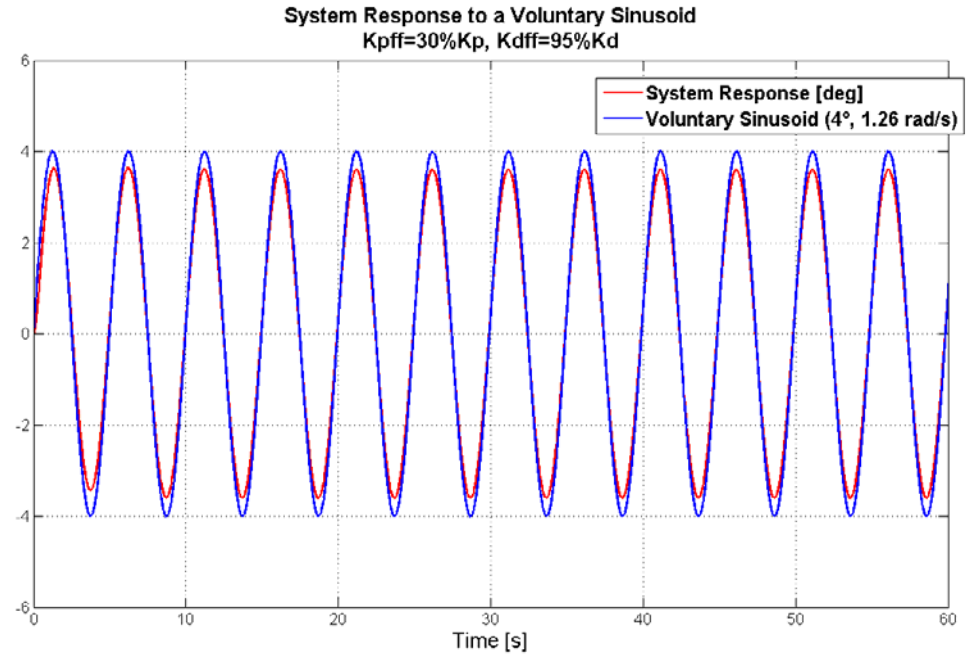

Figure 4.21 - Response to a desired voluntary sinusoid of 4° and 1.26 rad/s with Feed-Forward controller $\left(K_{P_{ff}} = 30\%K_P, K_{D_{ff}} = 95\%K_D\right)$

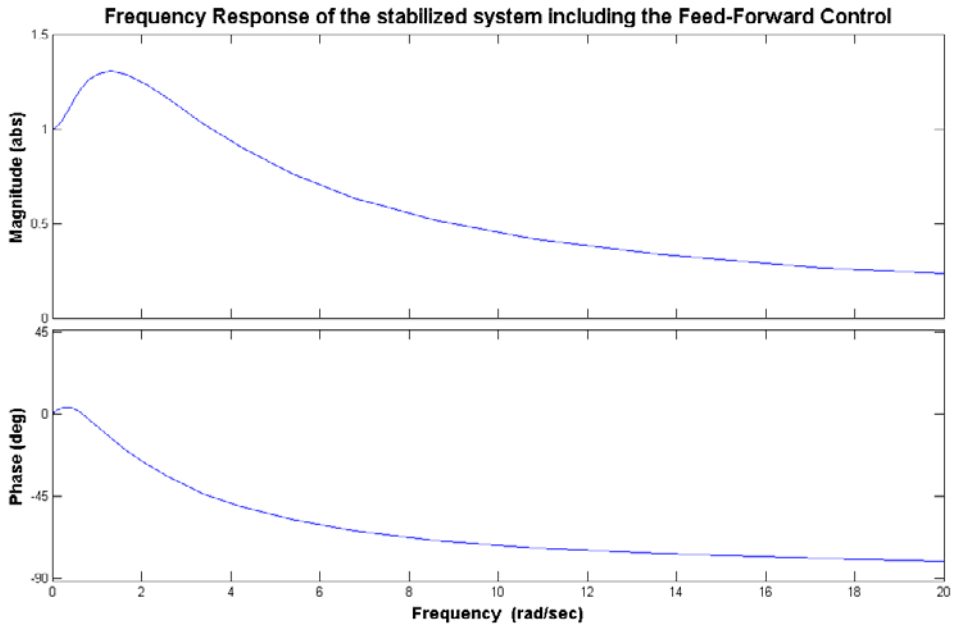

Figure 4.22 - Frequency response of the stabilised inverted pendulum system with Feed-Forward controller $\left(K_{P_{ff}} = 50\%K_P, K_{D_{ff}} = 95\%K_D\right)$

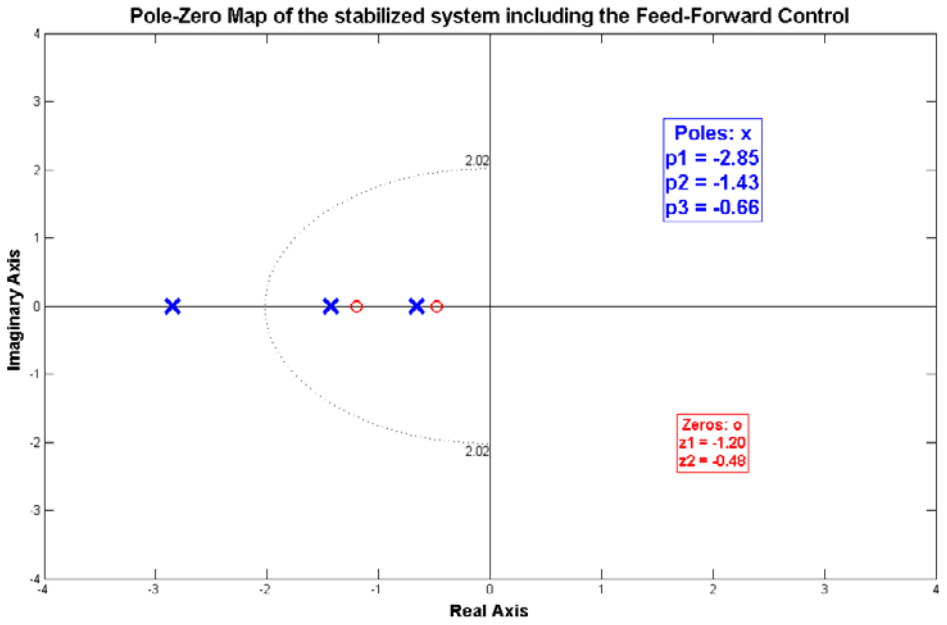

Figure 4.23 - Pole-Zero Map of the stabilised inverted pendulum system with Feed-Forward controller $\left(K_{P_{ff}} = 50\%K_P, K_{D_{ff}} = 95\%K_D\right)$

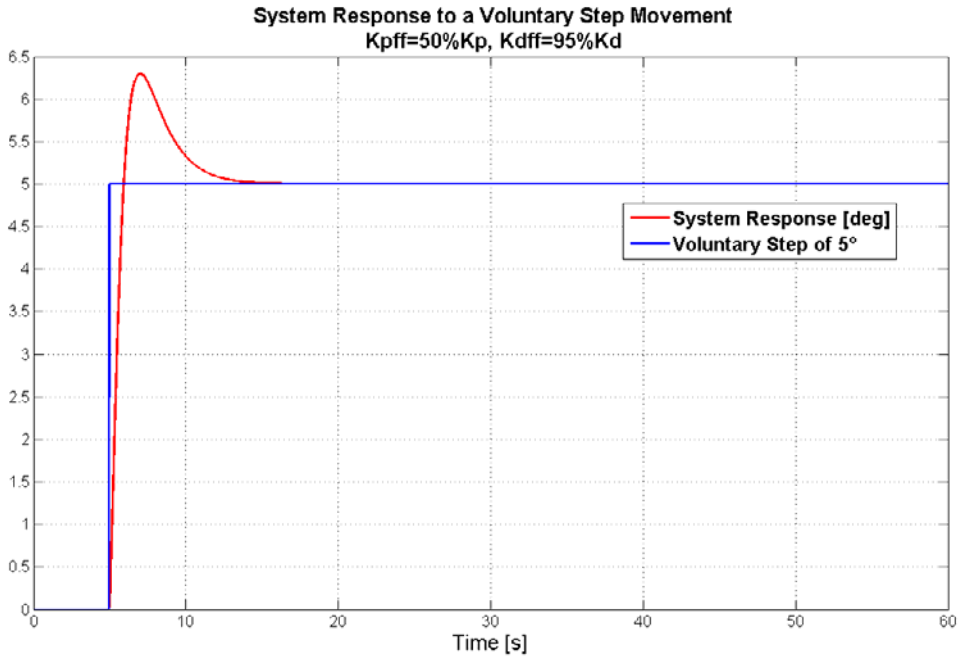

Figure 4.24 - Response to a desired voluntary step of 5° with Feed-Forward controller $\left(K_{P_{ff}} = 50\%K_P, K_{D_{ff}} = 95\%K_D\right)$

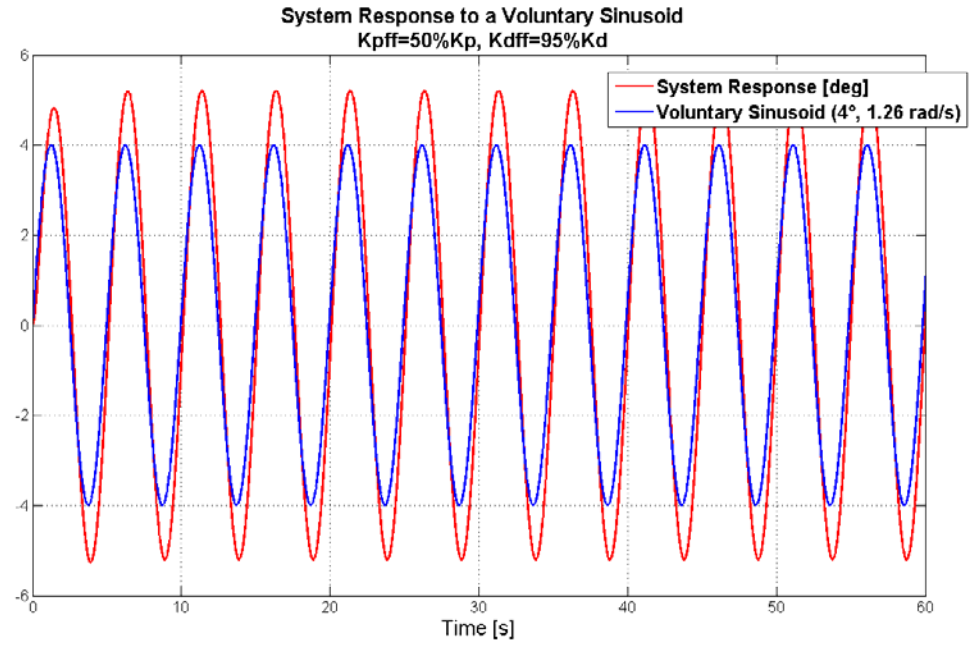

Figure 4.25 - Response to a desired voluntary sinusoid of 4° and 1.26 rad/s with Feed-Forward controller $\left(K_{P_{ff}} = 50\%K_P, K_{D_{ff}} = 95\%K_D\right)$

The values for feed-forward contributions that produce the best tracking response to a voluntary sinusoid motion of 4° and 1.26 rad/s are respectively (Figure 4.26):

- $K_{P_{ff}} = 35\%K_P = 430.70$ Nm/rad (4.68)
- $K_{D_{ff}} = 93\%K_D = 358.55$ Nms/rad (4.69)

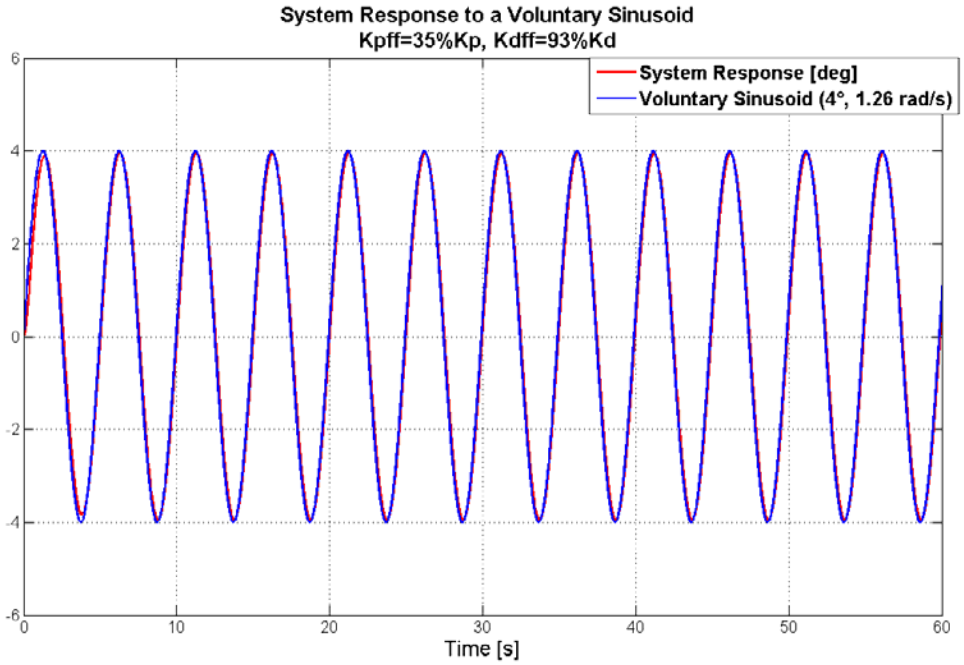

Figure 4.26 - Response to a desired voluntary sinusoid of 4° and 1.26 rad/s with Feed-Forward controller $\left(K_{P_{ff}} = 35\%K_P, K_{D_{ff}} = 93\%K_D\right)$

The values (4.68) and (4.69) have also been tested changing the parameters for the voluntary sinusoid motion. The results show that the tracking performance varies with the frequency characterising the input signal (from Figure 4.27 to Figure 4.30).

The analysis of the frequency response (Figure 4.18) also stressed the same outcomes.

The examples here reported show that the contribution of feed-forward control produces the desired tracking ability, but it has to be varied (or adapted) as the dynamics of voluntary motion change.

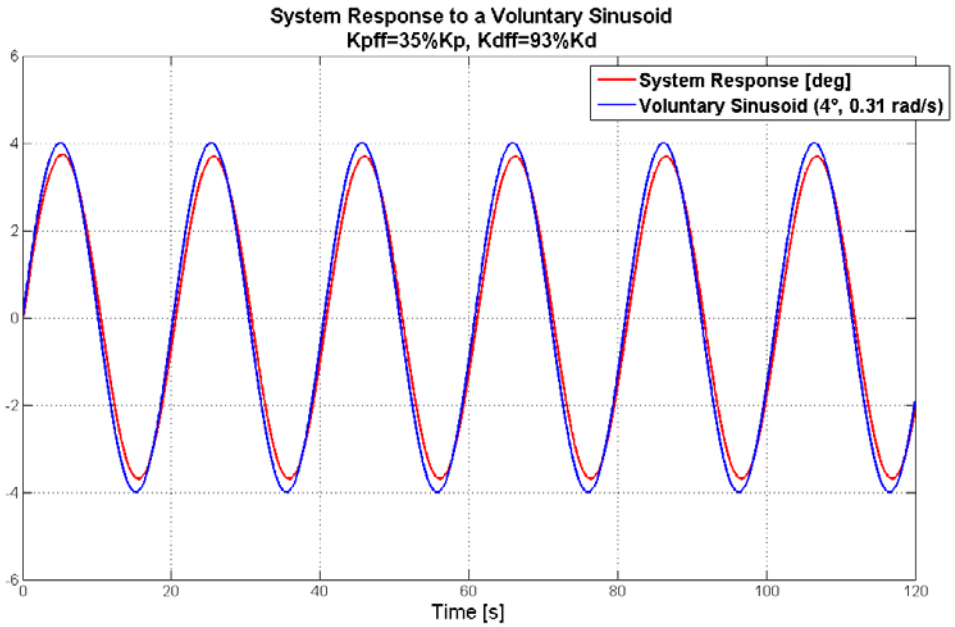

Figure 4.27 - Response to a desired voluntary sinusoid of 4° and 0.31 rad/s with Feed-Forward controller $\left(K_{P_{ff}} = 35\%K_P, K_{D_{ff}} = 93\%K_D\right)$

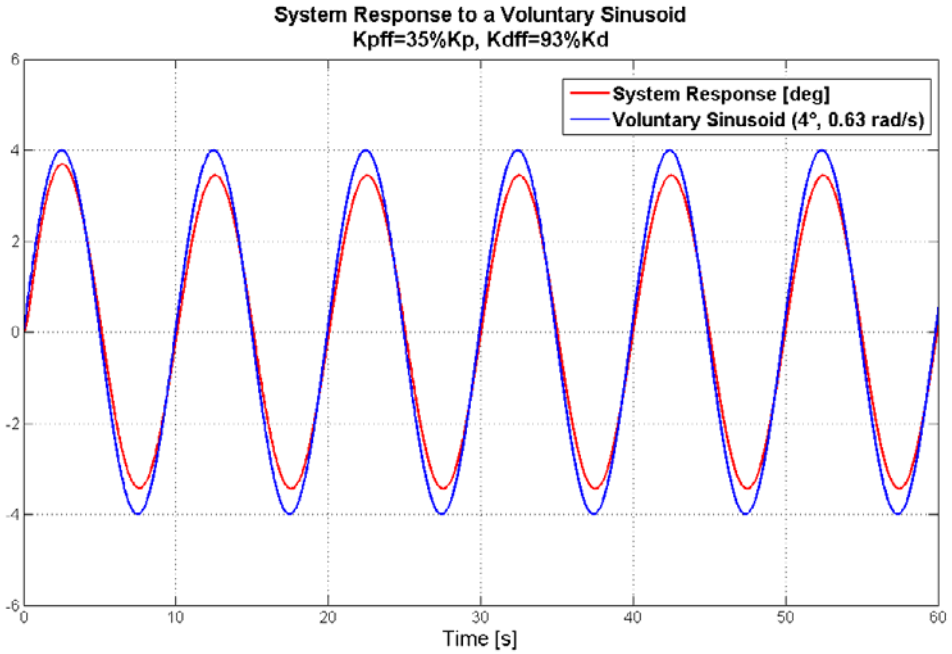

Figure 4.28 - Response to a desired voluntary sinusoid of 4° and 0.63 rad/s with Feed-Forward controller $\left(K_{P_{ff}} = 35\%K_P, K_{D_{ff}} = 93\%K_D\right)$

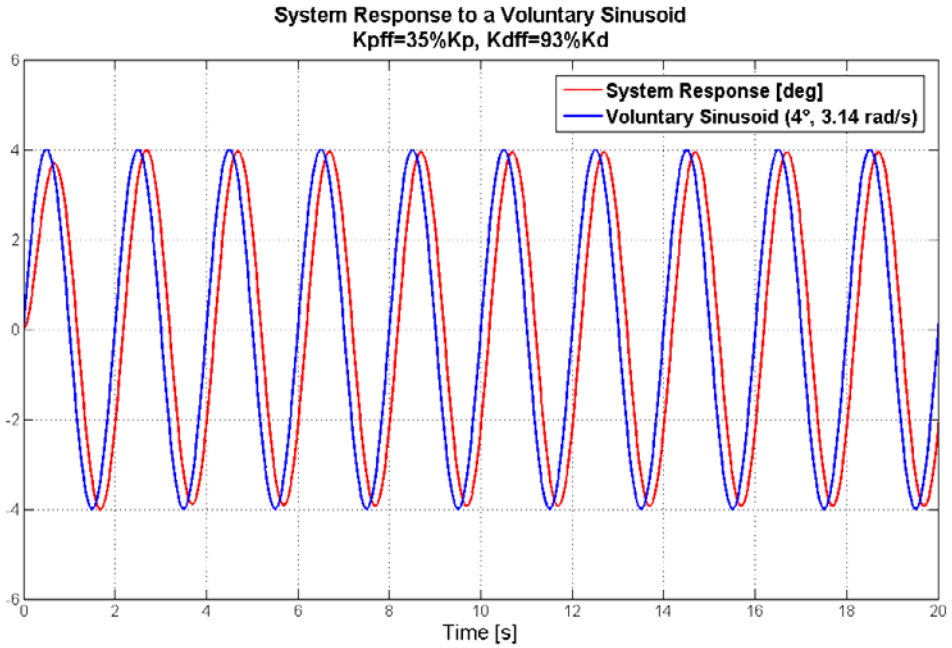

Figure 4.29 - Response to a desired voluntary sinusoid of 4° and 3.14 rad/s with Feed-Forward controller $\left(K_{P_{ff}} = 35\%K_P, K_{D_{ff}} = 93\%K_D\right)$

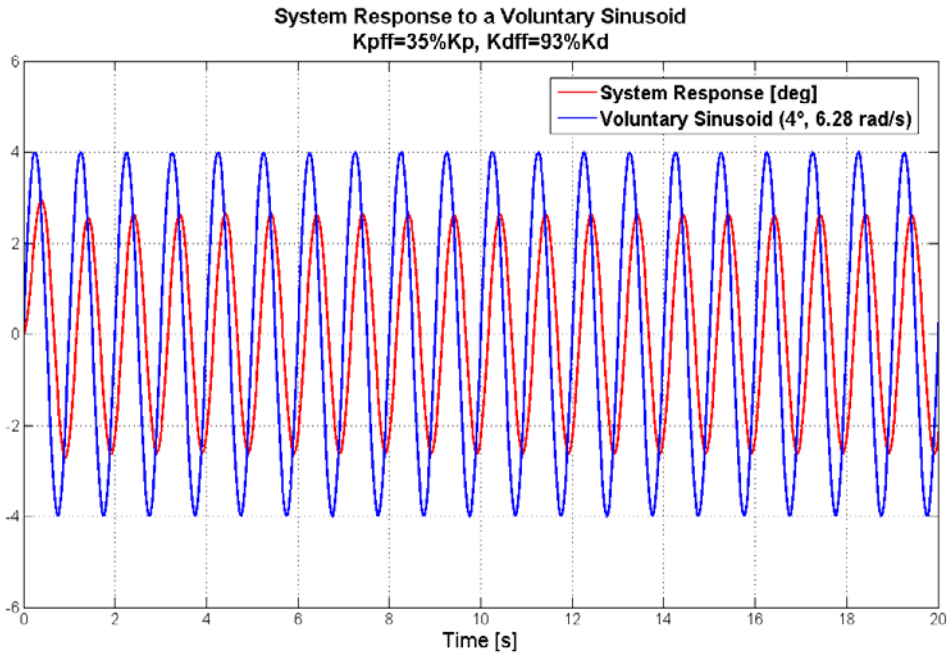

Figure 4.30 - Response to a desired voluntary sinusoid of 4° and 6.28 rad/s with Feed-Forward controller $\left(K_{P_{ff}} = 35\%K_P, K_{D_{ff}} = 93\%K_D\right)$

4.5 MODELLING THE POSTURAL CONTROL SYSTEM: ESTIMATION OF SHIP MOTIONS

The postural control scheme discussed above, made up of three components (PD controller for stabilising the naturally unstable system, Integral part for robust tracking, Feed-Forward for anticipatory control), has to be completed to face external disturbances like ship motions (Figure 4.31).

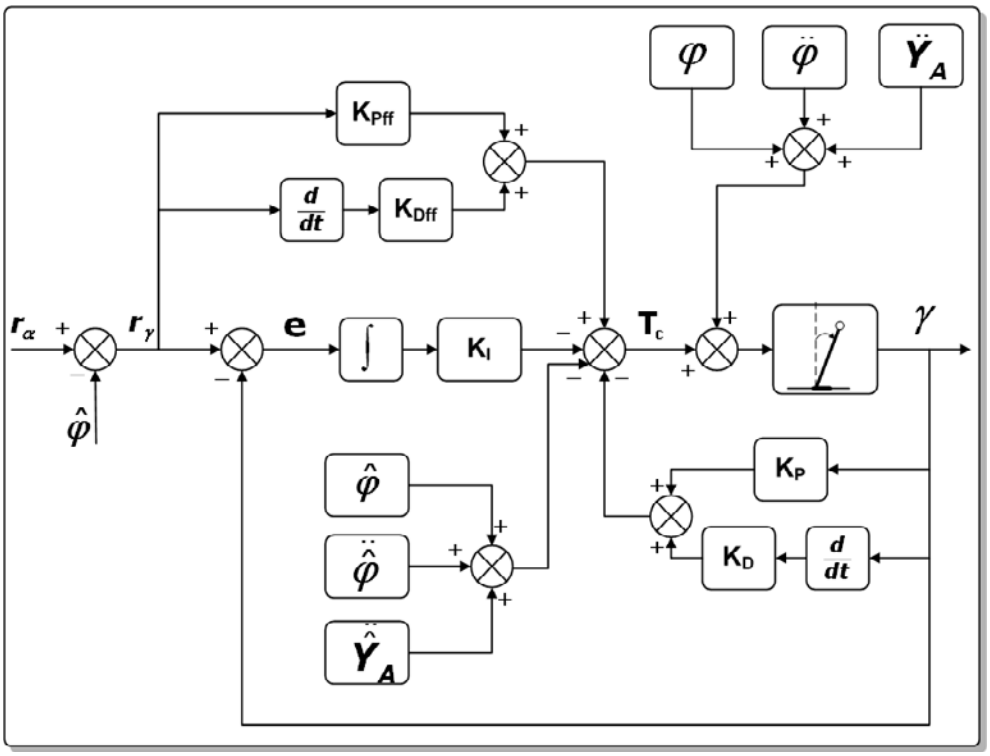

Figure 4.31 - Modelling the human postural control system: State-feedback PD control, Integral Tracking, Feed-Forward control and ship motion Estimation

As reported in (section 3.5.1), several studies demonstrated that the human postural control system can estimate platform motions (tilt and acceleration), as well as external forces, and compensate for their destabilising effects. Diverse control schemes for reproducing the mechanisms underlying the estimation, representation and compensation of external disturbances have been suggested. In this work, the estimation method proposed by Tahboub

([Tahboub, 2009], [Tahboub & Mergner, 2007]) has been followed and modified for taking into account the specific issues of interest.

The starting idea is that the ship motions in equation (4.18) here repeated:

$$J_A\left(\ddot{\gamma}(t)+\ddot{\varphi}(t)\right) - mgh\left(\gamma(t)+\varphi(t)\right)-mh\ddot{Y}_A(t)= T_C(t) \tag{4.70}$$

are for the human postural control system external unknown disturbances, that have to be estimated and counterbalanced.

Also Figure 4.1 is here (partly) reproduced for making the analysis of the following section easier:

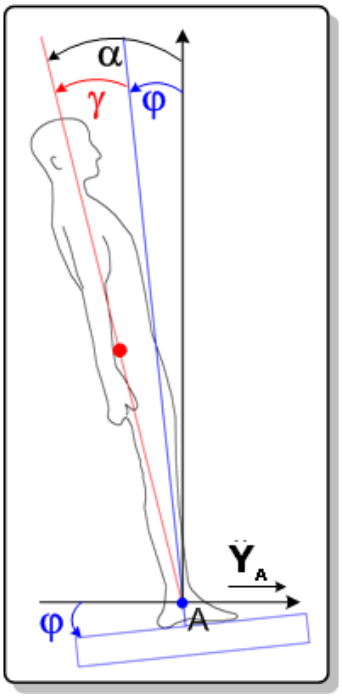

Figure 4.32 – A single inverted-pendulum model representing a crewmember standing on a moving deck. (after [Tahboub, 2009])

where:

- γ is the leaning angle from the ankle joint;
- φ is the deck roll angle;
- α is the inclination angle of body COM relative to the vertical;
- $\ddot{Y}_A$ is the deck lateral acceleration;

Equation (4.70) can be written in the state-space form

$$\begin{aligned}\dot{\mathbf{x}} &= \mathbf{A}\mathbf{x} + \mathbf{B}u + \mathbf{W}_1\mathbf{w}_1 + \mathbf{W}_2\mathbf{w}_2 \\ y &= \mathbf{C}\mathbf{x}\end{aligned} \tag{4.71}$$

$$\begin{aligned}\begin{bmatrix}\dot{x}_1 \\ \dot{x}_2\end{bmatrix} = \begin{bmatrix}\dot{\gamma} \\ \ddot{\gamma}\end{bmatrix} &= \begin{pmatrix}0 & 1 \\ \dfrac{mgh}{I_A} & 0\end{pmatrix}\begin{bmatrix}x_1 \\ x_2\end{bmatrix} + \begin{pmatrix}0 \\ \dfrac{1}{I_A}\end{pmatrix}u + \begin{pmatrix}0 & 0 & 0 \\ \dfrac{mgh}{I_A} & 0 & -1\end{pmatrix}\begin{bmatrix}w_1 \\ \dot{w}_1 \\ \ddot{w}_1\end{bmatrix} + \begin{pmatrix}mh \\ \overline{I_A}\end{pmatrix}w_2 \\ y &= \begin{bmatrix}1 & 0\end{bmatrix}\begin{bmatrix}x_1 \\ x_2\end{bmatrix}\end{aligned} \tag{4.72}$$

where:

- $\mathbf{W}_1 = \begin{pmatrix}0 & 0 & 0 \\ \dfrac{mgh}{I_A} & 0 & -1\end{pmatrix}$ (4.73)

  is the matrix connecting the system states to the roll disturbance vector

- $\mathbf{W}_2 = \begin{pmatrix}mh \\ \overline{I_A}\end{pmatrix}$ (4.74)

  is the matrix connecting the system states to the deck lateral acceleration disturbance vector;

- $\mathbf{w}_1 = \begin{bmatrix}w_1 \\ \dot{w}_1 \\ \ddot{w}_1\end{bmatrix} = \begin{bmatrix}\varphi \\ \dot{\varphi} \\ \ddot{\varphi}\end{bmatrix}$ (4.75)

  is the vector of roll disturbance terms;

- $\mathbf{w}_2 = \ddot{Y}_A$ (4.76)

  is the vector of lateral acceleration disturbance terms.

The implemented method is based on an extended observer that estimates the unknown disturbances (deck roll angle, roll acceleration, lateral acceleration) through an internal model reproducing the system dynamics. Conceptually, the human control system uses an internal representation that is stimulated by a copy of the control command (the controlling torque) for

generating a predicted response. This predicted response is compared with the actual measured system response to estimate the effects that are not part of the internal model but are due to the external disturbances.

At first, two distinct observers for estimating the angular and linear disturbances in equation (4.70) and system (4.71) have been employed (Figure 4.33).

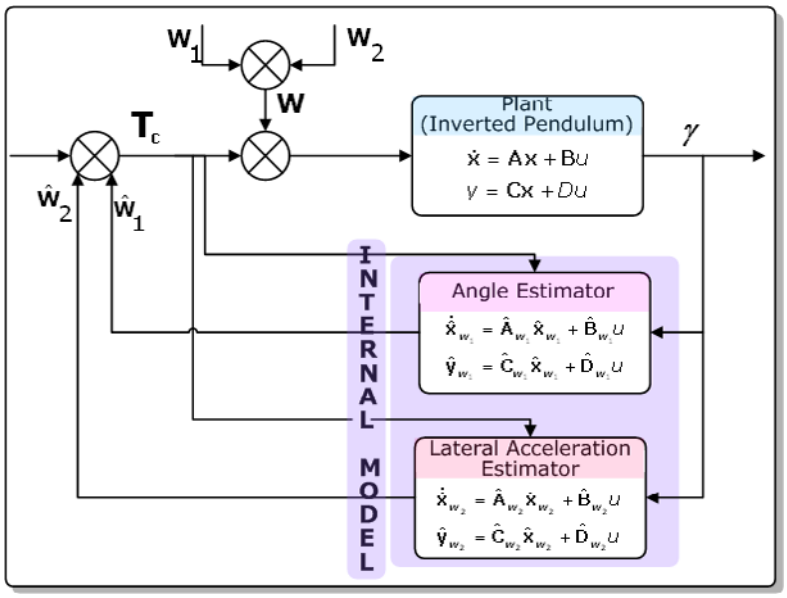

Figure 4.33 – Block diagram of the system with two distinct observers for ship motion rejection

From the control theory perspective, when a control system is designed, a method for rejecting external disturbances is needed. A very powerful techniques is based on augmenting an observer, also called estimator, with the disturbance equations in a way that permits to cancel out their effects on the output [Franklin et al., 1994]. An estimator is a key element in a feed-back control scheme that allows to reconstruct all the state variables of a system from a few measurements.

An extended estimator is a classical estimator where the external disturbances are assumed to be additional regular state [Tahboub & Mergner, 2007]:

$$\begin{aligned}\hat{\mathbf{x}}_{w_1} &= \begin{bmatrix} x_1 & x_2 & w_1 & \dot{w}_1 & \ddot{w}_1 \end{bmatrix}^T = \\ &= \begin{bmatrix} \gamma & \dot{\gamma} & \varphi & \dot{\varphi} & \ddot{\varphi} \end{bmatrix}^T \end{aligned} \tag{4.77}$$

$$\begin{aligned}\hat{\mathbf{x}}_{w_2} &= \begin{bmatrix} x_1 & x_2 & w_2 \end{bmatrix}^T = \\ &= \begin{bmatrix} \gamma & \dot{\gamma} & \ddot{Y}_A \end{bmatrix}^T \end{aligned} \tag{4.78}$$

However, since these states are originally extraneous to the system, the differential equations governing their behaviour in the time domain are supposed to be unknown. Rather, the external unknown disturbances can be approximated by a piece-wise constant function [Tahboub, 2010a]:

$$\begin{bmatrix} \dot{w}_1 \\ \ddot{w}_1 \\ \dddot{w}_1 \end{bmatrix} = \mathbf{A}_{w_1} \begin{bmatrix} w_1 \\ \dot{w}_1 \\ \ddot{w}_1 \end{bmatrix} = \begin{pmatrix} 0 & 1 & 0 \\ 0 & 0 & 1 \\ 0 & 0 & 0 \end{pmatrix} \begin{bmatrix} w_1 \\ \dot{w}_1 \\ \ddot{w}_1 \end{bmatrix} \tag{4.79}$$

$$\dot{w}_2 = \mathbf{A}_{w2} w_2 = \begin{pmatrix} 0 \end{pmatrix} w_2 \tag{4.80}$$

In the state-space form, the full-order estimator for roll disturbances is given by:

$$\begin{aligned} \dot{\hat{\mathbf{x}}}_{w_1} &= \hat{\mathbf{A}}_{w_1} \hat{\mathbf{x}}_{w_1} + \hat{\mathbf{B}}_{w_1} u \\ \hat{\mathbf{y}}_{w_1} &= \hat{\mathbf{C}}_{w_1} \hat{\mathbf{x}}_{w_1} + \hat{\mathbf{D}}_{w_1} u \end{aligned} \tag{4.81}$$

where:

$$\begin{bmatrix} \dot{\mathbf{x}} \\ \dot{\mathbf{w}}_1 \end{bmatrix} = \begin{bmatrix} \mathbf{A} & \mathbf{W} \\ \mathbf{0} & \mathbf{A}_{w_1} \end{bmatrix} \hat{\mathbf{x}}_{w_1} + \begin{bmatrix} \mathbf{B} \\ \mathbf{0} \end{bmatrix} u$$

$$\begin{bmatrix} \dot{x}_1 \\ \dot{x}_2 \\ \dot{w}_1 \\ \ddot{w}_1 \\ \dddot{w}_1 \end{bmatrix} = \begin{pmatrix} 0 & 1 & 0 & 0 & 0 \\ \dfrac{mgh}{I_A} & 0 & \dfrac{mgh}{I_A} & 0 & -1 \\ 0 & 0 & 0 & 1 & 0 \\ 0 & 0 & 0 & 0 & 1 \\ 0 & 0 & 0 & 0 & 0 \end{pmatrix} \begin{bmatrix} x_1 \\ x_2 \\ w_1 \\ \dot{w}_1 \\ \ddot{w}_1 \end{bmatrix} + \begin{pmatrix} 0 \\ \dfrac{1}{I_A} \\ 0 \\ 0 \\ 0 \end{pmatrix} u \tag{4.82}$$

Analogously, for the deck lateral acceleration the extended observer results:

$$\begin{aligned}\dot{\hat{\mathbf{x}}}_{w_2} &= \hat{\mathbf{A}}_{w_2}\hat{\mathbf{x}}_{w_2} + \hat{\mathbf{B}}_{w_2}u \\ \hat{\mathbf{y}}_{w_2} &= \hat{\mathbf{C}}_{w_2}\hat{\mathbf{x}}_{w_2} + \hat{\mathbf{D}}_{w_2}u\end{aligned} \tag{4.83}$$

$$\begin{bmatrix}\dot{\mathbf{x}} \\ \dot{\mathbf{w}}_2\end{bmatrix} = \begin{bmatrix}\mathbf{A} & \mathbf{W} \\ \mathbf{0} & \mathbf{A}_{w2}\end{bmatrix}\hat{\mathbf{x}}_{w_2} + \begin{bmatrix}\mathbf{B} \\ \mathbf{0}\end{bmatrix}u$$
$$\begin{bmatrix}\dot{x}_1 \\ \dot{x}_2 \\ \dot{w}_2\end{bmatrix} = \begin{pmatrix}0 & 1 & 0 \\ \dfrac{mgh}{I_A} & 0 & \dfrac{mh}{I_A} \\ 0 & 0 & 0\end{pmatrix}\begin{bmatrix}x_1 \\ x_2 \\ w_2\end{bmatrix} + \begin{pmatrix}0 \\ \dfrac{1}{I_A} \\ 0\end{pmatrix}u \tag{4.84}$$

In both systems (4.81) and (4.83), $\hat{\mathbf{y}}_{w_1}$ and $\hat{\mathbf{y}}_{w_2}$ represent the vectors of the measurements stemming from human sensory systems:

- $\hat{\mathbf{y}}_{w_1} = \begin{bmatrix}x_1 & x_2 & \omega & a\end{bmatrix}^T$ (4.85)
- $\hat{\mathbf{y}}_{w_1} = \begin{bmatrix}x_1 & x_2\end{bmatrix}^T$ (4.86)

Based on the studies reported in 3.4 and 3.5, it has been supposed that:

- $\begin{bmatrix}x_1 \\ x_2\end{bmatrix} = \begin{bmatrix}\gamma \\ \dot{\gamma}\end{bmatrix}$ (4.87)

  the pendulum angle and angular velocity are available from ankle proprioceptive sensors;
- $\omega = x_2 + \dot{w}_1 = \dot{\gamma} + \dot{\varphi}$ (4.88)

  the total actual angular velocity (sum of both pendulum and ship angular velocity) is measured by the semicircular organ;
- $$\begin{aligned}a &\cong w_2 - h_{ot}\left(\dot{x}_2 + \ddot{w}_1\right) - g\left(x_1 + w_1\right) = \\ &= \ddot{Y}_A - h_{ot}\left(\ddot{\gamma} + \ddot{\varphi}\right) - g\left(\gamma + \varphi\right)\end{aligned}$$ (4.89)

  the tangential acceleration is sensed by the otolith organ, whose height from the ankle joint has been fixed equal to:
- $h_{ot} = \left(0.94 - 0.04\right)\cdot h_{Body} = 1.579 \text{ m}$ (4.90)

It has to be highlighted that the noise and drift characterising the sensory systems are neglected in this contest.

The output measurement equations are then equal to:

$$\begin{aligned}\hat{\mathbf{y}}_{w_1} &= \hat{\mathbf{C}}_{w_1}\hat{\mathbf{x}}_{w_1} + \hat{\mathbf{D}}_{w_1}u \\ \begin{bmatrix} x_1 \\ x_2 \\ \omega \\ a \end{bmatrix} &= \begin{pmatrix} 1 & 0 & 0 & 0 & 0 \\ 0 & 1 & 0 & 0 & 0 \\ 0 & 1 & 0 & 1 & 0 \\ \left(-g - h_{ot}\dfrac{mgh}{I_A}\right) & 0 & \left(-g - h_{ot}\dfrac{mgh}{I_A}\right) & 0 & 0 \end{pmatrix}\begin{bmatrix} x_1 \\ x_2 \\ w_1 \\ \dot{w}_1 \\ \ddot{w}_1 \end{bmatrix} + \begin{pmatrix} 0 \\ 0 \\ 0 \\ -h_{ot}\dfrac{1}{I_A} \end{pmatrix} u\end{aligned} \tag{4.91}$$

for the roll observer, and

$$\begin{aligned}\hat{\mathbf{y}}_{w_2} &= \hat{\mathbf{C}}_{w_2}\hat{\mathbf{x}}_{w_2} + \hat{\mathbf{D}}_{w_2}u \\ \begin{bmatrix} x_1 \\ x_2 \end{bmatrix} &= \begin{pmatrix} 1 & 0 & 0 \\ 0 & 1 & 0 \\ 0 & 0 & 0 \end{pmatrix}\begin{bmatrix} x_1 \\ x_2 \\ w_2 \end{bmatrix} + \begin{pmatrix} 0 \\ 0 \\ 0 \end{pmatrix} u\end{aligned} \tag{4.92}$$

for the lateral acceleration observer.

The pairs $\left(\hat{\mathbf{A}}_{w_1}, \hat{\mathbf{C}}_{w_1}\right)$ in (4.81) and $\left(\hat{\mathbf{A}}_{w_2}, \hat{\mathbf{C}}_{w_2}\right)$ in (4.83) are observable, which means that the extended states (4.77) and (4.78) of the systems can be deduced by monitoring the sensed outputs. In other words, the extended-state vectors $\hat{\mathbf{x}}_{w_1}$ and $\hat{\mathbf{x}}_{w_2}$ can be estimated given the measurements (4.85) and (4.86).

The estimator equations for roll and deck acceleration disturbances can be then written as:

$$\begin{aligned}\dot{\hat{\mathbf{x}}}_{w_1} &= \hat{\mathbf{A}}_{w_1}\hat{\mathbf{x}}_{w_1} + \hat{\mathbf{B}}_{w_1}u + \mathbf{L}_{w_1}\left(\hat{\mathbf{y}}_{w_1} - \hat{\mathbf{C}}_{w_1}\hat{\mathbf{x}}_{w_1} - \hat{\mathbf{D}}_{w_1}u\right) = \\ &= \left(\hat{\mathbf{A}}_{w_1} - \mathbf{L}_{w_1}\hat{\mathbf{C}}_{w_1}\right)\hat{\mathbf{x}}_{w_1} + \left(\hat{\mathbf{B}}_{w_1} - \mathbf{L}_{w_1}\hat{\mathbf{D}}_{w_1}\right)u + \mathbf{L}_{w_1}\hat{\mathbf{y}}_{w_1}\end{aligned} \tag{4.93}$$

- $$\begin{aligned}\dot{\hat{\mathbf{x}}}_{w_2} &= \hat{\mathbf{A}}_{w_2}\hat{\mathbf{x}}_{w_2} + \hat{\mathbf{B}}_{w_2}u + \mathbf{L}_{w_2}\left(\hat{\mathbf{y}}_{w_2} - \hat{\mathbf{C}}_{w_2}\hat{\mathbf{x}}_{w_2} - \hat{\mathbf{D}}_{w_2}u\right) = \\ &= \left(\hat{\mathbf{A}}_{w_2} - \mathbf{L}_{w_2}\hat{\mathbf{C}}_{w_2}\right)\hat{\mathbf{x}}_{w_2} + \left(\hat{\mathbf{B}}_{w_2} - \mathbf{L}_{w_2}\hat{\mathbf{D}}_{w_2}\right)u + \mathbf{L}_{w_2}\hat{\mathbf{y}}_{w_2}\end{aligned} \tag{4.94}$$

The matrices $\mathbf{L}_{w_1}$ and $\mathbf{L}_{w_2}$ contain the gains for the two observers, whose values can be found by pole placement. It has to be kept in mind that the assumption the external disturbances to be piece-wise constant calls for fast observers [Tahboub, 2010a].

Definitely, the control law comprising all the control elements results:

$$\begin{aligned}T_C(t) &= T_{PD}(t) + T_I(t) + T_{P_{ff}}(t) + T_E = \\ &= -\left(K_P\gamma(t) + K_D\dot{\gamma}(t) + K_I\int^t\left(r_\gamma(t) - \gamma(t)\right)\,dt\right) + \\ &+K_{P_{ff}}r_\gamma(t) + K_{D_{ff}}\dot{r}_\gamma(t) + \\ &-\left(J_A\ddot{\hat{\varphi}}(t) - mgh\hat{\varphi}(t) - mh\ddot{\hat{Y}}_A(t)\right)\end{aligned} \tag{4.95}$$

where:

- $\hat{\varphi}(t)$ (4.96)

  is the estimated deck roll angle;

- $\ddot{\hat{\varphi}}(t)$ (4.97)

  is the estimated deck roll acceleration;

- $\ddot{\hat{Y}}_A$ (4.98)

  is the estimated deck lateral acceleration.

With the control scheme here proposed, several tests have been conducted. Some results, highlighting important and interesting features of the proposed model are shown.

In Figure 4.34 and Figure 4.35 the system response to a 5-degree step and a 0.02g lateral acceleration of the platform are reported separately. In both the cases, only the feedback PID and feed-forward PD have been employed.

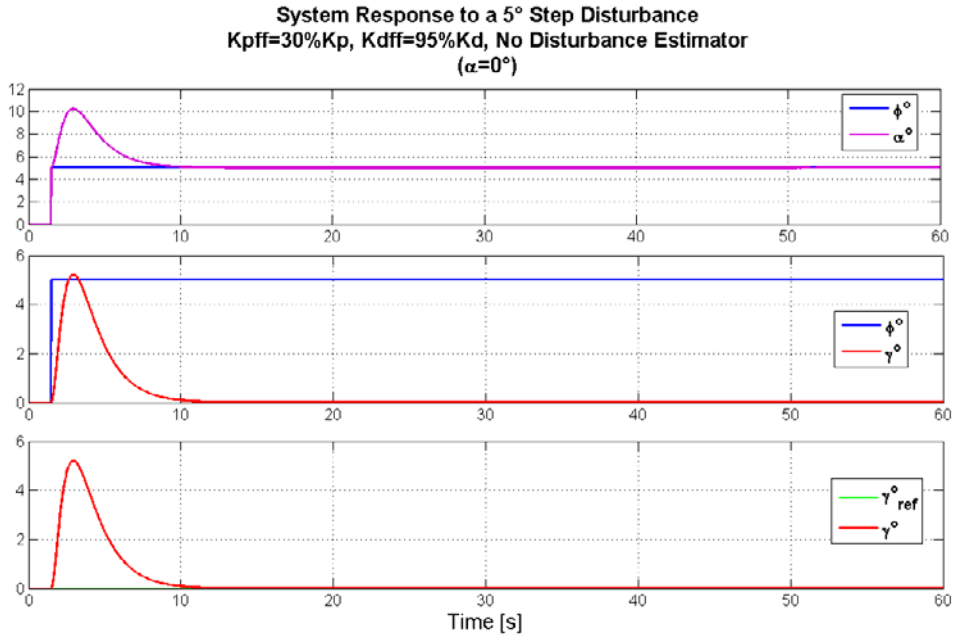

Figure 4.34- Response to a 5° step disturbance with Feed-Forward controller $\left(K_{P_{ff}} = 30\%K_P, K_{D_{ff}} = 95\%K_D\right)$

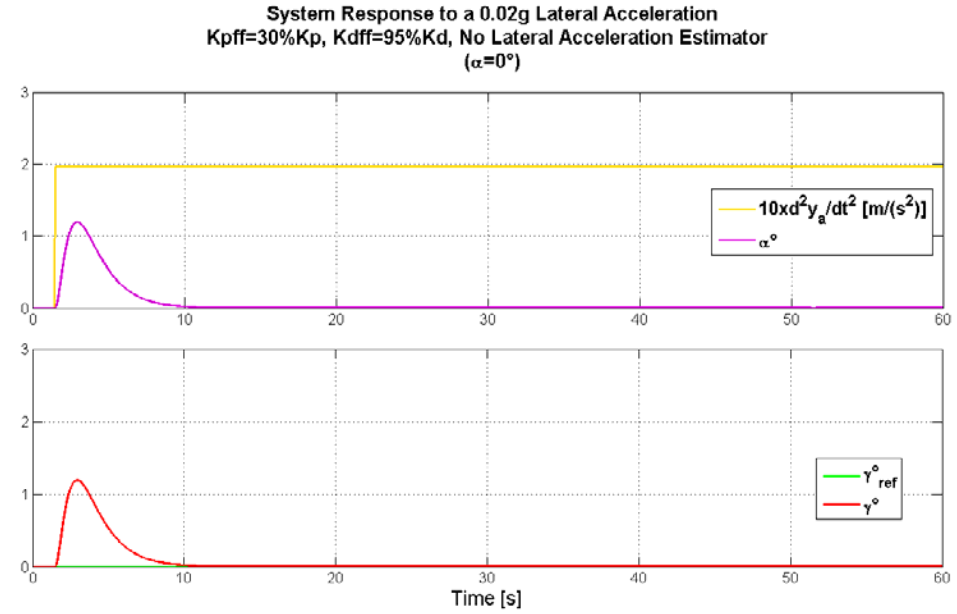

Figure 4.35 - Response to a 0.02g lateral acceleration disturbance with Feed-Forward controller $\left(K_{P_{ff}} = 30\%K_P, K_{D_{ff}} = 95\%K_D\right)$

By adding the roll estimator and reducing the feed-forward gains, the response to the angle step disturbance improves in terms of both overshoot

and settling time (Figure 4.36). In Figure 4.37 the estimated angle is shown against to the true external disturbance angle.

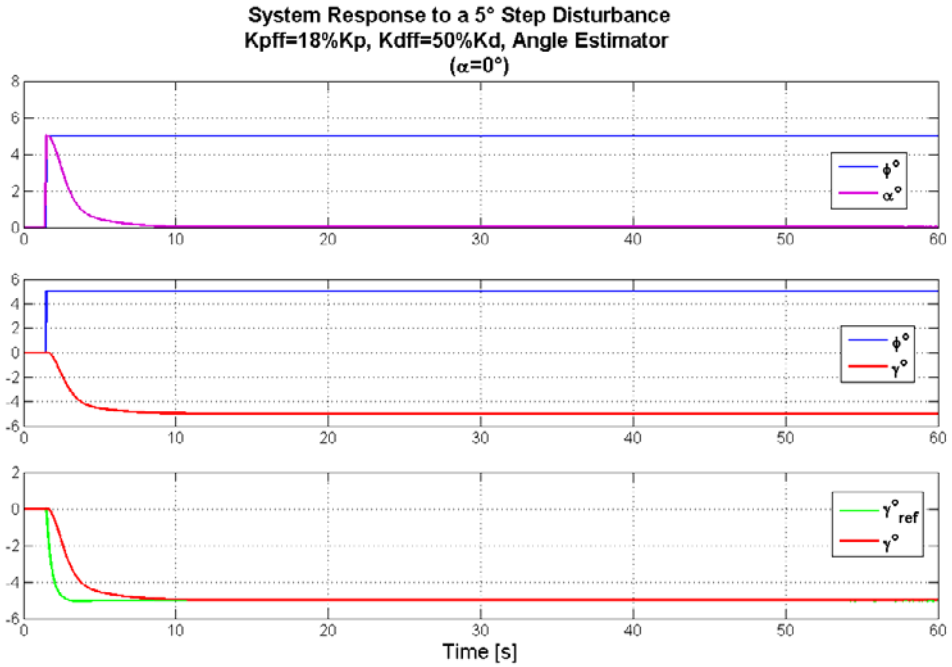

Figure 4.36 - Response to a 5° step disturbance with Feed-Forward controller $\left(K_{P_{ff}} = 18\%K_P, K_{D_{ff}} = 50\%K_D, \right)$ **and Angle Estimator**

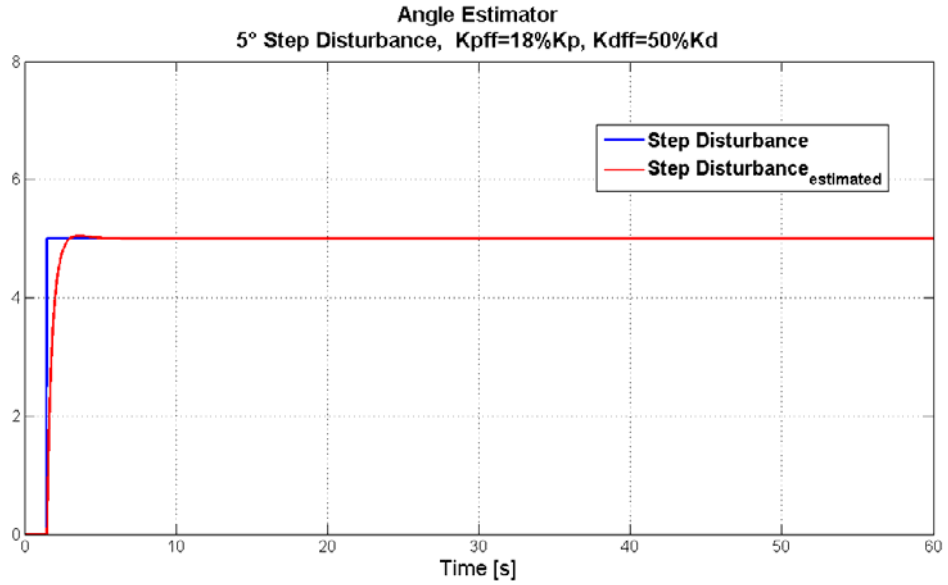

Figure 4.37 - Angle Estimator to a 5° step disturbance of with Feed-Forward controller $\left(K_{P_{ff}} = 18\%K_P, K_{D_{ff}} = 50\%K_D, \right)$

The overshoot is reduced also when the lateral acceleration is applied and the disturbance estimator is employed, but it takes longer time the system transients to decay (Figure 4.38). In Figure 4.39 the estimated lateral acceleration is shown; in this case, the external observer is not able to estimate the external disturbance properly.

If the system is excited with both the external disturbances, the response employing the two distinct observers is reproduced in Figure 4.40.

Figure 4.41 and Figure 4.42 show the estimated external disturbances when both step and lateral perturbations are applied at the same time.

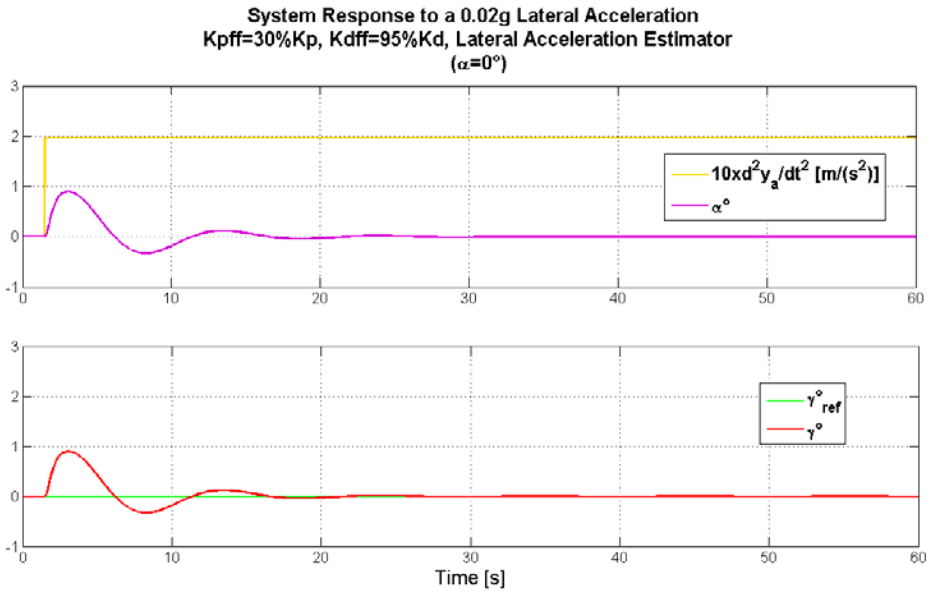

Figure 4.38 - Response to a 0.02g lateral acceleration disturbance with Feed-Forward controller $\left(K_{P_{ff}} = 30\%K_P, K_{D_{ff}} = 95\%K_D\right)$ and Lateral Acceleration Estimator

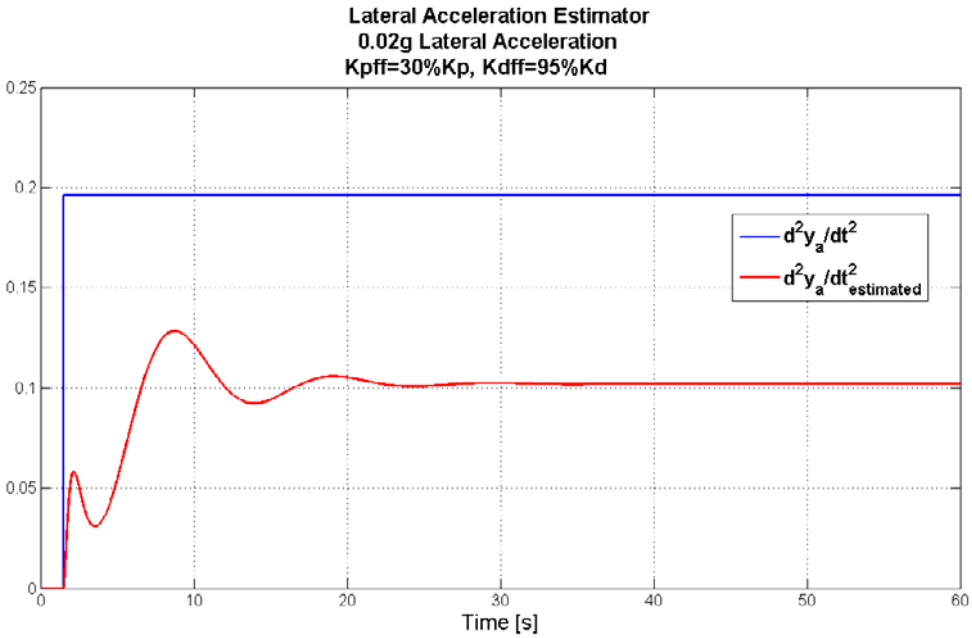

Figure 4.39 - Lateral Acceleration Estimator to 0.02g lateral acceleration disturbance of with Feed-Forward controller $\left(K_{P_{ff}} = 30\%K_P, K_{D_{ff}} = 95\%K_D\right)$

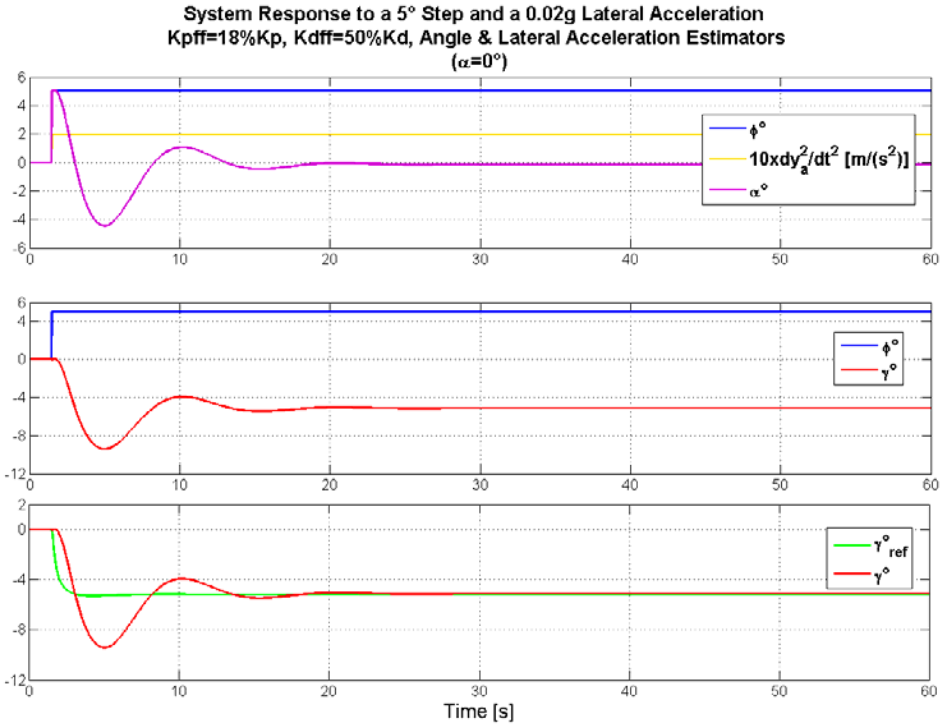

Figure 4.40 - System Response to a 5° step disturbance and a 0.02g lateral acceleration disturbance with Feed-Forward controller $\left(K_{P_{ff}} = 18\%K_P, K_{D_{ff}} = 50\%K_D\right)$**, Angle and Lateral Acceleration Estimators**

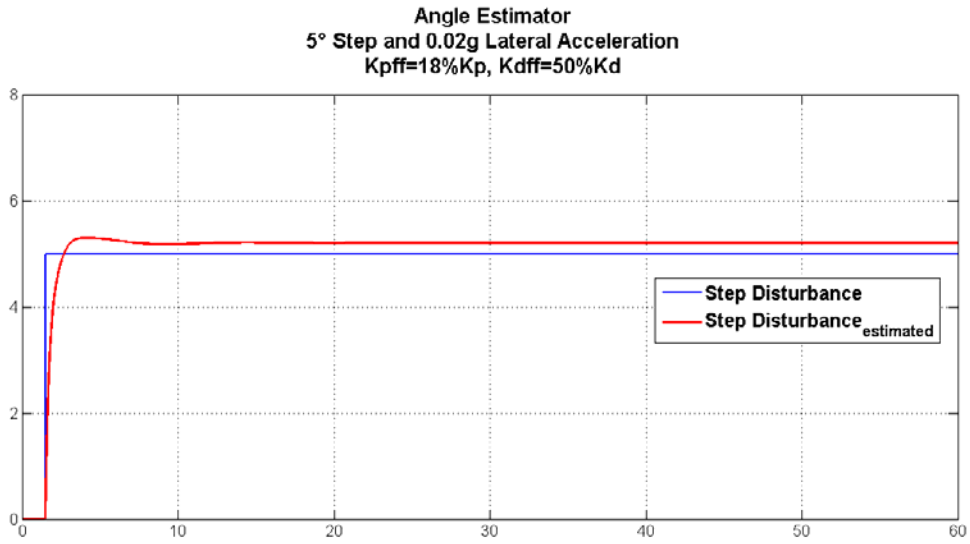

Figure 4.41 - Angle Estimator to a 5° step disturbance a 0.02g lateral acceleration disturbance with Feed-Forward controller $\left(K_{P_{ff}} = 18\%K_P, K_{D_{ff}} = 50\%K_D\right)$, Angle and Lateral Acceleration Estimators

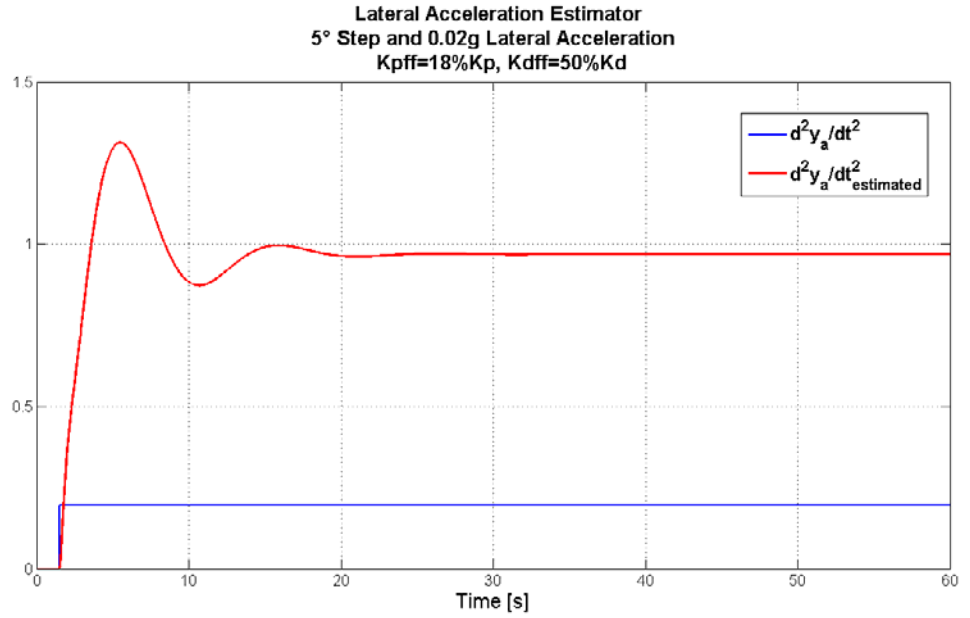

Figure 4.42 - Lateral Acceleration Estimator to a 5° step disturbance a 0.02g lateral acceleration disturbance with Feed-Forward controller $\left(K_{P_{ff}} = 18\%K_P, K_{D_{ff}} = 50\%K_D\right)$, Angle and Lateral Acceleration Estimators

For achieving a better response (lower negative overshoot and shorter transients) a further configuration has been implemented: a single extended observer, compensating for both roll and lateral acceleration, has been tested (Figure 4.43).

The full-order complete estimator for ship disturbances is given by:

$$\begin{aligned}\dot{\hat{\mathbf{x}}}_w &= \hat{\mathbf{A}}_w\hat{\mathbf{x}}_w + \hat{\mathbf{B}}_w u \\ \hat{\mathbf{y}}_w &= \hat{\mathbf{C}}_w\hat{\mathbf{x}}_w + \hat{\mathbf{D}}_w u\end{aligned} \tag{4.99}$$

where:

$$\begin{bmatrix}\dot{x}_1\\ \dot{x}_2\\ \dot{w}_1\\ \ddot{w}_1\\ \dddot{w}_1\\ \dot{w}_2\end{bmatrix} = \begin{pmatrix}0 & 1 & 0 & 0 & 0 & 0\\ \frac{mgh}{I_A} & 0 & \frac{mgh}{I_A} & 0 & -1 & \frac{mh}{I_A}\\ 0 & 0 & 0 & 1 & 0 & 0\\ 0 & 0 & 0 & 0 & 1 & 0\\ 0 & 0 & 0 & 0 & 0 & 0\\ 0 & 0 & 0 & 0 & 0 & 0\end{pmatrix}\begin{bmatrix}x_1\\ x_2\\ w_1\\ \dot{w}_1\\ \ddot{w}_1\\ w_2\end{bmatrix} + \begin{pmatrix}0\\ \frac{1}{I_A}\\ 0\\ 0\\ 0\\ 0\end{pmatrix}u$$

$$\begin{bmatrix}x_1\\ x_2\\ \omega\\ a\end{bmatrix} = \begin{pmatrix}1 & 0 & 0 & 0 & 0 & 0\\ 0 & 1 & 0 & 0 & 0 & 0\\ 0 & 1 & 0 & 1 & 0 & 0\\ \left(-g - h_{ot}\frac{mgh}{I_A}\right) & 0 & \left(-g - h_{ot}\frac{mgh}{I_A}\right) & 0 & 0 & \left(1 - h_{ot}\frac{mh}{I_A}\right)\end{pmatrix}\begin{bmatrix}x_1\\ x_2\\ w_1\\ \dot{w}_1\\ \ddot{w}_1\\ w_2\end{bmatrix} + \begin{pmatrix}0\\ 0\\ 0\\ -h_{ot}\frac{1}{I_A}\end{pmatrix}u \tag{4.100}$$

The pair $\left(\hat{\mathbf{A}}_w, \hat{\mathbf{C}}_w\right)$ in (4.99) is still observable, and the estimator equation becomes:

$$\begin{aligned}\dot{\hat{\mathbf{x}}}_w &= \hat{\mathbf{A}}_w\hat{\mathbf{x}}_w + \hat{\mathbf{B}}_w u + \mathbf{L}_w\left(\hat{\mathbf{y}}_w - \hat{\mathbf{C}}_w\hat{\mathbf{x}}_w - \hat{\mathbf{D}}_w u\right) = \\ &= \left(\hat{\mathbf{A}}_w - \mathbf{L}_w\hat{\mathbf{C}}_w\right)\hat{\mathbf{x}}_w + \left(\hat{\mathbf{B}}_w - \mathbf{L}_w\hat{\mathbf{D}}_w\right)u + \mathbf{L}_w\hat{\mathbf{y}}_w\end{aligned} \tag{4.101}$$

The system response is improved, since the undesirable negative overshoot is reduced, but the transients are still quite long (Figure 4.44). The full-order complete observer (4.99) shows a better performance in estimating both the angle (Figure 4.45) and the lateral acceleration (Figure 4.46).

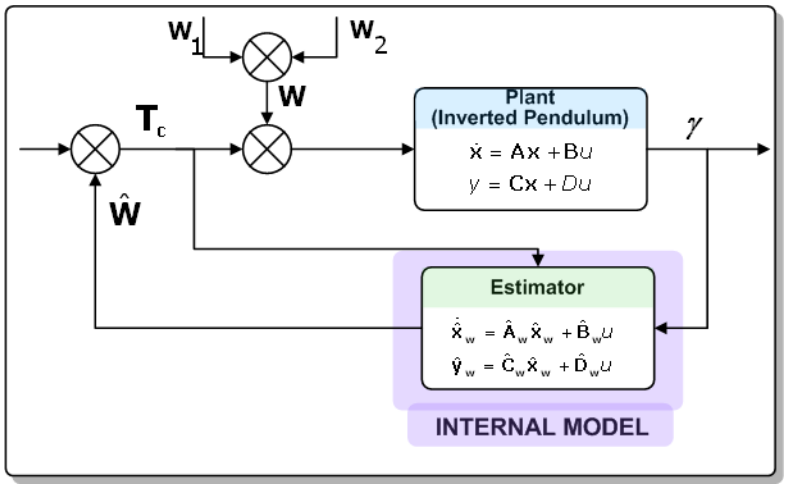

Figure 4.43 - Block diagram of the system with a single observer for ship motion rejection

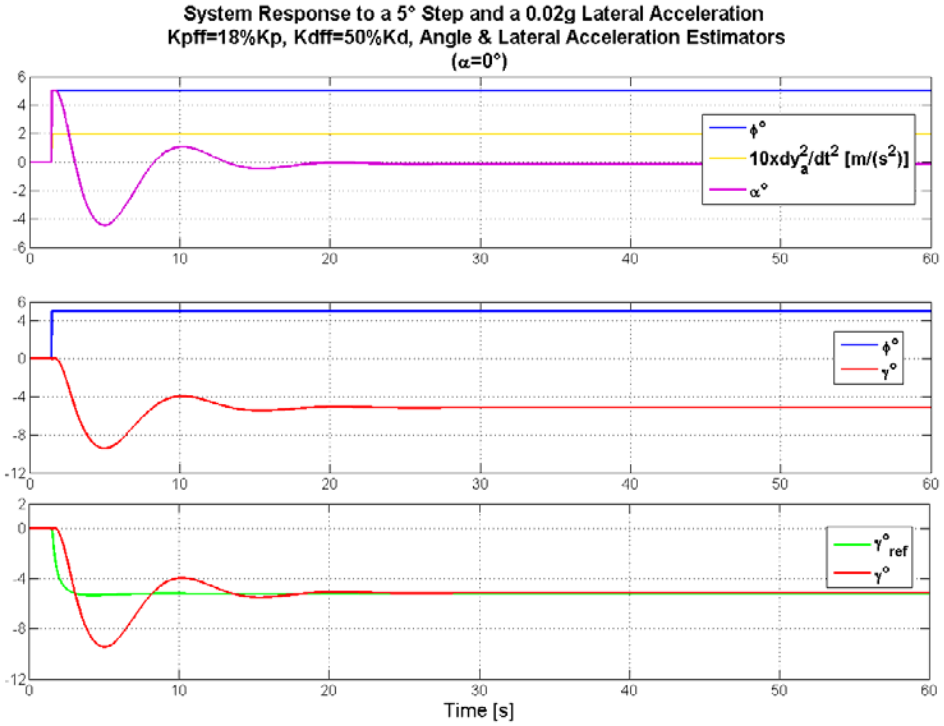

Figure 4.44 - System Response to a 5° step disturbance and a 0.02g lateral acceleration disturbance with Feed-Forward controller $\left(K_{P_{ff}} = 18\%K_P, K_{D_{ff}} = 6\%K_D\right)$, single disturbance Estimator

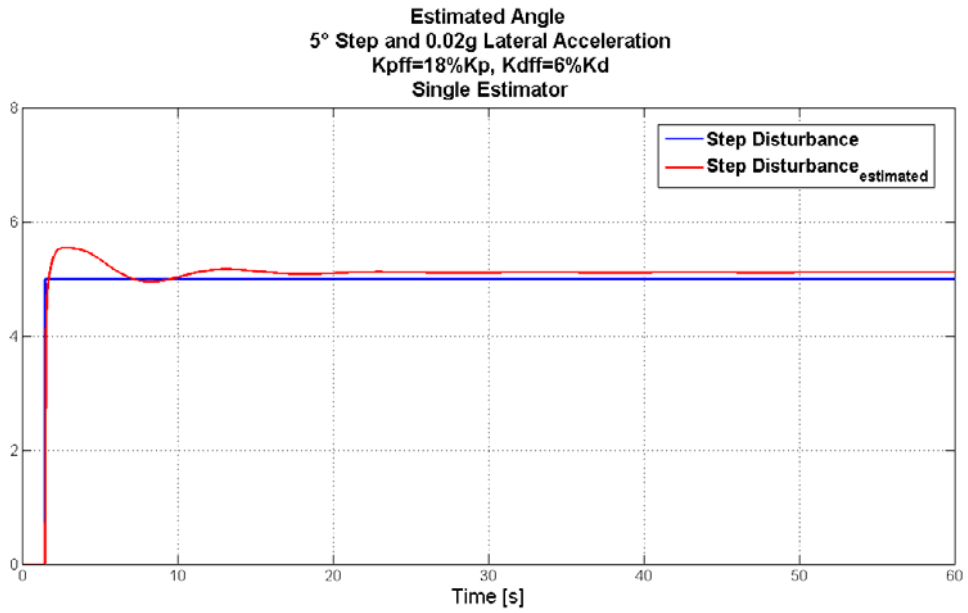

Figure 4.45 - Roll Angle Estimator to a 5° step disturbance and a 0.02g lateral acceleration disturbance with Feed-Forward controller $\left(K_{P_{ff}} = 18\%K_P, K_{D_{ff}} = 6\%K_D\right)$, single disturbance Estimator

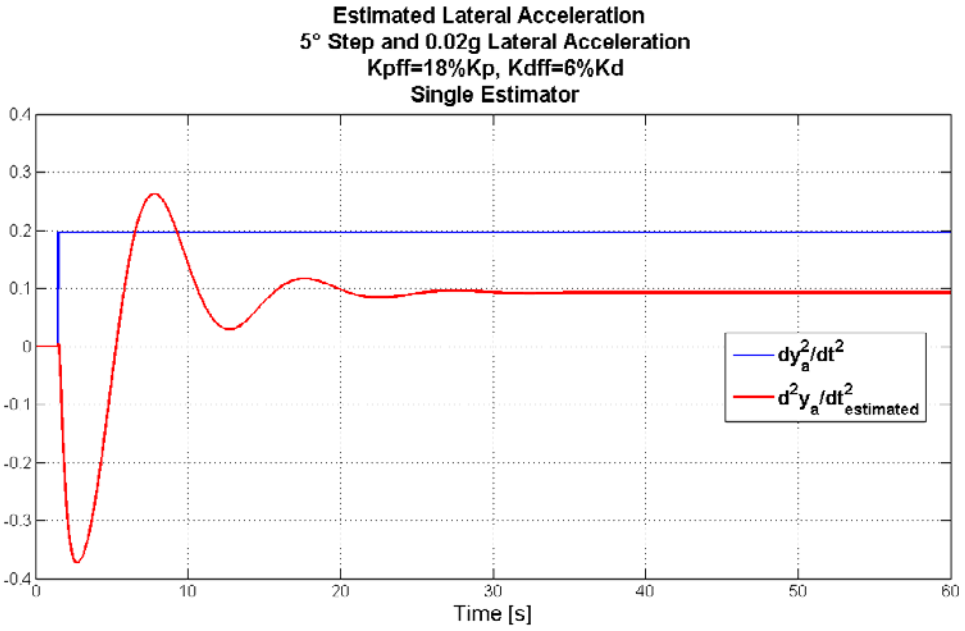

Figure 4.46 - Lateral Acceleration to a 5° step disturbance and a 0.02g lateral acceleration disturbance with Feed-Forward controller $\left(K_{P_{ff}} = 18\%K_P, K_{D_{ff}} = 6\%K_D\right)$, single disturbance Estimator

Hereinafter, additional simulations are reported. On one hand, these results show how the system reacts to a sinusoid perturbation. On the other, they illustrate that different system responses can be produced by varying the system parameters and the reference angle α. For example, Figure 4.49 and Figure 4.50 have been obtained by changing not only the feed-forward gains, but also the poles of the disturbance estimator.

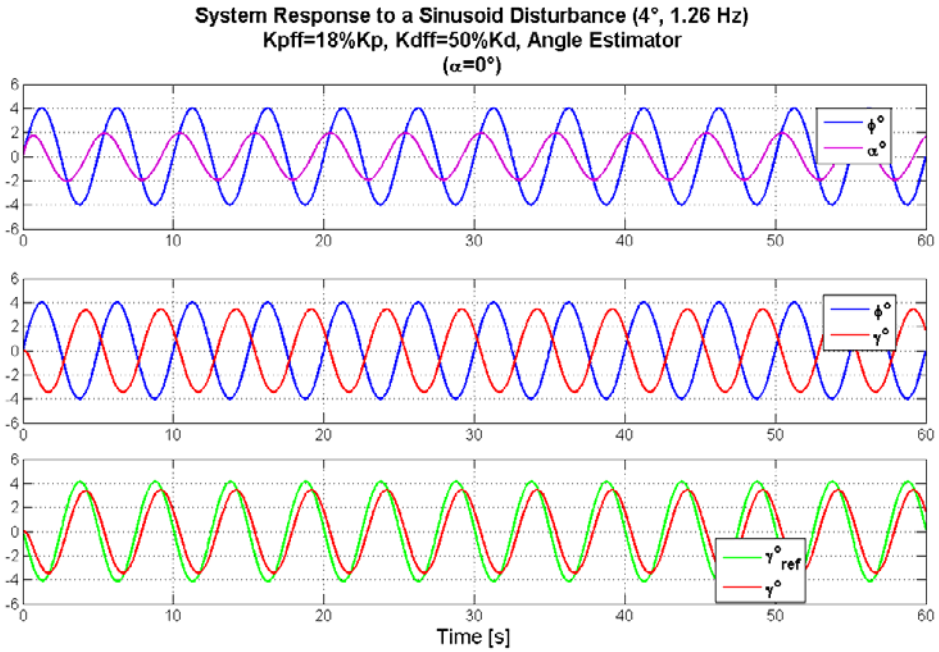

Figure 4.47 - System Response to a 4°, 1.26 Hz sinusoid disturbance with Feed-Forward controller $\left(K_{P_{ff}} = 18\%K_P, K_{D_{ff}} = 50\%K_D\right)$**, Angle Estimator,** $\alpha = 0°$**, Observer poles** $\left[-3, -3.31, -7.15, -10, -25\right]$

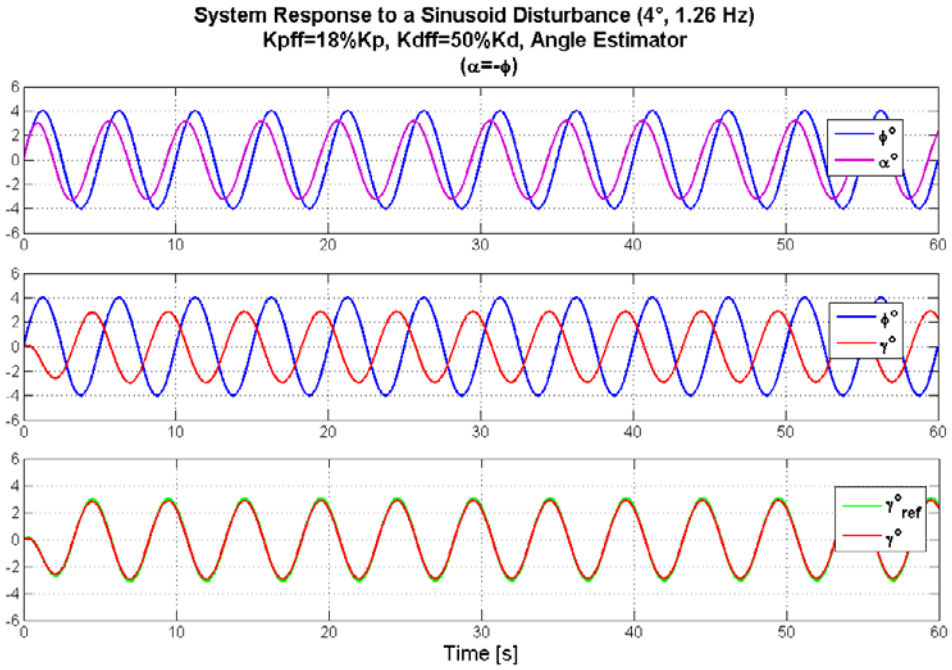

Figure 4.48 - System Response to a 4°, 1.26 Hz sinusoid disturbance with Feed-Forward controller $\left(K_{P_{ff}} = 18\%K_P, K_{D_{ff}} = 50\%K_D\right)$**, Angle Estimator,** $\alpha = -\varphi$**, Observer poles** $\left[-3, -3.31, -7.15, -10, -25\right]$

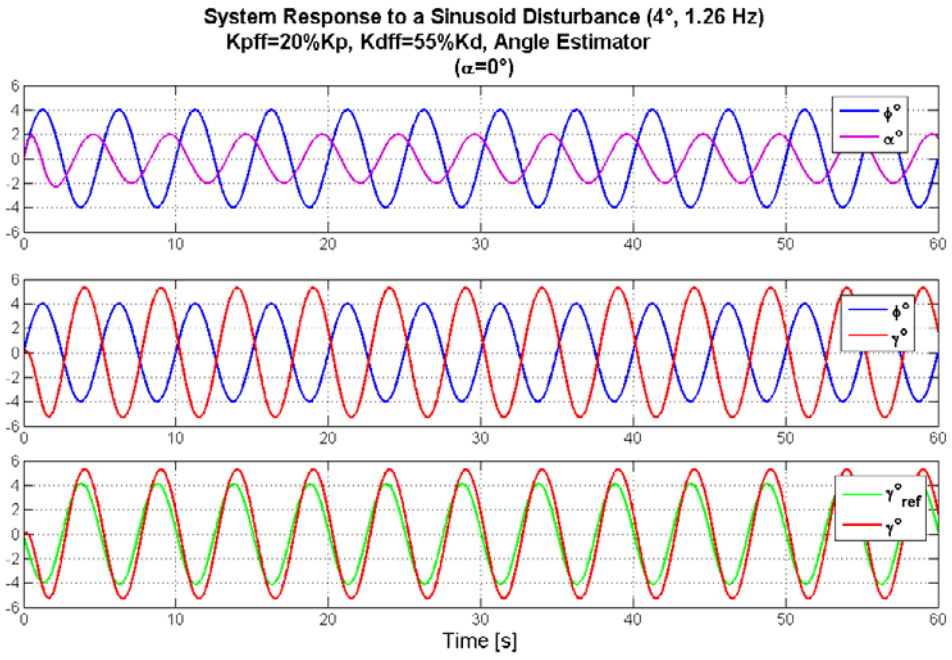

Figure 4.49 - System Response to a 4°, 1.26 Hz sinusoid disturbance with Feed-Forward controller $\left(K_{P_{ff}} = 20\%K_P, K_{D_{ff}} = 50\%K_D\right)$**, Angle Estimator,** $\alpha = 0°$**, Observer poles** $\left[-1.32, -2.86, -3, -10, -25\right]$

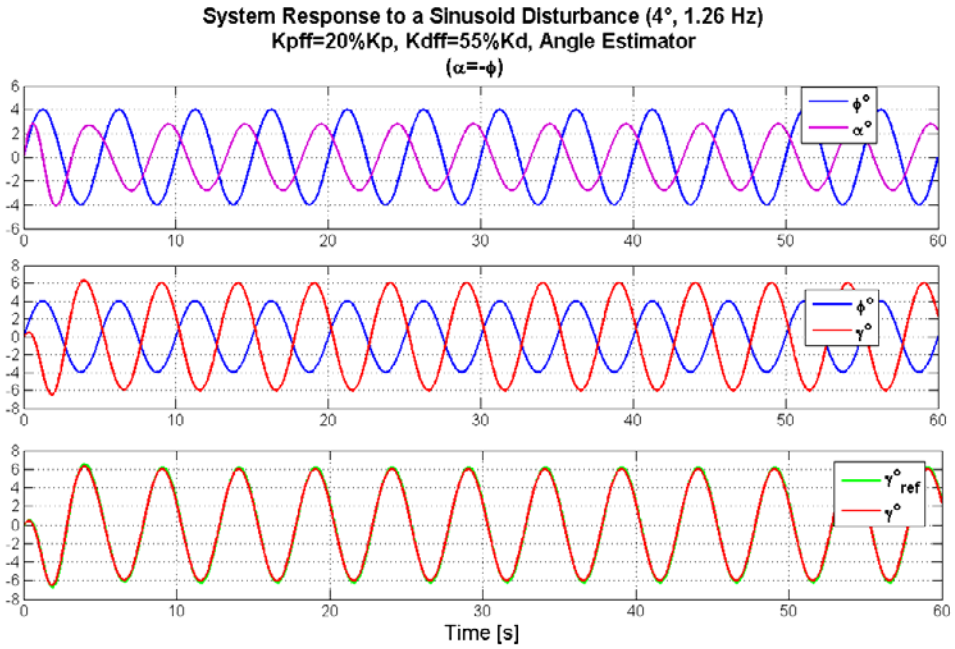

Figure 4.50 - System Response to a 4°, 1.26 Hz sinusoid disturbance with Feed-Forward controller $\left(K_{P_{ff}} = 20\%K_P, K_{D_{ff}} = 50\%K_D\right)$**, Angle Estimator,** $\alpha = -\varphi$**, Observer poles** $\left[-1.32, -2.86, -3, -10, -25\right]$

Appendix 4.A: HALYAS – Human posturAL stabilitY Aboard Ships

For testing the proposed model and simulating different inputs and configurations, an articulated software, called HALYAS, has been developed by the author in Matlab/Simulink environment.

4.A.1 MATLAB CODE AND SIMULINK MODEL

The development and implementation of HALYAS for simulating human postural stability onboard ships have several purposes:

- to analyse the model behaviour under different conditions;
- to study the system response with different model configuration;
- to assess the influence of assigning different values to the model parameters.

HALAYS is composed of three main parts:

- SIPMO – SImulating shiP MOtion: is a Matlab code including several Matlab functions that, starting from the RAO computed from commercial frequency domain seakeeping software[1], generates ship motion time series at different ship locations;
- ASOOS – ASsigning cOntrl mOdel parameterS: is an interactive Matlab code by which the user can set:
  - the kind of control scheme that has to be considered (e.g., if the feedforward path or the disturbance estimators have to be included or excluded in the current simulation);
  - the assigned values to the control gains;
  - the number and type of external disturbances:
    - ◇ step,

[1] At the moment, the code has been implemented for working with the output of Shipmo by Marin. It is the author's intention to extend the code for taking in input calculations from other commercial software.

◇ regular waves (sinusoids),

◇ irregular waves (from simulated or measured ship motions).

ASOOS also checks and warns the user about important system properties (e.g., if the system is controllable and observable).

- SPOSTA – Simulation of POstural STAbility: is a Simulink model made up of many interacting subsystems that implement the different elements composing the entire model. The fundamental modules are:
  - the system plant or biomechanical model that represents the human body (inverted pendulum);
  - the single controllers that form the complex, modular stabilising and controlling scheme:
    - ◇ the state-feedback PD control for stabilising the naturally unstable plant and the Integral control for robust tracking,
    - ◇ the feed-forward control for anticipatory response,
    - ◇ the extended observers for disturbance estimation.

  Other components have been included for determining additional parameters, such as the COP and COM displacement during the simulation. The assessment of MII occurrence has also been included and, at the moment, is under verification.

All the graphics and simulation results show in the present thesis have been produced using the own-developed software HALYAS.

Figure 4.A.1 describes the flowchart behind the software HALYAS.

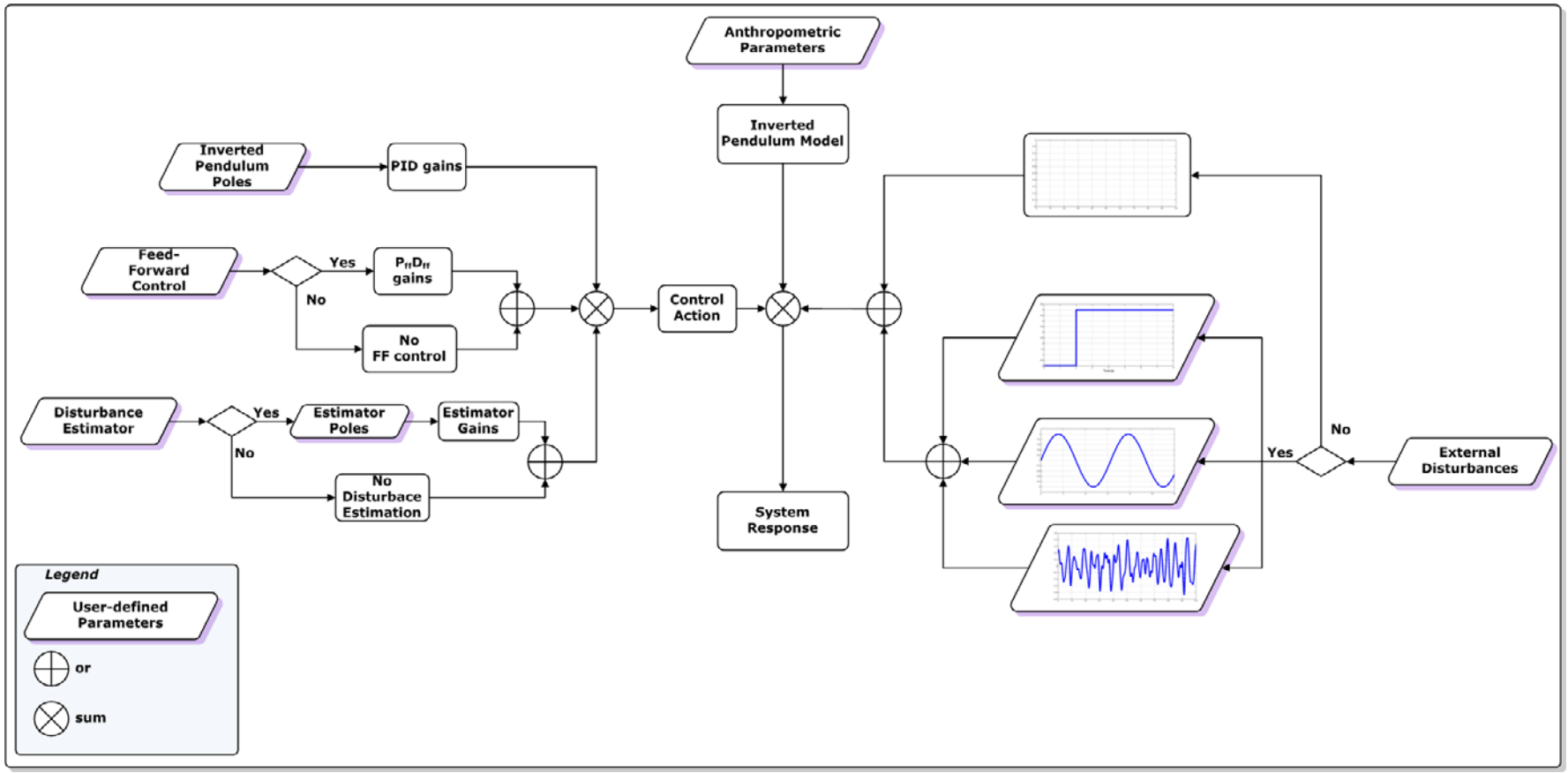

Figure 4.A.1 – Flowchart of HALYAS

Chapter 5: Experimental Procedures for Validating Human Postural Control Model

5.1 INTRODUCTION

In Chapter 4 a modular model for reproducing human postural control onboard ship has been incrementally built up and described. Some interesting results have been shown. These demonstrate interesting potentialities of the model in reproducing different dynamics.

The strength of the proposed model consists in its flexibility: by properly tuning the model parameters (controller gains), a desired response can be produced and adapted to emulate human behaviour.

The value assigned to each model gain mainly depends on the selected poles of the system, that determine the system response to various inputs and external conditions.

Experiments are required to validate the proposed control architecture and tune the system parameters.

Because of the peculiarities of the issue, the only practicable solution is to execute experiments in motion simulators or full-scale sea trials. Unfortunately, the classical and well-established method in the naval architecture field of towing-tank tests is impracticable in the case of interest (unless a proper human scale model is built!).

Trials in motion simulators have the advantage that the same sequence of motions may be reproduced to obtain controlled experiments on a large number of subjects. However, some simulators cannot reproduce all six

degrees of freedom or very large ship motions (in particular as well as translational motions are concerned). Practical experiments are limited since it is not possible to simulate all the tasks or phenomena occurring on a real ship. In addition, the costs for using such facilities can be very high, even prohibitive if the research is not supported by appropriate funding.

Onboard experiments allow studying postural stability in the field and correlating impaired balance with ship motions and onboard conditions in the real environment.

Up to now, standard procedures for conducting experiments onboard and validating human postural model have not been established yet. Few studies focused on this topic have been conducted and published. Moreover, the most part of them was interested in experimentally determining tipping coefficients for improving the prediction of MIIs (Motion Induced Interruptions) occurrence employing the standard model by Graham (section 2.3.1).

In the case of more complex human stability models, full-scale trials had principally the aim of tuning the proposed models in order to reproduce the MII rate and time of occurrence observed during the tests (section 2.3.3). The investigators were not focused in verifying the agreement between the simulated response of the balance control model and the measured behaviour of an individual working onboard vessels.

In this Chapter, a procedure for measuring human motion onboard ships is presented. The designed acquisition system results from the collaboration among researchers involved in many scientific fields. Diverse techniques (photogrammetry, inertial measurements, global positioning system) and instruments (digital cameras, inertial and positioning sensors) have been integrated with the ultimate goal of acquiring both ship and human motions.

The whole process of planning, designing, calibrating, and assessing the accuracy of the motion capture system is reported and discussed. The motivations that were at the basis of setting up this "ad hoc" acquisition system are analysed.

Laboratory tests were conducted for testing and validating the complex measurement system before executing preliminary trials onboard a fishing vessel.

The results from the first measurement campaign are presented and compared with the simulated motion obtained from the proposed postural control model.

5.2 HUMAN POSTURAL STABILITY TESTS ONBOARD SHIPS

Full-scale sea experiments have been planned for validating the proposed human stability control model discussed in Chapter 4. They combine elements characterising the classical seakeeping trials with procedures of human motion analysis.

While the main goal of full-scale seakeeping tests is to assess and compare the performance of ships in rough weather [Lloyd, 1989], the full-scale tests, conducted in the context of the present study, move from different motivations. The main purpose is to observe and record the postural stability behaviour of sailors in the real working environment. The crucial interest is to examine the actual movement of subjects trying to maintain balance, rather than to assess only the seakeeping qualities of the tested ship. These requirements demand for a multidisciplinary approach, involving the *classical* seakeeping method, mentioned above, together with human motion capture techniques.

The need of measuring at the same time both ship and individual motions has called for an acquisition system integrating different sensors and techniques.

5.2.1 SEAKEEPING FULL-SCALE TRIALS

Seakeeping trials, by their nature, are highly-costly and time consuming. They require careful planning, even if the final result is strongly related to the environmental conditions. During the execution, the sea state and weather in general can significantly change, causing the tests to be not practicable or

the result not reliable. Evidently, the ship is subtracted from the daily service with heavy costs for the owner.

Adequate instruments for recording all the relevant physical quantities are required.

First of all, a reliable method for measuring the actual sea-state during the test execution is necessary. Different kinds of pressure gauges and wave buoys exist, spanning from the simplest models that measure only the vertical displacement of sea free-surface ([Begovic et al., 2008], [Begovic et al., 2010]) up to more sophisticated buoys which give also information on the directional spreading of waves or the predominant wave direction, current direction and speed ([Cumming, 2005], [Scamardella, 2008] [Skey & Miles, 2005]). In addition, relative wind speed and direction can be recorded with directional anemometers fastened on masts [Cumming & Fleming, 2005].

Seakeeping trials are specifically performed for acquiring ship's motion in the six degrees of freedom. Until some years ago, instruments used for seakeeping tests were very expensive; for example angular motions were usually measured employing electromechanical gyros of the type used in aircraft navigation systems. Direct measurements of linear motion displacements were practically impossible, because they were not determinable without a suitable fixed reference datum. Ship's linear accelerations were recorded by means of accelerometers, and linear velocities and displacements were obtained by integrating the accelerometer data.

With the advent of new technologies, flexible and low-cost instrumentations for measuring the motion of objects are now available. Advances of Micro-Electro-Mechanical System (MEMS) technology have permitted the development of low-cost inertial sensors (composed of a cluster of accelerometers and gyroscopes), that can be used for evaluating both ship's angular motions and linear accelerations [Koning, 2009].

Global Navigation Satellite Systems (GNSS), such as the American Global Positioning System (GPS) or the Russian GLObal Navigation Satellite System (GLONASS) together with augmentation systems (e.g. the European Geostationary Navigation Overlay Service - EGNOS), provide satisfactory

accuracy in determining craft position even during high speed dynamic manoeuvres ([Nocerino & Scamardella, 2008], [Pacifico et al., 2009]).

If the objective of the tests is to acquire full scale motion data to validate physical model methodology as well as numerical simulation models, additional parameters have to be collected [Cumming & Fleming, 2005]: rudder angle can be measured with a yo-yo potentiometer; propeller shaft speed can be recorded using optical sensors, such as laser tachometers.

Each trial run must be of sufficient duration in order to ensure a reasonably estimate of the physical parameters to be assessed [Lloyd, 1989].

5.2.2 KINEMATICS AND HUMAN MOTION ANALYSIS

In this framework, kinematics deals with human movements, included linear and angular displacements, velocities, and accelerations. The type and the number of kinematic variables that have to be captured and assessed depend on the analysis required. For example, to describe the movement of the lower limb in the sagittal plane during one stride can require up to fifty variables [Winter, 2005]. To the purpose of testing the proposed control model, the angular displacement of the individual Centre of Mass (COM) with respect to the vertical is necessary.

Many different disciplines use motion analysis techniques for recording human movements and posture, including medicine, biomechanics, computer animation, virtual reality, etc. ([D'Apuzzo, 2003], [Roetenberg, 2006]).

Both research and commercial applications involve measurement, modelling and motion capture of the whole body or single parts (as human face). Consequently, different approaches and systems have been developed and they vary depending on the requirements. For example, high accuracy is needed for medical application, as in gait analysis of cerebral palsy patients [Winter, 2005]. In sport applications, high data acquisition rate is necessary for better understanding athlete movements and improving performances [Brodie, 2009]. For character animation in film and game industries, virtual reality, video surveillance the photorealistic aspect is fundamental ([D'apuzzo, 2003], [Roetenberg, 2006]).

Systems for body measurement and motion capture can be classified in direct measurement techniques (mechanical, magnetic, acoustic and inertial trackers) and optical methods (structured light systems, laser scanning, image-based techniques).

In the past, direct measurement techniques made use of goniometers, electrical potentiometers that were attached to body's limbs to measure joint angles ([Winter, 2005]). In the last decade, inertial sensors, often integrated with magnetic sensors or GPS receivers, have become quite common for motion capturing and measuring ([Brodie, 2009], [Ferrari et al., 2009], [Roetenberg, 2006]).

Optical sensors encompass a wide range of technologies, among which image-based systems are nowadays very popular in movement analysis ([D'Apuzzo, 2003], [Chiari et al., 2005], [Roetenberg, 2006], [Winter, 2005]).

Among the wide range of methodologies and technologies described above, the choice of instrumentations and sensors depends on the requirement of the specific experimentation.

The location where the experiments have been conducted differs substantially from any conventional ashore laboratories. The need of capturing the motion of an individual standing on a ship during its daily service has not permitted to employ the optical systems commonly used for human motion analysis. Commercial optical systems (e.g., Motion Analysis™, Vicon™), made up of many cameras, provide real time 3D data, but are costly and not sufficiently flexible. They have to be installed in specific locations and connected to a dedicated computer; the subject is required to move in a precise area, that is the measurement volume where the system accuracy is optimised. These sensors are not designed to operate in disadvantageous environmental conditions (water, wetness, saltiness) and with not optimal lightning.

The testing and validation of the proposed human control model has entailed the design and realization of a flexible and low-cost acquisition system.

5.3 A HIGH–FLEXIBLE MULTI–TECHNIQUE MOTION ACQUISITION SYSTEM

Validating theoretical models necessitates a lot of experiments to be conducted, in order to obtain relevant (statistically) data and infer significant results. A general procedure should require to have one or more ships completely available for executing a set of trials in different environmental conditions, testing many individuals involved in several tasks. This would be an "optimum" for obtaining data in a real environment, without the limitation on motion magnitude imposed by motion simulators, but would result in unbearable costs.

The solution adopted in this study has consisted in developing a motion acquisition system that could be easily usable onboard ships while accomplishing their daily mission. Furthermore, the system has been thought to work and be handled even by only one person in order to minimise the encumbrance onboard.

These characteristics and drawbacks have led to set up an "ad-hoc" motion capture system, whose peculiarities were:

- ease to use and calibrate even in disadvantageous conditions, as on a ship's deck;
- speed in setting up in different configurations and removing it in order to not hinder the normal execution of onboard tasks;
- flexibility for being employed on a movable platform, in cramped spaces, in unfavourable lighting conditions (also in the dark);
- taking up a minimal amount of space;
- to be integrated with sensors for measuring ship's motions;
- to be portable on different platforms, without interfering with onboard work.

Taking into account the specified requirements, the measurement system has been realised by integrating:

- an Inertial Measurement Unit (IMU), based on MEMES technology and integrated with a GPS antenna (Xsens MTi-G), for tracking and measuring ship's motion in the six degrees of freedom;
- a wearable device controlling multiple MEMES inertial sensors (Xsens Xbus kit) for acquiring 3D orientation as well as kinematic data of individuals onboard ships;
- three digital High-Definition video cameras for capturing human motion onboard (Sony HDR-CX106E).

This system is the core of a wider "mobile laboratory" for the assessment of manoeuvrability, seakeeping and personnel safety onboard developed in cooperation with the Laboratory of Topography and Photogrammetry of the University "Parthenope" of Naples. Within this project, other sensors have been also acquired:

- PCI data acquisition board;
- weather station with anemometer;
- triaxial accelerometers;
- biaxial inclinometers;
- linear displacement transducer for measuring rudder angle;
- magnetic and photoelectric sensors for measuring propeller shaft RPM.

Moreover, further instrumentations, such as, for example, wave buoy, will be available.

At the moment, the whole system is under development and testing, with the final goal of realizing:

- a complete data acquisition system for gathering all the important variables during a campaign in the field (section 5.2.1)
- a modular, flexible and "light" measuring tool, that could be installed on different (for both size and typology) vessels.

5.3.1 SHIP MOTION MEASUREMENT

For measuring ship motions in the six degrees of freedom an integrated GPS and Inertial Measurement Unit (IMU) has been used. The Motion Tracker MTi-G (Figure 5.1), produced by XSens Technologies [Xsens Technologies, Website], makes use of MEMS technology and consists of three accelerometers, three gyros, three magnetometers and static pressure (barometer).

Figure 5.1 – MTi-G with GPS antenna for measuring ship motion

The MTi-G dimensions are shown in Table 5.1

Table 5.1 – Mti-G dimensions

MTi-G	**Weight**	58 grams
	Housing dimensions (L×W×H)	(58×58×33) mm
GPS Antenna	**Housing dimensions (L×W×H)**	(2.32×2.05×0.53) mm

In order to improve the IMU accuracy and correct for drift, the vendor provides a GPS antenna, whose data are integrated through an extended Kalman filter. As clearly stated in the sensor manual and technical documentations, the implemented navigation algorithm uses different sources of information or assumptions (called "scenario") which vary depending on the field of application. The user has to determine the assumptions suitable for the application of interest, since, depending on the selected scenario, the sensor accuracy may significantly vary.

In Table 5.2, the sensor performance characteristics, as declared by the vendor, are reported.

Table 5.2 – Mti-G performance characteristics

GPS Receiver	**Type**	50 channels GPS L1, C/A code GALILEO OpenService L1
	GPS Update Rate	4 Hz
	Position/velocity Update Rate	120 Hz
	Accuracy Position SPS	2.5 m CEP* (3 m RMS)
	Accuracy Position SBAS	2.0 m CEP* (2.4 m RMS)
	Timing Accuracy	30 ns RMS
	Operational Limits	
	Maximum Altitude	18 km
	Maximum Velocity	600 m/s (2160 km/h)
	Max Dynamics GPS	4 g
Attitude and Heading from IMU and GPS	**Dynamic Range**	
	Pitch	± 90°
	Roll	± 180°
	Heading	± 180° (0°-360°)
	Angular Resolution	0.05°
	Static Accuracy	
	Roll/Pitch	<0.5°
	Heading	<1°
	Dynamic Accuracy	
	Roll/Pitch	1° RMS
	Heading	2° RMS
	Max Update Rate	120 Hz

* The Circular Error Probable (CEP) or circle of equal probability is defined as the radius of that circle, centred about the mean, the boundary of which is expected to include 50% of the population within it.

5.3.2 HUMAN MOTION CAPTURE

Kontaxis et al. [2009] define a motion analysis protocol as the means of measuring parameters required to test the hypotheses at the base of the study research question. The authors state that, when constructing a motion analysis protocol, the first issue that has to be addressed is to specify whether joint and/or segment kinematics is of interest, and to identify the joints and segments involved.

In the case study, experiments have been planned and conducted for testing a model that considers the planar motion of a rigid body with respect to the equilibrium position. Therefore, by considering the individual onboard an inverted pendulum, the motion of the subject COM in the direction of interest is the key parameter that has to be captured. Comparing the angle of the subject/pendulum with respect to the vertical measured onboard with the analogous output of the proposed model provides a proof of the model validity. For this purpose, two methodologies, motion measurement with inertial sensors and motion capture with videogrammetry, have been employed.

Unlike other motion capture systems, the use of video cameras also allows for retrieving semantic and general information that can help in better understand and reconstruct the overall dynamics to be studied.

5.3.2a INERTIAL MEASUREMENT OF HUMAN MOTION

The Xbus Kit (Figure 5.2) is a lightweight, portable system that incorporates a master (Xbus Master) and up to ten IMU or Motion Trackers (MTx) [Xsens Technologies, Website] made up of three accelerometers, three gyros and three magnetometers. Table 5.3 shows the system dimensions.

The master powers and synchronises the inertial sensors and transmits the inertial data to a PC also via Bluetooth connection. This kind of connection is particularly suitable for biomechanics, rehabilitation, and all the applications that need to acquire human movement without any mechanical interference or constraint. The master can be attached to a belt and fasten around the waist, while the single inertial units can be fixed to body limbs.

Figure 5.2 – Xbus Kit for measuring human motion

Table 5.3 – Xbus kit dimensions

Xbus Master	**Weight**	330 grams (batteries included)
	Housing dimensions (L×W×H)	(150×100×20) mm
MTx	**Weight**	30 grams
	Housing dimensions (L×W×H)	(53×38×21) mm

Table 5.4 – MTx performance characteristics

Angular Resolution	0.05°
Repeatability	0.2°
Static Accuracy	
Roll/Pitch	0.5°
Heading	1.0°
Dynamic Accuracy	2° RMS
Max Update Rate	120 Hz

The MTx are provided by the vendor with a Kalman Filter for computing 3D orientation (attitude and heading). The factory fusion algorithm employs the measurement of gravity, by the three accelerometers, and Earth magnetic field, by the three magnetometers, for compensating for gyro drift. As for the MTi-G used for measuring ship motion, also in this case, depending on the

expected movement to be measured, the user has to select the proper scenario, that determines the assumptions for combing the data.

Table 5.4 shows the orientation performance characteristics for MTx, as reported in the factory technical documentation:

5.3.2b VIDEOGRAMMETRY FOR HUMAN MOTION CAPTURE

The image-based motion capture system is made up of three low-cost, light and compact video cameras (Sony HDR-CX106E, Figure 5.3) and different kind of supports (three solid tripods or clamps with respective ball heads).

Figure 5.3 - Low-cost High-Definition video camera for the videogrammetric system

The camcorders have a resolution of 1920×1080 pixels, a frame-rate of maximum 25 Hz and employ a CMOS (Complimentary Metal-Oxide Semiconductor) image sensor. Such sensors are usually less expensive, but have lower quality than CCD (Charge Coupled Device) sensor used in digital cameras.

A very common drawback in consumer video cameras with CMOS sensor is the interlace effect. Each frame is divided into two consecutive fields, one containing all even lines, another with the odd lines. The fields are captured separately at a rate twice that of the nominal frame rate. The two separate fields are then combined (interlaced) with each other for forming the frame. The employed Sony cameras capture 50 fields every second (25 odd and 25 even); the two sets of 25 fields are joined together to create a full frame every 1/25th of a second. This results in a saw pattern effect when the enclosed object is moving (Figure 5.4 left).

For solving this problem, a deinterlacing process has to be applied. For each original frame, the two fields are split, obtaining two separate frames consisting of only even or odd lines (Figure 5.4 right). The empty lines are then filled by interpolating the upper and lower fields. The resulted video has a frame rate identical to the field rate, namely a frame rate twice that the original rate.

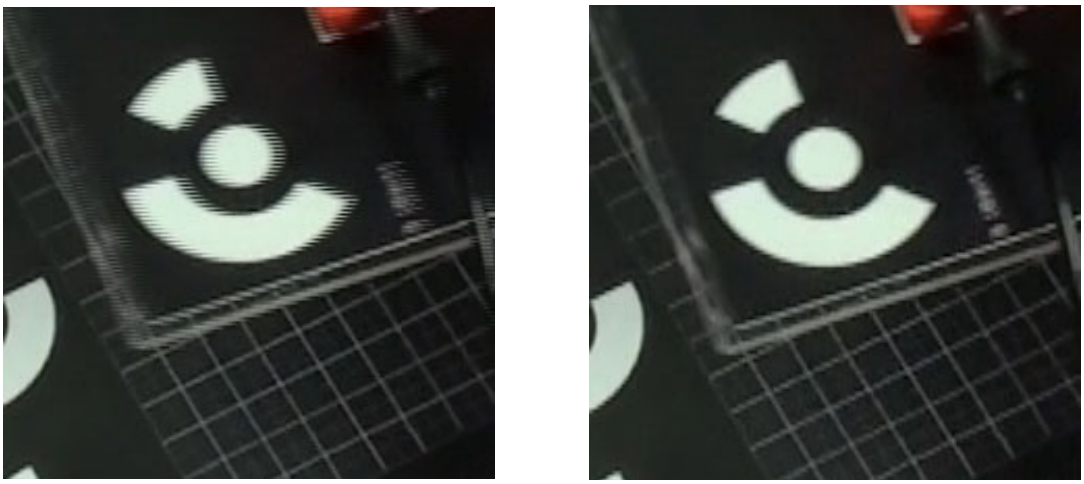

Figure 5.4 - Image processing.
Left: Image frame before deinterlacing process.
Right: Image frame after deinterlacing process

SYSTEM CALIBRATION

For calibrating the videogrammetric system two stages are necessary: calibration of each video camera and computation of exterior orientation of the system respect to object reference frame.

1) Camera Calibration

   The first stage is necessary for obtaining the geometric characteristics of each video camera and is usually repeated over time (some months) due to the instability of the camera mechanics and manufacture [Wackrow et al., 2007]. Each single camera is calibrated through a computational procedure [Akca & Gruen, 2009].

With each video camera, a 3D testfield was recorded from different points of view. The video was processed and an image sequence of 18 images was rendered. The image sequence was imported into a commercial package (Photomodeler) for computing the camera calibration parameters (Figure 5.5).

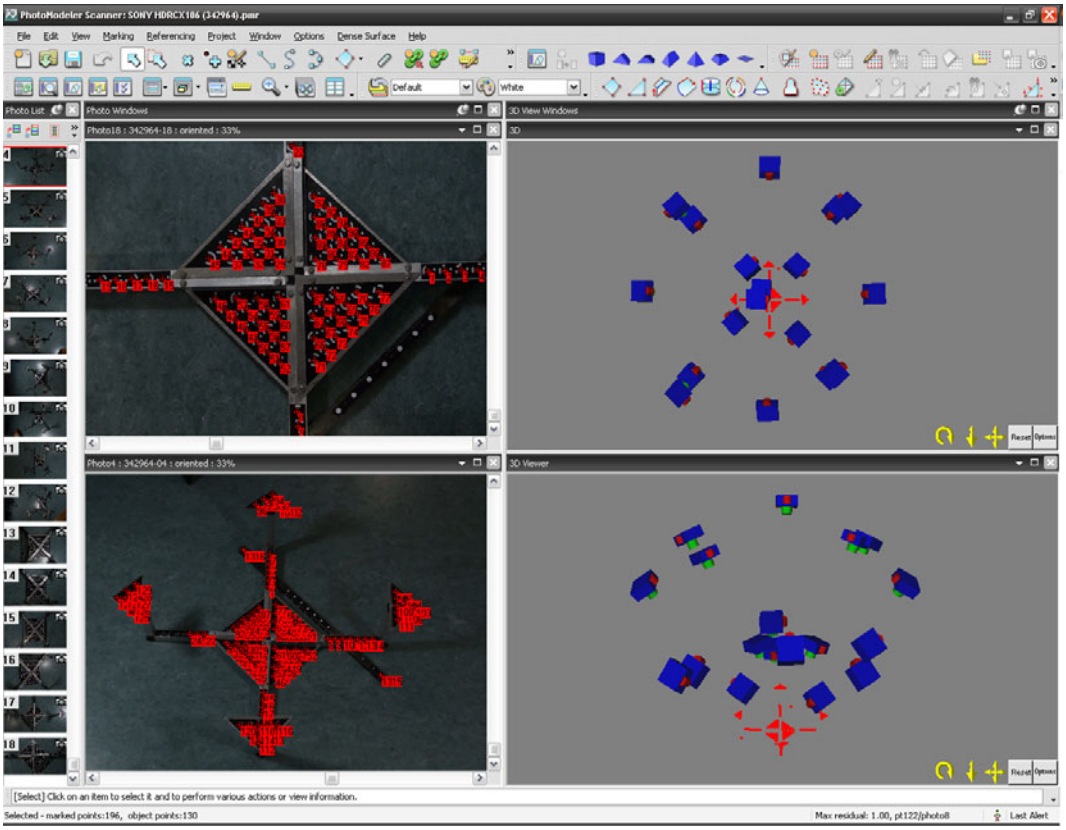

Figure 5.5 - Graphical User Interface of Photomodeler for camera calibration.
Left: 3D testfield with marked points.
Right: 3D points and camera stations after the calibration process

2) Exterior Orientation

This stage has to be repeated every time the cameras are arranged in a new configuration and location.

Once the camera calibration parameters have been calculated, as described in section 5.C.1 a minimum number of homologous points have to be marked on the frames for obtaining the exterior orientation parameters.

A very flexible method to orient the cameras has been employed. First of all, the cameras are synchronised by turning on (off) a high intensity LED during the video registration; the first (last) instant time in which the LED is visible is taken as the synchronization event. Then, the LED is moved within the measurement volume (Figure 5.6). Its image position is easily recognisable on the three synchronous frames from the video cameras and can be marked on them, as homologous point, with simple image processing algorithms.

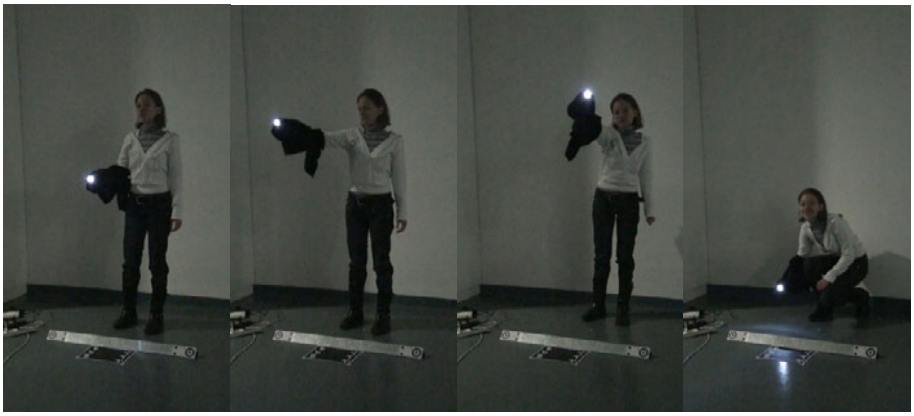

Figure 5.6 - Some frames of the image sequence used for orienting the three video cameras.
The LED is visible within the measurement volume

If the cameras remain still in their positions, the exterior orientation does not vary during the recording. After some seconds, hundreds of homologous points are automatically marked allowing to compute the exterior orientation with high redundancy, being five the minimum number of points that should be marked (Figure 5.7).

Once the system has been calibrated and video cameras oriented, measurements can be taken within the measurement volume. Since the system can be arranged in different configurations, different accuracy in measuring a well-targeted point can be reached depending mainly on the distance between the object and the video cameras. Typically, for the applications of interest accuracy ranges from 0.1 mm at a distance of 1 m, to 2 mm at a distance of 5 m.

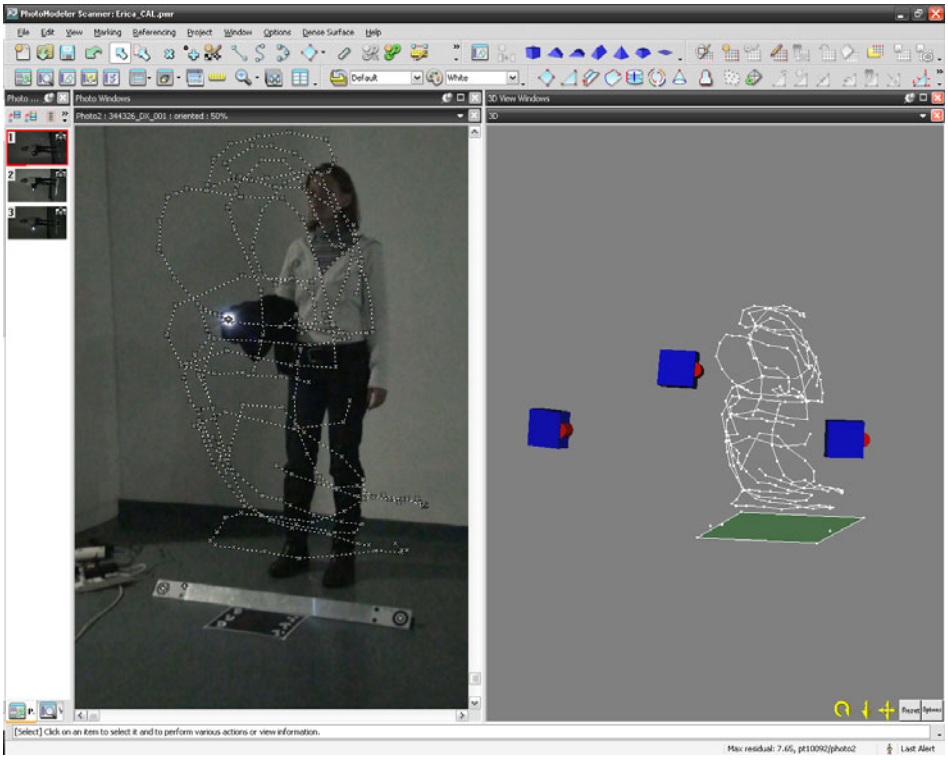

Figure 5.7 - Graphical User Interface of Photomodeler for exterior orientation.
Left: LED trajectory (made up of about 300 points) automatically marked for computing the exterior orientation.
Right: 3D positions of cameras and LED trajectory

5.4 PRELIMINARY TESTS

As widely discussed and motivated in literature (e.g., [Chang et al., 2008], [Roetenberg, 2006]) there are important limitations in the current motion measurement systems based on MEMS IMU. These arise mainly because the inherent drift of the orientation and position estimates limits long-term stability. Brodie [2009] showed that the Xbus kit is capable to capture some types of motion, as slow movements, but it fails to accurately capture rapid movements, as under continuous rotation.

The problem of calibration of low-cost inertial units has been previously faced by the author [Angrisano et al., 2009]. Within the present experimentation, the factory calibration data have been used, since they have been considered suitable for the planned purposes.

In order to verify reliability of the inertial sensors for the application of interest, several static and dynamic tests have been conducted.

5.4.1 STATIC TESTS

Laboratory indoor tests have been conducted in order to verify the orientation output provided by the inertial sensors (Mti-G without the GPS antenna and MTx) in static conditions.

The units were fastened to a high-precision electronic theodolite (WILD T2000, Figure 5.8) that was turned into different orientations. In each position, calibrated data from the sensors were acquired using the factory software and recorded for at least 60 seconds.

Figure 5.8 - Static tests: inertial sensor MTx fastened on the telescope of the WILD T2000 theodolite

The tests showed that the inertial sensors, after short transients, were able to measure attitude (roll and pitch) with an accuracy of about 0.15°. Moreover, during the time interval of each single trial, the drift was not significant. Troubles were found in determining the yaw (heading), since the

magnetometers were strongly influenced by the magnetic field generated by the electric circuits of the theodolite.

It was concluded that in static conditions the inertial sensors work well as inclinometers. Unfortunately, they can not be used for heading assessment if strong and variable magnetic fields are expected. As far as the MTi-G is concerned, improvements are presumed if data from GPS are integrated.

5.4.2 DYNAMIC TESTS

The motion capture system described in section 5.3.2b was used as reference for testing the reliability of the inertial units in dynamic conditions.

Two different set of trials have been conducted. The videogrammetric system was arranged into the laboratory (indoor) for executing the experiments with the MTx (Figure 5.9), the IMU for measuring human motion. In the case of the MTi-G employed for recording the ship motion, the experiments were carried on outside (on a terrace for heaving the skyline free from obstruction), in order to test the integration with the GPS.

Figure 5.9 - Dynamic tests: indoor laboratory set-up

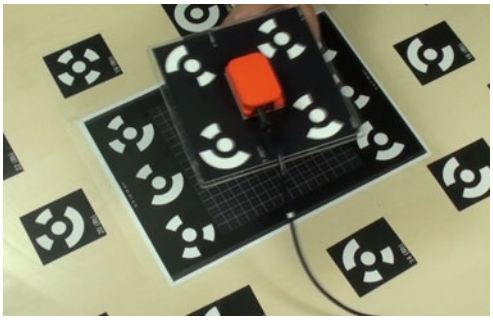

Figure 5.10 - Inertial sensor fastened on the non-magnetic base of support with photogrammetric targets

A suitable base of support was built of non-magnetic rigid material (Figure 5.10). The IMUs were fastened on the top of the plate, where a recognisable path with four coded targets was drawn. In order to synchronise the videos and the record from the IMUs, a suitable system has been assembled. A mechanic switch simultaneously hits the inertial sensor and turns on a LED fixed to the IMU housing.

The plate was manually moved by an operator, simulating dynamics of interest. The motion of the plate was recorded by the three camcorders (50 frames per second) and, simultaneously, calibrated data from the inertial sensors were acquired and sampled at 100 Hz using the factory software.

Each trial lasted about 90 seconds and was composed of three phases:

1) an initial phase in which the plate remained still;
2) a central phase in which the dynamics was gradually increasing;
3) a final phase in which the plate was placed again in the original position.

The videogrammetric techniques made it possible to retrieve both the linear and angular movements of the plate and, consequently, the sensor motion in the six degrees of freedom. The coded targets were tracked using a procedure involving both commercial and own-developed software. The accelerations were obtained by integrating twice the tracked plate motion. In this way, only the accelerations due to the motion were measured. In order to obtain the proper accelerations and compare them with the accelerations

from the inertial units, the components due to gravity were calculated and added. The acceleration obtained from this procedure were quite noisy as shown in fig. However, the comparison is reported since it gives a qualitative idea of the accordance between the data from the different techniques.

The tests have demonstrated that the outputs provided by the inertial sensors are in accordance with the specifics declared by the vendor.

Moreover, it has been proved that within a time interval of about 80 seconds the roll and pitch angles do not show a significant drift for both the MTx and the MTi-G. This conclusion also holds for the yaw angle provided by the MTi-G, thanks to the integration with the GPS, while the yaw angle provided by the MTx is not sufficiently reliable.

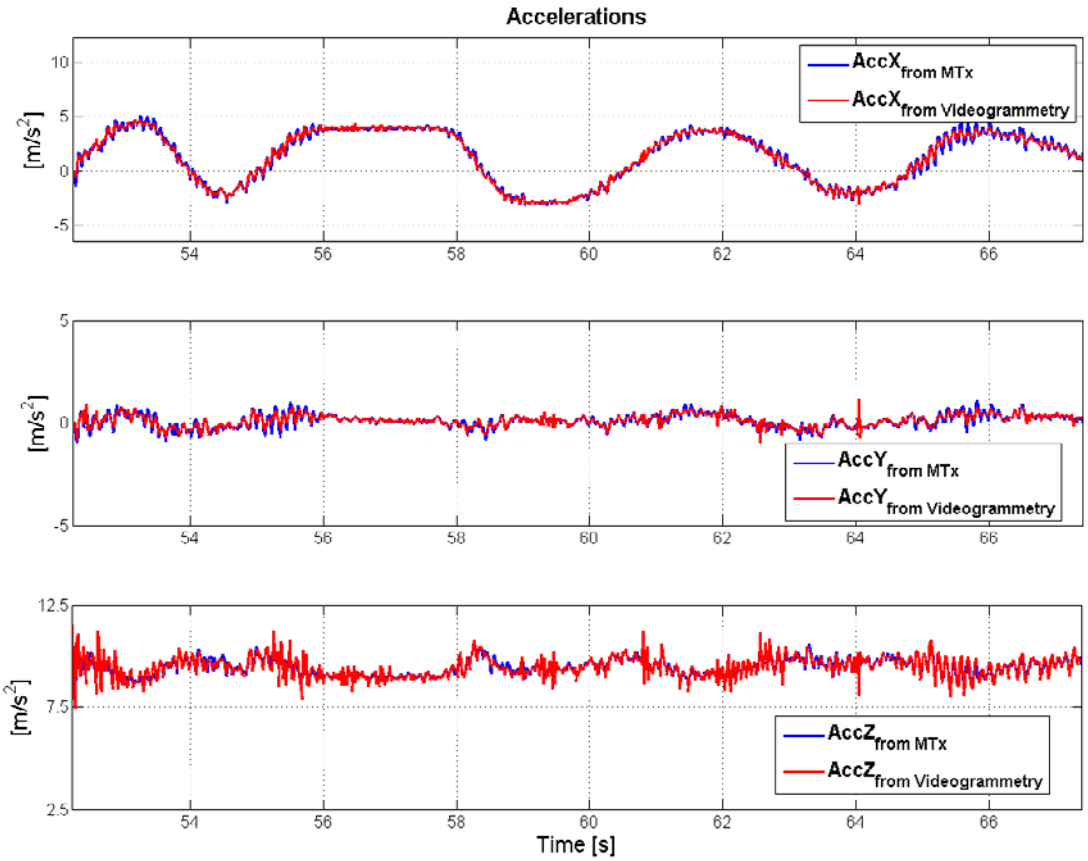

Figure 5.11 – Comparison between the accelerations from videogrammetry and MTx

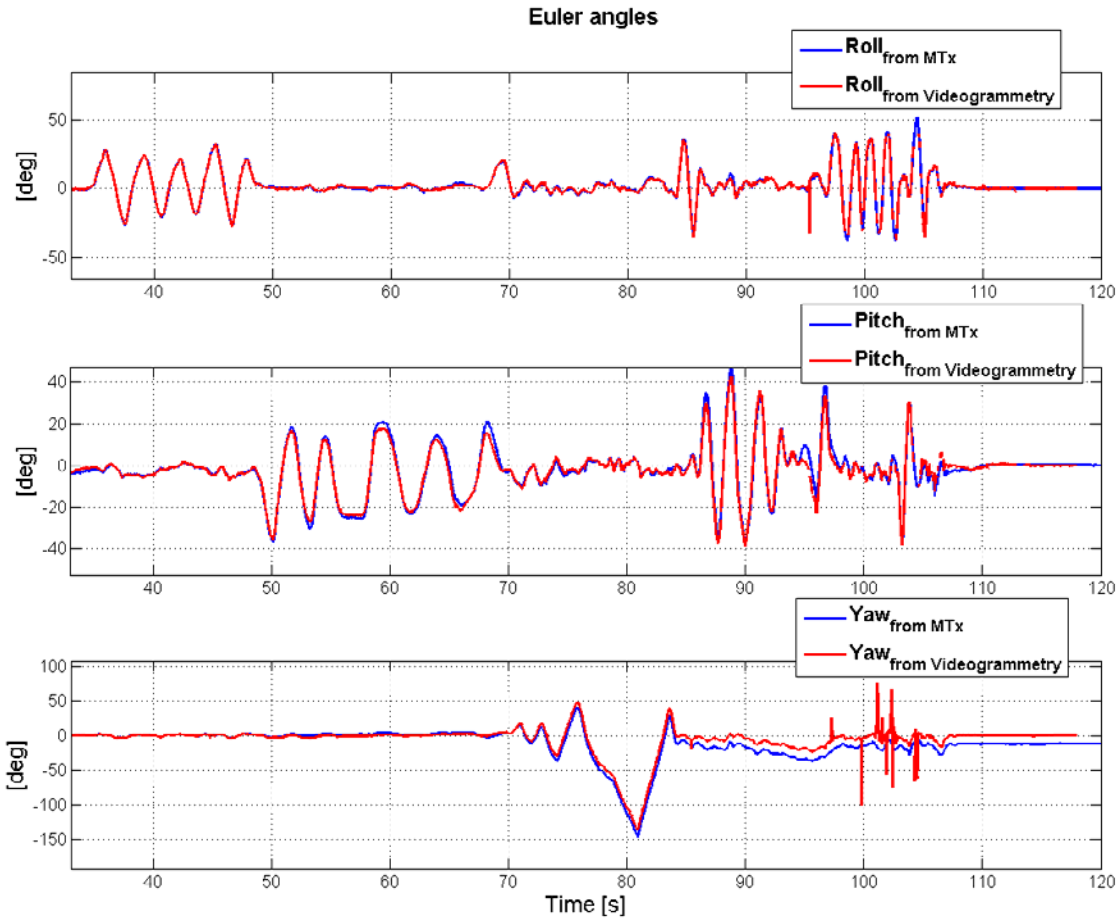

Figure 5.12 - Comparison between the Euler angles from videogrammetry and MTx

Figure 5.11 and Figure 5.12 show a representative comparison between the accelerations and the Euler angles measured by the MTx and calculated with videogrammetry.

5.4.3 CALCULATION OF HUMAN CENTRE OF MASS

Because the model to be validated considers only the simple movement in the antero/posterior direction, for the set of tests here presented it was not necessary to employ a crewmember, subtracting him from his tasks. Instead, subjects from the research group were employed.

Before the execution of onboard trials, the COM in three dimensions of subjects successively employed in the stability tests have been measured in laboratory. Accurate determination of the COM position requires a fully body kinematics analysis [Eames et al., 1999], which is usually performed, for example, in clinical studies. In the present application, evaluating the COM's height was necessary in order to obtain an approximated location for placing the inertial sensor and videogrammetric targets. This estimation was important for the trials in the onboard setting characterised by cramped spaces, where to perform a fully body kinematics analysis was not easy (sometimes not possible).

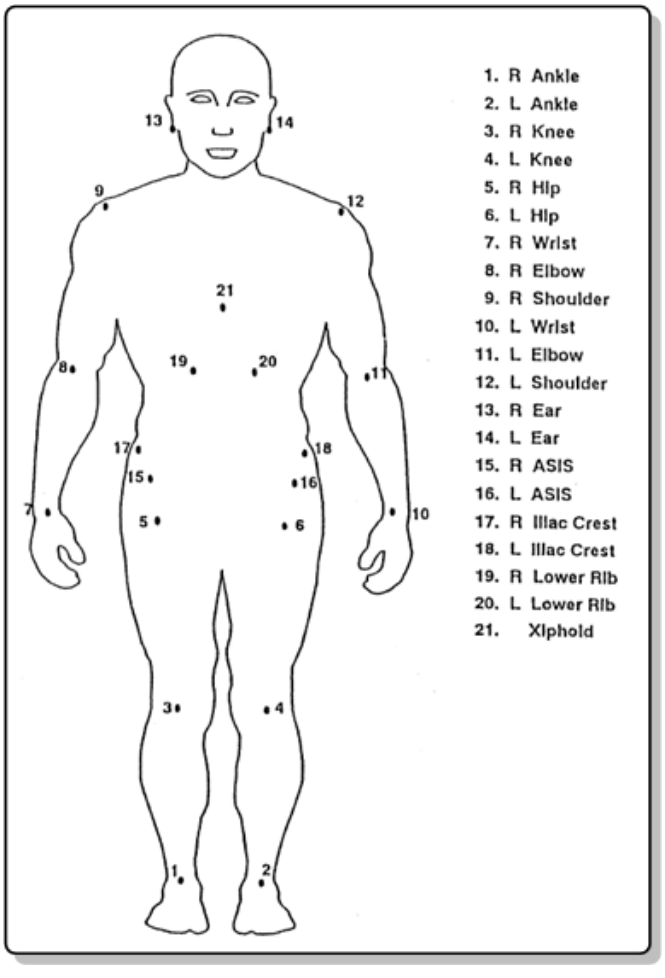

Figure 5.13 - Location of 21 markers in the 14 segment 3D model to estimate total body COM (after [Winter, 2005])

To this purpose, the model proposed by Winter [2005] for determining the mechanisms of balance during quiet standing has been used. The model subdivides the body into 14 segments, identified by 21 markers; the mass of each segment is expressed as a percentage of the total body mass. Figure 5.13 shows the location of the markers and Table 5.5 gives the definition of each of the 14 segments, along with mass fraction and COM definition of each segment.

Table 5.5 - Definition of the 14 segments, mass fraction and COM (after [Winter, 2005])

SEGMENT	MASS FRACTION	DEFINITION OF SEGMENT COM
Head	$f_1 = 0.081$	$\mathrm{COM}_1 = \frac{13+14}{2}$
Trunk 4	$f_2 = 0.136$	$\mathrm{COM}_2 = \frac{9+12+21}{3}$
Trunk 3	$f_3 = 0.078$	$\mathrm{COM}_3 = \frac{\left((19+20)/2\right)+21}{2}$
Trunk 2	$f_4 = 0.065$	$\mathrm{COM}_4 = \frac{17+18+19+20}{4}$
Trunk 1	$f_5 = 0.078$	$\mathrm{COM}_5 = \frac{17+18+15+16}{4}$
Pelvis	$f_6 = 0.142$	$\mathrm{COM}_6 = \frac{15+16}{2}$
Thighs	$f_7 = f_8 = 0.100$	$\mathrm{COM}_7 = 0.433\times 3 + 0.567\times 5$ $\mathrm{COM}_8 = 0.433\times 4 + 0.567\times 6$
Legs & Feet	$f_9 = f_{10} = 0.060$	$\mathrm{COM}_9 = 0.606\times 1 + 0.394\times 3$ $\mathrm{COM}_{10} = 0.606\times 2 + 0.394\times 4$
Upper arms	$f_{11} = f_{12} = 0.028$	$\mathrm{COM}_{11} = 0.436\times 8 + 0.564\times 9$ $\mathrm{COM}_{12} = 0.436\times 11 + 0.564\times 12$
Lower arms	$f_{13} = f_{14} = 0.078$	$\mathrm{COM}_{13} = 0.682\times 7 + 0.318\times 8$ $\mathrm{COM}_{14} = 0.682\times 10 + 0.318\times 11$
Total	$\sum_{i=1}^{14} f_i = M_{body} = 1$	$\mathrm{COM}_{\mathrm{body}} = f_1\cdot\mathrm{COM}_1 + f_2\cdot\mathrm{COM}_2 + \ldots + f_{14}\cdot\mathrm{COM}_{14}$

Measured the 3D coordinates of the 21 markers by a videogrammetric system, the COM of each segment can be calculated according to formulae reported in Table 5.5. The COM position in 3D at a given frame is then determined according to equation (5.1):

$$\begin{cases} x_{COM} = f_1 x_1 + f_2 x_2 + \ldots + f_{14} x_{14} \\ y_{COM} = f_1 y_1 + f_2 y_2 + \ldots + f_{14} y_{14} \\ z_{COM} = f_1 z_1 + f_2 z_2 + \ldots + f_{14} z_{14} \end{cases} \quad (5.1)$$

where

- $f_1, f_2, \ldots, f_{14}$ are the mass of each of the 14 segments expressed as a percentage of the total body mass (Table 5.5);
- $(x_i, y_i, z_i)_{i=1,2,\ldots,14}$ are the coordinates of the COM of each single body segment (Table 5.5).

In a suitable space, the capture system described in section 5.3.2b was set up and calibrated. A set of 21 adhesive bandage markers was prepared for each individual that had to be measured (Figure 5.14). The markers were drawn as black circles on a white background, in order to ensure a high contrast; this made easier the point measurement phase with the photogrammetric software (Photomodeler).

Figure 5.14 - Calculation of human centre of mass: laboratory set-up

The result of COM calculation for one of the tested subjects is shown in Figure 5.15.

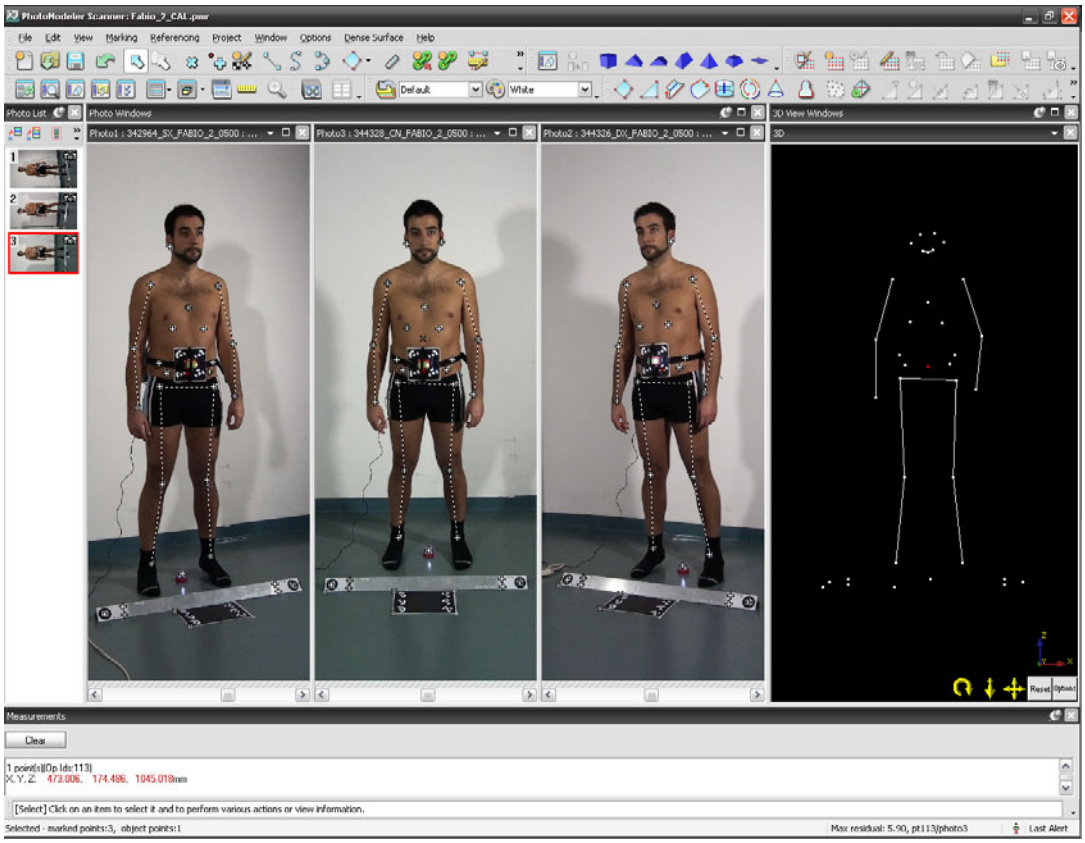

Figure 5.15 - Graphical User Interface of Photomodeler for COM calculation. Left: Synchronised image frames from the three video cameras. Right: 3D positions of body COM (red dot)

Each subject was also instrumented with the IMU placed on the reference plate and a high-intensity LED attached to the sensor housing.

Assuming that the person body is rigid, the COM motion can be tracked recording the displacement of the LED positioned at the measured COM height. Figure 5.16 reports the two-dimensional displacement of the COM for a 80-second record in quiet standing. The graphic shows that the main motion component is in the antero/posterior direction, in agreement with that discussed in Chapter 3.

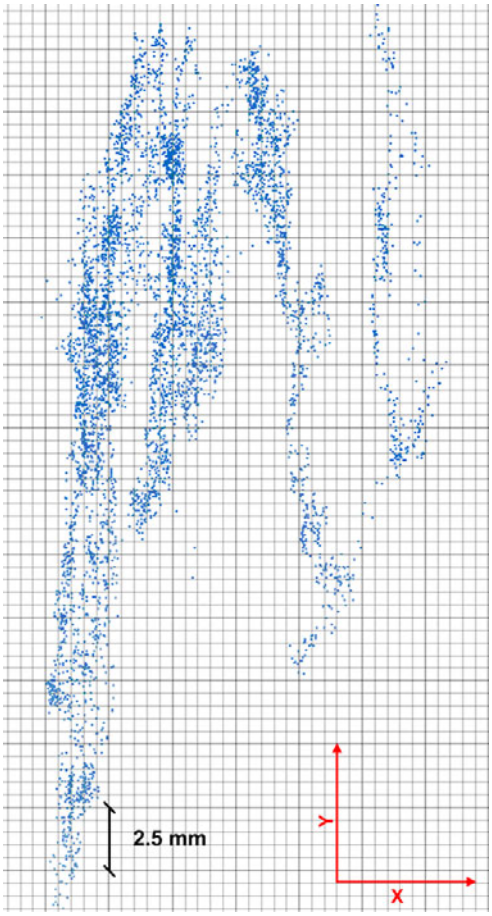

Figure 5.16 – 2D displacement of the COM for a 80-second record in quiet standing

In Chapter 4 the angles α and γ have been defined. The videogrammetric system is able to retrieve the angle γ between the inverted pendulum and the normal to the base of support. On the contrary, the inertial unit provides the angle α relative to the absolute vertical. If the platform where the individual is standing remains still (horizontally), the angle γ coincides with α. This condition was verified during the quiet postural stability tests here presented, making possible to compare directly the angles measured by the two different systems. The results from this comparison (Figure 5.17) show that the two measurements slightly differ and that the angle from the MTx is systematically larger (in the order of instrumental accuracy).

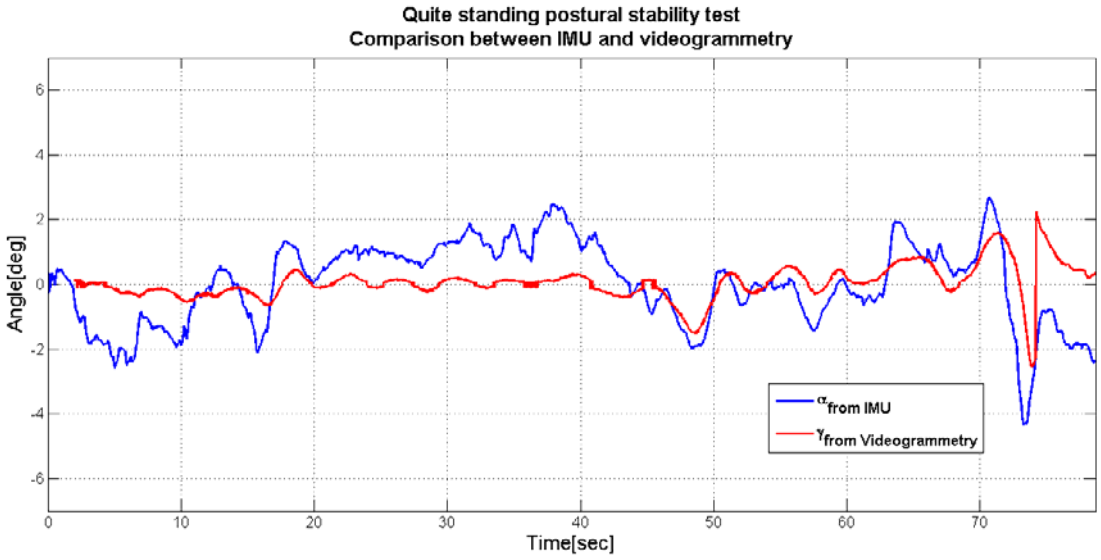

Figure 5.17 – Quite standing postural stability test: comparison between inertial sensor and videogrammetry

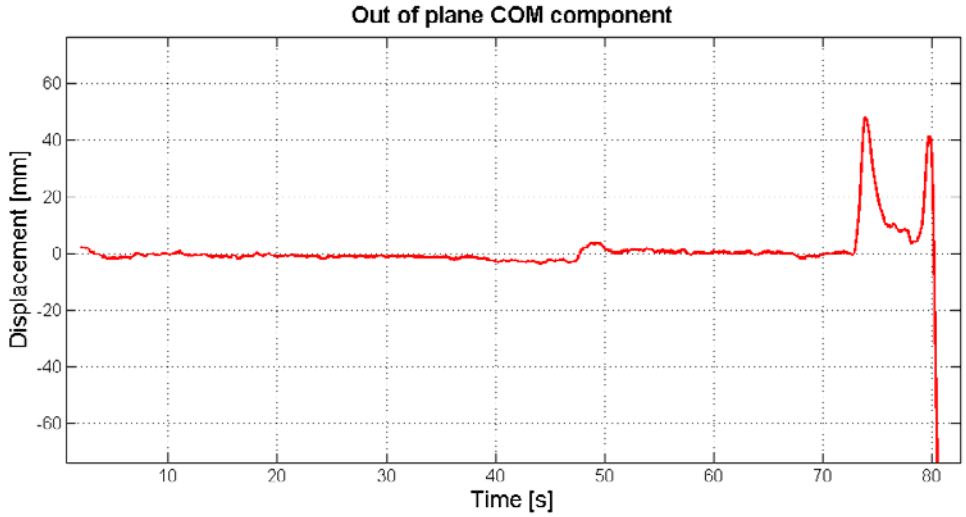

Figure 5.18 – Out-of-plane COM component from videogrammetry

So far, a person has been modelled as an inverted pendulum whose motion is allowed only in a plane, namely the sagittal plane (see Chapter 3 and Chapter 4). Figure 5.18 reports the motion component outside of this plane and gives information about the validity of the "inverted pendulum" hypothesis. If the magnitude of the out-of-plane component increased

significantly, the "inverted pendulum" model would be no longer suitable for describing the individual postural stability. The final part of the displayed trace shows that the out-of plane COM component is increasing: this corresponds to the moment where the recorded subject is moving at the end of the quiet standing test.

5.5 ONBOARD TRIALS

The presented trials have been conducted with the twofold aim of testing the designed data acquisition system in the real environment and trying a first validation of the proposed human control model.

Many practical difficulties have been faced, mainly related to the setting where the tests have been conducted. First of all, to find an operating ship available to host a research group (with its instrumentation) is not a minor matter. Other unexpected troubles have arisen onboard during the trial execution. For example, a set of tests was unusable because one of the video cameras was locked to an element of the cabin wall not completely fixed with the ship. The relative motion (in terms of vibrations) of this camcorder with respect to the other was not perceptible during the trials execution. Only during the post processing, this problem was detected by analysing the videos. However, the data from the video cameras were an important support in analysing and understanding the measurements from the inertial sensor.

Important lessons have been learned from this first experience, as far as both the execution of similar experiments and the tuning of the proposed postural model are concerned.

5.5.1 THE SHIP

The ship employed to this purpose is a 16.30-meter long wooden ship. The "San Gaetano" is a purse seiner inshore fisheries vessel (Figure 5.19), built by a long-established shipyard of carpenters in the South of Italy.

Figure 5.19 – The purse seiner "San Gaetano" with the "bug boat" in the port of Mergellina (Napoli, Italy)

By tradition, small wooden fishing vessels are built by templates, often without the related lines drawing being produced. Also in the case of "San Gaetano", the paper lines drawing does not exist, and an underwater survey has been carried out for retrieving it (Figure 5.20).

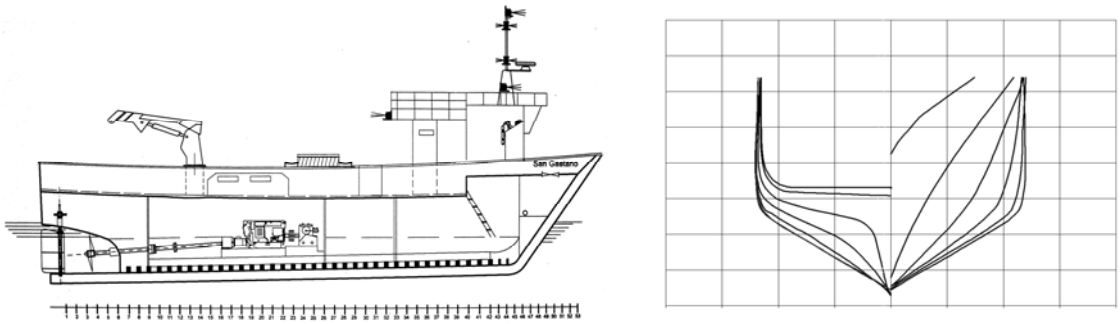

Figure 5.20 – Left: Longitudinal plane of the "San Gaetano". Right: Transversal plane of the "San Gaetano" (from underwater photogrammetry)

The "San Gaetano" performs night fishing activity in the Bay of Naples and surroundings, catching aggregating pelagic species (sardines, mackerel, anchovies, garfishes, etc.) near the surface of the sea.

The most important part of the fishing operation is searching for the fish shoals and assessing their size and direction of movement. The "San Gaetano" is equipped with sophisticated electronics (echosounders, sonar and track plotter) used to search for and track schools, assess their size and movement, and keep in contact with the school while it is surrounded with the seine net1 (Figure 5.21).

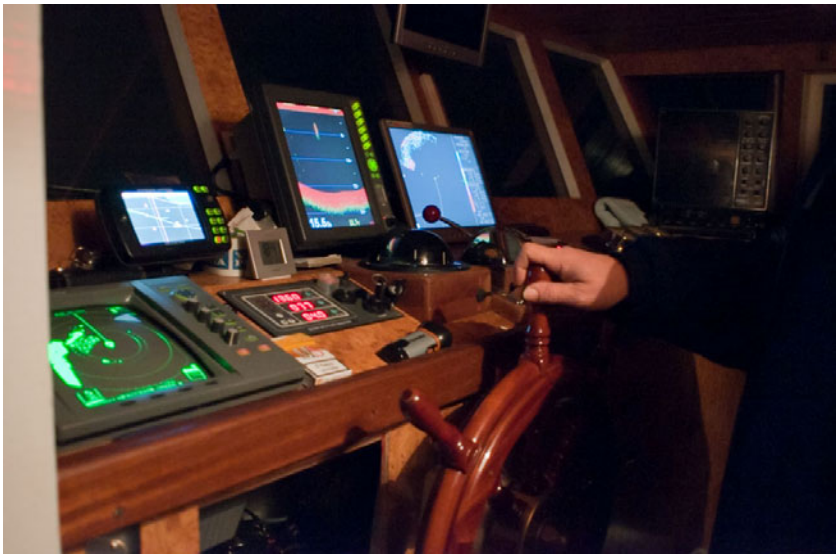

Figure 5.21 – Pilot bridge of the "San Gaetano". Electronics for searching and tracking the schools

Detected the school, the fishing process starts with the release of the "bug boat". The bug boat motors in place, while holding one end of the net, and the seiner rapidly circles the shoal. Once the "San Gaetano" reaches the bug boat, this motors to the opposite side of the seiner and powers away from the seine net to insure that the mass of fish and net do not drift below the seiner. No lights are used during this phase.

[1] A seine is a large fishing net that hangs in the water due to weights along the bottom edge and floats along the top. A purse seine presents along the bottom a number of rings; a rope passes through all the rings, and when pulled, draws the rings close to one another. The bottom of the net is then closed, trapping the catch inside and preventing the fish from escaping.

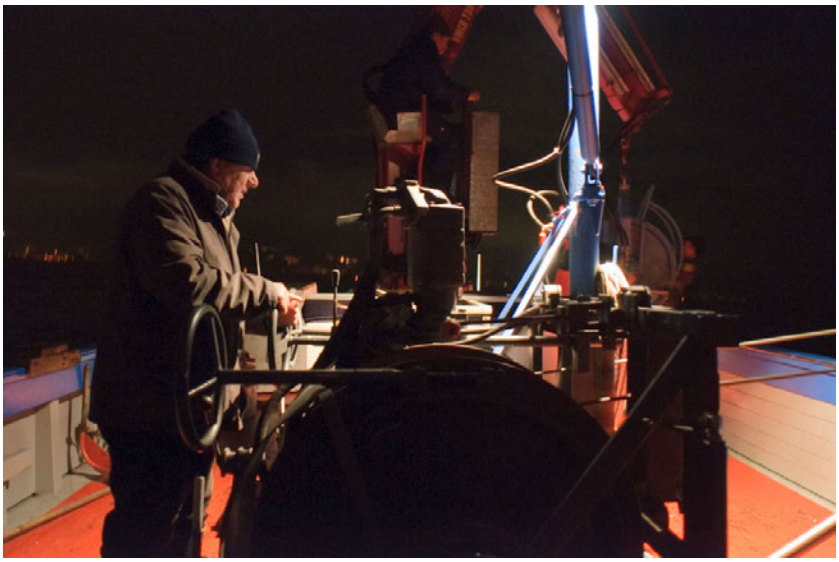

Figure 5.22 – The "San Gaetano" is equipped with a winch for pulling in both ends of the purse line

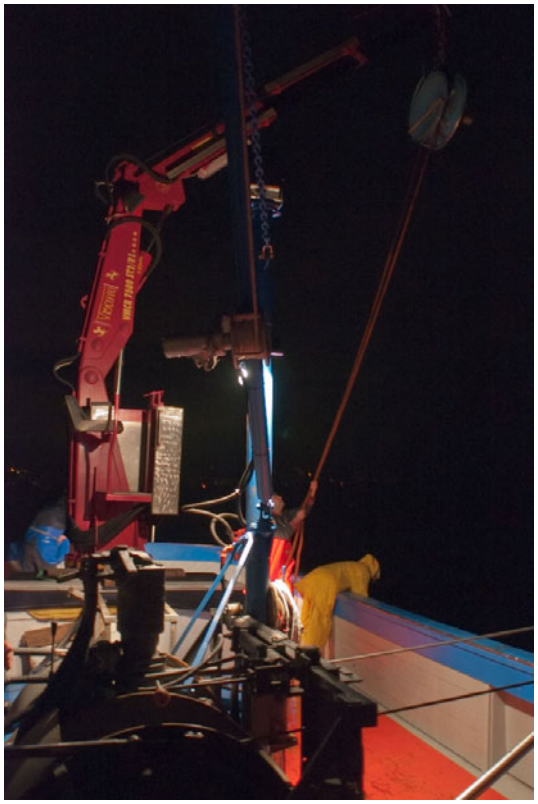

Figure 5.23 –Fishing operations the seine net is running through the "power block"

The "San Gaetano" is fitted out with a winch on the deck. When the bug boat is in place, the winch pulls in both ends of the purse line (Figure 5.22), closing (pursing) the bottom of the net underneath the fish shoal. Deck lights are then turned on and one end of the seine net is run through a large, hydraulically driven "power block" (a mechanized pulley) located at the top of a crane (Figure 5.23).

Part of the catch is picked by hand and part transferred using a brailer operated partly by hand and partly by power (Figure 5.24). Fishes are storage in crates arranged on deck (Figure 5.25).

At last, the net is lowered through the power block and stacked on deck in preparation for the next set (Figure 5.26).

The whole fishing process is really striking, in particular when the net is kept by the power block forming a high wall with the slender fishes shining in the dark (Figure 5.27).

However, it has to be kept in mind that fishing is a very hazardous activity [ILO, 2007]. During seine fishing, the crew can experience many dangerous situations: ropes are subjected to high stress; the deck is wetted and covered with fishes; fishing tasks are often performed without protective gauntlets (Figure 5.28). These factors explain further the choice of "San Gaetano" within the present research.

Figure 5.24 – Fishing operations: the brailer is used for transferring part of the catch

Figure 5.25 – Fishing operations: the crates are arranged on deck for storing the catch

Figure 5.26 – Fishing operations: a crewmember is stacking the net on deck

Figure 5.27 –Fishing operations: the net is kept by the power block forming a high wall with the slender fishes shining in the dark

Figure 5.28 – A crewmember cut one's hand

The postural stability tests were conducted during different phases of the fishing operation: i) while the ship was transferring to the fishing area, keeping a route quite straight at the cruising speed; ii) while fishermen were getting back the net onboard and picking the catch, with the boat kept at zero speed. These represent the most hazardous moments since the crewmembers are usually involved in the execution of the allotted tasks.

Measurements were not taken while the seiner was rapidly circling the shoal because during this phase the fishermen are usually not working and they can lean against or grasp some props.

5.5.2 THE ONBOARD SETTING

Before executing the trials, a first survey was made during ordinary fishing operations. The first outing onboard the "San Gaetano" was necessary for learning about the catching method, and, above all, identifying a proper location where to install the measurement equipment and to carry on the successive experiments.

The setting was chosen in order to not cause interference with onboard activities. The motion capture system was mounted inside the cabin located behind the deck house. The camcorders were secured to the cabin walls with the clamps mounting the ball heads. Two video cameras were placed for viewing simultaneously an individual facing forwards or backwards. The third was arranged in order to form a base with one of the other two cameras and record an individual facing laterally (Figure 5.29 and Figure 5.30).

Figure 5.29 – Onboard tests: experimental setting. The white circles indicate two of the three employed camcorders

Figure 5.30 - Onboard tests: experimental setting. The white circles indicate the tird video camera. A member of the research group is instrumented with the MTx on the photogrammetric plate (green circle)

The tested subjects were instrumented with the Xbus kit (Figure 5.30): the master was attached to a belt and fasten around the waist; the MTx on its photogrammetric plate was placed next to the COM height evaluated during the quiet standing stability tests (section 5.4.3).

The MTi-G for ship motion measurement was positioned on the cabin deck close to the vertical projection of the individual's COM. For assuring adequate performance and avoiding aliasing phenomena, the sensor was mechanically isolated, by using a layer of sponge, from deck vibrations. The GPS antenna was located outside the cabin at a known distance from the inertial unit, for guaranteeing satellite visibility.

The two separate inertial sensors were connected to the same PC and the data from both the MTi-G and the Xbus master were collected via the factory

software at a 100-Hz acquisition rate. This allowed to reduce the hardware required onboard and, at the same time, to synchronise the data from the two inertial units.

Once the videogrammetric system had been synchronised with the inertial sensors, each measurement session lasted about 90 seconds.

5.5.3 COMPARISON WITH THE SIMULATED RESULTS

In this section, the results from a postural stability test with the subject facing in the lateral port (positive) direction are presented as illustrative case.

In order to evaluate the potentialities of the proposed postural stability control model in simulating human motion onboard ships, the ship motions measured during the full scale trials (Figure 5.31) have been used as input for the software described in Appendix 4.A.

To this purpose, an own-developed software procedure, implemented in Matlab, has been employed for post processing the data acquired by the inertial units during the tests onboard.

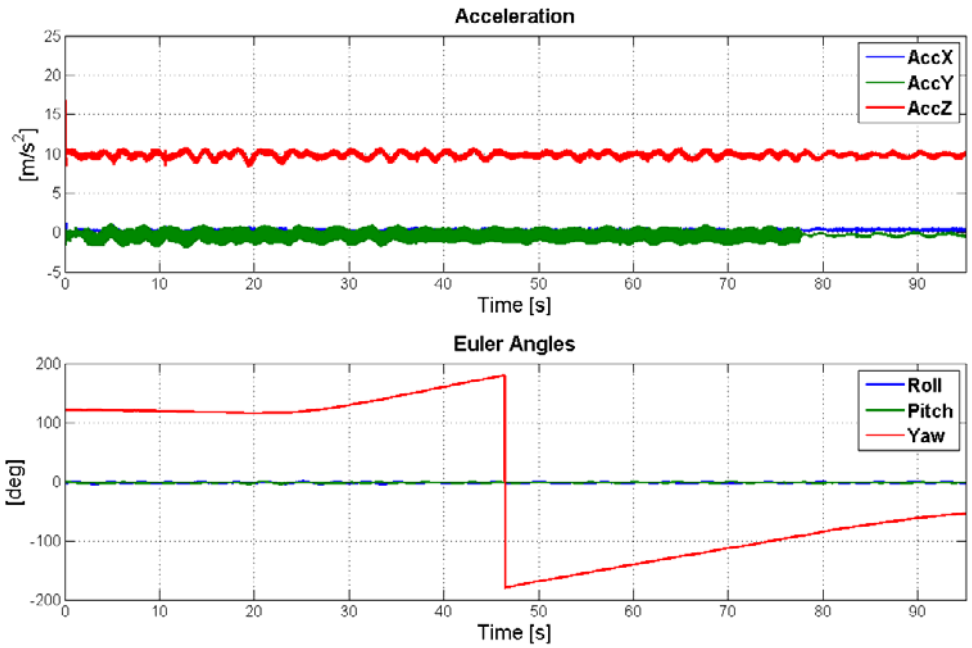

Figure 5.31 – Mti-G data: ship motion during tests onboard before filtering

The components due to gravity along each sensor axis have been subtracted from the measured proper accelerations (Figure 5.32). In this way, the accelerations due to ship motion alone have been obtained.

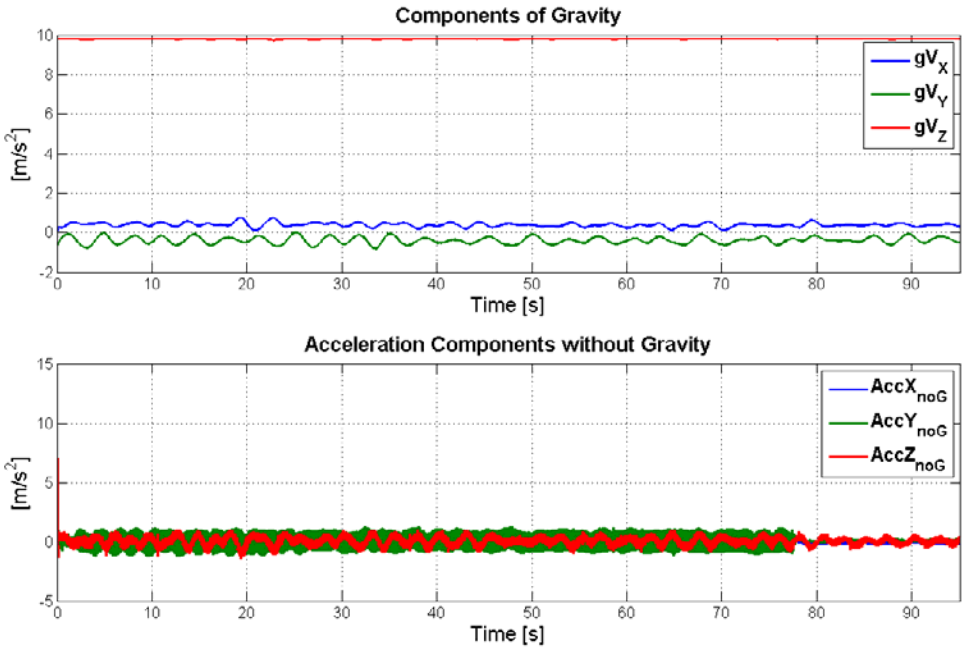

Figure 5.32– Accelerations from Mti-G without gravity

Both the accelerations, the Euler angles and the gyro outputs (rates of turn) have been filtered with an ideal bandpass filter2 (Figure 5.33 and Figure 5.34), in order to retrieve the motion components within the frequency range of interest and remove the undesirable components (noise and vibrations). The accelerations of the Euler angles have been obtained by making the time derivative of the filtered gyro outputs.

[2] The Matlab function *idealfilter* has been used.

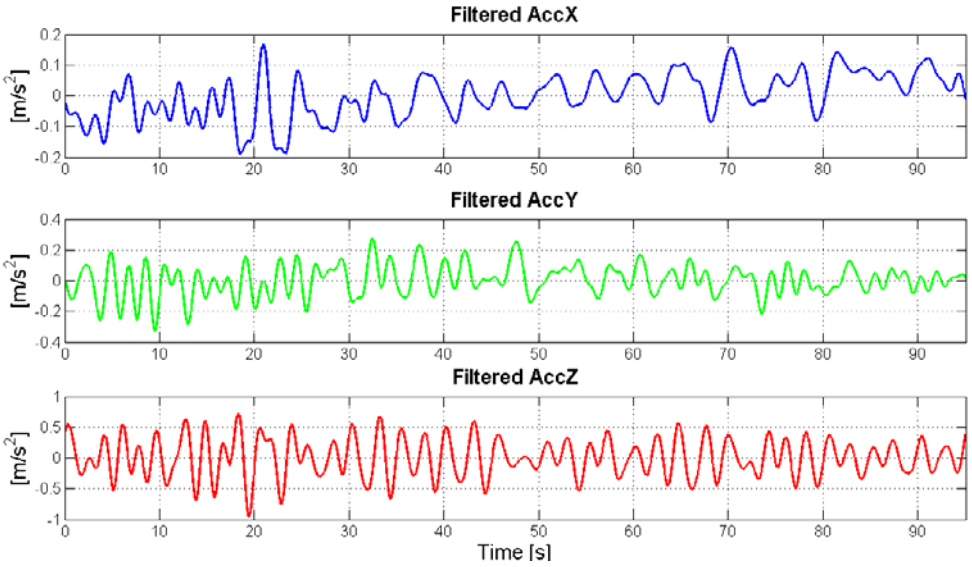

Figure 5.33 – Ship Accelerations from Mti-G after filtering

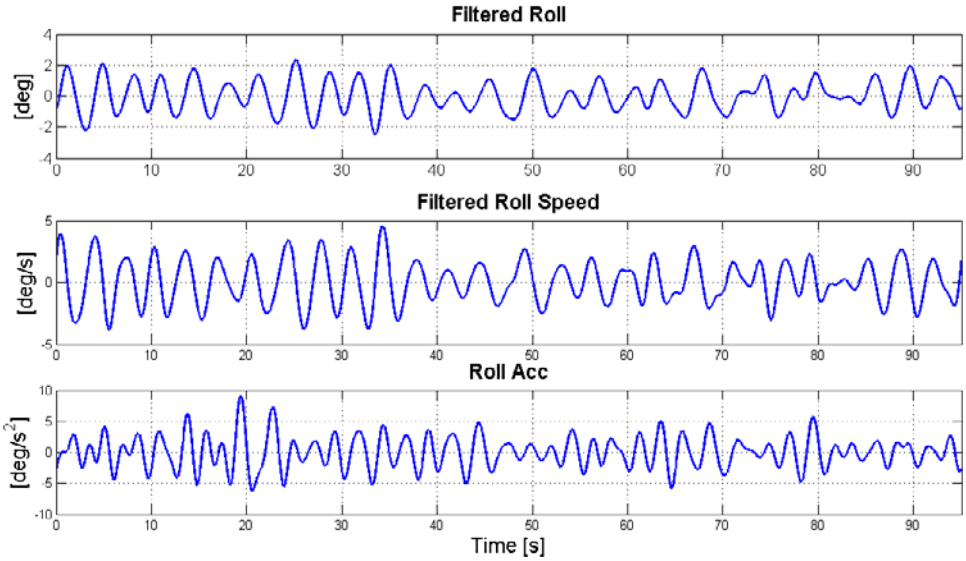

Figure 5.34 – Ship Roll from MTi-G after filtering

In Figure 5.35 the ship roll angle (blue line) and deck lateral acceleration (dark yellow line) from the MTi-G together with the inclination angle of the individual COM relative to the vertical (magenta line) from the MTx are shown.

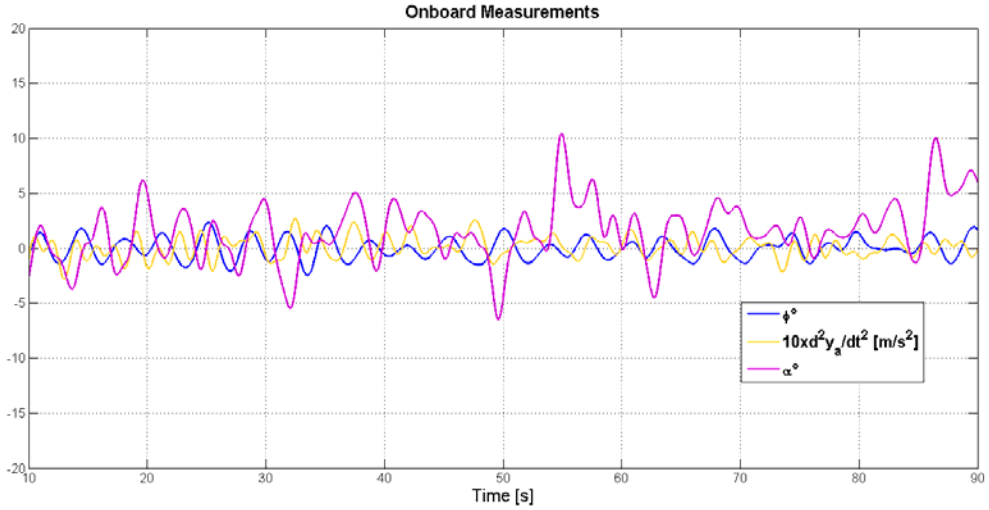

Figure 5.35– Ship Roll angle and Deck Lateral Acceleration from MTi-G and Inclination Angle of person COM relative to the vertical from MTx

The first ten seconds have been ignored since the subject was not ready to execute the trial. After this time period, the person seems to over-correct the deck angle, being in phase opposition with the roll angle and quite in phase with the deck lateral acceleration.

In Figure 5.36 the response simulated with the implemented control model, whose parameters have been adequately set, is reported.

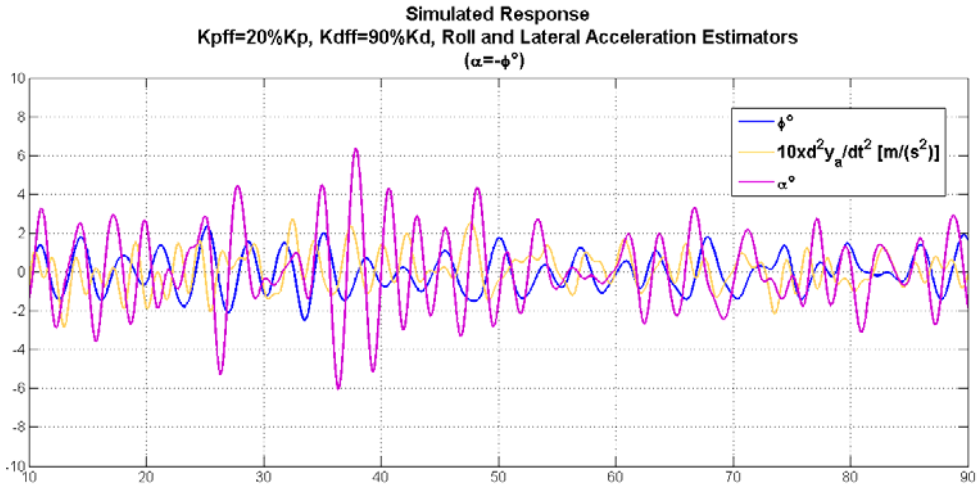

Figure 5.36– Simulated Ship Roll angle and Inclination Angle of person COM relative to the vertical

Even if the human motion is not perfectly replicated, salient aspects are simulated:

- the model reacts over-correcting for the input disturbances;
- in several time instants during the simulation, the response is in phase opposition with the ship roll angle and in phase with the deck lateral acceleration.

Appendix 5.A: INERTIAL SENSORS

An Inertial Measurement Unit - IMU is a device used for determining object orientation and is composed of a cluster of accelerometers and gyros. IMUs making use of MEMS technology have became widely used, for their low-cost and small size. They are employed in several fields, from control and navigation of aircraft, ships, unmanned vehicles, up to human motion capture.

MEMS IMUs have lower performance with respect to more expensive, high-accuracy sensors which use, for example, fiber-optic or spinning mass technologies. MEMS sensors have significant bias instability and noise level, and the short-term bias instability (drift) of gyros is the main concern [El-Sheimy, 2009]. At the end of 2007 the best published accuracy for a MEMS gyroscope was about one degree drift per hour, while combining three gyros into a single virtual sensor the bias drift can be reduced to 0.53 degree per hour [Chang et al., 2008].

For improving MEMS IMUs accuracy, data from additional sensors (like GPS receivers, magnetometers, barometers, optical sensors) are combining together, as it has been extensively shown in literature ([Brodie, 2009], [Chang et al., 2008], [El-Sheimy, 2009], [Ferrari et al., 2009], [Roetenberg, 2006]). Kalman filters are very commonly used data fusion algorithms.

5.A.1 MEMS TECHNOLOGY

Microelectromechanical systems (MEMS), also referred to as micromachines, is the technology of very small mechanical devices driven by electricity. MEMS are made up of components between 0.001 to 0.1 mm in size and MEMS devices generally range in size from 20 micrometres to a millimetre (Figure 5.A.1). They usually consist of a central unit, the microprocessor, that processes data, and several components, such as the microsensors, that interact with the outside.

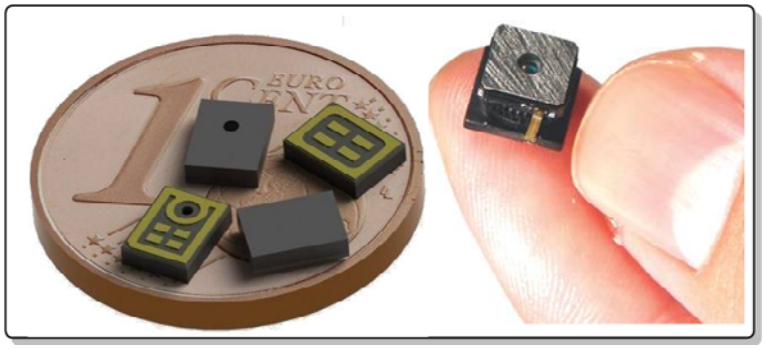

Figure 5.A.1 – Examples of MEMS tesserae

5.A.2 ACCELEROMETERS

A single axis accelerometer consists of a proof mass, suspended by a spring in a housing (Figure 5.A.2).

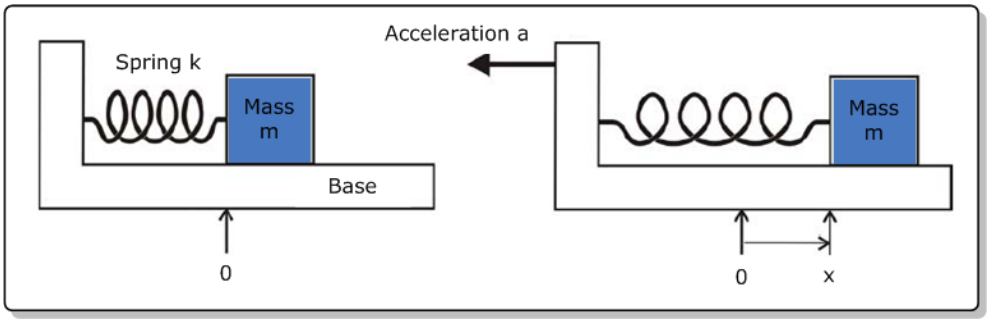

Figure 5.A.2 - A single axis accelerometer consisting of a mass suspended by a spring.
Left: no acceleration.
Right: acceleration of base to the left resulting in an expanded spring.
(after, [Roetenberg, 2006])

According to Hooke's law, the spring exhibits a restoring force that is proportional to the amount it has been expanded or compressed:

$$F = kx \tag{5.A.1}$$

where

- k is a constant called the rate or spring constant;

- x is the displacement of the end of the spring from its equilibrium position;
- F is the restoring force exerted by the spring.

For Newton's second law, the proof mass m subject to a force F undergoes an acceleration a that has the same direction as the force and a magnitude that is directly proportional to the force and inversely proportional to the mass

$$F = ma \tag{5.A.2}$$

This force causes the mass either compress or expand the spring, if the condition

$$F = ma = kx \tag{5.A.3}$$

holds. Hence an acceleration a causes the mass to be displaced by:

$$x = \frac{ma}{k} \tag{5.A.4}$$

or vice versa, considering the displacement, the mass experiences an acceleration equal to:

$$a = \frac{kx}{m} \tag{5.A.5}$$

In this way, for measuring the acceleration it is sufficient to measure the displacement of the proof mass connected to the spring.

In commercial devices, piezoelectric, piezoresistive and capacitive components are commonly used to convert the mechanical motion into an electrical signal.

An accelerometer measures proper acceleration: an accelerometer at rest relative to the Earth's surface indicates approximately 1g upwards, because

any point on the Earth's surface is accelerating upwards relative to the local inertial frame. To obtain the acceleration due to motion with respect to the Earth, this "gravity offset" must be subtracted and corrections for effects caused by the Earth's rotation relative to the inertial frame have to be applied. The reason for this gravitational offset is Einstein's equivalence principle, which states that the effects of gravity on an object are indistinguishable from acceleration.

In order to measure accelerations relative to multiple axes, the system has to be replicated along each required axis.

5.A.3 GYROSCOPES

A gyroscope is a device for measuring angular motion or orientation. A mechanical gyro operates on the basis of the principles of conservation of angular momentum, sensing the change in direction of an angular momentum. According to Newton's second law, the angular momentum of a body remains unchanged unless a torque acts upon the body itself. The equation describing the behaviour of the gyroscope is:

$$\tau = \frac{dL}{dt} = \frac{d\left(I\omega\right)}{dt} = I\alpha \qquad (5.A.6)$$

where

- τ is the torque of the gyroscope;
- L is its angular momentum;
- I is the moment of inertia;
- ω is the vector of gyro's angular velocity;
- α is the vector of gyro's angular acceleration.

Micromachined inertial sensors usually incorporate vibrating structure gyroscopes, also known as Coriolis vibratory gyros. The underlying physical principle is that a vibrating element (vibrating resonator) tends to continue vibrating in the same plane as its support rotates.

The basic element can be modelled as a spring-mass system, where the mass has two degrees of freedom (Figure 5.A.3). The mass is caused to vibrate along one axis, and this mode is called "drive mode". If the gyroscope rotes, the mass will experience the Coriolis force F_C perpendicular to the drive mode, given by:

$$F_C = -2m(\boldsymbol{\omega} \times \mathbf{v}) \tag{5.A.7}$$

where

- m is the mass of the vibrating element;
- $\boldsymbol{\omega}$ is the angular velocity due to the gyro rotation;
- $\mathbf{v}$ is the mass speed along the principal axis (drive mode).

The Coriolis force causes a secondary vibration (sense mode) along the axis perpendicular to the drive mode. By sensing the secondary vibration, the rate of turn $\boldsymbol{\omega}$ can be measured.

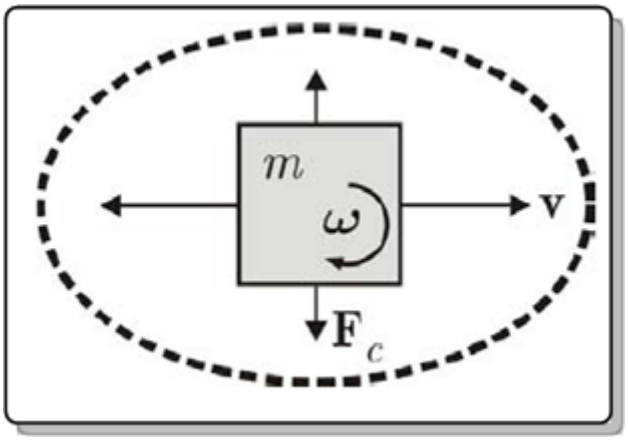

Figure 5.A.3 - A vibrating mass gyroscope consists of mass, which is rought into vibration v. When the gyroscope is rotated, the mass will undergo a small additional displacement caused by the Corolis force F_C in the direction perpendicular to the original displacement (after, [Roetenberg, 2006])

Appendix 5.B: The Global Positioning System

The Global Positioning System (GPS) is a worldwide radio-navigation system made up of a constellation satellites orbiting around the Earth. GPS uses these satellites as reference points to calculate positions on the Earth. GPS was developed by the United States Department of Defence.

5.B.1 BASIC PRINCIPLES

A GPS receiver calculates its position using the travel time of radio signals sent by the constellation of GPS satellites.

Each satellite continually transmits messages containing the time the message was sent, a precise orbit for the satellite sending the message (the ephemeris), and the general system health and rough orbits of all GPS satellites (the almanac). These messages are transmitted on two carrier frequencies:

- the L1 carrier (1575.42 MHz), carrying both the navigation message (ephemeris, clock corrections and almanac) and a Pseudo-Random Code (PRC[3]) for timing, also known as Coarse Acquisition (C/A) code. The GPS L1 frequency also contains a precision (P) code that is reserved for military use;
- the L2 carrier (1227.60 MHz), used for more precise positioning.

Two GPS services are provided. The Precise Positioning Service (PPS) is available primarily to the military of the United States and its allies for users properly equipped with PPS receivers. The Standard Positioning Service (SPS) is designed to provide a less accurate positioning capability than PPS for civil and all other users throughout the world.

For the determination of its position on earth, the GPS receiver compares the time when the signal was sent by the satellite with the time the signal was received. By multiplying this time difference by the speed of light, the distance from the satellite can be computed.

[3] The Pseudo-Random Code is a complicated digital code unique for each satellite.

Let the satellite position and the time the message is sent be respectively:

$$\begin{cases} X_i^S, Y_i^S, Z_i^S \\ T_i^S \end{cases}, \; i = 1,2,3,4 \tag{5.B.1}$$

where the subscript i is the satellite number. If T^R is the time the message was received, the GPS receiver can compute the transit time of the message and, assuming the message travelled at the speed of light c, the distance travelled is equal to:

$$p_i = \left(T^R - T_i^S\right)c \tag{5.B.2}$$

The observation equation (5.B.2) does not give the true range from the satellite, because both the clock of the satellite and the clock of the receiver are affected from a bias. Due to the these errors, the range measurement is called 'Pseudorange'.

Introducing a clock bias for both the receiver and satellite clocks in (5.B.2), the pseudorange equation becomes:

$$\begin{aligned} p_i &= \left(T^R - T_i^S\right)c = \left[\left(t^R + \tau^R\right) - \left(t_i^S + \tau_i^S\right)\right]c = \\ &= \left(t^R - t_i^S\right)c + c\tau^R - c\tau_i^S = \\ &= \rho_i\left(t^R, t_i^S\right) + c\tau^R - c\tau_i^S \end{aligned} \tag{5.B.3}$$

where $\rho_i\left(t^R, t_i^S\right)$ is the range from receiver (at receive time) to the satellite (at transmit time):

$$\rho_i\left(t^R, t_i^S\right) = \sqrt{\left(X_i^S\left(t_i^S\right) - X^R\left(t^R\right)\right)^2 + \left(Y_i^S\left(t_i^S\right) - Y^R\left(t^R\right)\right)^2 + \left(Z_i^S\left(t_i^S\right) - Z^R\left(t^R\right)\right)^2} \tag{5.B.4}$$

The navigation message allows to compute the satellite position $\left(X_i^S, Y_i^S, Z_i^S\right)$ and the satellite clock bias τ_i^S. The four unknowns, the receiver position

$\left(X^R, Y^R, Z^R\right)$ and the receiver clock bias τ^R, can be computed if, at least, four satellites are in view of the receiver.

A satellite's position and pseudorange define a sphere, centred on the satellite with radius equal to the pseudorange. The position of the receiver is somewhere on the surface of this sphere. Thus with four satellites, the indicated position of the GPS receiver is at or near the intersection of the surfaces of four spheres.

By constantly recalculating its position, the GPS receiver can additionally determine speed and direction (referred to as "ground speed" and "ground track"). Another possibility of determining the speed is by using the Doppler's effect which occurs due to the movement of the receiver while receiving the signals.

Several errors can affect the accuracy in the GPS measure, such as atmospheric distortion (predominantly in the ionosphere), satellite clock inaccuracies, travel delays of the satellite signals, etc.. Altogether they can produce an average error of ± 15 meters. The introduction of augmentation systems, known as Satellite-Based Augmentation System – SBAS (e.g., Wide Area Augmentation System – WAAS, European Geostationary Navigation Overlay Service - EGNOS) can improve the system accuracy (± 3-5 meters), by correcting the pseudoranges mainly for the ionospheric delay. The accuracy in measuring the speed of a GPS receiver can reach 0.05 m/s in steady state.

Appendix 5.C: The Videogrammetric Technique

Videogrammetry is the application of the photogrammetric technique to dynamic phenomena.

5.C.1 BASIC PRINCIPLES OF PHOTOGRAMMETRY

Photogrammetry is a three-dimensional (3D) measurement technique which uses central projection imaging as its fundamental mathematical model often associated to a simple device called the "pinhole camera". Three elements are sufficient to fully describe the perspective of a pinhole camera: the focal distance and the two coordinates of the point where the optical axis intersects the image plane (Interior Orientation), referring to a specific frame on the image plane. Nevertheless, such a model is very different from the real one (e.g. a digital camera) for many reasons such as (i) the presence of a complex objective lens, (ii) a camera housing which is not built to be stable over time and an image recording surface (film or digital sensor) which may be (iii) neither planar (i.e. especially for analogue cameras) (iv) nor perpendicular to the optical axis. All these differences from the ideal central projection model have to be found by means of a calculation stage called camera calibration procedure. The camera calibration procedure retrieves perspective elements, known as Interior Orientation (IO) parameters, together with the radial and decentring lens distortion parameters, known as Additional Parameters (AP).

Photogrammetry is able to get three-dimensional (3D) data of an object from images in a way that is very similar to theodolite survey techniques, since it is based on the intersection between two or more optical rays (redundancy) called collinearity straight lines in photogrammetric terminology. Within the perspective model, the object point, perspective centre and image point lie on the same collinearity straight line.

The image acquisition stage consists in taking photographs of the object from different view positions, ensuring good intersection between collinearity straight lines.

The photogrammetric process is strictly linked to marking some homologous object points on the images to determine both camera positions and

orientations, called Exterior Orientation (EO), as well as 3D point coordinates. The recognition of the same object point on two or more images (image correspondences) requires the object surface to have enough texture information (such as natural points and/or edges, etc.). If no features are visible on the images, then artificial targets must be positioned and/or synthetic patterns must be projected or painted on the surface object [Menna et al., 2009]. For some applications, i.e. for high automation and accuracy purposes, circular coded targets should be positioned on the object to automatically recognize image correspondences.

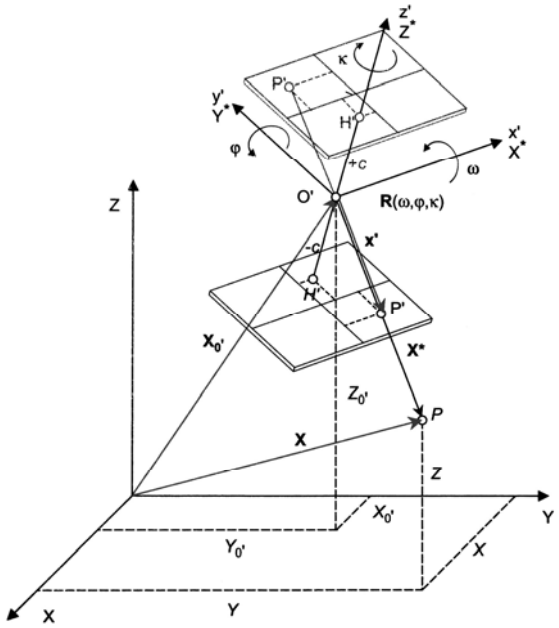

Figure 5.C.1 - Image space to object space frames [Luhmann 2006].

The image space to object space mathematical model, shown in Figure 5.C.1, can be described by equation (5.C.1):

$$\mathbf{X}_P = \boldsymbol{X}_{O'} + \boldsymbol{X}^*_P = \boldsymbol{X}_{O'} + \lambda \cdot \boldsymbol{R} \cdot \boldsymbol{x}'_P$$

$$\mathbf{X}_P = \begin{bmatrix} X_P \\ Y_P \\ Z_P \end{bmatrix} = \begin{bmatrix} X_{O'} \\ Y_{O'} \\ Z_{O'} \end{bmatrix} + \lambda \begin{bmatrix} r_{11} & r_{12} & r_{13} \\ r_{21} & r_{22} & r_{23} \\ r_{31} & r_{32} & r_{33} \end{bmatrix} \begin{bmatrix} x'_P \\ y'_P \\ z'_P \end{bmatrix} \tag{5.C.1}$$

$$\mathbf{x}'_P = \begin{bmatrix} x'_P \\ y'_P \\ z'_P \end{bmatrix} = \begin{bmatrix} x'_{P'} - x'_0 - \Delta x' \\ y'_{P'} - y'_0 - \Delta y' \\ -c \end{bmatrix}$$

where

- (X_P, Y_P, Z_P) are the coordinates of a generic point P in the object space reference system;
- $(X_{O'}, Y_{O'}, Z_{O'})$ are the camera station coordinates
- λ is the scale factor between the object and the camera frames;
- $\boldsymbol{R}$ is the orthogonal rotation matrix containing the three camera station (roll, pitch, yaw) angles $(\omega, \varphi, \kappa)$
- (x'_P, y'_P, z'_P) are the coordinates of a generic point P in the camera station reference system;
- (x'_0, y'_0, c) are interior orientation parameters;
- $(x'_{P'}, y'_{P'})$ are the coordinates of point P' in the image plane frame;
- $(\Delta x', \Delta y')$ are the corrections for radial and decentring lens distortions.

The (5.C.1) represents the equation of a collinearity straight line passing through point P, perspective centre O’ and point P’ imaged by the camera on the digital sensor or film.

While IO establishes the geometric characteristics of a bundle of rays (the bundle of collinearity straight lines), the EO establishes its position and orientation with respect to the object space coordinate system. Each bundle requires six independent parameters: three for position and three for orientation. These parameters can be calculated either through the knowledge of at least three object points coordinates (single image orienting or resection method) or by marking the same object points (at least five) on two or more images (image pairs orienting or relative orientation method). Once the approximate values for exterior orientation parameters have been computed or estimated, a least square evaluation by means of a bundle adjustment process (multi image orienting) is performed in order to improve accuracy [Gruen and Beyer, 2001]. Once the exterior orientation parameters have been computed, 3D measurements are possible.

Generally, a rough approximation of accuracy achievable with photogrammetric measurements can be derived directly from uncertainty in marking the imaged geometric primitives.

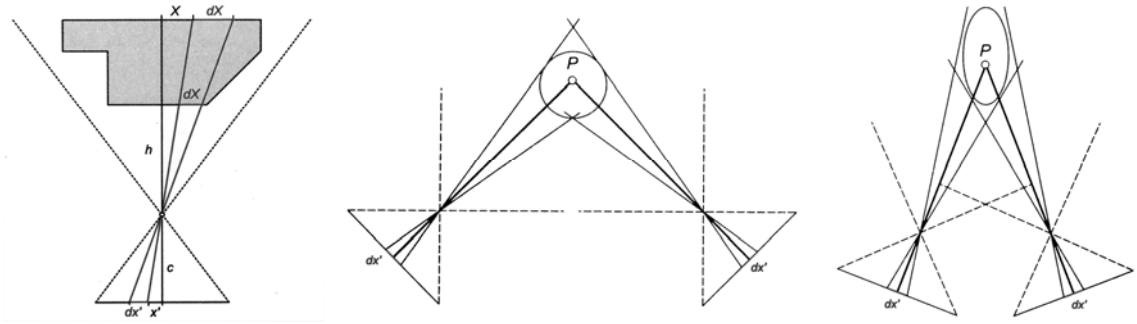

Figure 5.C.2 - Relationship between image and object space errors (after [Luhmann, 2006])

Figure 5.C.2 left shows the relationship between a measurement error dx' on the image and the correspondent error in the object space dX which is essentially a function of the image scale number m (the ratio of object distance h to the principal distance c of the camera used):

$$dX = m \cdot dx' \tag{5.C.2}$$

The 3D points in the object space are obtained from the intersection between collinearity straight lines that start from their projections on at least two images (Figure 5.C.3). This represents the simplest, most reliable and accurate kind of photogrammetric 3D measurement.

An empirical formula for the achievable accuracy by means of photogrammetric methodologies is given by Fraser [2001]:

$$dX = \left(\frac{q}{\sqrt{k}} \right) \cdot m \cdot dx \tag{5.C.3}$$

where

- q is a coefficient depending on the configuration of camera stations:
  - $q = 0.4 \div 0.8$ for convergent images, Figure 5.C.2 centre,

- $q = 1.5 \div 3.0$ for stereo or near parallel axes, Figure 5.C.2 right;

▪ k is the number of images per station.

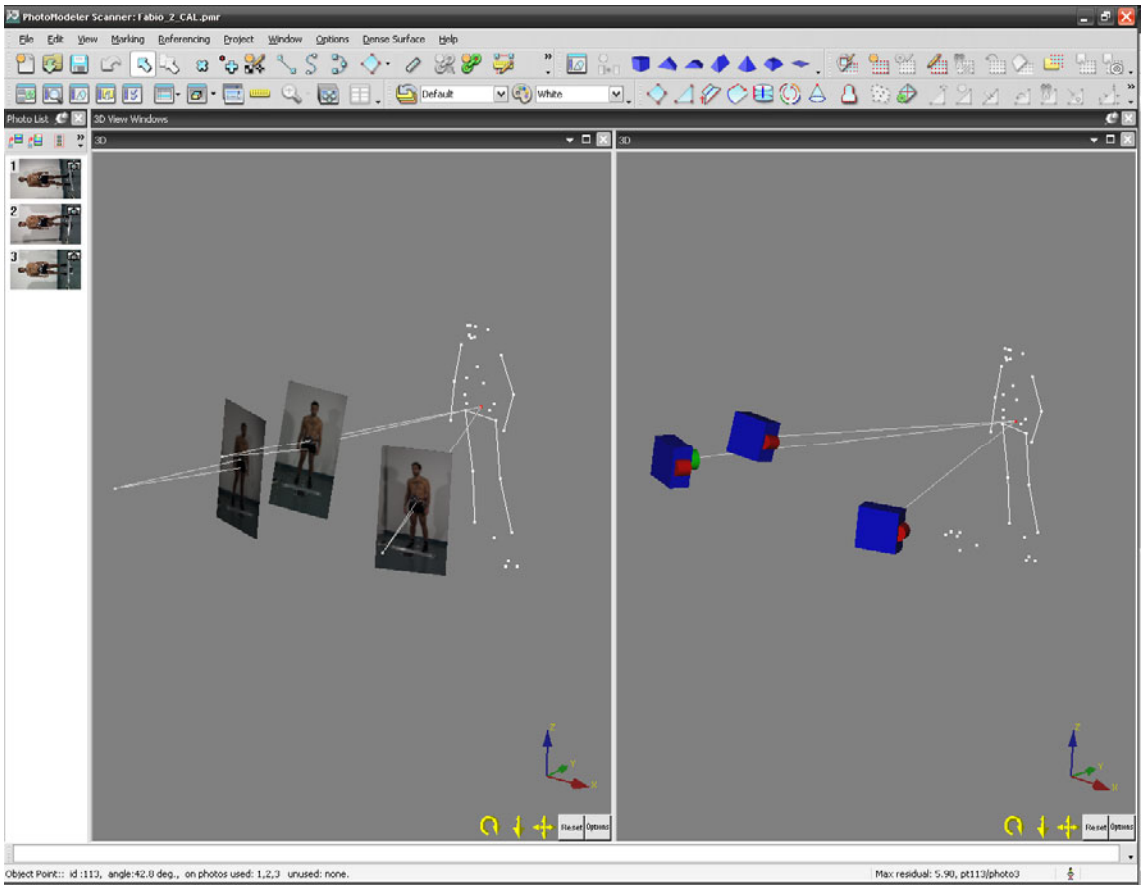

Figure 5.C.3 - Graphical User Interface of Photomodeler.
The 3D red point in the object space is obtained from the intersection among collinearity straight lines that start from its projection on three images

Nowadays, in the field of digital photogrammetry, different methods for measuring points exist: manual, semi-automatic and automatic. Manual measurement requires human interaction and experience. It is time-consuming, but furnishes reliable results because of human supervision. It consists in recognizing and marking the same object point on the images. Commonly, uncertainty in marking points with this procedure is about one pixel.

In semi-automatic techniques, the user marks a point on an image and a proper algorithm (image matching) automatically finds the corresponding

point on the other images where it is projected. This procedure gives the best results in terms of accuracy and reliability (human supervision), being suitable for reverse engineering applications. Accuracy in marking the homologous points ranges from 1/10 to 1/100 pixel (sub-pixel point marking method) depending on the algorithm [Luhmann, 2006].

Fully automated procedures find and mark homologous points from a set of images. An image, taken as a reference, is properly gridded (or some interest points are sampled) then, using suitable algorithms, correspondences are found. This method supplies results as accurate as the semi-automatic procedures, but is less reliable since in finding correspondences some mismatches are possible. For this reason, though automatic measurement is fast, post-processing has to be performed to detect outliers.

Another automatic approach consists in using specific coded targets to provide an accurate sub-pixel point marking. Usually, coded targets are high contrast circles with some additional geometric shapes such as lines, rings or regions arranged around its centre. The point codes can be automatically recognized by algorithms during the marking process.

The procedure described above assumes the object to be a rigid body during the image acquisition stage, namely the object's shape is not deforming during the measurements. If this assumption holds, the images can be taken not necessarily at the same instant time.

If the body is moving and the aim of the survey is to retrieve its dynamics, images from different points of view have to be taken simultaneously. This is the case of videogrammetric measurements where synchronised digital cameras or videocameras record the moving object from two or more different positions. The movement is sampled according to the videocamera frame rate and it is reconstructed by tracking points of interest across the epochs (frames). For videogrammetric measurements, the most common coded targets (markers) are in the form of high intensity LEDs.

Chapter 6: Conclusions and Avenues for Future Investigation

6.1 GENERAL DISCUSSION

The research presented in this thesis has investigated human postural stability, topic that has important consequences on the safety of persons working onboard ships.

At the beginning of the avenue of study, two main objectives have been identified:

1) the development of a model reproducing human postural control on a moving platform;
2) the realization of experimental procedures for testing and validating the proposed control architecture.

To achieve the established research purposes, a broad state-of-art investigation has been conducted. Since human postural stability is a multidisciplinary topic involving several sciences and disciplines, many issues have been faced and examined. The result of this investigation has been reported in the first three chapters of the present work. These sections provide the salient elements for approaching the topic of interest.

Chapter 1 and 2 tackle the problem from the marine engineering point of view. Introduced the key features of seakeeping and discussed the personnel criteria that relate the human factors to ship operability, the current human models for evaluating the influence of ship motions on crew safety and performance have been reviewed.

Chapter 3 provides an understating of human postural control through the explanation of the relevant physiological and neurological concepts. This Chapter constitutes the basis for developing the postural control model proposed by the author and presented in Chapter 4.

Chapter 4 and 5 are the core of the conducted investigation; the author's proposals to the established research questions are here given and motivated.

6.2 THESIS OBJECTIVE 1

A stance control model for modelling postural behaviour of a crewmember onboard ship has been proposed.

The model has been conceived with the twofold aim of modelling a person in a dynamic and realistic manner, and developing, at the same time, a simple and flexible theoretical framework.

The principles of human stance control have been extracted from literature review and revised for reproducing an individual that tries to restore postural equilibrium on a moving ship. The proposed model has been implemented into a modular own-developed software procedure for being simulated and tested in different conditions.

As a first step in model development, the biomechanics of human body were simplified by assuming that the body was represented by a single-link inverted pendulum. The linearised equations of motion describing the inverted pendulum dynamics onboard ships have been derived.

As a second step, the main features of postural equilibrium as a biological process have been translated into a control engineering approach to model the human upright control system.

Several simulations have been performed stimulating the model with different kinds of disturbances (steps, regular sinusoids, random signals) and meaningful results have been presented. Interesting potentialities of the model in reproducing different dynamics have been demonstrated.

6.3 THESIS OBJECTIVE 2

For validating the proposed model in the real environment it was designed for working in, experiments are required to be executed in the field.

Due to the lack of standard procedures for conducting experiments onboard and validating human postural model, a procedure for measuring human motion onboard ships has been proposed. Diverse techniques (photogrammetry, inertial measurements, global positioning system) and instruments (digital cameras, inertial and positioning sensors) have been integrated with the ultimate goal of acquiring both ship and human motions.

The whole process of planning, designing, calibrating, and assessing the accuracy of the motion capture system has been reported and discussed. The motivations that were at the basis of setting up this "ad hoc" acquisition system have been analysed.

Laboratory tests were conducted for testing and validating the complex measurement system before executing preliminary trials onboard a fishing vessel.

Many practical and unexpected difficulties have been faced during the first measurement campaigns, conducted with the twofold aim of testing the designed data acquisition system in the real environment and trying a first validation of the proposed human control model.

The results from postural stability tests onboard have been compared with the simulations obtained from the proposed control model. To this purpose, the ship motions measured during the full scale trials have been used as input for the implemented software.

The comparisons have shown that, even if the human motion is not perfectly replicated, the model has the capability of reproducing salient aspects of human behaviour onboard ships.

The strength of the proposed model, consisting in its flexibility, has been illustrated: by properly tuning the model parameters a desired response can be produced.

6.4 SUGGESTIONS FOR FUTURE DEVELOPMENTS

In the author's opinion, further developments and improvements can be suggested for both the thesis objectives.

6.4.1 HUMAN POSTURAL CONTROL MODEL

The model here proposed simulates human postural stability in a single plane (in the antero/posterior direction). In future research, the model should be extended for allowing motion also in the lateral direction and in three dimensions.

Modelling a person as a dynamic and active system would result in a more realistic scenario than the reference model by Graham. This model regards an individual as a dummy unable to counteract the external disturbances due to ship motions. The better performance of the proposed model in predicting loss of balance events onboard ship should be verified through a comparative analysis between the proposed and the classical model.

Collaboration with other institutions and research centres is required for obtaining further data against which to test and validate the control model presented in this work.

Once the human postural control model has been validated, a suitable criterion for human stability onboard ships should be identified. If the current Motion Induced Interruption - MII criterion were chosen, the maximum tolerable frequency of loss of balance events would be estimated trough an extensive experimental program.

The human postural stability model and stability criterion will be then incorporate into a more general procedure for assessing and predicting safety working conditions aboard.

6.4.2 EXPERIMENTAL PROCEDURES FOR TESTING AND VALIDATING HUMAN POSTURAL MODELS

Executing further (numerous) trials in different environmental conditions onboard different ships, testing many individuals involved in several tasks will be necessary in order to obtain relevant (statistically) data and infer significant results for validating the theoretical model.

The designed acquisition system has shown satisfactory performance onboard, but it should be useful to include additional instrumentations for extending the number of parameters collected in the field.

Cooperation with international research group is desirable in order to realize a standardization of the procedures for conducting experiments onboard with the aim of validating human postural model.

References

Akca, D., Gruen, A., 2009: Comparative Geometric and Radiometric Evaluation of Mobile Phone and Still Video Cameras. The Photogrammetric Record, vol. 24(127), pp. 217–245. The Remote Sensing and Photogrammetry Society and Blackwell Publishing Ltd.

Alexandrov, A.V., Frolov, A.A., Horak F.B., Carlson-Kuhta, P., Park S., 2005: Feedback Equilibrium Control During Human Standing. Biol Cybern, vol. 93(5), pp. 309–322. National Institute Of Health.

Amoud, H., Snoussi, H., Hewson, D., Duchêne, J., 2008: Univariate and Bivariate Empirical Model Decomposition for Postural Stability Analysis. EURASIP Journal on Advances in Signal Processing. Hindawi Publishing Corporation.

Angrisano A., Nocerino E., Troisi S., Del Core G., 2009: IMU Low Cost Calibration Method ENC09 - European Navigation Conference 2009. Naples, Italy, 3-6 May 2009.

Baitis, A.E., Applebee, T.R., McNamara T.M., 1984: Human Factor Considerations Applied to Operations of the FFG-8 and LAMPS MK III. Naval Engineers Journal, vol. 97(4), pp. 191-199.

Beck, R., Reed, A., 2001: Modern Computational Methods for Ships in a Seaway. Transactions, Society of Naval Architects and Marine Engineers, Vol. 109, pp. 1-52.

Begovic E., Nocerino E., Scamardella A., 2008: Study on Wake Wash Generated by HSC in the Bay of Naples. HSMV 2008 - 8th International Symposium on High Speed Marine Vehicles, pp. 23-30. Naples, Italy. 21-23 May 2008. ISBN 888-898-704-5.

Begovic E., Nocerino E., Scamardella A., 2010: Analisi Teorico-Sperimentale delle onde prodotte da High Speed Craft nel Golfo di Napoli. Rivista "Annali della Facoltà di Scienze e Tecnologie" della Facoltà di Scienze e Tecnologie dell'Università degli Studi di Napoli "Parthenope", vol. LXX. ISSN: 1825-1331. *In press.*

Boccadamo, G., 1999: Seakeeping Performance, operability and safety of personnel onboard fishing vessels. Biennial Symposium: Techniques and Technology in Fishing Vessels, Italy.

Boccadamo, G., Scamardella, A., 2003: Methods for Evaluating the Motion Induced Interruptions on Fishing Vessels. The 3-rd Safety and Reliability International Conference to Safer Life and Environment. Gdynia, PL, 27-30 May 2003. ISSN 1642-9311.

References

Bolzern, P., Scattolini, R., Schiavoni, N., 1998: Fondamenti di Controlli Automatici. McGraw-Hill Libri Italia srl. ISBN: 88-386-0747-8.

Borg, F.G., 2005: An Inverted Pendulum with a Springy Control as a Model of Human Standing. Website: arXiv:physics/0512122v1.

Bos, J.E., Valk, P.J.L., Hogervorst, M.A., Munnoch, K., Perrault, D., Colwell, J.L., 2008: TNO contribution to the Quest 303 trial – Human performance assessed by a vigilance and tracking test, a multi-attribute task, and by dynamic visual acuity. TNO report, TNO Human Factors, Soesterberg, the Netherlands TNO-DV 2008 A267.

Brodie, M.A.D., 2009: Development of Fusion Motion Capture for Optimisation of Performance in Alpine Ski Racing. Ph.D. Thesis. Massey University, Wellington, New Zealand.

Chang, H., Xue, L., Qin, W., Yuan G., Yuan, W., 2008: An Integrated MEMS Gyroscope Array with Higher Accuracy Output. Sensors vol. 8, pp. 2886-2899. MDPI. ISSN 1424-8220

Chiari, L., Della Croce, U., Leardini, A., Cappozzo, A., 2005: Human Movement Analysis Using Stereophotogrammetry. Part 2: Instrumental Errors. Gait and Posture, vol. 21,pp. 197–211. Elsevier B.V.

Cnyrim, C., Mergner, T., Maurer, C., 2009: Potential roles of force cues in human stance control. Exp Brain Res. Springer-Verlag. DOI 10.1007/s00221-009-1715-7

Colwell, J. L., 1989: Human factors in the Naval environment: A review of motion sickness and biodynamic problems. DREA Technical Memorandum 89/220.

Colwell, J.L.,2005: Modeling Ship Motion Effects on Human Performance for Real Time Simulation. Naval Engineers Journal, Winter 2005, pp. 77-90.

Colwell, J.L.,2006: Human Performance at Sea. Presentation at the ABCD Symposium on the Influence of Ship Motions on Biomechanics and Fatigue. 25-26 April, 2006. Panama City, Florida.

References

Crossland, P., Evans, M.J., Grist, D., Lowten, M., Jones, H., Bridger, R.S., 2007: Motion-induced interruptions aboard ship: Model development and application to ship design. Occupational Ergonomics, IOS Press, vol. 7(3), pp. 183-199

Crossland, P., Rich, K.J., 1998: Validating a Model of the Effects of Ship Motion on Postural Stability. ICEE - International Conference on Environmental Ergonomics, San Diego, USA.

Cumming, D., 2005: Comparison of Neptune and Datawell Direction Wave Buoy Data Acquired Fall 2004. Laboratory Memorandum LM-2005-13. Institute for Ocean Technology - IOT. Memorial University of Newfoundland – MUN. Canada.

Cumming, D., Fleming, T., 2005: Practical Considerations Related to Carrying Out Seakeeping Trials on Small Fishing Vessels. 7th Canadian Marine Hydromechanics and Structures Conference Halifax, NS.
http://nparc.cisti-icist.nrc-cnrc.gc.ca/npsi/ctrl?action=shwart&index=an&req=8895994&lang=en

D'Apuzzo, N., 2003: Surface Measurement and Tracking of Human Body Parts from Multi Station Video Sequences. Ph.D. Thesis. Swiss Federal Institute Of Technology Zurich. ISSN 0252-9335.

Davidson, B.S., 2007: Experimental and Simulation-Based Assessment of the Human Postural Response to Sagittal Plane Perturbations with Localized Muscle Fatigue and Aging. Ph.D Thesis. Virginia Polytechnic Institute and Wake State University. Blacksburg, Virginia, USA.

Dobbins, T., Rowley, I., Campbell, L., 2008: High Speed Craft Human Factors Engineering Design Guide. ABCD-TR-08-01 V1.0.

Dobie, T. G., 2003: Critical Significance of Human Factors in Ship Design. Proceedings of the 2003 RVOC Meeting, 8 – 10 October, 2003. Large Lakes Observatory, University of Minnesota.

Duncan, C.A., 2007: Biomechanical Adaptations Required to Maintain Postural Stability in Moving Environments when Performing Manual Materials Handling Activities. Master's Thesis. University of New Brunswick, Frederickton, Canada.

References

Eames, M.H.A., Cosgove, A., Baker, R., 1999: Comparing Methods of Estimating the Total Body Centre of Mass in Three-Dimensions in Normal and Pathological Gaits. Human Movement Science, vol. 18, pp. 637-646. Elsevier Science B.V.

El-Sheimy, N., 2009: Emerging MEMS IMU and Its Impact on Mapping Applications. Photogrammetric Week 2009. Institute for Photogrammetry, University of Stuttgart. Germany. Dieter Fritsch (Ed.)

Faltinsen, O.M., Zhao, R., 1991: Numerical predictions of ship motions at high forward speed. Phil. Trans. R. Soc. Lond. A, vol. 334, pp. 241–252.

Faltinsen, O.M., 1990: Sea Loads on Ships and Offshore Structures. Cambridge University Press.

Faltinsen, O.M., 2005: Hydrodynamics of High-Speed Marine Vehicles. Cambridge University Press 2005. ISBN 0-521-84568-8.

Fathi, D., 2010: SHIPX Vessel Responses (VERES). Ship Motions and Global Loads. Users' Manual. MARINTEK - Norwegian Marine Technology Research Institute Report.

Ferrari, A., Cutti, A.G., Garofalo, P., Raggi, M., Heijboer, M., Cappello, A., Davalli, A., 2009: First in Vivo Assessment of ''Outwalk'': a Novel Protocol for Clinical Gait Analysis Based on Inertial and Magnetic Sensors. Med Biol Eng Comput, vol. 48, pp. 1–15. International Federation for Medical and Biological Engineering.

Franklin, G.F., Powell, J.D., Emami-Naeini, A., 1994: Feedback Control of Dynamic Systems. Third Edition. Addison-Wesley Publishing Company, Inc. ISBN 0-201-53487-8.

Graham, R., 1990: Motion-Induced Interruptions on Ship Operability Criteria. Naval Engineers Journal, vol. 102, n. 2, pp. 65-71.

Graham, R., Baitis, A.E., Meyers, W.G., 1991: A Frequency-Domain Method for Estimating the Incidence and Severity of Sliding. David Taylor Research Center, Ship Hydromechanics Department. DTRC/SHD-1361-01.

Graham, R., Baitis, A.E., Meyers, W.G., 1992: On the Development of Seakeeping Criteria. Naval Engineers Journal, vol. 104(3), pp. 259-275.

References

Gruen, A., Beyer, H. A.: 2001. System calibration through self-calibration. Calibration and Orientation of Cameras in Computer Vision. Information Sciences, vol. 34, pp. 163-193. Springer Verlag. ISBN: 3-540-65283-3.

Hay, L., Rendon, C., 1999: Feedforward Versus Feedback Control in Children and Adults Subjected to a Postural Disturbance. Exp Brain Res, vol. 125, pp. 153–162. Springer-Verlag.

Henry, S.M., Fung, J., Horak, F.B., 2001: Effect of Stance Width on Multidirectional Postural Responses. Journal of Neurophysiology, vol. 85, pp. 559-570. The American Physiological Society.

Hidenori, K., Jiang, Y., 2006: A PID Model of Human Balance Keeping. IEEE Control Systems Magazine, December 2006, pp. 18-23.

Hof, A.L., Gazendam, M.G.L., Sinke, W.E., 2005: The condition for dynamic stability. Journal of Biomechanics, vol. 38, pp. 1-8.

Hsu, W.L., Scholz, J.P., Schoner, G., Jeka, J.J., Kiemel, T., 2007: Control and Estimation of Posture During Quiet Stance Depends on Multijoint Coordination, Journal of Neurophysiology, vol. 97, pp. 3024–3035. The American Physiological Society. ISSN: 0022-3077.

ILO – International Labour Organization, 2007: Work in fishing. Convention No. 188 Recommendation No. 199. 978-92-2-120869-3.

Ito, S., Asano, H., Kawasaki, H., 2003: A Balance Control in Biped Double Support Phase Based on Center of Pressure of Ground Reaction Forces. 7th IFAC Symposium on Robot Control, pp. 205–210.

Journée, J.M.J., 1993: Hydromechanic Coefficients for Calculating Time Domain Motions of Cutter Suction Dredges by Cummins Equations. Report 968. Delft University of Technology, Ship Hydromechanics Laboratory.

Journée, J.M.J., 2001: User Manual of SEAWAY. Release 4.19 (12-02-2001). Report 1212a. Delft University of Technology, Ship Hydromechanics Laboratory.

Journée, J.M.J., Pinkster, J., 2002: Introduction in Ship Hydromechanics. Lecture MT519. Delft University of Technology.

Journée, J.M.J., Adegeest, L.J.M., 2003: Theoretical Manual of Strip Theory Program "SEAWAY for Windows". Ship Hydromechanics Laboratory, Delft University of Technology. Advanced Maritime Consulting, www.amarcon.com.

Khalid, H., Turan, O., Bos, J.E., Kurt, R.E., Cleland, D., 2010: A Comparison of The Descriptive and Physiological Motion Sickness Models in their Ability to Predict Seasickness Aboard Contemporary High Speed Craft. International Conference on Human Performance at Sea HPAS 2010, Glasgow, Scotland, UK, 16-18 June, 2010.

Kimura, N., Amagi, K., Inaba, Y. 1988: On the Relationship between the Maintenance of Human Posture and The Ship Oscillatory Motions. World Symposium on Fishing Gear and Fishing Vessel Design. Marine Institute, St. John's, Newfoundland, Canada, pp, 564-568.

Koning, J., 2009:Lashing@Sea. Executive Summary. Report No. 19717-20-TM. MARIN - MAritime Research Institute Netherlands. Wageningen, The Netherlands. http://www.mcga.gov.uk/c4mca/19717-20-tm---executive_summary.pdf

Kontaxis, A., Cutti, A.G., Johnson, G.R., Veeger, H.E.J. , : 2009: A Framework for the Definition of Standardized Protocols for Measuring Upper-Extremity Kinematics. Clinical Biomechanics, vol. 24, pp. 246–253. Elsevier Ltd.

Krell, J.B., Cinelli, M.E., Patla, A.E., 1998: Postural Responses to Unexpected Perturbations Are Unaffected by Stance Conditions. NACOB98 - North American Congress on Biomechanics. Canadian Society for Biomechanics - American Society of Biomechanics. University of Waterloo, Waterloo, Ontario, Canada. August 14-18, 1998.

Kuo, A.D., 1995: An Optimal Control Model for Analyzing Human Postural Balance. IEEE Transactions on Biomedical Engineering, vol. 42(1), pp. 87-101.

Langlois, R.G., 2010: Development of a Spatial Inverted Pendulum Shipboard Postural Stability Model. International Conference on Human Performance at Sea HPAS 2010, Glasgow, Scotland, UK, 16-18 June, 2010.

Langlois, R.G., Chan, A., Ahmadi, M., Martin, J., 2010: Experimental Investigation of Postural Stability Actuation and Response while Performing Common Shipboard Tasks.

International Conference on Human Performance at Sea HPAS 2010, Glasgow, Scotland, UK, 16-18 June, 2010.

Langlois, R.G., MacKinnon, S.N., Duncan, C.A., 2009: Modelling Sea Trial Motion Induced Interruption Data Using an Inverted Pendulum Articulated Postural Stability. The Transactions of The Royal Institution of Naval Architects, International Journal of Maritime Engineering, vol. 151(A1), pp. 1-9. ISSN 1479-8751.

Lenzi, D., Cappello A., Chiari, L., 2003: Influence of Body Segment Parameters and Modeling Assumptions on the Estimate of Center of Mass Trajectory. Journal of Biomechanics, v. 36, pp. 1335–1341. Elsevier Ltd.

Levin, O., Mizrahi, J., 1995: An Iterative Model for Estimation of the Trajectory of Center of Gravity from Bilateral Reactive Force Measurements in Standing Sway. Gait & Posture, vol. 4, pp. 89-99. Elsevier Science.

Lloyd, A.R.J.M., 1989: Seakeeping, Ship Behaviour in Rough Weather. Ellis Horwood Limited. ISBN: 0-7458-0230-3.

Luhmann, T., Robson, S., Kyle, S., Harley, I., 2006: Close Range Photogrammetry. Principles, methods and Applications. Wiley. ISBN: 978-0470106334.

Mahboobin, A., 2007: Computational and Robotic Models of Human Postural Control. Ph.D. Thesis. University of Pittsburgh. Pittsburgh, USA.

Mahboobin, A., Loughlin, P.J., Redfern, M.S., Andersonc, S.O., 2008: Sensory Adaptation in Human Balance Control: Lessons for Biomimetic Robotic Bipeds. Neural Networks, vol. 21, pp. 621–627. Elsevier Ltd.

Marais, J.F., Basset, F.A., Duncan, C.A., MacKinnon, S.N., 2010: Measurement of Aerobic Demands Associated with Moving Platforms. International Conference on Human Performance at Sea HPAS 2010, Glasgow, Scotland, UK, 16-18 June, 2010.

Matsangas, P., Johnston, J.,.McCauley, M.E, Miller, N.L., 2010: Personnel Physical Activity Levels on Naval Vessels - Evidence for Soporific and Fatigue Effects?. International Conference on Human Performance at Sea HPAS 2010, Glasgow, Scotland, UK, 16-18 June, 2010.

Matsuo, A., Ozawa, H., Godat, K., Fukunaga, T., 1995: Moment of Inertia of Whole Body Using an Oscillating Table in Adolescent Boys. Journal of Biomechanics, v. 28(2), pp. 219-223. Elsevier Science Ltd.

Maurer, C., Mergner, T., Peterka, J., 2006: Multisensory Control of Human Upright Stance. Exp Brain Res., vol. 171, pp. 231–250. Springer-Verlag DOI 10.1007/s00221-005-0256-y.

Maurer, C., Peterka, J., 2005: A New Interpretation of Spontaneous Sway Measures Based on a Simple Model of Human Postural Control. Journal of Neurophysiology, vol. 93, pp. 189–200. The American Physiological Society. ISSN: 0022-3077.

McCauley, M.E., Pierce, E., 2008: Evaluation of Motion Sickness and Motion Induced Interruptions on FSF-1. Pacific International Maritime Conference. Sydney, Australia, 29 January - 1 February, 2008.

Menna F., Ackermann S., Nocerino E., Scamardella A., Troisi S., 2009: Digital photogrammetry: a useful tool for shipbuilding applications. IMAM 2009 - 13th Congress of International Maritime Association of Mediterranean. Towards the Sustainable Marine Technology and Transportation. Vol. 2, pp. 607-614. İstanbul, Turkey, 12-15 October. 2009. ISBN (SET) 978-975-561-357-4.

Mergner, T., 2004: Meta level Concept versus classic reflex concept for the control of posture and movement. Archives Italiennes de Biologie, vol. 142 (2004), pp. 197-198.

Mergner, T., 2007: Modeling Sensorimotor Control of Human Upright Stance. Progress in Brain Research, vol. 165, pp. 283-297. Elsevier B.V.

Mergner, T., Glasauer, S., 1999: A Simple Model of Vestibular Canal-Otolith Signal Fusion. Annals New York Academy of Sciences, vol. 871, pp. 430-434.

Mergner, T., Huethe, F., Maurer, C., Ament, C., 2006: Human equilibrium control principles implemented into a biped robot. In: Robot Design, Dynamics, and Control (Romansy 16, Proceedings of the sixteenth CISM-IFToMM Symposium). T. Zielinska and C. Zielinski (Eds.), CISM Courses and Lectures 487, pp 271-279

Mergner, T., Maurer, C., Peterka, R.J., 2003: A Multisensory Posture Control Model of Human Upright Stance. Progress in Brain Research, vol. 142, pp. 189-201. Elsevier B.V.

References

Mergner, T., Schweigart, G., Fennel, L., 2009: Vestibular Humanoid Postural Control. Journal of Physiology, vol. 103, pp. 178–194. Elsevier Ltd.

Mergner, T., Schweigart, G., Maurer, C., Blümle, A., 2005: Human Postural Responses to Motion of Real and Virtual Visual Environments Under Different Support Base Conditions. Exp Brain Res, vol. 167, pp.535–556. Springer-Verlag. DOI 10.1007/s00221-005-0065-3

Miller, J. French, J., 2005: Estimating the Effects of Stress during Operational Conditions. Simulation Conference, 4-7 December 2005. ISBN: 0-7803-9519-0.

Moss, S., Wang, Z., Salloum, M., 2000: Anthropometry for WorldSID A World-Harmonized Midsize Male Side Impact Crash Dummy. SAE Technical Paper Series. The Engineering Society For Advancing Mobility Land Sea Air and Space – SAE International. Society of Automotive Engineers, Inc. ISSN 0148-7191.

Nabergoj, R., 2007: Fondamenti di Tenuta della Nave al Mare.

NATO RTO - Research and Technology Organisation, 2008: Seakeeping and Habitability in the Design of Vessels with Novel Hull Forms. Final Report of Task Group AVT-112, RTO-TR-AVT-112.

Nocerino E., Scamardella A., 2008: Full-Scale Measurements of Manoeuvrability: Implementation and Testing of an Innovative and Flexible Positioning System. SEAMED 2008. Messina, Italy, 4 July 2008.

Pacifico A., Nocerino E., Scamardella A., Vultaggio M., 2009: Implementation and testing of EGNOS full-scale dynamic trials onboard of HSC. Atti dell'Istituto Italiano di Navigazione, vol. 190, pp. 142-152, ISSN: 1120-6977.

Pattison, J.H., Sheridan, D,J., 2004: Human Performance Factors and Measures in Hull Form Selection. RTO AVT Symposium on "Habitability of Combat and Transport Vehicles: Noise, Vibration and Motion", Prague, Czech Republic, 4-7 October 2004, RTO-MP-AVT-110.

Perez, T., 2005: Ship Motion Control. Course Keeping and Roll Stabilisation using Rudder and Fins. Springer-Verlag London Limited 2005, ISBN-10: 1-85233-959-4.

Perez, T., Fossen, T.I., 2007: Kinematics and Kinetics of Marine Vessels (Module 3). Presentation at One-day Tutorial, CAMS'07, Bol, Croatia.

Perez, T., Fossen, T.I., 2009: A Matlab Toolbox for Parametric Identification of Radiation-Force Models of Ships and Offshore Structures. Modeling, Identification and Control. Vol. 30, No. 1, 2009, pp. 1-15. Norwegian Society of Automatic Control. ISSN 1890-1328

Peterka, R.J., 2002: Sensorimotor integration in human postural control. Journal of Neurophysiology, vol. 88 (2002), pp. 1097-1118.

Peterka, R.J., 2003: Simplifying the Complexities of Maintaining Balance. Insights Provided by Simple Closed-Loop Models of Human Postural Control. IEEE Engineering in Medicine and Biology Magazine.

Peterka, R.J., Loughlin, P.J., 2004: Dynamic Regulation of Sensorimotor Integration in Human Postural Control. Journal of Neurophysiology, vol. 92, pp. 400-423. The American Physiological Society. ISSN: 0022-3077.

Punakallio, A, 2005: Balance Abilities of Workers in Physically Demanding Jobs: with Special Reference To Firefighters Of Different Ages. Journal of sports science & medicine, vol. 4(8). http://www.jssm.org.

Qu, X., 2008: Development and Evaluation of Postural Control Models for Lifting Motions and Balance Control. Ph.D Thesis. Virginia Polytechnic Institute and State University. Blacksburg, Virginia, USA.

Rao, G., Amarantini, D., Berton, E., Favier, D., 2005: Influence of Body Segments' Parameters Estimation Models on Inverse Dynamics Solutions During Gait. Journal of Biomechanics, vol. 39, pp. 1531–1536. Elsevier Ltd.

Riola, J.M., Esteban, S., Giron-Sierra, J.M., Aranda J., 2004: Motion and Seasickness of Fast Warships. Research and Technology Organization RTO, Symposium on "Habitability of Combat and Transport Vehicles: Noise, Vibration and Motion", Prague, Czech Republic, 4-7 October 2004, RTO-MP-AVT-110.

Rocchi, L., Chiari, L. Horak, F.B., 2002: Effects of Deep Brain Stimulation and Levodopa on Postural Sway in Parkinson's Disease. J Neurol Neurosurg Psychiatry, vol. 73, pp. 267–274.

Roetenberg, D., 2006: Inertial and Magnetic Sensing of Human Motion. Ph.D. Thesis. University of Twente. The Netherlands. ISBN-10: 90-9020620-5.

Salvesen, N., Tuck, E.O., Faltinsen, O.M., 1970: Ship motions and sea loads. Transactions of the Society of Naval Architects and Marine Engineers, vol. 78, pp. 250–287.

Scamardella, A., 2008: Studio delle Onde Prodotte dal Mezzo Veloce Snav "Don Francesco" e Loro Impatto sulla Costa del Golfo Di Napoli. Department of Applied Sciences, University of Naples "Parthenope", Italy. Internal Report.

Schweigart, G., Mergner, T., 2008: Human Stance Control Beyond Steady State Response and Inverted Pendulum Simplification. Exp Brain Res, vol. 185 pp. 635–653. Springer-Verlag. DOI 10.1007/s00221-007-1189-4

Skey, S.G.P., Miles, M.D., 2005: Advances in Buoy Technology for Wind/Wave Data Collection and Analysis.
http://www.envirtech.org/doc/Paper%20-%20Advances%20in%20Buoy%20Technology.pdf

SNAME – The Society of Naval Architects and Marine Engineers, 1989: Principles of Naval Architecture, Second Revision. Volume III, Motions in Waves and Controllability. Edward V. Lewis, Editor. 0-939773-02-3.

Spirduso, W.W., Francis, K.L., MacRae, P.G., 2005: Physical dimensions of aging. Human Kinetics. ISBN: 0-7360-3315-7

Stevens, S.C., Parson, M.G., 2002: Effects of Motion at Sea on Crew Performance: A Survey. Marine Technology, Vol. 39, No. 1, January 2002, pp. 29–47.

Stockwel, C.W., Koozekanani, S.H., Barin, K., 1981: A Physical Model of Human Postural Dynamics. Annals New York Academy of Sciences.

Tahboub, K.A., 2009: Biologically-inspired humanoid control. Journal of Physiology – Paris, vol. 103 (2009), pp. 195-210.

References

Tahboub, K.A., 2010a: Optimal estimation of supporting-ground orientation for multi-segment body based on otolith-canal fusion. World Academy of Science, Engineering and Technology, vol. 63 (2010).

Tahboub, K.A., 2010b: Biologically-Inspired Postural and Reaching Control of a Multi-Segment Humanoid Robot. IEEE/ASME International Conference on Mechatronic and Embedded Systems and Applications. July 15-17, 2010, Qingdao, ShanDong, China

Tahboub, K.A, Mergner, T., 2007: Biological and engineering approach to human postural control. Integrated Computer-Aided Engineering, vol. 14 (2007), pp. 15-31.

Tahboub, K.A, Mergner, T., Ament, C., 2006: Neurological and Engineering Approaches to Human Postural Control. ICINCO 2006 – 3rd International Conference on Informatics in Control, Automation and Robotics. 1-5 August, 2006. Setúbal, Portugal.

Tang, C.P., 2006: Lagrangian Dynamic Formulation of a Four-Bar Mechanism with Minimal Coordinates. Internal Report. Erik Jonsson School of Engineering & Computer Science, The University of Texas at Dallas.

Valk, P., Grech, M., Bos, J., 2010: A Multi-Factorial Analysis of Human Performance During a 9-Day Sea Trial. International Conference on Human Performance at Sea HPAS 2010, Glasgow, Scotland, UK, 16-18 June, 2010.

Valles, B.K.D., Schneider, J.M., Long, J.T., Riedel, S.A., Johnson, M.J., Harris, G.F., 2006: Combined Sagittal and Coronal Plane Postural Stability Model. 28th IEEE EMBS Annual International Conference. New York City, USA, August 30 – September 3,2006.

Valles, B.K.D., Long, J.T., Riedel, S.A., Graf, A., Krzak, J., Hassani, S., Smith, P.A., Harris, G.F., 2008: Application of a Bi-Planar Postural Stability Model in Children with Cerebral Palsy. 30th IEEE EMBS Annual International Conference. Vancouver, British Columbia, Canada, August 20-24, 2008.

van der Kooij, H., Jacobs, R., Koopman, B., Grootenboer, H., 1999: A Multisensory Integration Model of Human Stance Control. Biol. Cybern., vol. 80, pp. 299-308. Spinger-Verlag.

van der Kooij, H., van Asseldonk, E., van der Helm, F.C.T., 2005: Comparison of different methods to identify and quantify balance control. Journal of Neuroscience Methods, vol. 145(2005), pp. 175-203.

Vibration Injury Network, 2001: Review of methods for evaluating human exposure to Whole–Body Vibration. Appendix W4A to Final Report. EC Biomed II concerted action BMH4-CT98-3291.

Wackrow, R., Chandler, J.H., Bryan, P., 2007: Geometric Consistency and Stability of Consumer-Grade Digital Cameras for Accurate Spatial Measurement. The Photogrammetric Record, vol. 22(118), pp. 121–134. The Remote Sensing and Photogrammetry Society and Blackwell Publishing Ltd.

Wagner, M.J., Smith, M.A., 2008: Shared Internal Models for Feedforward and Feedback Control. The Journal of Neuroscience, vol. 28(42), pp. 10663–10673. Society for Neuroscience.

Wedge, J., Langlois, R.G., 2003: Simulated the Effects of Ship Motion on Postural Stability using Articulated Dynamic Models. The Society for Modeling and Simulation, International Summer Computer Simulation Conference, SCSC Liophant & SCS, Montreal, 20-23 July, 2003.

Wertheim, A. H., 1998: Working in a moving environment. Ergonomics, Vol. 41, n. 12, pp. 1845–1858, Taylor & Francis Ltd.

Wing, A.M., Clapp, S., Burgess-Limerick, R., 1995: Standing Stability in The Frontal Plane Determined by Lateral Forces Applied to the Hip. Gait & Posture, vol. 3, pp. 38-42. Elsevier Science.

Winter, D.A., 1995: Human balance and posture control during standing and walking. Gait & Posture, vol. 3(4), pp. 193-214. Elsevier Science.

Winter, D.A., Prince, F., Frank, J.S., Powell, C., Zabjek, K.F., 1996: Unified Theory Regarding A/P and M/L Balance in Quiet Stance. Journal of Neurophysiology, vol. 75(6), pp. 2334-2343.

References

Winter, D.A., Patla, A.E., Prince F., Ishac, M.G., Gielo-Perczak K, 1998:. Stiffness control of balance in quiet standing. Journal of Neurophysiology, vol.80, pp. 1211–1221. The American Physiological Society. ISSN: 0022-3077.

Winter, D.A., 2005: Biomechanics and Motor Control of Human Movement. John Wiley and Sons Inc. ISBN 0-471-44989-X.

WEBSITES

Gambino, S., Mirochnik, M., Schechter, S., 2006: Center of Mass of a Human. The Physics Factbook™. Edited by Glenn Elert. Website: http://hypertextbook.com/facts/2006/centerofmass.shtml

Gibbs, P., Sugihara, H., 1997: What is Occam's Razor? Website: http://www.phys.ncku.edu.tw/mirrors/physicsfaq/General/occam.html

IEA - International Ergonomics Association: What is Ergonomics. Website: iea.cc/01_what/What%20is%20Ergonomics.html.

McKeough, D.M. 2010: Balance Concept Map. Website: http://www.csus.edu/indiv/m/mckeoughd/

NeuroCom International, Inc. 2009: Balance Control. Website: http://resourcesonbalance.com/clinical_info/BalanceControl.aspx

PostuRob. Website: http://www.uniklinik-freiburg.de/neurologie/live/forschung/sensorfusion/posturob.html

thefreedictionary.com, Proactive. Website: http://www.thefreedictionary.com/proactive

thefreedictionary.com, Proprioceptor. Website: http://www.thefreedictionary.com/Proprioceptor

thefreedictionary.com, Somatosensation. Website: http://medical-dictionary.thefreedictionary.com/Somatosensation

References

Wikipedia, Anatomical terms of location. Website:
http://en.wikipedia.org/wiki/Anatomical_terms_of_location

Wikipedia, Central Nervous System. Website:
http://en.wikipedia.org/wiki/Central_nervous_system

Wikipedia, Electromyography. Website:
http://en.wikipedia.org/wiki/Electromyography

Wikipedia, Human factors. Website:
http://en.wikipedia.org/wiki/Human_factors#Application_of_Human_Factors_Engineering

Wikipedia, PID controller. Website:
http://en.wikipedia.org/wiki/PID_controller

Wikipedia, Reflex. Website:
http://en.wikipedia.org/wiki/Reflex

Wikipedia, Sopite Syndrome. Website:
http://en.wikipedia.org/wiki/Sopite_syndrome

Wikipedia, Vestibular system. Website:
http://en.wikipedia.org/wiki/Vestibular_system

Xsens Technologies, Website:
http://www.xsens.com/

Acknowledgments

Three years have gone and I would like to express my deepest gratitude to all the persons that have supported me along this way.

I would to thank prof. Guido Boccadamo for having introduced me to such an interesting topic. When I started, I could have never thought that it would be so stimulating and challenging.

I would like to express sincerely thanks to prof. Antonio Scamardella for his unfailing assistance, patience and encouragement all along my course of study. His positive disposition has encouraged me to face the difficulties encountered during these years.

I am particularly grateful to Dr. Ermina Begovic for her advises and support. Her willingness to discuss my research work has been remarkable for me.

Next, I would also to show appreciation to prof. Salvatore Troisi. With his passion and patience, he has shown me what a "researcher" should be.

The experimental part of this research would not have been possible if it was not for my colleagues and friends of the Laboratory of Topography and Photogrammetry (University of Naples Parthenope). Dr. Sebastiano Ackermann, Silvio Del Pizzo and Dr. Fabio Menna have provided me invaluable support and friendship. Their keenness and passion for the challenges and new research questions have been extremely motivating. I look forward to collaborating with them in the future.

Thanks to Arturo, Alessandra, Andrea and Mario: their love assists me constantly, against all the difficulties.

This work would not have been possible without the continuous support and encouragement of Fabio. Every day, you are the most precious *find* for me!